The development and evaluation of a novel hybrid PLGA nanoparticle-Pheroid® with the potential to improve tuberculosis therapy

MP Chelopo-Mgobozi

orcid.org/ 0000-0002-3348-1635

M.Sc. Med Pharmaceutical Chemistry (UKZN)

Thesis submitted for the degree *Doctor of Philosophy* in Pharmaceutical Chemistry at the North-West University

Promoter:	Prof Rose Hayeshi
Co-Promoter:	Prof Anne Grobler
	Mr Lonji Kalombo

Graduation May 2018

Student number: 24408646

"There are two possible outcomes: if the result confirms the hypothesis, then you've made a measurement. If the result is contrary to the hypothesis, then you've made a discovery"

— Enrico Fermi

This thesis is dedicated to my precious daughter, Sipho-esihle Amare Mgobozi.

Acknowledgements

To the Almighty God, praise and glory be unto You. You have provided all the strength and wisdom to complete this work through every trial. Your word has given me great hope that I can do all things through the strength of our Saviour Lord Jesus Christ. "*Oh Lord God! Behold, You have made the heavens and the earth by Your great power and by Your outstretched arm! Nothing is too difficult for You*" **Jeremiah 32:17**.

I would like to express my sincere gratitude and appreciation to the following:

- **Prof Rose Hayeshi,** my study leader for the opportunity you offered me to do my PhD under your supervision and for being the best supervisor I could ever find. Thank you for your patience, persistence guidance, and insightful criticism through the planning and execution of all this work. Your dedication and work ethic have been a great inspiration to me.

- To my co-supervisors: **Prof Anne Grobler**, for the opportunity to do my PhD studies in Pharmaceutical Chemistry at NWU under your supervision and for all your guidance, wisdom and support towards a better quality of my PhD work; **Mr Lonji Kalombo**, for the countless times you offered comfort through challenging times and your critical thinking through the experimental planning and interpretation of the results, especially in the design of the nanoparticles.

- To the individuals who offered technical support in this work: **Dr James Wesley-Smith**, for your enormous knowledge and help in conducting the transmission electron microscopy (TEM); Dr **Matthew Glyn**, for your time and effort in capturing the confocal laser scanning microscopy (CLSM) images; **Dr Pascaline Fonteh**, for your valuable time in conducting cell viability experiment and assistance in the use of the xCELLIgence® technology; **Antoinette Fick** and **Hylton Buntting,** for your enthusiastic aid in handling the mice and conducting the mice experiments and **Brendon Naicker**, for your dedication and assistance in the analysis of the mice samples.

- To **Colin Pillai**, for your mentorship and guidance in ensuring that I finally submit my PhD thesis as an alumnus of the "Next Generation Scientist" program. You are one of the greatest leaders I have ever encountered in my life.

- To my loving husband and my best friend, **Tham'sanqa Mgobozi**, for your love and belief in me. Through this journey, you were my boyfriend, fiancé and ultimately my husband. Thank you for being there through times of tears and for the all the sacrifices you have made for us. We have been blessed with such a precious daughter, **Sipho-esihle Amare Mgobozi**, during this journey, who has given me the greatest strength and to whom I dedicate this thesis.

- To my Mother, **Salphinah R Chelop**o, for always being a pillar of strength up to this point in my life and through all my decisions to study; To my late father, **Albert S Chelopo**, for his commitment to see me thrive through education; I am dedicated to keeping your legacy of love and kindness alive. I want to thank my family for all the support and love they gave to me, especially my siblings **Mosima**, **Makgomo, Motlatjo, Mancha** and **Moloko Chelopo**, my aunt **Mosima Chelopo**, my uncle **Phineas Boshomane**, my aunt-in-law **Lungile Mgobozi** and the my new loving family **Irene (Dube), Sbonelo, Mary, Bonga, Nosisa, Makaziwe (Nana) and Nosipho Mgobozi.**

- To my loving friends: **Mbali Zulu**, **Thobekile Gambu**, **Senabelo Chiliza**, **Kholofelo Kgole**, **Rose Matjie** and **Blessing Monyai**. You guys are God-sent angels to me. Thank you for all your prayers, inspiration and encouragements through this journey.

- My colleagues: **Nomvuyo Nomadolo**, **Dr Vongani Chauke**, **Dr Goitsi Phiri**, **Dr Lindo Nhlanhla**, **Nthwaleng Mogamme** and **Thulile Khanyile** for all your advice and for such a vibrant working environment. My PhD buddies: **Vusani Mandiwana**, **Dr Clinton Rambanapasi** and **Dr Isaac Mutingwende** for all the motivation and drive to get this PhD and a constant reminder that I am never alone in this journey.

- To the institutions that have supported and funded to fund this PhD project: the National Research Foundation (**NRF**), through professional development program (PDP), for providing financial support; the Council for Scientific and Industrial Research (**CSIR**) for hosting me and providing additional funding for all my running costs; my academic institution North-West University (**NWU**) for administering my PhD registration and for additional funding.

Preface

This thesis is submitted in fulfilment of the requirements for a Doctor of Philosophy in Pharmaceutical Chemistry, using the article format in accordance with the General Academic Rules (A.7.5.7.4) of the North-West University (NWU). Chapters 3 to 5 include the following sections: an abstract; introduction; experimental or materials and methods; results and discussions as well as a conclusion. References are provided at the end of each chapter (1-6). Harvard style referencing was used throughout the thesis. Permissions for all cited images and illustrations in this thesis were obtained from the copyright office of the journal articles or books. All the experimental work demonstrated in chapters 3-5 was conducted as part of the PhD studentship contract between myself and the Council for Scientific and Industrial Research (CSIR) while registered as a full-time student at NWU. The National Research Foundation (NRF), the Department of Science and Technology (DST), the CSIR and NWU provided all the funding for this research.

I Madichaba Phuti Chelopo-Mgobozi, the student, did the following in the work presented in this thesis:

- Planned and designed the experiments, in consultation with study promoters;
- Carried out all the experimental work and participated in all the experiments done at external laboratories, which include the DST/CSIR National Centre for Nanostructured Materials and Department of Biochemistry at the University of Pretoria;
- Interpreted the results and discussed them with promoter and co-promoters;
- Wrote the complete thesis;
- Drafted the manuscripts.

The promoter and co-promoters significantly contributed in the following manner:

- Supervised the planning and design of studies;
- Assisted in the interpretation of the results;
- Critically reviewed the drafted thesis and manuscripts;
- Co-authored the manuscripts

Manuscript 1 (Chapter 3) has been published in the *Journal of Material Science*, while manuscript 2 (Chapter 5) will be submitted to the *International Journal of Pharmaceutics*. All the co-authors have given permission that the manuscripts may be submitted for degree purposes, as stipulated in the Manual for Post Graduate Students of the North-West University.

Abstract

The development of drug delivery technologies has the potential to bring both therapeutic and commercial value to future healthcare products. Drug delivery technologies are transport vehicles that help overcome the disadvantages, such as poor bioavailability and limited aqueous solubility, associated with free drugs, and enable drugs to function to their full potential. Case in point: tuberculosis (TB) is still a major health threat in South Africa, even though anti-TB drugs are available for its treatment. These anti-TB drugs have poor pharmacokinetic (PK) properties and have to be taken for lengthy periods at high daily dosage for them to be effective. Several drug delivery systems (DDS) have been investigated to improve the current TB therapy so as to reduce dosing frequency and shorten the treatment period. However, the advancement of these systems for improved TB therapy is limited by certain drawbacks of each of these DDS. Hybrid (or combined) DDS composed of a polymeric nanoparticle (NP) core and a lipid-based outer shell have recently emerged in an effort to mitigate some limitations associated with the individual DDS.

The research described here explores the combination of two delivery systems with unique properties, namely poly (DL-lactic-*co*-glycolic acid) (PLGA) NP and Pheroid® technology. The solid PLGA NP were combined with Pheroid® vesicles using two types of mixing approaches namely, pre-mix (the addition of preformed NP during the Pheroid® manufacturing) and post-mix (the combination of the two individual preformed systems). The particle size of the hybrid system ranged from approximately 2250 nm to 2850 nm, depending on the surface properties of the NP, while the zeta potential (ZP or ζ-potential) ranged from -19 to -25 mV, measured using laser diffraction and electrophoretic velocity methods, respectively. There was an increase in the size of the Pheroid® vesicles when combined with NP that had a positive ZP, suggesting a possible electrostatic interaction between the two systems. Further physicochemical properties of this novel hybrid system were obtained through transmission electron microscopy (TEM) and confocal laser scanning microscopy (CLSM), both of which revealed possible co-localisation of the NP with the Pheroid® vesicles. The effect of the NP/Pheroid® ratio when combining the two systems showed that the stability of the hybrid system is compromised at ratios above 2.5% (w/v) NP.

In vitro experiments were conducted to evaluate the effect of the hybrid system on cytotoxicity, permeability as well as intracellular uptake using the Caco-2 cell line. The use

of high concentrations of Pheroid® in the cell culture environment has previously been shown to compromise cell viability through the prevention of nutrients and gas exchange between the culture media and cells. The real-time cell analysis (RTCA) used in this study indicated that it was imperative to dilute NP, Pheroid® and the hybrid DDS for use in Caco-2 cell permeability experiments. The appropriate dilutions that showed prolonged safety for the Caco-2 cells over 24 hours (h) period using the RTCA were confirmed to be 0.004% (v/v) for the Pheroid® vesicles and a maximum of 1% (w/v) for the NP. However, the hybrid DSS did not show any significant effect on the permeability of coumarin 6 (C6) in comparison with the individual DDS. The C6 was found to be associated with the Caco-2 cell membrane rather than taken up into the cytoplasm.

An *in vivo* evaluation of this novel hybrid system was undertaken to investigate its potential application to address challenges in tuberculosis (TB) therapy. Three types of formulations were prepared for each of the two selected anti-TB drugs, rifampicin (RIF) and isoniazid (INH). These formulations included free drug, drug-loaded PLGA NP and drug-loaded NP–Pheroid® hybrid system. A single oral dose of each formulation was administered to healthy female BALB/c mice, and the levels of RIF and INH were measured in the plasma and selected organs at several time points to determine the effect of the hybrid delivery system on the PK of these drugs. The plasma data did not provide evidence of the NP–Pheroid® hybrid formulation on improving the PK parameters for both drugs. However, the effect of the hybrid formulation was observed in the RIF distribution to the lung tissue, where there was a significant reduction of T_{max} from 11 to 4 h in comparison to the RIF NP, and to the kidney, where the half-life of RIF was significantly increased to 16 h in comparison to the 4 h by the free RIF. The hybrid system also led to an increased retention of RIF in the lungs up to a period of 5 days (d), compared to the 3 d RIF circulation from free RIF and RIF NP.

In conclusion, the fabrication of the PLGA NP-Pheroid® hybrid DDS was successful, as determined through size and ζ-potential measurement. Co-localisation of the NP with the Pheroid® vesicles was demonstrated by microscopy techniques, namely, TEM and CLSM. The optimal NP/Pheroid® mixing ratio for a stable hybrid system was found to be a maximum of 2.5% (w/v). The permeability of C6 was enhanced when encapsulated in all the delivery systems: NP, Pheroid®, and NP-Pheroid®. However, C6 cell uptake was not altered when formulated in any those above-mentioned delivery systems. The NP-Pheroid® hybrid system did not alter the PK parameters of either INH or RIF in the plasma. However, the effect of the novel hybrid DDS was observed on RIF distribution to the lungs and kidney.

Keywords: PLGA nanoparticles, Pheroid® vesicles, drug delivery, hybrid drug delivery systems, lipid-polymer hybrid nanoparticles, Caco-2 cells, real-time cell analysis, tuberculosis, rifampicin, isoniazid, and pharmacokinetics

Uittreksel

Die ontwikkeling van tegnieke deur middel waarvan medisyne gelewer word, het die potensiaal van beide terapeutiese en kommersiële waardetoevoeging in die toekoms tot porodukte vir gesondheidsorg. Die leweringstegnieke van medisyne waardeur dit moontlik gemaak word dat medisyne se funksie hulle volle volle potensiaal bereik, is vervoermiddele wat help om nadele soos onvoldoende bio-beskikbaarheid en beperkte oplosbaarheid in water teë te werk. In hierdie verband moet daarop gelet word dat tuberkulose (TB) steeds ‘n belangrike gesondheidsgevaar is, ten spyte daarvan dat anti-tuberkulosemiddels vir behandeling beskikbaar is. Hierdie anti-tuberkulosemiddels beskik egter oor gebrekkige farmokinetiese eienskappe en moet, om effektief te wees, oor lang periodes en met hoë daaglikse dosisse ingeneem word. Verskeie sisteme deur middel waarvan medisyne gelewer word is ondersoek ten einde die huidige tuberkuloseterapie te verbeter deur die vermindering van die frekwensie van die dosisse en die verkorting van die behandelingsperiode. Die vordering en vooruitgang van hierdie sisteme vir die verbetering van tuberkuloseterapie, word egter beperk deur sekere belemmerings in elk van hierdie sisteme. Hibridiese (of gekombineerde) sisteme wat saamgestel is uit ‘n gepolimeerde nanodeeltjiekern en ‘n lipiedgebaseerde buite-omhulsel het onlangs die lig gesien in ‘n poging om sommige van die beperkings, wat met die individuele sisteme geassosieer word, te versag,

In die onderhawige navorsing word ‘n kombinasie van twee sisteme met unieke eienskappe, naamlik poli (DL-laktiese-*co*-glukolaktiese suur), NP en Pheroid® -tegnolgie ondersoek. Die soliede PLGA NP is gekombineer met Pheroid® -blasies deur gebruikmaking van twee benaderings met betrekking tot die vermenging, naamlik pre-vermenging (die homogenisering van voorafgevormde NP gedurende die bereiding van Pheroid®) en post-vermenging (die kombinering van die twee individuele voorafgevormde sisteme). Die deeltjiegrootte van die hibridiese sisteem wissel vanaf ongeveer 2250 nm tot 2850 nm, afhangend van die oppervlakte-eienskappe van die NP, terwyl die zeta-potensiaal strek vanaf -19 tot 25 mV, wat gemeet is aan die hand van laserstraalbuiging en elektroforesiese snelheidsmetodes, respektiewelik.. Daar was ‘n toename in die populasiegrootte van die Pheroid® -deeltjies wanneer dit gekombineer is met die NP wat ‘n positiewe ZP het; dit dui op ‘n moontlike elektrostatiese wisselwerking tussen die twee sisteme. Voorts is fisikochemiese eienskappe van hierdie nuwe hibridiese sisteem verkry deur transmissie electron- mikroskopie en noukeurige laserskandering-mikroskopie wat beide dui op moontlike gelyktydige lokalisering

van die NP met die Pheroid® -deeltjies. Die effek van die NP/ Pheroid® -ratio wanneer die gekombineer word, dui daarop dat die stabiliteit van die hibridiese sisteem geraak word by ratio's bo 2,5% (w/v) NP.

In vitro-eksperimente is uitgevoer om die effek van die hibridiese sisteem op sitotoksisiteit, deurdringbaarheid sowel as intrasellulêre opneming deur midel van die Caco-2-sellyn te evalueer. Dit is reeds bevind dat die gebruik van hoë konsentrasies Pheroid® in die kultuuromgewing van die sel seltoksisiteit veroorsaak deur die voorkoming van voedingstowwe en gasruiling tussen die kultuurmedia en selle. Die reële tyd wat in hierdie studie aan selanalise bestee is, het bewys dat dit van die uiterste belang is om NP, Pheroid® en die leweringsisteme van die hibriede te verdun vir aanwending in Caco-2 eksperimente op seldeurdringbaarheid. Die gepaste verdunnings wat gelei het tot die verlengde veiligheid vir die Caco-selle oor 'n periode van 24 uur met die gebruikmaking van die RTCA is vasgestel op 0.004% (v/v) vir die Pheroid® -deeltjies en 'n maksimum van 1% (w/v) vir die NP. Die hibried se leweringsisteem het egter geen betekenisvolle effek getoon met betrekking tot die deurdringbaarheid van coumarin (C6) in vergelyking met die individuele sisteem nie. Dit is bevind dat die C6 meer met die Caco-2 selmembraan assosieer eerder as opname in die sitoplasma.

'n *In vito*-evaluering van hierdie nuwe hibridiese sisteem is onderneem om die potensiële aanwending daarvan vir die uitdagings van tuberkuloseterapie vas te stel. Drie tipes formules is voorberei vir elk van die twee geselekteerde twee anti-TB-middels, rifampicin (RIF) en osoniazid. Hierdie formules sluit in behandelinglose, behandelinggelaaide PLGA NP en behandelinggelaaide NP-Pheroid® hibridiese sisteem. 'n Enkele mondelikse dosis van elke formule is aan vroulike gesonde BALB/c muise toegedien en die vlakke van RIF en INH in die plasma en geselekteerde organe is op verskillende tye gemeet om die effek van die hibridiese leweringsisteem op die PK van hierdie middels vas te stel. Die plasma-data het geen bewyse gelewer omtrent die invloed van die NP–Pheroid® hibridiese formule ten opsgte van die verbetering van die PK-parameters vir beide middels nie. Die effek van die hibriedformule is egter waargeneem in die RIF-distribusie in die longweefsel van 'n betekenisvolle afname van T_{max} van 11 tot 4 uur in vergelyking met die RIF NP. Die hibridiese sisteem het ook gelei tot 'n toename in die retensie van RIF in die longe tot 'n periode van 5 dae, vergeleke met die 3 dae RIF-sirkulasie van RIF-vrye en RIF NP-vrye.

Ten slotte word gestel dat die fabrisering van die PLGA NP-Pheroid® -hibridiese leweringsisteem suksesvol was soos op indirekte wyse aangedui deur grootte en ZP-meting.

Die gelyktydige lokalisering van die NP met die Pheroid®-deeltjies is gedemonstreer deur middle van mikroskopie-tegnieke, naamlik TEM en CLSM. Dit is vasgestel dat die optimale NP/Pheroid®-mengratio vir ‘n stabiele hibridiese sisteem ‘n maksimum van 2.5% (w/v) is. Die deurdringbaarheid van C6 is verhoog toe dit saamgevat is in al die leweringsisteme: NP, Pheroid® en NP-Pheroid®. Die C6-selopname is egter in geen van die sisteme gewysig toe dit in die bogenoemde sisteme saamgevat is nie. Die NP-Pheroid® hibridiese sisteem het nie die PK-parameters van die INH en die RIF in die plasma® verander nie. Die effek van die nuwe hibridiese sisteem is egter waargeneem in die RIF-distribusie na die longe.

Sleutelwoorde: PLGA-nanodeeltjies, Pheroid®-blasies, lewering van middels; hibridiese sisteme vir lewering van middels, lipiede-veeltallige hibridiese nanodeeltjies, Caco-2-selle, reële tyd van selanalise, tuberkulose, rifampicin, isoniazid en farmokinetika.

Table of Contents

Acknowledgements iv
Preface vi
Abstract vii
Uittreksel x
Table of Contents xiii
List of Figures xviii
List of Tables xxiii
Abbreviations xxv

CHAPTER 1: PROBLEM STATEMENT AND AIMS OF THE RESEARCH STUDY 2
1. Problem in the progress of drug delivery systems for tuberculosis therapy 2
2. The combination of DDS as a solution 2
3. Research focus 6
3.1. Research questions and hypothesis 8
3.2. Research aim and objectives 8
4. Thesis chapters breakdown 9
5. References 10

CHAPTER 2: A REVIEW ON THE ADVANCEMENT OF DRUG DELIVERY SYSTEMS FOR THERAPY IMPROVEMENT 15
1. Drug delivery systems 15
2. Brief history – Advancement to nano-based DDS 16
3. Oral drug delivery route 20
4. Polymeric drug delivery systems 21
4.1. Chemically-controlled systems 23
4.2. Biodegradable polymeric systems 23
4.2.1. Poly (DL-lactic-*co*-glycolic acid) nanoparticles 23
5. Lipid-based drug delivery systems 25
5.1. Liposomes 25
5.2. Pheroid® delivery system 27
6. Lipid-polymer hybrid drug delivery systems 32
6.1. Preparation methods for individual DDS and hybrid DDS 35

6.2. Characterisation of the physicochemical properties of the individual DDS and hybrid DDS ... 36
7. Biological application of hybrid DDS ... 39
8. Tuberculosis – a neglected poverty-related disease ... 41
8.1. The pathogenesis of TB ... 43
8.2. Current TB chemotherapy ... 45
8.3. Drug delivery systems for TB ... 48
9. References ... 52

CHAPTER 3: THE FABRICATION AND CHARACTERIZATION OF PLGA NANOPARTICLE-PHEROID® COMBINED DRUG DELIVERY SYSTEM ... 69
1. Abstract…. ... 69
2. Introduction ... 70
3. Experimental ... 71
3.1. Materials ... 71
3.2. Preparation of PLGA NP ... 72
3.3. Preparation of Pheroid® vesicles ... 72
3.4. Combination of PLGA NP with Pheroid® vesicles ... 72
3.5. NP/Pheroid® mixing Ratio ... 73
3.6. Size, distribution, and zeta potential measurements ... 73
3.7. Microscopy ... 73
4. Results…. ... 75
4.1. Preparation and characterization of PLGA NP and Pheroid® individual systems ... 75
4.2. Preparation and characterization of combined PLGA NP-Pheroid® system ... 76
4.3. Microscopy ... 77
4.4. NP/Pheroid® mixing Ratio ... 81
5. Discussion ... 83
5.1. Preparation and characterization of PLGA NP and Pheroid® individual systems ... 83
5.2. Preparation and characterisation of the combined PLGA NP- Pheroid® system ... 84
5.3. Microscopy analysis ... 86
5.4. NP/Pheroid® mixing Ratio ... 88
6. Conclusions ... 90
6.1. Acknowledgements ... 90
7. References ... 91

CHAPTER 4: THE EFFECT OF THE NP-PHEROID® HYBRID SYSTEM ON THE VIABILITY OF AND TRANSPORT ACROSS CACO-2 CELLS 96
1. Abstract… 96
2. Introduction 97
3. Materials and methods 100
3.1. Materials 100
3.2. Methods 100
3.2.1. Cell culture 100
3.2.2. Trypan blue assay 101
3.2.3. MTT assay 101
3.2.4. Real-time cell analysis (RTCA) 103
3.2.5. Permeability and uptake studies 104
4. Results and discussion 106
4.1. *In vitro* viability - Trypan blue 106
4.2. *In vitro* viability - MTT and xCELLigence® assay 107
4.2.1. Effect of the NP on Caco-2 cells (MTT and xCELLigence®) 109
4.2.2. Effect of the Pheroid® vesicles on Caco-2 cells (xCELLigence®) 112
4.2.3. Effect of the NP-Pheroid® on Caco-2cells (xCELLigence) 113
4.3. *In vitro* permeability and uptake study 117
4.3.1. Cell monolayer integrity 117
4.3.2. Cell permeability 118
4.3.3. Cell uptake 120
8. Conclusion 123
5.1. Acknowledgements 123
9. References 124

CHAPTER 5: PHARMACOKINETIC EVALUATION OF ANTI-TB DRUGS IN A NP – PHEROID® HYBRID DRUG DELIVERY SYSTEM 132
1. Abstract…. 132
2. Introduction 132
3. Materials and methods 135
3.1. Materials 135
3.2. Methods 136
3.2.1. Preparation and characterisation of drug- loaded NP–Pheroid® 136
3.2.2. Drug loading and encapsulation efficiency determination 137

3.2.3. Animals used for the study 138
3.2.4. Administration of the formulations to the mice and sample collection 139
3.2.5. Plasma sample preparation for LC-MS/MS analysis 141
3.2.6. Organ (liver, lungs, kidneys and intestines) sample preparation 141
3.2.7. Calibration curves 142
3.2.8. LC-MS/MS method 142
3.2.9. Data analysis 143
4. Results and discussion 144
4.1. Characterisation of the drug-loaded NP-Pheroid® hybrid system 144
4.1.1. Drug loading (DL) and encapsulation efficiency (EE) 146
4.2. LC-MS/MS detection and quantification of INH and RIF 147
4.3. PK analysis of INH and RIF in mouse plasma 149
4.3.1. Plasma PK of INH 150
4.3.2. Plasma PK of RIF 151
4.3.3. INH and RIF C_{max}/AUC graph 154
4.4. The distribution of INH and RIF in the organs of the mice 155
4.4.1. INH detection in the organs 156
4.4.2. RIF detection and PK analysis in the Organs 156
5. Conclusion 167
5.1. Acknowledgements 167
6. References 168

CHAPTER 6: THESIS SUMMARY 1766
1. Thesis outcomes 1766
2. Research contribution 1788
3. Study limitations 17979
4. Future recommendations 1811
5. References 1833

ANNEXURE A – Overall Flow of Experiments 187
ANNEXURE B - Journal Author Guidelines 189
Journal 1 – *Journal of Material Science* 190
Journal 2 - *International Journal of Pharmaceutics* 204

ANNEXURE C - Poster Presentations…….....2188

Poster 1 – 17th World Congress of Basic and Clinical Pharmacology (WCP 2014)……..21919

Poster 2 – From Rising Stars to a Nobel Star……2211

ANNEXURE D - Oral Presentations……223

Oral Presentation 1 – APSSA/ SAAPI Conference…….……22424

Oral Presentation 2 - 6th International Conference on Nanoscience & Nanotechnology in Africa (Nano Africa 2016)…….2255

Oral Presentation 3 – 2nd Edition of Nanotech France International Conference and Exhibition (Nanotech France 2016)…….226

Oral Presentation 4 – 2nd Symposium on Nanomedicine and HIV/AIDS……..227

ANNEXURE E – Language Editing Certificate..……...2238

List of Figures

CHAPTER 1

Figure 1: A TB patient holding a daily dose of anti-TB drugs. Photo reprinted with permission from the Guardian News & Media Ltd, (2016). 2

Figure 2: Structural components of a lipid-polymer hybrid DDS composed of PEG; lipid bilayer; polymeric NP and an encapsulated drug. 6

CHAPTER 2

Figure 1: A schematic diagram showing the progress of drug delivery systems (DDS) from macro and micro systems to the nano systems. The dates given represent early discovery and significant events after discovery. This diagram was reprinted with permission from Crommelin and Florence, (2013). 18

Figure 2: Examples of nano-based drug delivery systems. This image was reprinted with permission from Cho *et al*., (2008). ..... 19.

Figure 3: Diagram showing a broad overview of the essential factors to consider in the design of nano-based DDS from basic research to clinical applications. The diagram was reprinted with permission from Bennet and Kim, (2014) 20

Figure 4: The chemical structure of PLGA (x – number of lactic acid monomers and y – number of glycolic acid monomers). 24

Figure 5: Structure of liposome. The figure was reprinted with permission from Cukierman and Khan, (2010) 26

Figure 6: A hypothetical diagram of Pheroid® membrane demonstrating the red regions as the hydrophobic and blue regions as the hydrophilic domains of the fatty acid components of vitamin F. The pore structures or channels are formed by the Cremophor molecules. The figure was reprinted with permission from Grobler, (2009). 30

Figure 7: The components that make up the Structure of Pheroid® (left) and pro-Pheroid® (right). The figure was reprinted with permission from Grobler, (2009). 31

Figure 8: Three different types of Pheroid® observed using confocal laser scanning microscope (CLSM). A. Pheroid® Vesicle; B. Pro-Pheroid® and C. Pheroid® Sponges. The figure was reprinted with permission from Grobler, (2009). 32

Figure 9: Schematic illustration of a lipid-polymer hybrid DDS with its structural components. The figure was reprinted with permission from Zhang *et al.*, (2008). 34

Figure 10: The global TB incidences estimated in 2014. Figure reprinted with permission from WHO, (2015) 42

Figure 11: The global HIV prevalence in TB cases estimated in 2014. Figure reprinted with permission from WHO, (2015). 42

Figure 12: Graph showing the amount of antiretroviral therapy given to HIV-positive patients with TB. The graph was reprinted with permission from UNAIDS, (2014).....43

Figure 13: The transmission and pathogenesis *M.tb*. Diagram reprinted with permission from Pinheiro *et al.*, (2011).....45

Figure 14: The structures of the four first-line anti-TB drugs: INH (A); ETB (B); RIF (C); PYZ (D). Structures obtained with permission from DrugBank, (2005a-d).....46

Figure 15: Diagram illustrating the cell wall, cell membrane and the cytoplasm of *M.tb* and the site of action for each of the first-line anti-TB drugs. Diagram reprinted with permission from (du Toit *et al.*, 2006).....47

CHAPTER 3

Figure 1: The illustration of two combination methods for Pheroid® and NPs and the hypothetical structure of the NP-Pheroid® combined system. (A) Post-mix method, where preformed Pheroid® lipid vesicles are combined with the preformed PLGA NPs through vortex. (B) Pre-mix method, the pre-formed NPs are added to the oil phase constituents of the Pheroid® and the N_2O saturated water though homogenisation.....74

Figure 2: Typical micrographs of PLGA NPs shown by (A) SEM (scale bar= 1 µm) and (B) TEM (scale bar= 0.1 µm). The image of Pheroid® vesicles was vied using (C) light microscope (scale bar = 20 µm).....78

Figure 3: Confocal Images of 1% (w/v) C6 NP (Pos-NPs) combined with Pheroid® vesicles (stained with Nile red) by pre-mix method. Row A: Control Pheroid® vesicles shown in the Red and Green channels and Row B, C6 NP - Pheroid® Vesicles shown in the Red, Green and Red and Green channels. (Scale bars = 20 µm).....79

Figure 4: TEM images of free Pheroid® vesicles obtained after (A) Cryogenic method (cryo-TEM) and (B) air dried method (RT TEM). All samples were negatively stained using uranyl acetate (UA) (scale bar = 0.2 µm).....80

Figure 5: TEM images of neat Pheroid® vesicles: (A-B) Osmium tetraoxide (OsO_4) and (C) Uranyl acetate (UA). The second row images display NP-Pheroid® system (D-F) stained with uranyl acetate (UA) and were prepared using pre-mix method at 1% (w/v) NP (Pos NP).....81

Figure 6: Graphs showing the effect when varying NP/Pheroid® mixing ratio using neg-NPs (without CT and PEG) and pos-NPs (with CT and PEG) on the (A) Particle size and (B) Zeta Potential (ZP).....82

Figure 7: The percentage change in Size and ZP when 1% (w/v) of neg-NPs and pos-NPs are used to form the combined system.....85

Figure 8: (A) The size distribution curves of the Pheroid® vesicles with an increasing amount of pos NPs in percentages (% w/v) and (B) The confocal images of Pheroid® vesicles with varying ratios of C6 pos-NPs (Scale bars = 20 µm).....89

CHAPTER 4

Figure 1: The chemical structure of coumarin 6 (C6), composed of hydrophobic benzopyrone backbone and N-diethylamine or benzothiazole substituents. 99

Figure 2: The titration of Caco-2 cell density in the xCELLigence® E-plate wells to identify the ideal seeding density. The optimum density that was suitable for treatment where the cells were slowly proliferating, was determined to be 2.5 x 10^3. (n=2). 104

Figure 3: Cytotoxicity of various Pheroid® concentrations in Caco-2 cells determined using the trypan blue assay. This indicates a Pheroid® concentration-dependent response. (The NP % depict w/v; n=2). 107

Figure 4: MTT cell viability response to nanoparticles (NP) after 24 h. The curve shows dose-dependent decrease in cell viability. (The NP % depict w/v; n=2). 110

Figure 5: The RTCA profiles of the cells after treatment with PLGA NP over 24 h. The 5% NP resulted in cell death immediately on treatment. (The NP % depict w/v; n=2). 111

Figure 6: The RTCA profiles of the cells after treatment with Pheroid® vesicles (Phe V) over 3 h, showing no evidence of decreased cell viability. (The Phe V % depict v/v; n=2). 112

Figure 7: The RTCA profiles of the cells after treatment by Pheroid® vesicles (Phe V) over 24 h. A dose-response relation is evident, where 0.4% Pheroid® vesicles were the most cytotoxic concentration. (The Phe V % depict v/v; n=2). 113

Figure 8: xCELLigence® plot of cell response to 0.4% (v/v) Pheroid® vesicles (Phe V) combined with various NP concentrations over 24 h period. All combinations lead to an acute decline in the CI. (The Phe V % depict v/v; NP % depict w/v; n=2). 114

Figure 9: xCELLigence® plot of cell response to 0.04% (v/v) Pheroid® vesicles (Phe V) combined with various NP concentrations over 24 h period. A delayed decline in the CI is observed at the lowest NP concentration (1%) combined with the 0.04% Pheroid® vesicles. (The Phe V % depict v/v; NP % depict w/v; n=2). 115

Figure 10: xCELLigence® plot of cell response to 0.004% (v/v) Pheroid® vesicles (Phe V) combined with various NP concentrations over 24 h period. The 0.004% Phe V:1% NP ratio was not cytotoxic. (The Phe V % depict v/v; NP % depict w/v; n=2). 116

Figure 11: Before and after experiment TEER values and the % LY rejection for the Caco-2 cell monolayer. The TEER values were obtained from three wells before the experiment and two wells after the experiment. Each TEER value was subtracted from TEER without cells = 190 Ω. All Pheroid® (Phe) samples were 1000x dilutions. (n=2). 118

Figure 12: The permeability of C6 (at 2μg/ml) in apical-to-basolateral (A→B) directions. The P_{app} values are an average of three wells, and the error bars represent SD from the average P_{app}. (n=3). 120

Figure 13: Confocal images of Caco-2 Cells after 3 h treatment with C6 NP (A), C6 Pheroid® (B) and C6 NP-Pheroid® (C) formulations, showing the association of C6 with the cells. 121

Figure 14: The association of C6 (at 2μg/ml) in Caco-2 cells. Average concentrations (Conc) were calculated from three wells, and the error bars represent as SD from the average Conc. (n=3). ……122

CHAPTER 5

Figure 1: The hypothetical structure of drug-loaded NP-Pheroid® hybrid drug delivery system (DDS). This image illustrates the drug loaded-PLGA NP core enveloped by a Pheroid® lipid bilayer shell. 135

Figure 2: The illustration of four steps taken in handling and restraining a mouse for an oral gavage administration of drugs (Images obtained from (UIC, 2014).....140

Figure 3: Chemical structures and the mass-to-charge ratio (m/z) of the two anti-TB drugs, INH and RIF, as well as their internal standards (IS), RIB and 6-ANA. The arrow shows the anticipated points of fragmentation to form major ions for detection. 143

Figure 4: The CLSM images of Pheroid® vesicles produced from pro-Pheroid®, stained using Nile Red. (*Scale bar = 8.9 μm.*).....146

Figure 5: Typical LC-MS/MS chromatograms of INH and 6-ANA (Insert).....148

Figure 6: Typical LC-MS/MS chromatograms of RIF and RIB (Insert) 148

Figure 7: Concentration (Conc) of INH detected in mice plasma from free, NP and NP-Pheroid® formulations. All INH formulations were administered at a dose of 5 mg/kg. The error bars indicate the SD obtained from n=8 samples. (Phe = Pheroid®). 150

Figure 8: Concentration (Conc) RIF detected in mouse plasma from free, NP and NP-Pheroid®0formulations. All RIF formulations were administered at a dose of 10 mg/kg. The error bars indicate the SD obtained from n=8 samples. (Phe = Pheroid®)..... 152

Figure 9: The C_{max}: AUC ratio of INH and RIF in plasma from the free drug, drug in NP and drug in NP-Pheroid® post oral administration. INH dose = 5 mg/kg and RIF dose = 10 mg/kg/. 155

Figure 10: Blood circulation and passage through tissues. Redrawn with permission from Shin et al., (2016). 156

Figure 11: The concentration (Conc) of RIF in the liver following oral administration of free RIF (G1B), RIF NP (G2B) and RIF NP-Pheroid® (G3B). The dose level of RIF was 10 mg/kg in each formulation. The error bars indicate SD from the mean concentration that was obtained from n=8 samples. (Phe = Pheroid®)……..…157

Figure 12: The circulation time of RIF in lungs, intestines, kidneys and liver from Free RIF, RIF NP and RIF NP-Pheroid® after oral administration. RIF dose = 10 mg/kg. 159

Figure 13: The tissue concentration (Conc) of RIF in the lungs following oral administration of free RIF (G1B), RIF NP (G2B) and RIF NP-Pheroid® (G3B). The dose level of RIF was 10 mg/kg in each formulation. The error bars indicate SD from the mean concentration that was obtained from n=8 samples. (Phe = Pheroid®). 160

Figure 14: The concentration (Conc) of RIF in the kidneys following oral administration of free RIF (G1B), RIF NP (G2B)) and RIF NP-Pheroid® (G3B). The dose level of RIF was 10 mg/kg in each formulation. The error bars indicate SD from the mean concentration that was obtained from n=8 samples. (Phe = Pheroid®)..... 162

Figure 15: The tissue concentration (Conc) of RIF in the intestines following oral administration of free RIF (G1B), RIF NP (G2B)) and RIF NP-Pheroid® (G3B). The dose level of RIF was 10 mg/kg in each formulation. The error bars indicate SD from the mean concentration that was obtained from n=8 samples. (Phe = Pheroid®)……..……... 163

Figure 16: The AUC organ: AUC plasma ratio of RIF levels in lungs, intestines, kidneys and liver from Free RIF, RIF NP and RIF NP-Pheroid® after oral administration. RIF dose = 10 mg/kg…….. 165

CHAPTER 6

Figure 1: An illustration of the electrostatic interaction of Pheroid® vesicles (Negative Zeta Potential) with Nanoparticles (positive Zeta Potential) into a Nanoparticle-Pheroid® hybrid system. 177

List of Tables

CHAPTER 2

Table 1: The timeline for 1st, 2nd and 3rd Generation DDS. Table reprinted with permission from Yun *et al.*, (2015). 17

CHAPTER 3

Table 1: The average size, polydispersity index (PDI) and zeta potential (ZP) of the negatively (Neg-NPs) and positively charged NPs (Pos NPs). 76

Table 2 The average size, polydispersity index (PDI) and zeta potential (ZP) of the free Pheroid® and NP-Pheroid® system. The pre-mix and post-mix combination methods were used to prepare NP- Pheroid® combined system using 1% (w/v) neg-NPs (without CT and PEG). 77

Table 3: The average size, polydispersity index (PDI) and zeta potential (ZP) of the free Pheroid® and NP-Pheroid® system. The pre-mix and post-mix combination methods were used to prepare NP- Pheroid® combined system using 1% (w/v) pos-NPs (with CT and PEG). 77

CHAPTER 4

Table 1: The sample concentrations or dilutions for each formulation of NP, Pheroid® and NP-Pheroid® used for the MTT assay. The samples used for the xCELLigence® assay are indicated by an asterisk (*). 102

CHAPTER 5

Table 1: Test group assignment of the mice (INH was given at 5 mg/kg and RIF at 10 mg/kg) ... 139

Table 2: The particle size, polydispersity index (PDI) and zeta potential of the Pheroid® vesicles prepared from the pro- Pheroid® and their combination to INH/RIF-loaded NP). (n=2). 1444

Table 3: The amount of formulation calculated to be administered to mice. The weight of NP was calculated from the %DL..... 147

Table 4: The linear equations and coefficient of determination (R^2) values for each drug. (n=3). 147

Table 5: Summary of PK parameters previously obtained comparing free INH or Free RIF to the Pheroid® formulation. Data extracted from Nieuwoudt, (2009). 149

Table 6: The average mouse plasma PK parameters (T_{max}, C_{max}, AUC and $t_{1/2}$) for free INH, INH NP and INH NP-Pheroid®, presented as mean ± SD. INH was given at 5 mg/kg dose (n=8). (Phe = Pheroid®)..... 151

Table 7: The average mouse plasma PK parameters (T_{max}, C_{max}, AUC and $t_{1/2}$) for free RIF, RIF NP and RIF NP-Pheroid® (Phe), presented as mean ± SD. RIF was given at 10 mg/kg dose (n=8)……..152

Table 8: The average mouse liver PK parameters (T_{max}, C_{max}, AUC and $t_{1/2}$) for free RIF, RIF NP and RIF NP-Pheroid®, presented as mean ± SD. RIF was given at 10 mg/kg dose (n=8). (Phe = Pheroid®)……158

Table 9: The average mouse lung PK Parameters (T_{max}, C_{max}, AUC and $t_{1/2}$) for free RIF, RIF NP and RIF NP-Pheroid®, presented as Mean ± SD. RIF was given at 10 mg/kg dose (n=8). (Phe = Pheroid®). 161

Table 10: The average mouse kidney PK Parameters (T_{max}, C_{max}, AUC and $t_{1/2}$) for free RIF, RIF NP and RIF NP-Pheroid®, presented as Mean ± SD. RIF was given at 10 mg/kg dose (n=8). (Phe = Pheroid®)……162

Table 11: The average mouse intestine PK Parameters (T_{max}, C_{max}, AUC and $t_{1/2}$) for free RIF, RIF NP and RIF NP-Pheroid®, presented as Mean ± SD. RIF was given at 10 mg/kg dose (n=8). (Phe = Pheroid®). 165

Abbreviations

Δ – change

6-ANA – 6-aminonicotinic acid

ACN – acetonitrile

ADME – absorption, distribution, metabolism and excretion

AIDS – acquired immune deficiency syndrome

ANOVA – analysis of variance

ATCC – American Type Culture Collection

AUC – area under the curve

BCS – Biopharmaceutics Classification System

BHA – butylated hydroxyanisole

BHT – butylated hydroxytoluene

C6 – coumarin 6

CDC – Centre for Disease Control

CI – cell index

CLSM – confocal laser scanning microscopy

C_{max} – maximum concentration

Conc - concentration

cryo-TEM – cryogenic transmission electron microscopy

CSIR – Council for Scientific and Industrial Research

CT – chitosan

d – day(s)

DDS – drug delivery system(s)

DL – drug loading

DLS – dynamic light scattering

DMEM – Dulbecco's modified eagles medium

DOTS – Directly Observed Treatment, Short-course

DST – Department of Science and Technology

EA – ethyl acetate

EE – encapsulation efficiency

EMA – European Medicine Agency

ESI – electrospray ionisation

ETB – ethambutol

FA – formic acid

FBS – foetal bovine serum

FDA – Food and Drug Administration

FDC – fixed dose combination

GI – gastrointestinal

HBSS – Hanks' Balanced Salt Solution

HCl – hydrochloric acid

HEPES – 4-(2-hydroxyethyl)-1-piperazineethanesulfonic acid

HIV – human immunodeficiency virus

HPLC – High-Performance Liquid Chromatography

h – hour(s)

INH – isoniazid

IS – internal standards

IV – intravenous

JMSC - Journal of Material Science

LC-MS/MS – liquid chromatography-tandem mass Spectrometry

LPHN – lipid-polymer hybrid nanoparticles

LY – lucifer yellow

MDR – multi-drug resistant

MIC – minimum inhibitory concentration

min – minute(s)

M.tb – *Mycobacterium tuberculosis*

MTT – 3-(4, 5-dimethylthiazolyl-2)-2, 5-diphenyltetrazolium bromide

N_2O – nitrous oxide

NaOH – sodium hydroxide

neg-NPs – negatively charged nanoparticles

NP – nanoparticle(s)

NRF – National Research Foundation

NWU – North-West University

OsO_4 – osmium tetroxide

P_{app} – apparent permeability

P-gp – P-glycoprotein

PBS - phosphate buffered saline

PC – phosphatidylcholine

PD – pharmacodynamics

PDI – polydispersity index

PEG – polyethylene glycol

PK – pharmacokinetics

PLGA – poly (DL-lactic-*co*-glycolic acid)

pos-NPs – positively charged nanoparticles

PRD – poverty-related disease

PVA – polyvinyl alcohol

PYZ – pyrazinamide

RES – reticuloendothelial system

RIB – rifabutin

RIF – rifampicin

RNA – ribonucleic acid

RTCA – real-time cell analysis

SADOH – South African Department of Health

SD – standard deviation

SEM – scanning electron microscopy

$t_{1/2}$ – half-life

TB – tuberculosis

TEER – transepithelial electrical resistance

TEM – transmission electron microscopy

T_g – transition temperature

T_{max} – time for the drug to reach the maximum concentration

UA – uranyl acetate

UV – ultra-violet

vs - versus

WHO – World Health Organization

w/o – water-in-oil

w/o/w – water-in-oil-in-water

XDR – extensively drug-resistant

ζ-potential or ZP – Zeta potential

CHAPTER 1

This chapter is an introduction to the thesis. The problem statement (or research question), the hypothesis, and the objectives of the study are discussed in this chapter.

CHAPTER 1: PROBLEM STATEMENT AND AIMS OF THE RESEARCH STUDY

Figure 1: A TB patient holding a daily dose of anti-TB drugs. Photo reprinted with permission from the Guardian News & Media Ltd, (2016).

1. Problem in the progress of drug delivery systems for tuberculosis therapy

Despite the significant progress made, many clinically approved drugs formulated within efficient drug delivery systems (DDS) have not been targeted for neglected infectious diseases such as tuberculosis (TB), but rather for cancer (Pham *et al*., 2015, Wang *et al*., 2013). DDS are aimed at improving the effectiveness of therapeutically active drugs and therefore assisting them to function to their full potential (Tiwari *et al.*, 2012). TB is still a major health threat that burdens a large number of poor communities in the developing world and is one of the major causes of death amongst a group of infectious diseases even though there are effective drugs approved for its treatment (Zumla *et al*., 2015, Sacks and Behrman, 2009, Jain, 2011). The current treatment for the primary TB infection requires a fixed dose combination (FDC)

of the following four potent drugs: rifampicin (RIF), isoniazid (INH), pyrazinamide (PYZ) and ethambutol (ETB), approved by the World Health Organization (WHO), to be taken daily for a period of up to six months (D'Ambrosio *et al.*, 2015). The first two months of treatment is called the initial or intensive phase where all four drugs are administered daily and the last four months is called the continuation phase in which only RIF and INH are taken daily (Pham *et al.*, 2015). The failure to control or reduce the number of TB cases is aggravated by the high dosage, long treatment duration, development of side effect and poor patient compliance, typically leading to the development of drug-resistant TB strains that presents yet more challenges in the treatment of TB (Sacks and Behrman, 2009). The burden of a high dose of drugs taken daily by a typical TB patient is shown in Figure 1 above. This failure to reduce the number of TB incidences has occurred regardless of the efforts to implement the "Directly Observed Treatment, Short-course" (DOTS) strategy (Harries *et al.*, 2008). There is, therefore, an urgent need for an effective and affordable anti-TB therapy with reduced dose for a shorter period to support the elimination of TB burden worldwide.

Previous attempts to improve the efficacy of anti-TB drugs that are formulated within a suitable DDS have included polymeric nanoparticles (NP) as well as lipid-based DDS (Sosnik *et al.*, 2010). When anti-TB drug-loaded NP, made of poly (DL-lactic-*co*-glycolic acid) (PLGA), were given to rodents (mice and guinea pigs) through oral administration, they were reported to have significantly improved the bioavailability, extended the release of drugs and reduced the drug dosage from daily to once every week when compared with the free drugs (Pandey and Khuller, 2006a). This NP formulation also resulted in an easy uptake of anti-TB drugs by alveolar macrophages that are susceptible to the *Mycobacterium tuberculosis (M.tb)* (Pandey and Khuller, 2006a). However, there is a lack of human trial studies conducted to evaluate the effect of polymeric NP on anti-TB drugs (Nasiruddin *et al.*, 2017, Laghari *et al.*, 2016). The use of lipid-based DDS in TB treatment has not been studied as extensively as the polymeric NP due to the possible low capacity for drug loading and low physical stability over time (Sosnik *et al.*, 2010). Lipid-based DDS such as liposomes have previously demonstrated overall increases in anti-TB activity with a significant decrease in toxicity of anti-TB drugs, however liposomes are readily degraded by intestinal lipase and can therefore not be administered orally but through the invasive intravenous (IV) method (Pinheiro *et al.*, 2011). Besides liposomes, one other recently explored lipid-based DDS includes the Pheroid® technology which has resulted in promising outcomes when formulated with anti-TB drugs (Grobler, 2009). Pheroid® is a stable lipid-based system that can be administered through

various routes including oral administration (Uys, 2006). This system was shown to enhance the bioavailability of anti-TB drugs by improving their intestinal absorption and increasing their half-life (Grobler, 2009, Nieuwoudt, 2009, Ludick, 2014). A comparative phase I clinical trial to evaluate the change of pharmacokinetic (PK) properties of anti-TB drugs when entrapped within Pheroid® DDS was conducted and provided evidence that the Pheroid® DDS extends the therapeutic window of the anti-TB drug and has potential to contribute to lowering the dosage and therefore improving the TB therapy (Grobler, 2009, Nieuwoudt, 2009). The disadvantage with this Pheroid® system is the lack of extended drug release and therefore more needs to be done to further its applications in TB therapy.

Despite the effectiveness of polymeric NP and lipid-based DDS for anti-TB drugs, sufficient data from clinical trials is still required in order to pave a way to bring them into the market. It was predicted that the use of nanomedicine to deliver effective conventional therapeutic agents would facilitate a faster transition of effective DDS formulated therapy to the clinic for a better control of poverty-related infectious diseases (Bell *et al*., 2013). However, the advancement of these DDS for TB is limited by pitfalls such as bio-accumulation, cumulative toxicity and side effects associated with these nanomedicines (Bell *et al*., 2013, Moghimi *et al*., 2005)). The lack of extensive research studies on safety and the long-term stability hinders the progress of new medicine formulations to human trials (Basavaraj and Betageri, 2014, Muller and Keck, 2004). Other major hurdles in advancing these delivery technologies, especially for the improvement of TB therapy to the clinical stage, include the high cost of the drug delivery materials, the inability to conduct large-scale production and the removal of residual organic solvents (Pandey and Ahmad, 2011). The high cost incurred in developing effective drug-loaded DDS for poverty-related infectious diseases leads to a reluctance by the pharmaceutical industries in advancing them to the market. Although new potential DDS continue to be proposed for the improvement of PK for the current anti-TB drugs, according to our knowledge novel strategies such as the combination of two effective DDS have not yet been explored.

2. The combination of DDS as a solution

The combination of unique DDS such as polymeric NP and lipid-based DDS has led to the design of hybrid DDS that can be referred to as lipid-polymer hybrid nanoparticles (LPHN) (Wu, 2016, Cheow and Hadinoto, 2011, Mandal *et al*., 2013) Hybrid DDS may enable one to

make the most out of the unique attributes that each delivery system provides. Lipid-based systems (liposomes) and biodegradable polymeric (PLGA) NP are two prevalent types of drug carriers that are frequently used to create hybrid delivery systems (Mufamadi *et al.*, 2011). These two DDS have unique properties, but sometimes they do not possess all the required characteristics for an overall improvement of a certain therapy, individually. PLGA NP are mechanically stable and slowly degrade in living systems to ensure the controlled release of the encapsulated substances, however depending on their molecular weight, they can retain the active ingredient for longer than necessary and can stimulate an immune response (Makadia and Siegel, 2011, Danhier *et al*., 2012, Soppimath *et al*., 2001). On the other hand, lipid-based DDS are more biocompatible due to their cell membrane-resembling properties, but they lack physical stability and control release capabilities (Torchilin, 2005, Pinheiro *et al.*, 2011). Therefore, when polymeric NP and lipid-based systems are combined to form lipid-polymer hybrid DDS, they present a more robust and promising delivery platform compared to the individual systems (Zhang *et al.*, 2008, Raemdonck *et al.*, 2013).

The structural components of the hybrid DDS or LPHNs feature three distinct functional units: (1) an inner biodegradable polymer that is enclosed by (2) a phospholipids bilayer shell and (3) polyethylene glycol (PEG) conjugated to the lipid bilayer (Figure 2). Drugs can either be encapsulated within the polymeric core or in the lipid bilayer membrane, depending on their polarity. This hybrid architecture can provide physicochemical advantages compared to non-hybrid systems. For example, entrapment of multiple drugs, high drug loading, tunable surface functionality and adjustable drug release profiles are possible with the hybrid systems (Mandal *et al.*, 2013). Previous studies have shown that a combination of drug-loaded and surface modified liposomes with polymeric scaffolds resulted in improved stability, enhanced compatibility as well as controlled release of drug over extended periods (Mufamadi *et al.*, 2011, Zhang *et al.*, 2008). It has also been shown that the hybrid DDS are easy to synthesise and may be altered for a production scale-up (Zhang *et al.*, 2008). Moreover, hybrid DDS exhibit good cellular targeting ability, have favourable stability in serum and superior *in vitro* cellular delivery efficacy compared to individual systems (Hadinoto *et al.*, 2013). Even though all these attributes make these hybrid systems a promising drug delivery strategy, adequate *in vivo* evaluation to confirm their promising *in vitro* results have not yet been widely explored (Hadinoto *et al.*, 2013). Furthermore, the scope of application for these hybrid systems has been limited mostly to enhancing anti-cancer drug properties (Ramasamy *et al.*, 2014) and less on improving therapy for infectious diseases such as TB. Hadinoto *et al.* (2013) reviewed other

applications of hybrid DDS besides the delivery for anticancer treatment, which included deliveries of gene therapeutics, vaccines, diagnostic imaging agents and their dynamic use in combinatorial and active targeted drug deliveries. Therefore there is an opportunity to evaluate the potential of such hybrid systems to deliver anti-TB drugs.

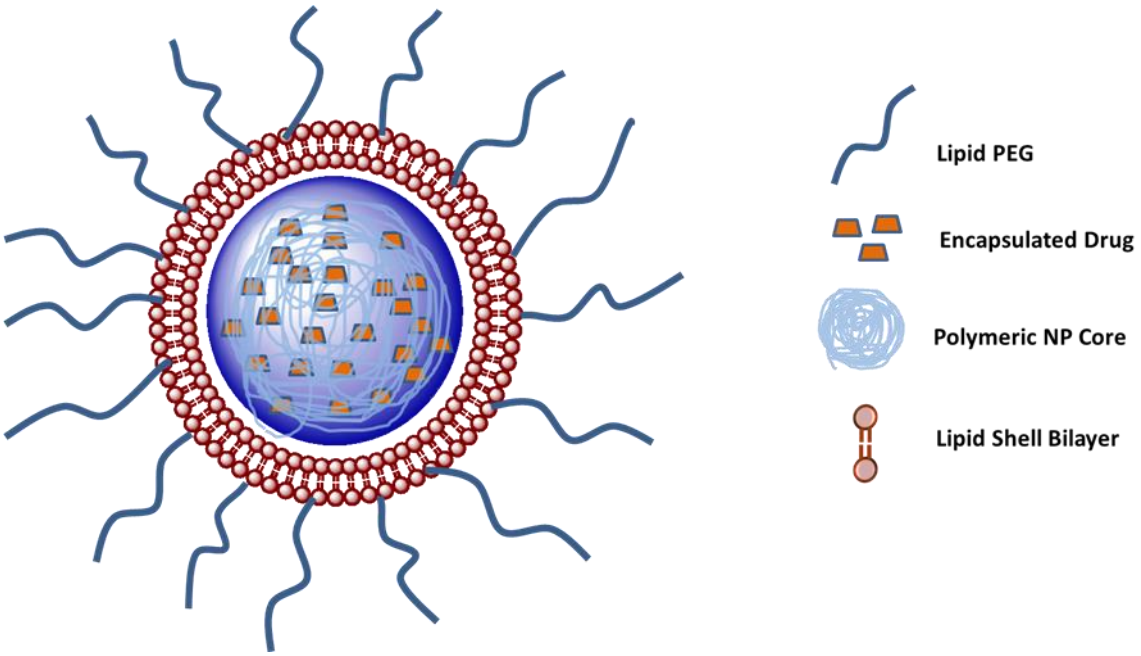

Figure 2: Structural components of a lipid-polymer hybrid DDS composed of PEG; lipid bilayer; polymeric NP and an encapsulated drug.

3. Research focus

The studies described in this thesis focused on the fabrication of a novel hybrid drug delivery system where biodegradable PLGA NP are entrapped within Pheroid® vesicles. The development and design of hybrid DDS have more often made use of liposomes as the lipid component, while PLGA is the polymeric component. Replacing the liposome with the Pheroid® system, which is more stable and can be administered orally, would lead to a novel hybrid DDS which could widen the scope of their applications for TB therapy. The features of this novel lipid-polymer hybrid DDS comprising PLGA NP and Pheroid® has the potential to enhance the PK properties of anti-TB drugs due to the unique advantages that these two systems have previously demonstrated as individual systems. The successful design of this novel

hybrid DDS could pave a way towards advancing the anti-TB drug-loaded DDS into the required clinical trials.

This research aims to capitalise the advantages of PLGA NP and Pheroid® system to yield a novel, robust and efficient hybrid delivery system for the improvement of TB therapy. The main advantages of these two systems are the slow degradation of PLGA NP and the absorption enhancing capability of the Pheroid® system. The PLGA NP–Pheroid® hybrid system would exist as a liquid suspension that is meant to be taken orally, which is the preferable form of drug administration (Ensign *et al.*, 2012). Oral administration is not common for other colloidal systems as it is often difficult to maintain stability in a liquid state (Mandal *et al.*, 2013). For example, liposomes have only been administered intravenously whereas Pheroid® can be administered through various routes including oral and pulmonary (Ludick, 2014, Bruyn, 2006). PLGA NP existing in a solid form as an individual system have also been reported as orally stable (Pandey and Khuller, 2006b, Semete *et al*., 2010).

This research focused on the delivery of two of the anti-TB drugs, namely RIF and INH entrapped within the PLGA NP–Pheroid® hybrid system. It has been shown that INH and RIF are two of the most effective anti-TB drugs, as they contribute to the eradication of about 99% of the *M.tb* bacilli during the initiation phase of TB therapy (Du Toit, 2006). However, the antagonistic interaction between these two drugs is of major concern (Shishoo *et al.*, 2001), and this will be addressed in this study by encapsulating each drug separately into PLGA NP to avoid their incompatibility. Physicochemical characterisation and an *in vivo* evaluation study will be carried out to obtain information about the potential of this novel hybrid DDS. The materials used for both these two systems are biodegradable and approved by the US Food and Drug Administration (FDA), which adds an advantage in advancing any positive outcomes of this work.

The *in vivo* applications of the combined or hybrid DDS have not yet been thoroughly explored as the design of this drug delivery platform has mainly focussed on their structure, physicochemical characteristics and *in vitro* efficacy of entrapped drugs (Mandal *et al.*, 2013). The intricacies of these hybrid systems may yield new challenges when decoding the *in vitro* efficacies into tangible medicine. It is necessary to fill the gap by investigating the effect of the novel hybrid system on the *in vivo* PK parameters of the loaded drugs. The current state and the applications of lipid-polymer hybrid DDS have been analysed to recognise future research studies required to convey them closer to clinical use (Hadinoto *et al.*, 2013). Some

in vivo results illustrating the advantages of using these hybrid systems for drug delivery in comparison to the non-hybrid systems have been reported (Hadinoto *et al.*, 2013), however further *in vivo* studies are still required. Due to the urgent need to find new approaches for an improved treatment of TB, the *in vivo* studies may demonstrate the potential of the PLGA NP–Pheroid® hybrid DDS loaded with anti-TB drugs.

3.1. Research questions and hypothesis

This study will attempt to answer the following central research questions:

1. Can PLGA NP and Pheroid® be optimally combined to form a stable hybrid system?
2. Can the combined effect of the PLGA NP and Pheroid® delivery systems alter the PK of anti-TB drugs by enhancing their bioavailability and biodistribution *in vivo*?

The hypothesis is that PLGA NP will be entrapped within (or localised with) Pheroid® vesicles, resulting in a novel NP–Pheroid® hybrid DDS that would lead to enhanced absorption and improved PK properties of anti-TB drugs.

3.2. Research aim and objectives

The principal aim of this research project is to combine two delivery technologies, PLGA-NP and Pheroid® vesicles, to create a novel efficient system, which will be evaluated for improving TB treatment. This study will, therefore, contribute knowledge to the field of hybrid DDS.

The specific objectives are as follows:

A. Preparation and characterisation of the NP-Pheroid® hybrid system:
    1. Explore various methods of developing a novel hybrid system where PLGA NP are entrapped within the Pheroid® vesicles;
    2. Perform physicochemical characterisation to obtain size, zeta potential (ζ-potential) and morphology of the NP-Pheroid® hybrid system.
B. Perform the *in vitro* biological characterisation of the hybrid drug delivery system as follows:
    1. Cell viability of the hybrid formulation compared to the individual components;

2. Trans-cellular permeability studies;
3. Intracellular uptake studies.

C. Conduct PK characterisation of the hybrid DDS by studying:

1. The effect of the hybrid system on the plasma levels of INH and RIF in healthy mice;
2. The influence of the hybrid system on the drug distribution across various organs of the mice.

4. Thesis chapters breakdown

This thesis has a total of six chapters. The current chapter introduces the study rationale of the thesis and describes the research objectives. A literature review, split into two sections, is covered in Chapter 2. The first section (Part A)focuses on relevant topics of this research such as the history and design of DDS; introduction of polymeric NP as well as lipid-based delivery systems; the aspects of Pheroid® DDS and finally an extensive look at the emerging hybrid system platforms. The second section (Part B) includes the literature review of the biological applications of hybrid DDS as well as a thorough review of TB and interventions to improve its therapy. Chapter 3 concentrates on the development of the NP-Pheroid hybrid DDS and includes the physicochemical characterization of this system. This chapter is presented in the article format in which it was published. The *in vitro* cellular studies done to further characterise this system are discussed in Chapter 4. Chapter 5 focuses on evaluating the effect of this novel hybrid system on the PK properties of two anti-TB drugs, INH and RIF. Chapter 6 concludes the thesis with a summary of the overall results obtained, discusses the major contributions and general limitations of the study as well as possible future work to further this study. An annexure section is added at the end of this thesis. This section includes an overall flow of the experimental work done, targeted journal author guidelines for the submission of manuscripts as well the conference (posters and oral presentations) contributions made from this research.

5. References

BASAVARAJ, S. & BETAGERI, G. V. 2014. Can formulation and drug delivery reduce attrition during drug discovery and development—review of feasibility, benefits and challenges. *Acta Pharmaceutica Sinica B,* 4**,** 3-17.

BELL, I. R., SCHWARTZ, G. E., BOYER, N. N., KOITHAN, M. & BROOKS, A. J. 2013. Advances in integrative nanomedicine for improving infectious disease treatment in public health. *European Journal of Integrative Medicine,* 5**,** 125-140.

BRUYN, T. D. 2006. *Nasal Delivery of Insulin with Pheroid Technology.* Master of Science, North-West University. https://dspace.nwu.ac.za/handle/10394/730 (Date accessed: 22 July 2013).

CHEOW, W. S. & HADINOTO, K. 2011. Factors affecting drug encapsulation and stability of lipid-polymer hybrid nanoparticles. *Colloids and Surfaces B: Biointerfaces,* 85**,** 214-220.

D'AMBROSIO, L., CENTIS, R., SOTGIU, G., PONTALI, E., SPANEVELLO, A. & MIGLIORI, G. B. 2015. New anti-tuberculosis drugs and regimens: 2015 update. *European Respiratory Journal Open Research,* 1**,** 1-15.

DANHIER, F., ANSORENA, E., SILVA, J. M., COCO, R., LE BRETON, A. & PRÉAT, V. 2012. PLGA-based nanoparticles: An overview of biomedical applications. *Journal of Controlled Release,* 161**,** 505-522.

ENSIGN, L. M., CONE, R. & HANES, J. 2012. Oral drug delivery with polymeric nanoparticles: The gastrointestinal mucus barriers. *Advanced Drug Delivery Reviews,* 64**,** 557-570.

GROBLER, A. F. 2009. *Pharmaceutical applications of Pheroid™ technology.* Doctor of Philosophy in Pharmaceutics, North-West University. https://dspace.nwu.ac.za/handle/10394/6701 (Date accessed: 22 August 2013).

HADINOTO, K., SUNDARESAN, A. & CHEOW, W. S. 2013. Lipid–polymer hybrid nanoparticles as a new generation therapeutic delivery platform: A review. *European Journal of Pharmaceutics and Biopharmaceutics,* 85**,** 427-443.

HARRIES, A. D., JAHN, A., ZACHARIAH, R. & ENARSON, D. 2008. Adapting the DOTS framework for tuberculosis control to the management of non-communicable diseases in Sub-Saharan Africa. *PLoS Medicine,* 5**,** 0859-0862.

JAIN, R. 2011. Tuberculosis—challenges and opportunities. *Indian Journal of Tuberculosis* 58**,** 148-154.

LAGHARI, M., DARWIS, Y., MEMON, A. H., KHAN, A. A., ABDULBAQI, I. M. T. & ASSI, R. A. 2016. Nanoformulations and clinical trial candidates as probably effective and safe therapy for tuberculosis. *Tropical Journal of Pharmaceutical Research,* 15**,** 201-211.

LUDICK, C. E. 2014. *The development of an oral single dose emulgel formulation for Pheroid® technology*. Doctor of Philosophy in Pharmaceutics, North-West University. https://dspace.nwu.ac.za/handle/10394/12246 (Date accessed: 05 May 2016).

MAKADIA, H. K. & SIEGEL, S. J. 2011. Poly Lactic-co-Glycolic Acid (PLGA) as Biodegradable Controlled Drug Delivery Carrier. *Polymers,* 3**,** 1377-1397.

MANDAL, B., BHATTACHARJEE, H., MITTAL, N., SAH, H., BALABATHULA, P., THOMA, L. A. & WOOD, G. C. 2013. Core–shell-type lipid-polymer hybrid nanoparticles as a drug delivery platform. *Nanomedicine: Nanotechnology, Biology and Medicine,* 9**,** 474-491.

MOGHIMI, S. M., HUNTER, A. C. & MURRAY, J. C. 2005. Nanomedicine: current status and future prospects. *The FASEB Journal,* 19**,** 311-330.

MUFAMADI, M. S., PILLAY, V., CHOONARA, Y. E., DU TOIT, L. C., MODI, G., NAIDOO, D. & NDESENDO, V. M. K. 2011. A Review on Composite Liposomal Technologies for Specialized Drug Delivery. *Journal of Drug Delivery,* 2011, 19 Pages.

MULLER, R. H. & KECK, C. M. 2004. Challenges and solutions for the delivery of biotech drugs – A review of drug nanocrystal technology and lipid nanoparticles. *Journal of Biotechnology,* 113**,** 151-170.

NASIRUDDIN, M., NEYAZ, M. K. & DAS, S. 2017. Nanotechnology-based approach in tuberculosis treatment. *Tuberculosis Research and Treatment,* 2017, 12 Pages. NIEUWOUDT, L. 2009. *The impact of Pheroid technology on the bioavailability and efficacy of anti-tuberculosis drugs in an animal model.* Master of Science, North-West University. https://dspace.nwu.ac.za/handle/10394/4316 (Date accessed: 13 January 2014).

PANDEY, R. & AHMAD, Z. 2011. Nanomedicine and experimental tuberculosis: facts, flaws, and future. *Nanomedicine: Nanotechnology, Biology and Medicine,* 7**,** 259-272.

PANDEY, R. & KHULLER, G. 2006a. Nanotechnology based drug delivery system (s) for the management of tuberculosis. *Indian Journal of Experimental Biology,* 44**,** 357-366.

PANDEY, R. & KHULLER, G. K. 2006b. Oral nanoparticle-based antituberculosis drug delivery to the brain in an experimental model. *Journal of Antimicrobial Chemotherapy,* 57**,** 1146-1152.

PHAM, D.-D., FATTAL, E. & TSAPIS, N. 2015. Pulmonary drug delivery systems for tuberculosis treatment. *International Journal of Pharmaceutics,* 478**,** 517-529.

PINHEIRO, M., LÚCIO, M., LIMA, J. L. F. C. & REIS, S. 2011. Liposomes as drug delivery systems for the treatment of TB. *Nanomedicine,* 6**,** 1413-1428.

RAEMDONCK, K., BRAECKMANS, K., DEMEESTER, J. & DE SMEDT, S. C. 2013. Merging the best of both worlds: Hybrid lipid-enveloped matrix nanocomposites in drug delivery. *Chemical Society Reviews,* 43**,** 444-472.

RAMASAMY, T., TRAN, T. H., CHOI, J. Y., CHO, H. J., KIM, J. H., YONG, C. S., CHOI, H.-G. & KIM, J. O. 2014. Layer-by-layer coated lipid-polymer hybrid nanoparticles designed for use in anticancer drug delivery. *Carbohydrate Polymers,* 102**,** 653-661.

SACKS, L. V. & BEHRMAN, R. E. 2009. Challenges, successes and hopes in the development of novel TB therapeutics. *Future Medicinal Chemistry,* 1**,** 749-756.

SEMETE, B., BOOYSEN, L. I. J., KALOMBO, L., VENTER, J. D., KATATA, L., RAMALAPA, B., VERSCHOOR, J. A. & SWAI, H. 2010. In vivo uptake and acute immune response to orally administered chitosan and PEG coated PLGA nanoparticles. *Toxicology and Applied Pharmacology,* 249**,** 158-165.

SHISHOO, C. J., SHAH, S. A., RATHOD, I. S., SAVALE, S. S. & VORA, M. J. 2001. Impaired bioavailability of rifampicin in presence of isoniazid from fixed dose combination (FDC) formulation. *International Journal of Pharmaceutics,* 228**,** 53-67.

SOPPIMATH, K. S., AMINABHAVI, T. M., KULKARNI, A. R. & RUDZINSKI, W. E. 2001. Biodegradable polymeric nanoparticles as drug delivery devices. *Journal of Controlled Release,* 70**,** 1-20.

SOSNIK, A., CARCABOSO, Á. M., GLISONI, R. J., MORETTON, M. A. & CHIAPPETTA, D. A. 2010. New old challenges in tuberculosis: Potentially effective nanotechnologies in drug delivery. *Advanced Drug Delivery Reviews,* 62**,** 547-559.

TIWARI, G., TIWARI, R., SRIWASTAWA, B., BHATI, L., PANDEY, S., PANDEY, P. & BANNERJEE, S. K. 2012. Drug delivery systems: An updated review. *International Journal of Pharmaceutical Investigation,* 2**,** 2-11.

TORCHILIN, V. P. 2005. Recent advances with liposomes as pharmaceutical carriers. *Nature Reviews Drug Discovery,* 4**,** 145-160.

UYS, C. E. 2006. *Preparation and characterization of Pheroids.* Master of Science, North-west University. https://dspace.nwu.ac.za/handle/10394/1669 (Date accessed: 25 April 2013).

WANG, R., BILLONE, P. S. & MULLETT, W. M. 2013. Nanomedicine in action: An overview of cancer nanomedicine on the market and in clinical trials. *Journal of Nanomaterials,* 2013, 12 Pages.

WU, X. Y. 2016. Strategies for optimizing polymer-lipid hybrid nanoparticle-mediated drug delivery. *Expert Opinion on Drug Delivery,* 13**,** 609-612.

ZHANG, L., CHAN, J. M., GU, F. X., RHEE, J.-W., WANG, A. Z., RADOVIC-MORENO, A. F., ALEXIS, F., LANGER, R. & FAROKHZAD, O. C. 2008. Self-assembled lipid−polymer hybrid nanoparticles: A robust drug delivery platform. *ACS Nano,* 2**,** 1696-1702.

ZUMLA, A., GEORGE, A., SHARMA, V., HERBERT, R. H. N., OXLEY, A. & OLIVER, M. 2015. The WHO 2014 Global tuberculosis report—further to go. *The Lancet Global Health,* 3**,** e10-e12.

CHAPTER 2

This chapter contains the literature review which focuses on various topics covered in this thesis. The topics include drug delivery systems, lipid-polymer hybrid nanoparticles, and tuberculosis.

CHAPTER 2: A REVIEW ON THE ADVANCEMENT OF DRUG DELIVERY SYSTEMS FOR THERAPY IMPROVEMENT

PART A

1. Drug delivery systems

A drug delivery system (DDS) is a device or a formulation which assists the transport of a therapeutic compound (drug) in a living system and enhances its safety and effectiveness through the control of its absorption, release location and time of release (Tiwari *et al.*, 2012, Jain, 2008). Most potent pharmaceutical drugs and many newly discovered drug candidates exhibit toxicity, limited water solubility, poor absorption and therefore display low bioavailability and biodistribution (Tiwari *et al.*, 2012). These drugs can have a limited therapeutic effect due to the possible enzymatic degradation or hydrolysis that may occur before they reach the target tissue or they may result in side effects caused by the body's response to the drug (Vogelson, 2001). Drug delivery technologies are therefore transport vehicles that may help overcome the disadvantages associated with the administration of free drugs and may improve their absorption as well as prolong their therapeutic activity (Jain, 2008, Parveen *et al.*, 2012). Dr Flynn (1982) defined drug delivery concepts as "the use of whatever means possible, be it chemical, physiochemical, or mechanical, to regulate a drug's access rate to the body's central compartment, or in some cases, directly to the involved tissue" (Ranade *et al.*, 2003, Flynn, 1982).

The design of DDS takes into consideration the route, the target tissue and the type of the drug being transported. A perfect delivery system must feature the following, amongst others: access to unreachable locations, protection of drug from undesirable degradation in the body, delivery to pharmacological receptors and controlled release rate of the drug (Tiwari *et al.*, 2012). It is therefore, beneficial to have targeted drug delivery and controlled release of the drug for reduced side effects, enhanced therapeutic index and improved bioavailability of the drug. The development of DDS is a key area of extensive research with the potential to convey therapeutic and commercial value to future therapeutic products. The ultimate goal in the use of drug delivery formulations is modulation of the pharmacological profiles, this is the

pharmacokinetics (PK) and pharmacodynamics (PD), of the therapeutic agents to ensure clinical potential (Park, 2014, Liu *et al*., 2016). Therefore, to design an efficient delivery system, important principles such as drug stability, drug solubility, drug safety, biocompatibility, therapeutic efficacy and industrial scale-up need to be taken into consideration from basic research to clinical applications (Liu *et al*., 2016).

Understanding the physicochemical characteristics of drugs is critical in determining the type of delivery material. The Biopharmaceutics Classification System (BCS) categorises therapeutic compounds based on their water solubility and intestinal permeability into four different categories (Ku, 2008), which can benefit the decision-making for a suitable DDS. Active compounds (drugs) are divided into four BCS classes as follows: Class I are highly permeable and highly soluble leading to high absorption rate; Class II have high permeability and low solubility, which leads to limited bioavailability; Class III have low permeability and high solubility, which reduces their absorption rate; Class IV possess both low permeability and low solubility, which results in both limited bioavailability and reduced absorption rate (Ku, 2008). In addition to the permeability and solubility classifications, other drug properties that need to be considered for choosing an appropriate DDS include their molecular weight, half-life and their route of delivery.

2. Brief history – Advancement to nano-based DDS

The use of DDS originated from the introduction of the first sustained release formulation in the 1950s (Park, 2014). The historical perspective and the progression of DDS have been categorised as the first, second and third generation, summarised in Table 1. The first generation (1950-1980, macroscopic era) was based on the development of sustained release systems for oral and transdermal administration while the second generation (1980-2010) involved self-regulated and nanotechnology-based DDS (Yun *et al.*, 2015). The third generation DDS are currently under production with a focus on overcoming physicochemical and biological barriers from the first and second generation that limited their progression to clinical applications (Park, 2014, Yun *et al.*, 2015). During the macroscopic era, various controlled drug release systems and devices, with large particle sizes, were designed and approved for clinical use. Examples include topical patches for the skin, ingestible capsules for the gastrointestinal (GI) tract, intramuscular implants and mucosal inserts for the eye (Hoffman, 2008).

Table 1: The timeline for 1st, 2nd and 3rd Generation DDS. Table reprinted with permission from Yun *et al.*, (2015).

1950	1980	2010	2040
1st Generation	**2nd Generation**	**3rd Generation**	
Basics of controlled release	Smart delivery systems	Modulated delivery systems	
Successful control of physicochemical properties of delivery systems	Inability to overcome biological barriers	Need to overcome both physicochemical and biological barriers	

The development of a controlled delivery skin patch called "bandage for administering drugs" and osmotic pump capsule to release drugs at a sustained rate in the GI tract are examples of macroscopic devices with a rate-controlling membrane that resulted in zero-order release kinetics for a steady drug concentration in the blood (Hoffman, 2008). The evolution of this controlled drug delivery field to microscopic devices or systems occurred in the 1970s and 1980s. Figure 1 illustrates the controlled DDS from the early stages in the macroscopic size range which progressed to microparticles and to the current nano-sized range DDS (Crommelin and Florence, 2013). The microscopic era involved the use of controlled release, polymeric microparticles and phase-separated long-term depot drug delivery formulations. During the early 1980's the first clinically-approved microparticle was an injectable and degradable depot DDS comprising leutinising hormone-releasing hormone used as a treatment for prostate cancer (Kent *et al.*, 1987).

Nanotechnology, in the 1970s, became the main drive in the growth of DDS and led to the availability of various delivery platforms that exist in the nanoscale. Nanoparticles (NP) are colloidal dispersions in the size range of 1-1000 nm, (Mohanraj and Chen, 2006). This concept originated at the Swiss Federal Institute of Technology (ETH) in Zürich in a group led by Professor Speiser, who in the late 1960s developed the first NP for vaccination and drug delivery purposes (Kreuter, 2007). Advances in this technology led to the currently active nanoscopic era which uses nanocarriers as advanced DDS that have been evolving into clinically successful products from the 1980s (Hoffman, 2008). The application of nanocarriers for delivering either diagnostic or therapeutic agent is referred to as nanomedicine (Kim *et al.*, 2010, Moghimi *et al.*, 2005). Nano-size range particles possess distinct chemical and physical properties that offer a number of unique advantages over micrometre-sized

particles, particularly in drug delivery (Chen *et al*., 2016). It has been demonstrated that NP (100 nm) have a greater intracellular uptake compared to microparticles (10 µm) in Caco-2 cell line studies (Desai *et al*., 1997, Gamboa and Leong, 2013). This attribute of cellular uptake is essential for the treatment of intracellular pathogens, which are responsible for most infectious diseases. The encapsulation of the drug within NP can therefore, ensure a more efficient intracellular delivery. Nano-sized particles also have very high surface area per unit volume, and this has had a significant influence in the field of drug delivery, where most drugs with generally poor bioavailability attained significantly improved bioavailability when encapsulated in NP (Jia, 2005, Chen *et al*., 2016).

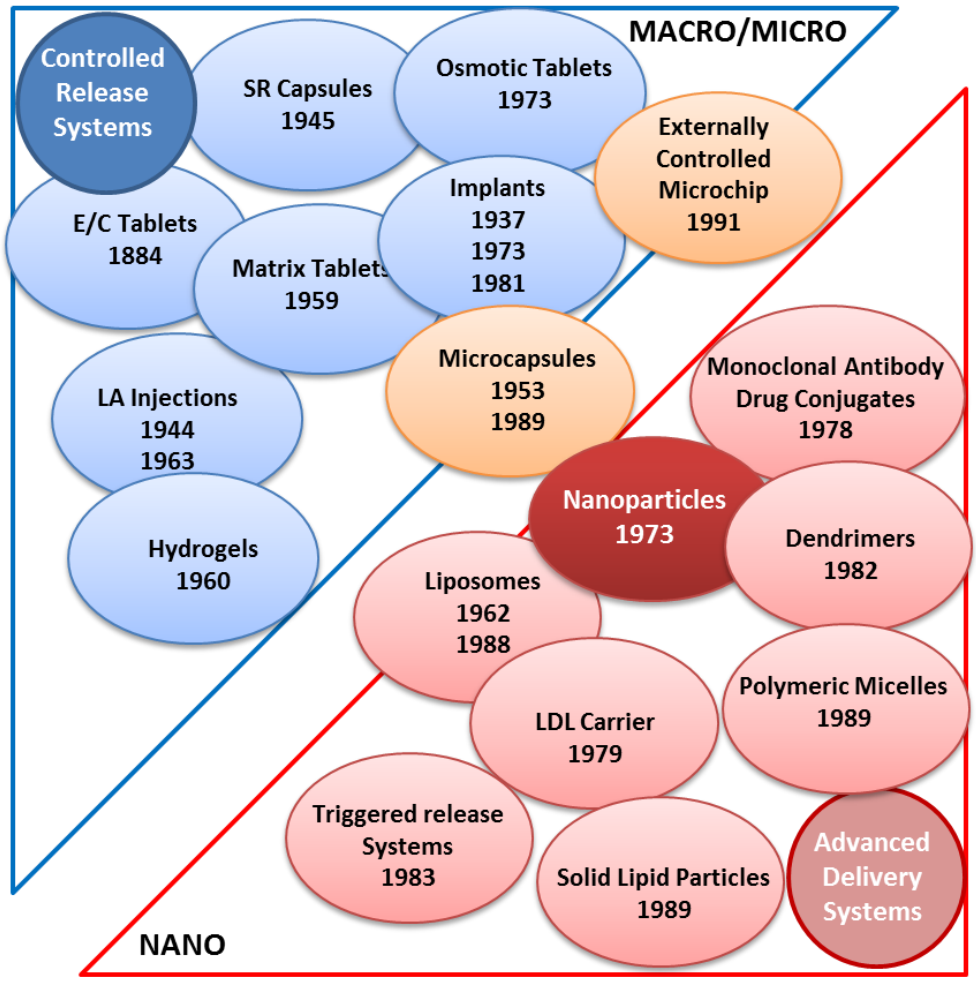

Figure 1: A schematic diagram showing the progress of DDS from macro and micro systems to the nano systems. The dates given represent early discovery and significant events after discovery. This diagram was reprinted with permission from Crommelin and Florence, (2013).

The field of nanomedicine encompasses the use of nanocarriers such as liposomes, carbon nanotubes, polymeric NP and much more, as depicted in Figure 2, to deliver drugs in the body (Janin, 2007). The widespread use of nanocarriers is primarily attributed to their potential to enable targeted drug delivery to the specific site of action of the drug for improved efficacy (Albanese *et al.*, 2012). Nano-based DDS have brought transformation to the field of pharmacotherapy through their capability to modify the PK properties of conventional drugs, which includes the extension of the drug circulation time, increase in the half-life of the drugs and reduced toxicity (Farokhzad and Langer, 2009, Bennet and Kim, 2014). Figure 3 summarises the factors to be taken into account in the fabrication of an efficient nano-based DDS (Bennet and Kim, 2014), however these can be applied to a wide variety of DDS.

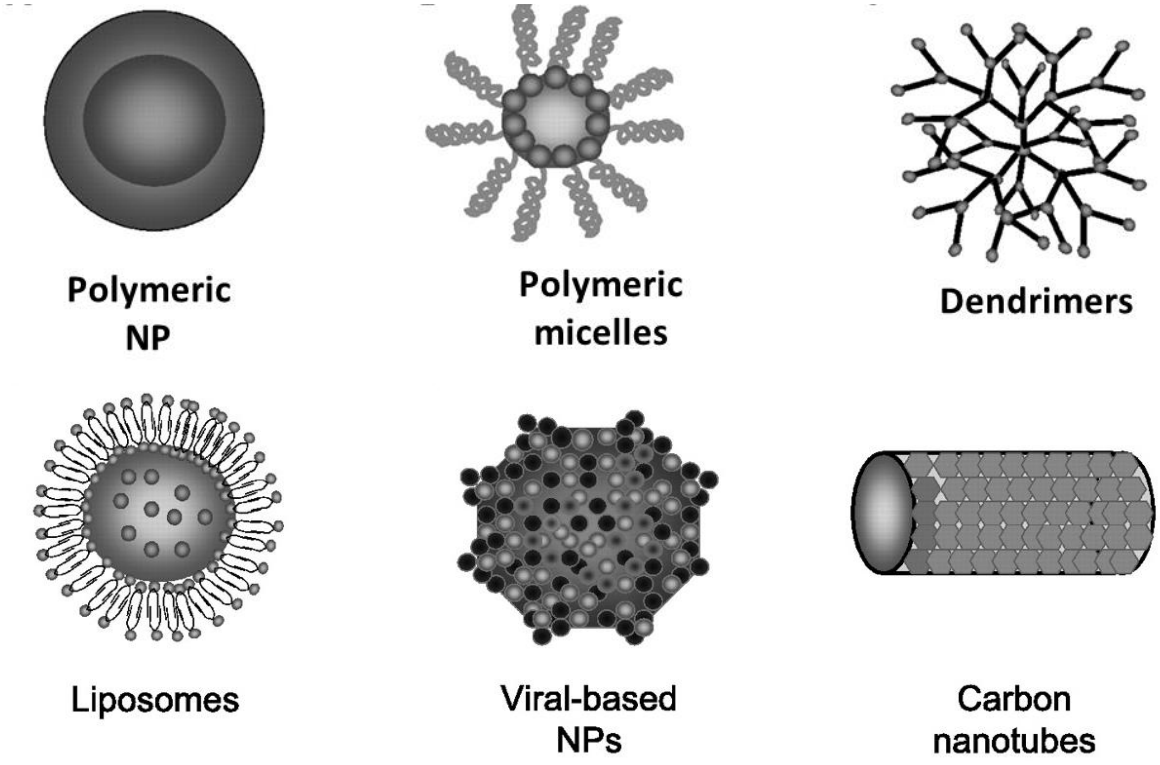

Figure 2: Examples of nano-based drug delivery systems. This image was reprinted with permission from Cho *et al*., (2008).

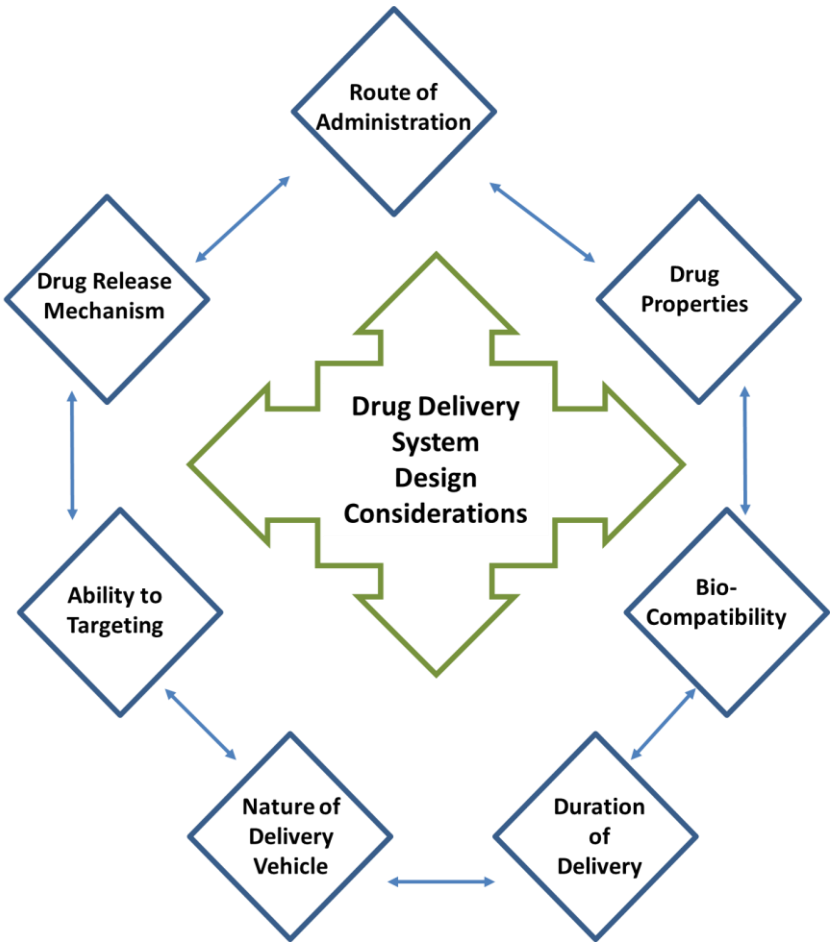

Figure 3: Diagram showing a broad overview of the essential factors to consider in the design DDS from basic research to clinical applications. The diagram was reprinted with permission from Bennet and Kim, (2014).

3. Oral drug delivery route

The choice of the route to administer therapeutics is governed by the following factors: the desired effect, the disease type and the type of drug. The administration route has an influence on the bioavailability of the drug in the bloodstream and determines whether the drug will reach the target tissue at a sufficient concentration. The most common routes of drug administration are oral, parenteral, nasal (inhalation) and transdermal (topical), where the oral route is the most accepted and preferred (Ensign *et al.*, 2012). The parenteral route involves the direct injection of drugs intravenously, intramuscularly and subcutaneously. It is an uncomfortable and painful route that requires sterilised equipment and can results in toxicity because of rapid release of the drug in the bloodstream. In contrast, the absorption of a drug can be insufficient or too slow following oral, transdermal and nasal administration routes. Nevertheless, oral

delivery is an attractive route due to its ease of administration and its widespread patient compliance and acceptability especially when multiple daily doses are required for treatment (Gamboa and Leong, 2013). Oral delivery has maintained commercial success in the past for the administration of many conventional drugs in various dosage forms.

Despite the numerous advantages of oral administration, the fabrication of oral DDS is a challenge considering all the barriers in the GI tract (Gamboa and Leong, 2013). These barriers include the acidic environment, the presence of degradative enzymes and mucus layer across a larger part of the GI tract as well as the tight junctions of the small intestine epithelial cells (Gamboa and Leong, 2013). It is therefore, worthwhile to understand the essential elements of the GI physiology as they influence factors concerning drug absorption and should be considered in the design of oral DDS.

Oral DDS should therefore preferably exhibit the following properties: the protection of the drug from degradative enzymes, improved mucoadhesion and prolonged retention in the GI tract (Ensign *et al.*, 2012). For instance, some lipid-based DDS are delivered through parenteral routes because they are vulnerable to breakdown by lipases in the GI tract. On the other hand, polymeric NP can evade degradative enzymes, which makes them suitable for oral drug delivery (Gamboa and Leong, 2013). It has been shown that drug-loaded NP coated with chitosan, which is a positively charged mucoadhesive polymer, improved the oral delivery of some poorly absorbed drugs due to the increased interaction with the negatively charged mucus layer of the intestine (Chen *et al.*, 2013).

4. Polymeric drug delivery systems

A polymer is a chemical compound made up of a recurrence of similar molecules known as monomers bonded together through a process called polymerisation. Over the past 30 years, there has been an escalation in the number of publications and patents focused on the use of polymers in DDS for controlled drug-release systems (Kaur and Kaur, 2014). Polymers used in DDS are grouped into the following three classes based on their source of formation: natural polymers, which include chitosan, gelatin, alginate, collagen, starch, dextrin, chitin and albumin; synthetic polymers which comprises examples such as poly (DL-lactic-*co*-glycolic acid) , poly (capro-lactone), poly (alkylcyano-acrylates) and poly (methyl-methacrylate) and semi-synthetic polymers, where modifications are made to natural polymers to result in altered

physicochemical properties of these polymers (Kaur and Kaur, 2014, Ranade *et al.*, 2003, Hans and Lowman, 2002). Natural polymers differ in their purity and may require cross-linking reactions that often alter the inherent qualities of the entrapped drug and this limits their use in DDS. Synthetic polymers have consequently attracted enormous attention for use in the fabrication of various DDS (Kumari *et al*., 2010, Kaur and Kaur, 2014).

Polymeric NP are solid colloidal particles or particulate dispersions ranging in size from 10 to 1000 nm and are used in nanomedicine to deliver drugs. Drugs may be entrapped, encapsulated, dissolved in or adsorbed on the surface of these NP. Advantages of polymeric NP include their high stability, capacity to encapsulate both hydrophilic and hydrophobic substances, slow release of the drug as a function of the polymer degradation rate, as well as their versatility in terms of polymer type and type of drug to be encapsulated (Bennet and Kim, 2014). From the drug delivery perspective, controlled-release polymers can be categorised into four groups: (1) diffusion-controlled; (2) solvent-activated; (3) externally-triggered and (4) chemically-controlled systems (Vilar *et al*., 2012, Liechty *et al*., 2010).

Diffusion-controlled systems consist of a drug core and non-biodegradable polymeric material surrounding the core, which allows slow diffusion of the drug (Laurent *et al*., 2011). The general difficulty with diffusion-controlled systems is that they require surgical removal as the polymer remains intact in the body after the drug has completely diffused. Solvent-activated systems exist in two types, namely the osmotically-controlled and the swelling-controlled (Srivastava *et al*., 2016). The drug is transported across a semi-permeable polymeric membrane from a high concentration to a low concentration of the external fluid in the osmotically-controlled systems, while the swelling-controlled systems consist of hydrogels (dehydrated crosslinked hydrophilic polymers), which when exposed to an aqueous environment, absorb water and swell (Gao *et al*., 2016, Peppas *et al*., 2000). Externally-triggered polymeric systems, also referred to as "smart polymers", are known for undergoing behavioural modification triggered by an external stimulus. These external stimuli can either be of physical nature, comprising light, ultrasound, electrical/magnetic fields, and temperature or of chemical nature, including molecular interactions between polymer and solvent or between polymer chains (Liechty *et al*., 2010, Gil and Hudson, 2004). Despite their proven efficiencies, more research is required to ensure reproducibility and clinical translation of these stimulus-sensitive DDS (Liu *et al*., 2016)

4.1. Chemically-controlled systems

Chemically-Controlled Systems are polymeric DDS known for their general capacity to constantly release the drug through the degradation of the polymer matrix. These include polymer-drug conjugate systems, where the drug is chemically linked to the backbone of the polymer via a linker group that can be cleaved enzymatically to release the drug at a controlled rate (Kopeček, 2013). Their lack of biodegradability is a drawback that limits the extent of their application (Bennet and Kim, 2014).

4.2. Biodegradable polymeric systems

Biodegradable polymeric systems are an essential class in drug delivery and have become a solution to one of the main drawbacks in other polymeric DDS (Li *et al*., 2016). This drawback is the toxicological reactions that occur in the body as a result of foreign, non-degradable polymer material left for an indefinite period after the drug has depleted. Biodegradable polymers contain monomers that are linked with hydrolytically and enzymatically labile bonds that break down to yield biocompatible non-toxic by-products that can be excreted via normal physiological pathways (Kumari *et al*., 2010). A biodegradable polymeric DDS must be designed to have permeability, biocompatibility and tensile strength (Nair and Laurencin, 2006). Commercially available polymers seldom have all these desired requirements, and therefore the custom synthesis of these polymers to meet these specifications is recommended (Vilar *et al*., 2012).

4.2.1. Poly (DL-lactic-*co*-glycolic acid) nanoparticles

Poly (DL-lactic-*co*-glycolic acid) (PLGA) is one of the most widely used synthetic biodegradable polymers in DDS (Makadia and Siegel, 2011). This polymer has been approved by the US Food and Drug Administration (FDA) for clinical use in the market. The biodegradation kinetics and tunable mechanical properties of the PLGA have made it attract considerable attention over the past two decades (Makadia and Siegel, 2011, Gentile *et al*., 2014). PLGA is composed of two biodegradable units of lactic acid and glycolic acid linked through an ester bond, see Figure 4. The lactic acid has an asymmetric α-carbon, which results in *D*- and *L*- enantiomeric lactic acid forms that can exist in equal ratio (50:50) in PLGA.

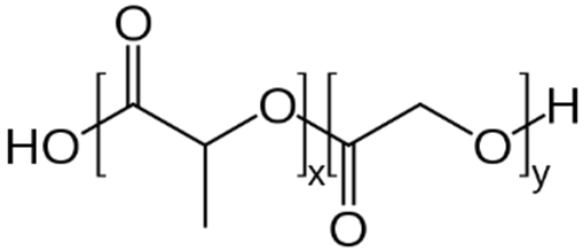

Figure 4: The chemical structure of PLGA (x – number of lactic acid monomers and y – number of glycolic acid monomers).

PLGA biodegrades through the hydrolysis process, where the ester bonds first break into oligomers and then into its monomers. The biodegradation rate of the PLGA depends on the following factors: molecular weight, the degree of crystallinity, the molar ratio of the lactic and glycolic acids in the polymer chain and the transition temperature (T_g) of the polymer (Danhier *et al.*, 2012, Keles *et al.*, 2015). The biodegradation of PLGA has been indicated to be purely through hydrolysis (Keles *et al.*, 2015) and does not involve any enzymatic activity (Correia *et al*., 2015). However, other studies have demonstrated the function of enzymes in PLGA breakdown depending on the distinct degradation rates *in vitro* and *in vivo* (Amann *et al.*, 2010). The lactic acid by-product enters an enzyme catalysed reaction referred to as Krebs cycle or tricarboxylic acid cycle *in vivo*; it is then metabolised and is eventually excreted as carbon dioxide gas from the body. The glycolic acid is eliminated from the body either unchanged through the kidney or it enters the Krebs cycle, where it is subsequently converted to carbon dioxide and water (Makadia and Siegel, 2011). PLGA is therefore, an ideal carrier material and its nano-sized NP provide an added advantage to its application. These NP have demonstrated the following properties: structural integrity, stability during storage and in biological fluids, versatile drug loading and controlled drug release (Danhier *et al*., 2012).

Copolymers of PLGA

Polyethylene glycol (PEG) is a hydrophilic polymer that is usually conjugated to PLGA to enhance the immune-compatibility of the NP (Gamucci *et al*., 2014). PEG can reduce non-

specific interactions of the hydrophobic PLGA NP with immune system proteins (opsonins) that bind to foreign substances to render them vulnerable to phagocytosis or reticuloendothelial system (RES) removal referred to as RES clearance (Jokerst et al., 2011, Mohanraj and Chen, 2006). Consequently, PEGylated PLGA NP evade RES clearance leading to prolonged *in vivo* circulation resulting in their high bioavailability (Kolate *et al.*, 2014).

Chitosan is a natural polysaccharide polymer that can be linked to PLGA for optimal drug delivery purposes. This copolymer offers properties such as permeation enhancement, efflux pump inhibition and mucoadhesion (Chen *et al.*, 2013). The capability of chitosan-coated PLGA for improved drug delivery has been demonstrated in various research studies (Bernkop-Schnürch and Dünnhaupt, 2012, Takeuchi *et al*., 2005, Chakravarthi and Robinson, 2011).

5. Lipid-based drug delivery systems

Lipids are a group of molecules comprised of fats and esters with analogous properties and are the chief structural components of cellular membranes consisting of both hydrophobic hydrocarbon chains and hydrophilic polar heads (Fahy *et al*., 2005). Lipid-based DDS are therefore recognised as biocompatible because they are compatible with the living system and evade immunological toxic reactions (Shrestha *et al*., 2014). The safety and efficacy of these lipid-based carriers have been established, which makes them attractive candidates for encapsulating therapeutics, diagnostics, and nutraceuticals (Attama *et al*., 2012). Lipid-based DDS are broadly classified as lipid vesicular, which include phytosomes, transfersomes, ethosomes, archaeosomes, vesosomes, niosomes and liposomes and lipid particulate systems such as solid lipid nanoparticles (SLN) (Saroj *et al.*, 2012).

5.1. Liposomes

Liposomes are the first type of lipid-based material that was applied in drug delivery (Allen and Cullis, 2013, Sercombe *et al*., 2015). They are composed of a bilayer of amphiphilic phospholipids that self-assemble spherically, where the hydrophilic polar heads are towards the aqueous phase, while the hydrophobic hydrocarbon chains stick to each other to form a closed bilayer lipid membrane separating aqueous compartments as shown in Figure 5. Drugs can either be intercalated into the bilayer or encapsulated into the aqueous space within the liposome vesicle (Jain *et al*., 2014). The location of the drug is determined by the

physicochemical properties of the drug and the composition of the lipid used. Liposomes are composed of phospholipids such as phosphatidylcholine (PC) in conjunction with cholesterol (Melzak *et al*., 2012). The function of cholesterol in the liposomes is to maintain the interior skeleton of the liposomes mechanically and to stabilise the phospholipids in the bilayer to help minimise the leakage of the encapsulated drugs (Briuglia *et al*., 2015).

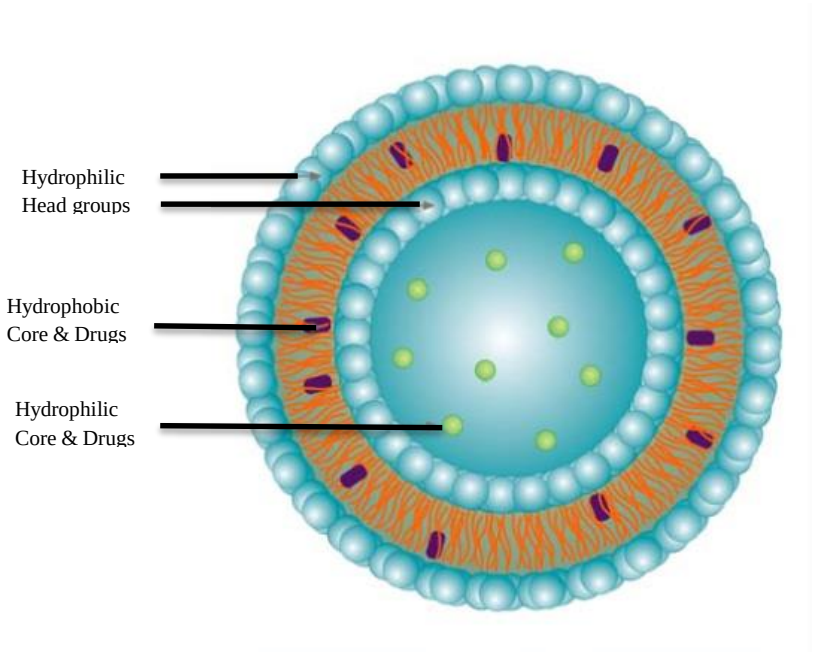

Figure 5: Structure of liposome. The figure was reprinted with permission from Cukierman and Khan, (2010).

Liposomes have been administered through various routes; however, the intravenous (IV) route is commonly used due to their instability when taken orally, caused by their susceptibility to being broken down by lipases in the GI tract (Pinheiro *et al.*, 2011). IV administration has always been the route that resulted in improved PK and efficacious results of liposomes (Allen *et al.*, 1993, Wilson *et al.*, 2007). The half-life ranges from minutes (min) to numerous hours (h) in the vascular system and is determined by their size and lipid constituents. Post administration, small liposomes (100 to 1000 nm) are taken up by the RES in the spleen and liver tissues, while larger ones accumulate within lungs. The RES uptake of liposomes has been advantageously used for transporting drugs to macrophages and tumours in the liver (Immordino *et al*., 2006); however, this can be a drawback when targeting other organs. To avoid liposome capture, their surfaces can be coated with PEG to form "stealth liposomes", known to improve the residence and the bioavailability of these liposomes in the vesicular system (Sercombe *et al*., 2015). Stealth liposomes could also have targeting ligands, such as antibodies, attached to the surface of the membrane for site-specific delivery of encapsulated

drugs (Immordino *et al*., 2006, Torchilin, 2005). Liposomal formulations have been shown to improve the PK and PD of various drugs and have been well-established as drug carriers for cancer therapy. The very first nanomedicine therapies to be approved by the FDA in 1995 were two liposomal products namely Doxil® and Myocet® for cancer treatment (Barenholz, 2012, Park, 2002). These two liposomal products both contain a anti-breast cancer drug, doxorubicin, and exhibited enhanced PK and PD properties when compared with free doxorubicin. However, the lipid bilayer surface of Doxil® is coated with PEG while Myocet® is not PEGylated. Lipo-Dox® is a subsequent PEGylated liposomal product that also contains doxorubicin (Chang and Yeh, 2012). In phase I clinical study, Lipo-Dox® displayed the longest residence time with a half-life of 65 h, but its activity against hepatocellular cancer was not enhanced in comparison to the free doxorubicin. The lipid composition of Doxil® and Myocet® is PC while Lipo-Dox® is made up of distearoyl phosphatidylcholine (DSPC). It has been said that phospholipids such as DSPC, comprising saturated fatty acids (stearic acid in this case), lead to liposomes with a higher stability than those containing kinky unsaturated fatty acid chains such as egg PC and hydrogenated soy PC (Li *et al*., 2015, Chang and Yeh, 2012). Despite the widespread applications and research on liposomes as a DDS, their use is limited due to their poor stability *in vivo* (Casals *et al.*, 2003). Since liposomes are not stable for oral administration, a waterless liposomal formulation called pro-liposomes, has been explored for oral delivery of drugs; however, the mechanism of this delivery method is still under investigation *in vitro* as well as in the pre-clinical trial stages (Shaji and Bhatia, 2013, Vijaykumar *et al.*, 2015).

5.2. Pheroid® delivery system

The Pheroid® DDS is a unique and a versatile lipid-based drug delivery technology that is based on colloidal emulsion. Patents for various applications of this technology have been registered globally due to its capability to improve the absorption and efficacy of a wide range of therapeutics (Grobler, 2009). The Pheroid® system has properties that contribute to its advantages over some of the other lipid-based DDS for example, the presence of essential fatty acids, rather than synthetic lipids (Uys, 2006). The essential fatty acids of Pheroid® particles (oil phase) such as ethyl esters of linolenic acid are emulsified in water (aqueous phase) that is saturated with nitrous oxide (gas phase) (Bruyn, 2006). Essential fatty acids are not produced by the body but have to be ingested to perform vital functions in cells, which include the regulation of energy homeostasis as well as programmed cell death, maintenance of membrane

integrity of cells and modulation of the immune system. However, it has been found that Western diets often lack in essential fatty acids that are components of the Pheroid® DDS, making this technology safe and highly biocompatible (Grobler, 2009). Potential application of the Pheroid technology in infectious diseases (such as tuberculosis, HIV, and malaria), chronic diseases (such as diabetes inflammation and pain), vaccines, cosmetics, and agriculture have been demonstrated (Grobler, 2009, Bruyn, 2006, Botha, 2007, Nieuwoudt, 2009, Grobler, 2014, Ludick, 2014).

Many challenges in the entrapment of drugs, manufacturing procedures and stability associated with liposomal DDS are not applicable to this technology. Unlike liposomes, Pheroid® can be used to deliver drugs through a number of administration routes, such as transdermal, nasal and oral without the need for further complicated stabilisation procedures. The interior bilayer structure of the Pheroid® system is stable without the addition of any stabilising lipids such as cholesterol used in liposomal systems (Uys, 2006, Chung *et al.*, 2006). While Pheroid® systems have a relatively high degree of elasticity and fluidity, liposomes tend to lose fluidity and elasticity due to the presence of cholesterol (Uys, 2006, Immordino *et al*., 2006). The key advantages of the Pheroid® delivery system include its effective delivery of pharmaceutically active compounds, improved therapeutic efficacy, high entrapment efficiency and capacity to penetrate many biological barriers that often seem challenging, which includes skin, keratinised tissue, intestinal lining and the vascular system as well as pathogens (Uys, 2006, Grobler, 2009, Steyn et al., 2011).

The historical perspective of the Pheroid®, as iterated in Grobler's thesis (2009), involves its origin in Emzaloid™ technology formulated by Piet Meyer and Steven Zall to cure psoriasis, an autoimmune disease that results in the appearance of red raised scaly patches on the skin (Grobler, 2008). Emzaloid™ consisted of micro and nano-sized vesicles into which the psoriasis drug, coal tar, was encapsulated for topical application. The MeyerZall laboratory was established to commercialise this psoriasis product and to optimise Emzaloid™ for the drug delivery of more active ingredients and a more extensive application. The intellectual property for Emzaloid™ technology was obtained by the North-West University (NWU) in 2003. Pheroid® and Emzaloid™ technologies are similar, with differences mainly in the manufacturing protocols where Emzaloid™ products are under-saturated with nitrous oxide (N_2O), low gas pressure (80 kPa) for a few hours, while Pheroid® formulations are over-saturated with N_2O as they are produced at higher gas pressure (200 kPa) for more than three

days. Furthermore, the constituents making up the two systems differ in that only the Pheroid® contains D/L-α-tocopherol also known as vitamin E (Grobler, 2009, Ludick, 2014).

The role of N_2O in the Pheroid® technology is to increase the miscibility of the fatty acids and contributes to the process of Pheroid® vesicle self-assembly (Uys, 2006, Grobler, 2009). N_2O is typically used as an inhalable anaesthetic and is both water and lipid soluble which tends to accumulate more in the lipid-rich region (King Jr and Coan, 1971, Becker and Rosenberg, 2008). This gas concentrates and accumulates in the lipid membrane, which helps to enhance the fluidity of the lipid vesicles and contributes to the easy movement of both hydrophobic and hydrophilic molecules through the membrane (Chin *et al.*, 1976, Grobler, 2009). The D/L-α-tocopherol or vitamin E component is fat-soluble and is widely distributed through the cellular membranes, acting as anti-oxidant (Grobler, 2009). This compound prevents the oxidation of unsaturated fatty acyl residues by reacting with oxidants such as peroxyl radicals of the cellular membrane (Wang and Quinn, 2002). Therefore this Pheroid® constituent, D/L-α-tocopherol, play a significant role during the entrapment of drugs that lead to the formation of reactive oxygen species (ROS). The vitamin F ethyl ester is the fatty acid component comprising the unsaturated (C=C bonds) hydrocarbon chain attached with ethyl ester, as shown in Figure 6. Other constituents of Pheroid® include Cremophor EL or Kolliphor EL, which functions as an emulsion stabiliser in the encapsulation of drugs that are especially lipophilic and it is also capable of exerting biological effect (Zeng *et al.*, 2017, Gelderblom *et al*., 2001). This constituent is a PEGylated glycerol of the C18 fatty acid and forms pores or channels in the bilayer membrane attached to the fatty acid components, see Figure 6. Cremophor EL administered through IV may elicit certain dose-dependent toxicity (Gelderblom *et al.*, 2001, Kiss *et al.*, 2013). However, an oral administration of drugs in combination with Cremophor EL has resulted in undetectable Cremophor levels in plasma suggesting no evidence of its toxicity for oral administration (Gelderblom *et al.*, 2001).

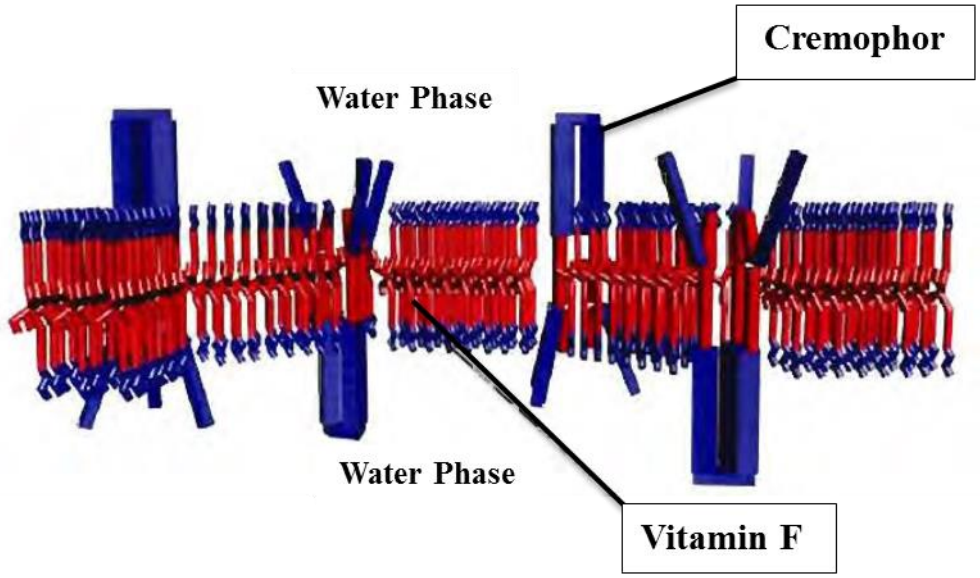

Figure 6: A hypothetical diagram of Pheroid® membrane demonstrating the red regions as the hydrophobic and blue regions as the hydrophilic domains of the fatty acid components of vitamin F. The pore structures or channels are formed by the Cremophor molecules. The figure was reprinted with permission from Grobler, (2009).

A Pheroid® is a stable structure that can be fine-tuned for a specific morphology, structure, size, and function. The size and the structure of the Pheroid® can be manipulated into three types of Pheroid® formulations based on the composition and method of preparation (Uys, 2006), see Figure 7. These three types of Pheroid® include

- Pheroid® vesicles: A colloidal emulsion in nanometre to micrometre size range, typically between 0.05 - 4 μm;
- pro-Pheroid®: Consists of N_2O-gassed oil phase and spontaneously forms Pheroid® vesicles upon contact with water;
- Pheroid® sponges: Have large particles in the micron size range between 1.5 - 6 μm

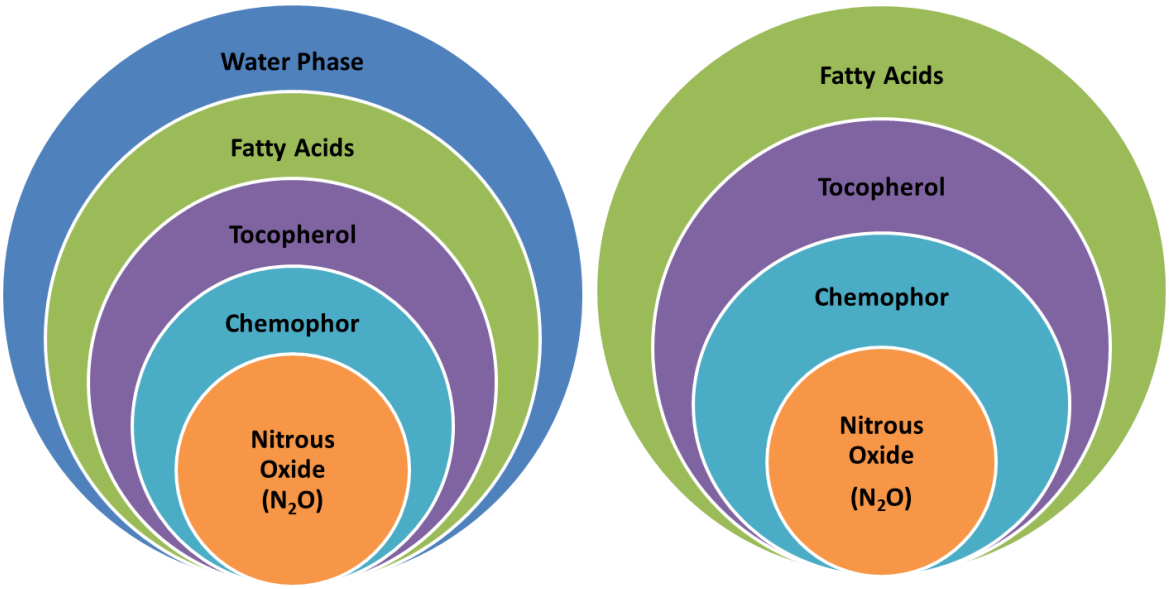

Figure 7: The components that make up the Structure of Pheroid® (left) and pro-Pheroid® (right). The figure was reprinted with permission from Grobler, (2009).

The choice of the Pheroid® type to use for drug delivery is dependent on the route of administration, properties of the drug, and the effect required (Uys, 2006). Pro-Pheroid® formulations have been said to unlock the ability of the system to be administered by various routes. The pro-Pheroid® is a precursor formulation suitable for oral administration and is usually used to entrap drugs that are unstable in water and these drugs are spontaneously entrapped into vesicles when exposed to an aqueous environment (Grobler, 2009, Sheen, 2010). The principles of pro-Pheroid® are similar to those of pro-liposomes, a precursor of liposomes (Shaji and Bhatia, 2013). Both pro-liposomes and pro-Pheroid® are based on the tendency of lipid membranes to form vesicle emulsions upon the addition of water. Pro-liposomes have been described as a potential breakthrough to stability issues associated with liposomes and could lead to the application of liposomes in oral administration (Shaji and Bhatia, 2013).

The original visualisation of Pheroid® relied mainly on confocal laser scanning microscopy (CLSM). This technique helped visualise and determine the structural characterisation and morphology of particles. In addition, CLSM is used to monitor quality and determine particle size distribution and crystallinity of the Pheroid®. Figure 8 shows confocal images of the three different types of Pheroid® (Grobler, 2009).

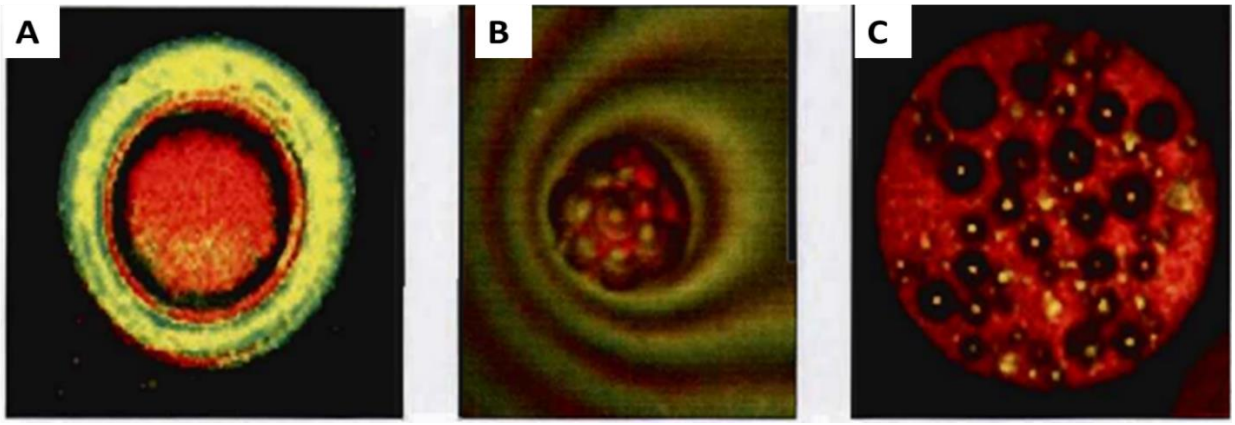

Figure 8: Three different types of Pheroid® observed using confocal laser scanning microscope (CLSM). A. Pheroid® Vesicle; B. Pro-Pheroid® and C. Pheroid® Sponges. The figure was reprinted with permission from Grobler, (2009).

6. Lipid-polymer hybrid drug delivery systems

In the above sections, it is clear that there is significant progress in the design and applications of numerous drug delivery approaches. However, one of the new approaches that has emerged is the combination of two delivery systems to obtain the combined effect of the unique attributes of each delivery technology. In the late 1990's, studies for this new approach showed potential towards improving cancer therapy. A polymeric-Doxil conjugate was encapsulated in a lipid-based delivery system to increase the blood circulation time and tumour uptake of the drug (Uchegbu and Duncan, 1997). Another study showed that entrapment of liposomes in dextran microspheres resulted in the sustained release of liposomes for up to 100 days (d) (Stenekes *et al.*, 2000). The integration of delivery systems advanced the development of drug-loaded lipid systems entrapped within a depot polymeric (natural or synthetic) system (Hara and Miyake, 2001, Chung *et al.*, 2006). These systems were acknowledged to be effective, however there was a high demand for further enhancements to allow a broader application of these integrated delivery systems (Mufamadi *et al.*, 2011). Liposomes and biodegradable polymeric NP are the most dominant classes of delivery systems that have been used to prepare hybrid systems as evidenced by the increasing numbers of research studies in recent reviews (Raemdonck *et al.*, 2013, Hallan *et al.*, 2016).

The use of polymeric NP to deliver drugs has gained much attention due to their controlled drug release capability and potential to reach therapeutic targets, however their limitations include polymer degradation prior to reaching target tissue, a very low degradation rate for high molecular weight PLGA and the inclusion of organic solvents during the preparation steps (Reis *et al*., 2005). As described earlier, liposomes have similarities with the biological membranes that are made up of phospholipids, which offers them superior biocompatibility. For this reason, they have been perceived as an ideal DDS for a long time (Torchilin, 2005). However, liposomal drug products have drawbacks, which include lack of structural integrity, poor batch-to-batch reproducibility and inefficient manufacturing scale-up (Sharma and Sharma, 1997).

Novel, integrated, hybrid DDS, where polymeric NP are enveloped within a liposomal system, have emerged to be a robust and promising delivery platform in an effort to address the limitations of polymeric NP and liposomes (Zhang *et al.*, 2008). This new generation of hybrid DDS, which combines characteristics of both polymeric NP and liposomes, are classified according to the structural organisation of the lipid and polymer components. They can be referred to as polymer core–lipid shell, core-shell-type, hollow lipid-polymer-lipid NP and polymer-caged liposomes (Mandal *et al.*, 2013). These combined DDS will henceforth be referred to as lipid-polymer hybrid nanoparticles (LPHNs) or hybrid DDS. They comprise the following three components, see Figure 9:

1. A biodegradable polymeric core (usually, PLGA), which encapsulates the drug and conveys controlled drug release;
2. A lipid shell covering the polymeric core, to provide more biocompatibility;
3. An outer lipid–PEG layer that offers steric stabilisation and prolonged *in vivo* circulation time.

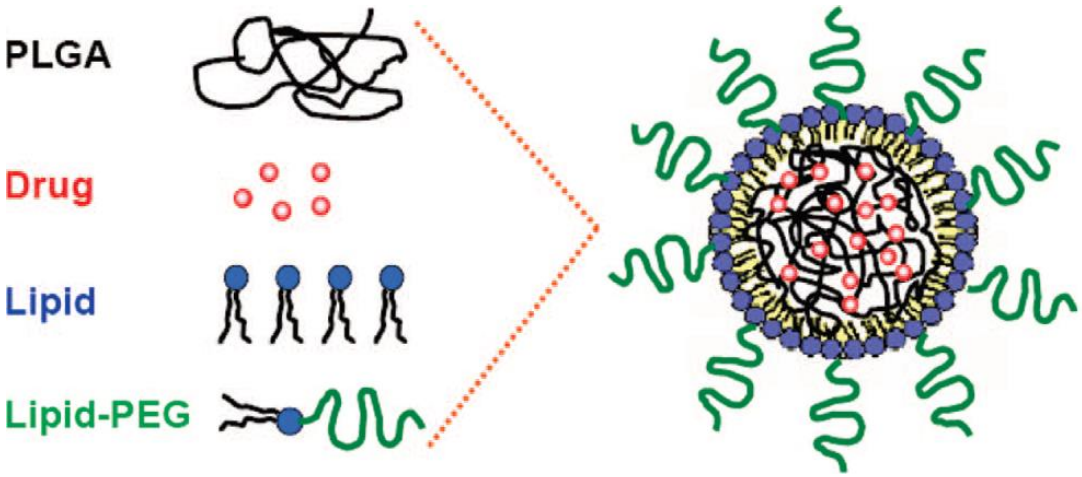

Figure 9: Schematic illustration of a lipid-polymer hybrid DDS with its structural components. The figure was reprinted with permission from Zhang *et al.*, (2008).

The polymeric core provides the skeleton that contributes to structural integrity and mechanical stability and controlled drug release (Grabnar and Kristl, 2011); The inner lipid layer reduces the leakage of the encapsulated drug during the preparation of hybrid DDS. Additionally, it displays similar behaviour to that of cell membranes, which confers high biocompatibility, bioavailability and the capability to interact with several molecules, also owed to the lipid–PEG layer (Zhang *et al.*, 2008). The lipid layer also minimises the rate of polymer degradation by regulating inward water diffusion and therefore allowing controlled release of the drug (Hadinoto *et al.*, 2013). The biodegradable polymers that are often chosen for this system are biocompatible, non-toxic and those previously used in approved products such as PLGA, dextran or albumin. The common choices for lipids are phospholipids that can be zwitterionic, cationic, anionic or neutral.

The lipid-polymer hybrid DDS are capable of encapsulating hydrophobic drugs with high entrapment efficiency and improved drug stability during storage, in comparison to individual liposomes or polymeric NP. For example, a previously studied hybrid system resulted in an enhanced encapsulation efficiency of 60–80% of doxorubicin and about 50% of this drug was released in the first few hours and an additional 10–20% was released over a period of 2 weeks (Wong *et al.*, 2006a). It was also indicated that hybrid DDS could efficiently deliver two drugs simultaneously for enhanced cancer therapy, namely the cytotoxic doxorubicin and chemosensitiser, GG918 (Wong *et al.*, 2006b). This property of the lipid-polymer hybrid DDS

to encapsulate and deliver hydrophilic and hydrophobic therapeutic agents can be due to the drug adsorption and inclusion onto the surface of the bilayer lipid as well as the polymeric core.

Several studies have indicated that hybrid DDS can also be conjugated with ligands such as folic acid, aptamers, transferrin and antibodies for targeted drug delivery of drugs to cancer tissues (Wang *et al.*, 2010, Hu *et al.*, 2010, Zhao *et al.*, 2012, Zhang *et al.*, 2015). When a system of folic acid conjugated LPHNs was developed for the delivery of an anti-cancer drug, docetaxel, it was shown that the combined system possessed more sustainable and controlled targeted delivery of the drug compared to the individual systems (Liu *et al.*, 2010a). Hybrid systems can be tuned by optimising the core-shell structure for a sustained drug release profile (Mandal *et al.*, 2013). These properties of lipid-polymer hybrid DDS are the reason for their quick progression into robust drug delivery platforms. In summary, these liposome-polymer combined systems showed improved properties, which include enhanced stability of the liposomes, controlled release of drugs from liposomes over extended periods of time as well as enhanced efficacy compared to that of the individual systems (Mufamadi *et al.*, 2011).

6.1. Preparation methods for individual DDS and hybrid DDS

The physicochemical properties of a DDS and its drug release characteristics are dependent on many factors such as drug solubility, the composition of the delivery system, rate of solvent evaporation and method of manufacture (Giri *et al.*, 2013). The previously described carriers such as NP, nanospheres and liposomes, are manufactured based on the preparation of emulsions. To obtain an emulsion, two immiscible liquids (aqueous and hydrophobic/organic) are mixed, and the dispersed droplets are stabilised by a surface-active agent called a surfactant. Surfactants are molecules characterised by the presence of both a polar and a nonpolar region and they stabilise the emulsion through the introduction of a mechanical barrier to delay the ultimate destruction of the system. The selection of the specific preparation method is primarily determined by the properties of the delivery material and the drugs which will partition between the aqueous and hydrophobic phases depending on their lipophilicity (Lamprecht *et al.*, 1999). Emulsion formulation methods are reproducible and consist of single or multiple stages with no high-tech equipment required (Saroj *et al.*, 2012). A double emulsion technique followed by a homogenisation process is necessary for preparing delivery systems that have narrow size ranges and also increases the encapsulation efficiency (Giri *et al.*, 2013).

The methods of preparing hybrid DDS have been widely classified as either a two-step or a one-step method. The two-step method is a conventionally used method that involves the combination of preformed polymeric NP and preformed lipid vesicles through either sonication, vortex or continuous stirring (Hadinoto *et al.*, 2013). In a study by Troutier *et al.* (2005b), it was concluded that electrostatic forces were responsible for the interaction between cationic lipid vesicles and anionic polymeric NP when using the two-step method. The advantages of this method include the accurate control of the particle size, drug release properties and drug loading (Troutier *et al.*, 2005b, Sengupta *et al.*, 2005). However, the two-step method can be time and energy consuming in terms of preparing the two systems separately. It has also been shown that this method could reduce the encapsulation efficiency of hydrophilic drugs due to the leakage from the polymeric core prior to the lipid shell coating (Cheow and Hadinoto, 2011). The recently explored one-step method combined the dual processes of the two-step approach into a single production process of the lipid-polymer hybrid DDS. This one-step method involves the combination of polymer and lipid solutions through either solvent evaporation or nano-precipitation approaches after which they self-assemble to form hybrid systems (Hadinoto *et al.*, 2013). The solvent evaporation approach has been used to entrap anti-cancer drugs in LPHNs (Chan *et al.*, 2009, Liu *et al.*, 2010b), while other studies applied the nano-precipitation approach for preparing LPHN (Valencia *et al.*, 2010). The one-step method of preparing the hybrid system has been demonstrated to be more efficient, with the potential to overcome the challenges associated with the two-step method (Wang *et al.*, 2016).

6.2. Characterisation of the physicochemical properties of the individual DDS and hybrid DDS

The parameters that specifically play a crucial role in DDS and have significant pharmacological effects include particle size, surface area, surface charge, crystallinity and encapsulation efficiency. The particle size parameter can be measured by various techniques, which include the measurements of the scattering pattern produced when the light is shone through the dispersed particles in a liquid. The size measurement of these particulate dispersions is based on the diffusion caused by Brownian motion, which is the random movement of nano-sized particles when suspended in a liquid medium resulting from collisions between them and the molecules of dispersing medium that prevent them from sedimenting. The size of the particle is then calculated through the Stokes-Einstein equation, which provides

the radius of a particle and therefore an estimation of the average hydrodynamic particle size and distribution of spherical particles in the sample (Gittings and Saville, 1998). Using one of the laser instrumentation technologies from Malvern called Zetasizer Nano ZS, this measuring principle is applied through dynamic light scattering (DLS) (MalvernInstruments, 2004, Sharma and Patankar, 2004). In this technique, laser light is passed through a sample with a suspension of particles; the light is scattered at different intensities because of the Brownian motion, and these intensities are used to determine the particle size. A laser diffraction technique is adopted to measure particles above the submicron size, where smaller particles scatter light at large angles while larger particles scatter light at small angles. Variations in the intensity of angular scattering is analysed to determine the size, based on the Mie theory of light scattering (Agrawal *et al.*, 2008, MalvernInstruments, 2004).

The zeta potential (ζ-potential) is an important parameter known to influence the stability of particles as it determines the surface charge of the particles that in turn controls the electrostatic force (repulsion/attraction) between particles (Honary and Zahir, 2013). The principle of calculating the ζ-potential involves the determination of the electrophoretic mobility, which is the velocity at which the particles move when an electric field is applied (Gittings and Saville, 1998, MalvernInstruments, 2004). The electrophoretic mobility is calculated using the Henry equation, which takes into account the strength of the electric field and the viscosity of the particle dispersion medium. The medium of dispersion as well the chemical composition of the particle have an effect on this mobility. NP with a highly positive or negative ζ-potential (±15 to ±40 mV) have been demonstrated to be stable in suspension (Muller and Keck, 2004). Highly positive or negative ζ-potential depicts an extended electronic double layer around the vesicle droplets, thus imparting significant electrostatic repulsion between them. This will prevent the aggregation between the NP that will eventually result in sedimentation of these NP as the Brownian motion is affected (Pfeiffer *et al.*, 2014). Furthermore, the steric hindrance owing to the presence of surfactant molecules surrounding the vesicles may contribute to the high ζ-potential value. A positive ζ-potential for orally administered NP can be obtained by coating their surface with positively charged polymers like chitosan, which helps enhance their attachment to the negatively charged cellular membrane, thus improving their intracellular uptake (Chen *et al.*, 2013). ζ-potential also influences the opsonisation process through electrostatic interactions, where NP with a highly negative ζ-potential value are more opsonisable (immunogenic) in serum than NP with positive ζ-potential (Honary and Zahir, 2013, Mohanraj and Chen, 2006).

The use of microscopy methods is an essential part of the physicochemical characterisation to gain more insight visually about the DDS. These methods may use light, photons or a beam of electrons to generate an image. Some hybrid systems have been characterised using various microscopy methods. Information on the structure of these particles can be acquired through fluorescence, laser and electron microscopy. Previous studies on hybrid DDS have used conventional fluorescence microscopy (Troutier *et al.*, 2005a, Wang *et al.*, 2010), CLSM (Bershteyn *et al.*, 2008, Liu *et al.*, 2010a, Ahmed *et al.*, 2002)) and cryogenic or normal transmission electron microscopy (TEM) (Mornet *et al.*, 2004, Bershteyn *et al.*, 2008, Troutier *et al.*, 2005a, Thevenot *et al.*, 2007). These techniques enabled analysis of the morphology, particle size, lipid shell thickness, lipid-shell permeability and the distribution of polymer particles within the lipid.

Further characterisation of hybrid DDS involved *in vitro* biological analysis, which included cellular permeability and uptake (Liu *et al.*, 2010b, Wang *et al.*, 2010) as well as cell viability and cytotoxicity (Wong *et al.*, 2006a, Liu *et al.*, 2010b). These latter characterisation techniques determine the capabilities of these hybrid systems as drug delivery technologies.

PART B

7. Biological application of hybrid DDS

The versatile character of hybrid DDS enables them to encapsulate an extensive range of therapeutic compounds, irrespective of their lipophilicity, hydrophilicity, aqueous solubility, and ionicity (Cheow and Hadinoto, 2011). In general, hybrid DDS bring about improved controlled release kinetics, enhanced encapsulation efficiency, and elevated cellular uptake (Mandal *et al.*, 2013, Zhang *et al.*, 2008).

The delivery of various anti-cancer drugs has dominated applications of hybrid DDS. Anti-cancer drug-loaded hybrid DDS have been recognised to induce increased cancer cell-kill effect while healthy cells remain protected from the exposure to cytotoxic effect for tumour-selective delivery (Mandal *et al.*, 2013). For example, a doxorubicin-loaded LPHN system comprising SLNs and hydrolysed polymer of epoxidised soybean oil was fabricated and was reported to have 65% – 80% encapsulation efficiency (Wong *et al.*, 2006c). This LPHN system was evaluated for activity against multi-drug resistant (MDR) breast cancer cells, and both the cell-kill activity as well as the intracellular uptake were significantly enhanced in comparison to the individual formulations. The mechanism of action for the doxorubicin-loaded hybrid system was assumed to be either of the following: the hybrid system released free doxorubicin that acted on the cells or the system was taken up intracellularly then released doxorubicin within the cells for action, which allowed the evasion of the P-glycoprotein (P-gp) efflux pump. This hybrid system allowed better retention of the doxorubicin, which led to enhanced activity against MDR breast cancer cells in comparison to the free-doxorubicin (Wong *et al.*, 2006c, Mandal *et al.*, 2013).

To the best of our knowledge, literature has only reported a few studies on the *in vivo* evaluation of drug-loaded hybrid systems in animal models (Zhao *et al.*, 2012, Mandal *et al.*, 2013). Sengupta *et al.* (2005) reported a ground-breaking research study, where dual-drug-loaded LPHNs, referred to as nanocells, were evaluated for an anti-cancer activity *in vivo* using a male C57BL/6 mouse model induced with tumour cells. The dual-drug loading comprised doxorubicin, a chemotherapeutic drug that was complexed to the polymeric core of this hybrid system, and combretastatin, which is an anti-angiogenic agent that was entrapped within the lipid shell. An IV administration of this hybrid system containing dual agents displayed a

significant reduction of the tumour volume as well as the increased percentage of mice survival in comparison with a single-agent-loaded hybrid DDS. This study also provided evidence of a dose-dependent inhibition of the tumour growth through the dual-agent loaded-hybrid DDS treatment with more susceptibility toward melanoma than lung carcinoma (Sengupta *et al.*, 2005, Wong *et al*., 2006a). In another *in vivo* animal xenograft study, a solid tumour was induced in BALB/c mice by injecting EMT6 mouse mammary cancer cells intramuscularly, into the hind legs of the mice, for evaluation of doxorubicin-loaded LPHNs (Wong *et al.*, 2006a). The tumour growth was delayed in mice after receiving doxorubicin–loaded LPHNs compared to when free doxorubicin or blank LPHNs were intratumorally administered. This administration reduced the healthy tissue toxicity post a single dose of intratumoral injection, suggesting the effectiveness of the LPHNs system for localised cancer treatment (Mandal *et al.*, 2013). The research studies mentioned above show the potential of the lipid-polymer hybrid systems to improve cancer treatment. However, a recent review has shown that hybrid DDS have been explored for further applications beyond anticancer therapy, which includes vaccine delivery, bio-imaging, treatment of vascular injury and lung infection (Hadinoto *et al.*, 2013).

In contrast, for the most part, studies involving applications for diseases other than cancer are still in the preliminary stage (Hadinoto *et al.*, 2013). For example, the delivery of fluoroquinolone antibiotics loaded in hybrid formulations has been developed with the purpose of effectively treating a lung infection (Cheow and Hadinoto, 2011). This study was driven by the knowledge that liposomes, a component of the hybrid DDS, have potential to efficiently penetrate the thick mucus layer surrounding the bacterial colonies that are prevalent in lung infection, leading to optimised local antibiotic exposure (Ahmed *et al*, 2002), and that the antibiotic-loaded polymeric NP release the antibiotic at the correct dose and therefore inhibit the growth of the infection (Cheow *et al.*, 2010). Despite the fact that more extensive applications of hybrid DDS are still at the proof-of-concept stage, the feasibility of formulating the antibiotic-loaded hybrid system as inhaled products has been established (Wang *et al.*, 2012). A recent publication has reviewed the possibilities and future perspectives of lipid-polymer hybrid DDS for the commonly accepted oral route of delivery as well as the extension of their applications (Hallan *et al*., 2016). The effect of hybrid DDS in the oral therapy for poverty-related infectious diseases is investigated in the studies described in this thesis.

8. Tuberculosis – a neglected poverty-related disease

Tuberculosis (TB) is an airborne, highly contagious infection that poses a significant threat to global health and is one of the leading causes of death by an infectious disease. The World Health Organization (WHO) has reported about 8.6 million TB cases and 1.3 million deaths in 2014 worldwide (WHO, 2015). South Africa is still ranked amongst the top 22 high burden countries, which accounts for 83% of the global TB incidence (WHO, 2015). TB thrives on poor and undernourished communities with lack of proper healthcare. The map in Figure 10 shows that the sub-Saharan African region accounts for the highest TB incidence globally. The TB epidemic in developing countries, with a particular reference to the African region, is aggravated by the high prevalence of the human immunodeficiency virus (HIV) or acquired immune deficiency syndrome (AIDS). These countries account for 74% of cases of TB co-infection with HIV worldwide, and in South Africa more than 50% of HIV-TB co-infected patients have been reported (UNAIDS, 2014). The recent global TB report also estimated that more than 50% of HIV prevalence in new TB cases were observed in the sub-Saharan African countries, see Figure 11. The synergistic infection between TB and HIV indicates that HIV increases the rate of latent TB infection activation and speeds progression of active TB (Alexander, 2007). This is a major problem especially in South Africa, which has the highest number of HIV positive people with TB, based on the requirement for antiretroviral therapy among TB patients, see Figure 12 (UNAIDS, 2014). TB and HIV infections are referred to as "poverty-related diseases" (PRDs) as they burden a large proportion of low-income countries aggravated by poor nutrition, lack of access to proper sanitation and difficulties to apply health-care interventions needed to eradicate them (Singh and Singh, 2008). These PRDs primarily affect young adults in the middle age group (WHO, 2013), which can further worsen the poverty status (Singh, 2008).

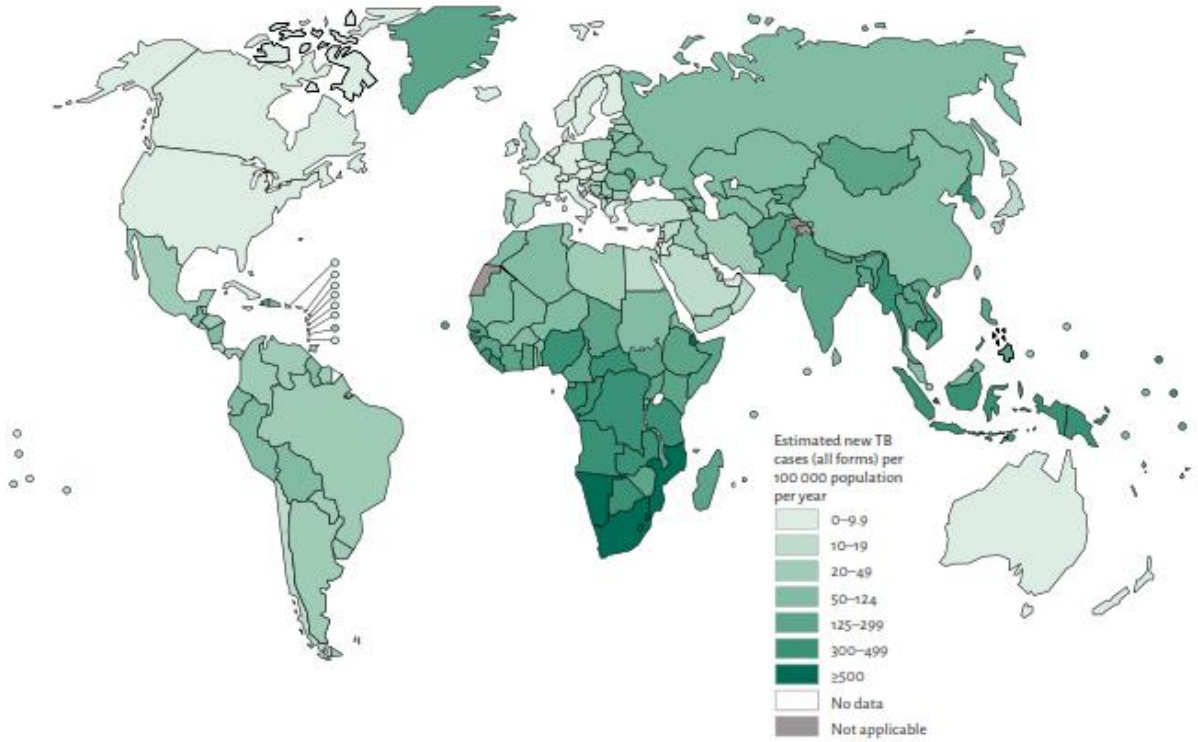

Figure 10: The global TB incidences estimated in 2014. Figure reprinted with permission from WHO, (2015).

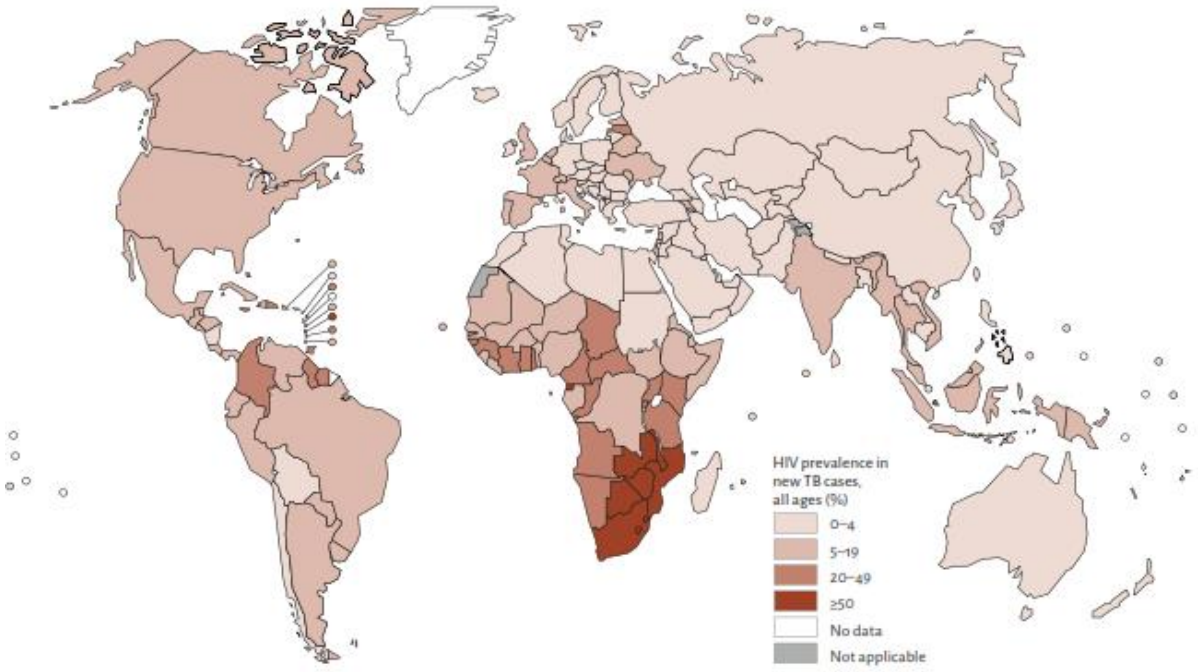

Figure 31: The global HIV prevalence in TB cases estimated in 2014. Figure reprinted with permission from WHO, (2015).

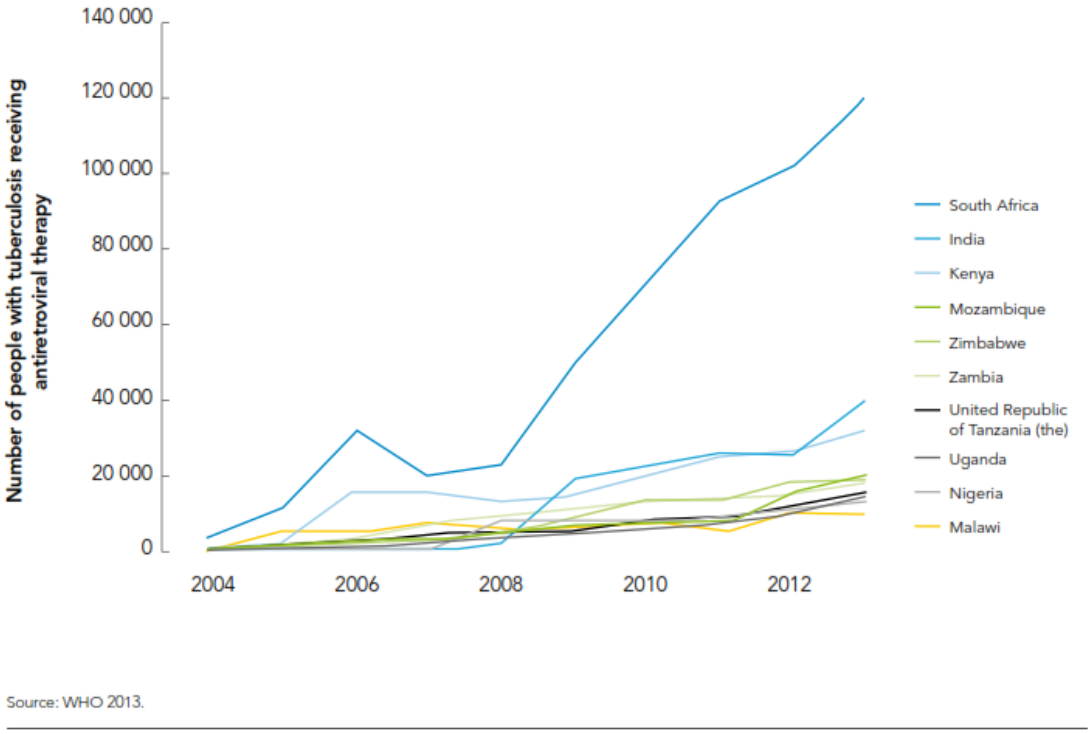

Figure 42: Graph showing the amount of antiretroviral therapy given to HIV-positive patients with TB. The graph was reprinted with permission from UNAIDS, (2014).

8.1. The pathogenesis of TB

The primary causative agent of TB, *Mycobacterium tuberculosis (M.tb)*, is a Gram-positive, aerobic, rod-shaped bacillus and slow-growing pathogen (Smith, 2003). *M.tb* is characterised by a strong, thick, lipid-rich and protective cell wall which provides the bacteria with the ability to persist for long periods despite being subjected to effective treatment (Brennan, 2003). The mycolic acids make up most of the cell wall lipids, which are impregnable and obstruct penetration. This pathogen has the ability to acquire resistance to treatment through genetic mutations. The extraordinary capability of the *M.tb* to adapt to environmental changes that include oxygen deprivation (hypoxia), lack of nutrients and various exogenous stress conditions is attributed to its surrounding cell wall (Pinheiro *et al.*, 2011). Humans are the primary host of *M.tb*, although there is a hypothetical theory that *M. bovis*, a TB-like infection in cattle, is an evolutional precursor that was passed to humans (Smith, 2003). The

pathogenesis of *M.tb* involves its inhalation and ingestion through phagocytosis by the lung alveolar macrophages, which initiates a non-specific response to the bacterium through a series of events that either lead to the defence or progression of active TB, as illustrated in Figure 13 (Schluger, 2005).

The primary TB infection is determined by the bacterial virulence and the microbicidal ability of the alveolar macrophage. If the *M.tb* organism persists beyond the initial defences, it can thrive and proliferate within the alveolar macrophage, leading to pulmonary TB where the pathogen spreads through the lymphatic circulation in the lungs (SADOH, 2014). After an extended period of infection, the bacilli can be scattered to distant organs resulting in extra-pulmonary TB that can cause death (Pieters, 2008). *M.tb* also has the ability to be dormant, where it can survive for many years without replication; this is referred to as latent TB. During latency, the bacteria is restrained within calcified tissues or granulomas, which are a collection of lymphocytes and macrophages that protect the alveolar tissues from the pathogen (Schluger, 2005, Rubins, 2003). These granulomas are vital in restricting the growth of the bacteria, tissue damage and the spreading from the lungs. The latent TB infection can, however, reactivate from dormancy to active TB, contributing to the worldwide TB epidemic, (Pinheiro *et al.*, 2011). If the host is immune-compromised, it provides the *M.tb* with the optimal conditions to multiply and thrive. In fact, it has been demonstrated that the worldwide spread of TB disease does not only result from the primary infection but the reactivation of latent TB carried in the host for a lifetime, and the high number of active TB incidence in low TB burden countries typically results from this reactivation (Ai *et al.*, 2016). Moreover, the WHO recently reported that out of two to three billion people that are infected with latent TB, about 5%-15% of these people would experience reactivation of TB (WHO, 2015).

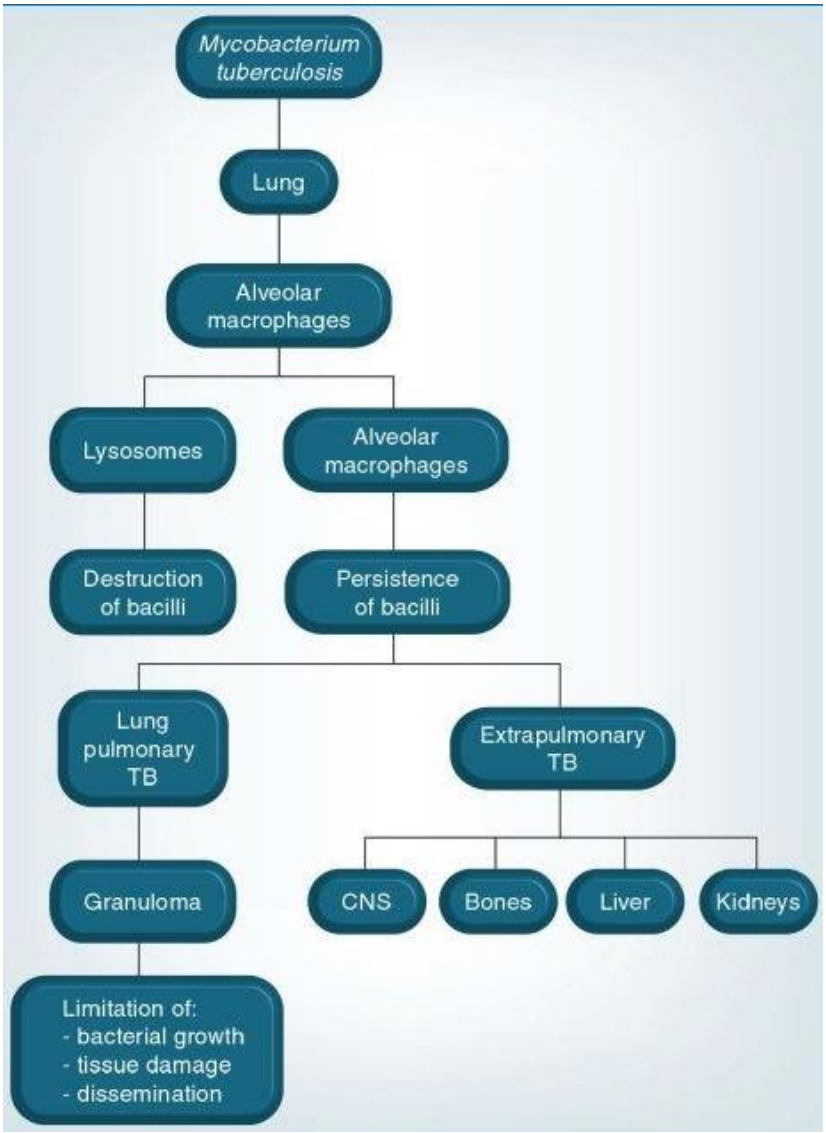

Figure 53: The transmission and pathogenesis *M.tb*. Diagram reprinted with permission from Pinheiro *et al.*, (2011).

8.2. Current TB chemotherapy

The current treatment for primary TB infection requires a fixed dose combination (FDC) of four potent drugs: rifampicin (RIF), isoniazid (INH), pyrazinamide (PYZ) and ethambutol (ETB), approved by the WHO and guaranteed to completely cure TB (Hari *et al.*, 2010, D'Ambrosio *et al.*, 2015), their chemical structures are shown in Figure 14. This FDC treatment has to be taken daily for a period of up to six months for effective eradication of primary TB infection. Figure 15 shows the target site on the *M.tb* cell wall and cytoplasm of these four anti-TB drugs, where they exert their therapeutic effect. RIF is a large hydrophobic compound,

which binds to ribonucleic acid (RNA) polymerase within the bacteria and prevents the synthesis of RNA, thereby leading to bacterial cell death (Kolyva and Karakousis, 2012). INH is a pro-drug that is first activated by the bacterial catalase enzyme (KatG) after which it inhibits the synthesis of mycolic acids, which are crucial components of the robust *M.tb* cell wall (Kolyva and Karakousis, 2012). ETB acts by hindering the activity of arabinosyl transferase, which plays an essential role in the polymerisation process to form arabinoglycan, a component of the bacterial cell wall (Kolyva and Karakousis, 2012). Lastly, PZA interrupts the synthesis of short chain fatty acid precursors in the cell membrane, thereby inhibiting the transport molecules across the *M.tb* membrane (Kolyva and Karakousis, 2012).

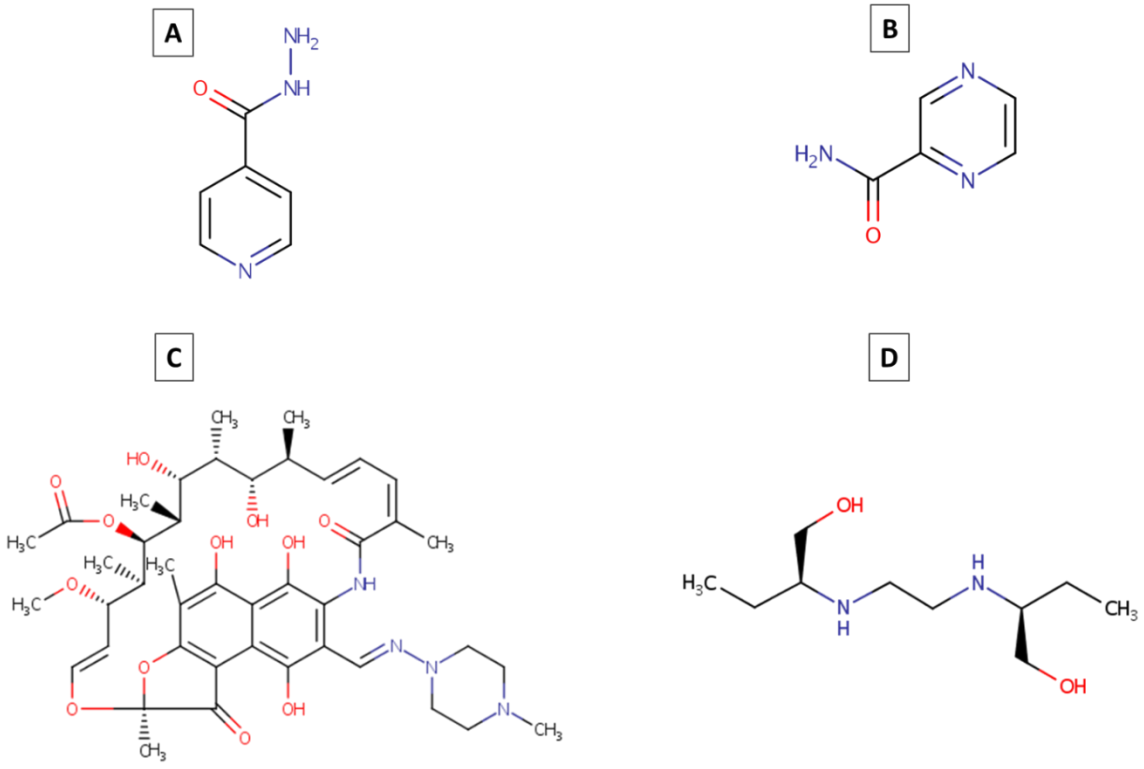

Figure 64: The structures of the four first-line anti-TB drugs: INH (A); ETB (B); RIF (C); PYZ (D). Structures obtained with permission from DrugBank, (2005a-d).

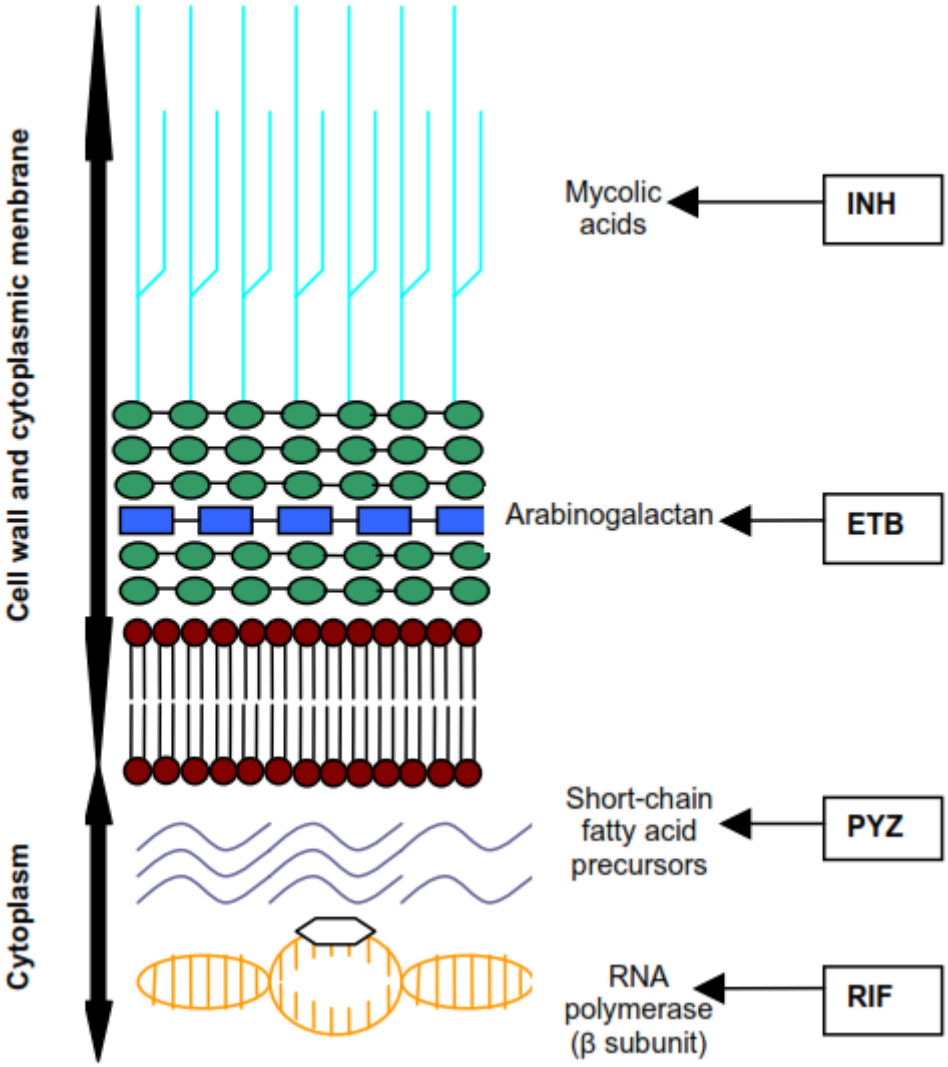

Figure 15: Diagram illustrating the cell wall, cell membrane and the cytoplasm of *M.tb* and the site of action for each of the first-line anti-TB drugs. Diagram reprinted with permission from (du Toit *et al.*, 2006).

Although the FDC is guaranteed to eradicate primary TB infection after a full six months of treatment, the drawbacks of the current treatment include toxicity and low bioavailability, which may lead to an ineffective eradication of this infectious disease. The long duration of therapy leads to the development of adverse side effects and poor patient compliance, which in turn leads to the formation of resistant strains of TB, which presents multiple challenges in the treatment of this TB (Sacks and Behrman, 2009). The emergence of multidrug-resistant TB (MDR-TB) and extensively drug-resistant TB (XDR-TB) is an escalating health crisis (Kwon *et al.*, 2014). MDR-TB had an estimated 450 000 cases and 170 000 deaths in 2012, and the

detection of XDR-TB was reported in 92 countries in 2014 (WHO, 2015, WHO, 2013). Furthermore, the second-line drugs approved for the treatment of drug-resistant TB strains are less potent and more toxic for use over an extended duration, making the treatment ineffective (Kwon *et al*., 2014). For instance, only about 48% of MDR-TB patients were reported to be treated successfully in 2014 (WHO, 2015). It has been more than 50 years since the discovery of the effective first-line anti-TB drugs. The previous years of a search for more potent anti-TB drugs have resulted in few novel compounds that have reached various stages of human trials (Sacks and Behrman, 2009). Two novel anti-TB drugs namely, bedaquiline and delamanid, were recently approved by the US FDA and the European Medicine Agency (EMA) for MDR-TB treatment (D'Ambrosio *et al.*, 2015).

Strategies and interventions implemented by the health ministry in South African to increase patient adherence to treatment and reduce the MDR TB burden have included FDC treatment under directly observed therapy (DOT) and health education (SADOH, 2014). The DOT strategy implies that a patient is supervised and monitored while taking treatment. This strategy guarantees patient compliance to treatment and a quick recognition of adverse side effects (Chaulk *et al.*, 1995). Patient education is vital for the prevention of deadly diseases such as TB and is essential for motivating patients to adopt healthy behaviour. Improved nutrition is another crucial element adopted in conjunction with other interventions to ensure a stronger immune system that would help to minimise the TB infection. In addition to the interventions for improved TB therapy or the discovery of novel TB drug candidates, a possible solution to this problem could be to use DDS suitable for modifying the PK properties of the current drugs used by TB patient and so to increase their therapeutic effectiveness by reducing drug toxicity, the dosage, as well as the treatment period. Therefore, along with the development of novel anti-TB drugs, the efficient delivery of the anti-TB drugs has demonstrated potential in the fight against TB in animal models (Sosnik *et al.*, 2010).

8.3. Drug delivery systems for TB

Novel therapeutic strategies such as nanotechnology-based DDS have been widely applied to mostly improve cancer therapy in preference to PRD therapies (Trouiller *et al.*, 2002). This is proven by the amount of research and nanomedicine-based drugs that are currently in the markets (Chang and Yeh, 2012). The success of basic research outcomes has been indicated by the introduction of a number of new nanomedicine products into clinical trials and then onto

the commercial market in recent years. For example, in addition to Doxil® that was approved for use by mid-1990s, the accomplishments of nanomedicine include the recently approved Abraxane®, an albumin-bound paclitaxel with significantly reduced side effects compared to paclitaxel (Wang *et al.*, 2013). Despite the rapid progress in the development of new nano-based pharmaceutical products, they have not been explored enough for treatment of PRDs to keep pace with the rate at which these diseases have reached high mortality in recent years. This situation calls for an urgent need for the development of innovative, scalable and cost-viable formulations to ensure that patients have access to appropriate medications for PRDs (Sosnik *et al.*, 2012).

The need for attaining novel dosage forms and new modes of delivery for anti-TB treatment was addressed through various investigations of potential nanomedicine-based DDS for anti-TB drugs (du Toit *et al.*, 2006, Kisich *et al.*, 2007, Nasiruddin *et al.*, 2017). Previous studies included targeted delivery of anti-TB drugs to the lungs in mice using Stealth® liposomes, and the evaluation of the therapeutic activity of RIF and INH encapsulated within liposomes (Deol and Khuller, 1997, Deol *et al.*, 1997). This study showed several advantages of liposomes as nano-DDS for TB therapy, which were an increase in the bioavailability of the first-line anti-TB drugs and a potential reduction in the frequency of dosage (Deol *et al.*, 1997, Pinheiro *et al.*, 2011). However, more extensive research was required to improve the PK of the anti-TB drugs further as liposomes had drawbacks such as the inability to be taken orally, which is the preferred administration route for TB therapy. In a previous comparison study, it was demonstrated that poly (*DL*-lactide-*co*-glycolide) (PLG) DDS exhibited a significant controlled release of INH and RIF in contrast to a liposomal DDS (Dutt and Khuller, 2001).

Nano-based polymeric DDS have been shown to display capability to optimise the PK of the current anti-TB drugs such as increasing the half-life and extending retention time of the drug. Initial studies showed that when the four first-line anti-TB drugs were loaded into PLGA NP and were administered to mice via oral gavage, the drugs were retained in the plasma for a period of up to 9 d and their concentrations were higher than the minimum inhibitory concentration (MIC) for more than 5 d, while free drugs were detected only up to 21 h (Pandey *et al.*, 2003). Additional experiments in this study showed that the *M.tb* pathogen was entirely eliminated from vital organs such as lungs, kidneys and spleen after only five oral doses of anti-TB drug-loaded PLGA NP were administered to mice over a period of 50 d (Pandey *et al.*, 2003). In another study, anti-TB drug-loaded PLGA NP prepared through a multiple emulsion technique were subcutaneously injected in a murine model of TB. The results revealed that the

encapsulated anti-TB drug plasma levels stayed above MIC for more than one month in the lungs as well as the spleen and that the bacterial counts were drastically reduced in most organs (Pandey and Khuller, 2004). The fate and toxicity of PLGA NP made via a patented double emulsion-solvent-evaporation technique, followed by spray drying was also investigated (Kalombo, 2011). It was found that after the oral administration of these NP to BALB/c mice, there was no specific anatomical pathological alteration or tissue damage in different organs (Semete *et al.*, 2010). In addition to the illustrated lack of toxicity, it was observed that these PLGA-based NP were still detected up to 7 d in the liver, lungs, kidneys, spleen, heart, and brain. In addition to liposomes and polymeric NP, other DDS have been studied in the treatment of TB such as solid lipid NP, nanodispersions, polymeric micelles and other self-assembled vesicles (Mohan *et al.*, 2013). These DDS including Pheroid® technology have displayed unique advantages with the potential to improve the TB treatment problem.

The effect of Pheroid® technology in the treatment of tuberculosis was evaluated on all four first-line anti-TB drugs. The entrapped drugs demonstrated promising PK results such as rapid absorption, increased time in the therapeutic window, increased drug plasma levels and reduced MIC (Matthee, 2007, Grobler, 2009). The low bioavailability of RIF in a fixed-dose combination (FDC) had been a matter of major concern because of its incompatibility or instability when it is formulated in combination with INH (Shishoo *et al.*, 2001). However, issues concerning the stability of RIF when formulated with other drugs, especially INH, were addressed by using pro-Pheroid® formulation, to entrap RIF with ETB and INH with PYZ (Sheen, 2010).

A pilot study using mice was set up to compare the plasma levels of the four anti-TB drugs, RIF, INH, ETB and PZY in a pro-Pheroid® formulation, with the current four-drug FDC (Rifafour e-275®), dissolved in water (Matthee, 2007). Increased levels of rifampicin (300%) were detected with the use of pro-Pheroid® formulation, in comparison with the commercial product, Rifafour e-275®. The absorption of all four anti-TB drugs across the intestinal epithelia in mice was significantly increased and led to improved bioavailability compared to the free drugs. A three-months accelerated stability study was also carried out under climatic conditions, where drug content and microbial growth were determined on a monthly basis (Matthee, 2007). Although the accelerated stability study was hampered with some apparatus-based inconsistencies, the pro-Pheroid® formulations were regarded as stable as the drug content remained between 90% and 110% of the initial values and there was no detectable microbial growth in the formulations (Matthee, 2007). These studies progressed to Phase I

clinical trials, where these four anti-TB drugs entrapped in the Pheroid® DDS were investigated for their safety and bioavailability in healthy human volunteers (Grobler, 2009). In this comparative phase I study, a group of 16 healthy human volunteers were orally given all four first-line anti-TB drugs entrapped within Pheroid® DDS while a second group was given Rifafour® e-200 (Matthee, 2007, Grobler, 2009). There were no significant side effects found with the Pheroid® treatments, and the results suggested that the interval between the dosages can be increased to decrease the dosage frequency (Grobler, 2009). The trial results demonstrated rapid absorption, overall improved bioavailability, increased drug plasma levels and an elevated time in the therapeutic window of the anti-TB drugs.

From all the reviewed studies, the use of well-designed DDS brings the potential to improve TB treatment outcomes. New delivery approaches continue to be proposed, however more research is required before the use of DDS for anti-TB drugs is translated to clinical applications (Dube *et al.*, 2013). It is noteworthy to mention that the application of Pheroid® technology to TB is focused on managing the same challenge that the polymeric NP addresses and that is, to decrease side effects, to lessen the daily drug dose burden, shorten the treatment period and increase patient adherence. Therefore the combination of polymeric NP and Pheroid® into a novel hybrid DDS could result in a better therapeutic method for TB.

9. References

AGRAWAL, Y., WHITMIRE, A., MIKKELSEN, O. A. & POTTSMITH, H. 2008. Light scattering by random shaped particles and consequences on measuring suspended sediments by laser diffraction. *Journal of Geophysical Research: Oceans,* 113, C04023, 17 Pages.

AHMED, K., GRIBBON, P. & JONES, M. N. 2002. The application of confocal microscopy to the study of liposome adsorption onto bacterial biofilms. *Journal of Liposome Research*, 12, 285-300.

AI, J.-W., RUAN, Q.-L., LIU, Q.-H. & ZHANG, W.-H. 2016. Updates on the risk factors for latent tuberculosis reactivation and their managements. *Emerging Microbes & Infections,* 5, e10, 8 Pages.

ALBANESE, A., TANG, P. S. & CHAN, W. C. W. 2012. The effect of nanoparticle size, shape, and surface chemistry on biological systems. *annual review of biomedical engineering,* 14**,** 1-16.

ALLEN, T., HANSEN, C. & GUO, L. 1993. Subcutaneous administration of liposomes: a comparison with the intravenous and intraperitoneal routes of injection. *Biochimica et Biophysica Acta (BBA)-Biomembranes,* 1150**,** 9-16.

ALLEN, T. M. & CULLIS, P. R. 2013. Liposomal drug delivery systems: From concept to clinical applications. *Advanced Drug Delivery Reviews,* 65**,** 36-48.

AMANN, L. C., GANDAL, M. J., LIN, R., LIANG, Y. & SIEGEL, S. J. 2010. In Vitro–In Vivo Correlations of Scalable PLGA-Risperidone Implants for the Treatment of Schizophrenia. *Pharmaceutical Research,* 27**,** 1730-1737.

ATTAMA, A. A., MOMOH, M. A. & BUILDERS, P. F. 2012. Recent advances in novel drug carrier systems (Chapter 5). *Lipid Nanoparticulate Drug Delivery Systems: A Revolution in Dosage Form Design and Development.* InTech, 107-140.

BARENHOLZ, Y. 2012. Doxil® — The first FDA-approved nano-drug: Lessons learned. *Journal of Controlled Release,* 160**,** 117-134.

BENNET, D. & KIM, S. 2014. Polymer nanoparticles for smart drug delivery (Chapter 8). *Application of Nanotechnology in Drug Delivery.* InTech, 257-310.

BERNKOP-SCHNÜRCH, A. & DÜNNHAUPT, S. 2012. Chitosan-based drug delivery systems. *European Journal of Pharmaceutics and Biopharmaceutics,* 81**,** 463-469.

BERSHTEYN, A., CHAPARRO, J., YAU, R., KIM, M., REINHERZ, E., FERREIRA-MOITA, L. & IRVINE, D. J. 2008. Polymer-supported lipid shells, onions, and flowers. *Soft Matter,* 4**,** 1787-1791.

BOTHA, M. M. 2007. *Pre-clinical evaluation of the possible enhancement of the efficacy of antiretroviral drugs by pheroid technology.* North-West University. https://www.researchgate.net/publication/26988859_Preclinical_evaluation_of_the_possible_enhancement_of_the_efficacy_of_antiretroviral_drugs_by_pheroid_technology_MM_Botha (Date accessed: 15 May 2017).

BRENNAN, P. J. 2003. Structure, function, and biogenesis of the cell wall of Mycobacterium tuberculosis. *Tuberculosis,* 83**,** 91-97.

BRIUGLIA, M.-L., ROTELLA, C., MCFARLANE, A. & LAMPROU, D. A. 2015. Influence of cholesterol on liposome stability and on in vitro drug release. *Drug Delivery and Translational Research,* 5**,** 231-242.

BRUYN, T. D. 2006. *Nasal Delivery of Insulin with Pheroid Technology.* Master of Science, North-West University. https://dspace.nwu.ac.za/handle/10394/730 (Date accessed: 22 July 2013).

CASALS, E., GALÁN, A. M. A., ESCOLAR, G., GALLARDO, M. & ESTELRICH, J. 2003. Physical stability of liposomes bearing hemostatic activity. *Chemistry and Physics of Lipids,* 125**,** 139-146.

CHAKRAVARTHI, S. S. & ROBINSON, D. H. 2011. Enhanced cellular association of paclitaxel delivered in chitosan-PLGA particles. *International Journal of Pharmaceutics,* 409**,** 111-120.

CHAN, J. M., ZHANG, L., YUET, K. P., LIAO, G., RHEE, J.-W., LANGER, R. & FAROKHZAD, O. C. 2009. PLGA–lecithin–PEG core-shell nanoparticles for controlled drug delivery. *Biomaterials,* 30**,** 1627-1634.

CHANG, H.-I. & YEH, M.-K. 2012. Clinical development of liposome-based drugs: formulation, characterization, and therapeutic efficacy. *International Journal of Nanomedicine,* 7**,** 49-60.

CHAULK, C., MOORE-RICE, K., RIZZO, R. & CHAISSON, R. E. 1995. Eleven years of community-based directly observed therapy for tuberculosis. *The Journal of American Medical Association,* 274**,** 945-951.

CHEN, G., ROY, I., YANG, C. & PRASAD, P. N. 2016. Nanochemistry and nanomedicine for nanoparticle-based diagnostics and therapy. *Chemical Reviews,* 116**,** 2826-2885.

CHEN, M.-C., MI, F.-L., LIAO, Z.-X., HSIAO, C.-W., SONAJE, K., CHUNG, M.-F., HSU, L.-W. & SUNG, H.-W. 2013. Recent advances in chitosan-based nanoparticles for oral delivery of macromolecules. *Advanced Drug Delivery Reviews,* 65**,** 865-879.

CHEOW, W. S. & HADINOTO, K. 2011. Factors affecting drug encapsulation and stability of lipid-polymer hybrid nanoparticles. *Colloids and Surfaces B: Biointerfaces,* 85**,** 214-220.

CHEOW, W. S., CHANG, M. W. & HADINOTO, K. 2010. Antibacterial efficacy of inhalable levofloxacin-loaded polymeric nanoparticles against *E. coli* Biofilm Cells: The effect of antibiotic release profile. *Pharmaceutical Research,* 27, 1597-1609.

CHIN, J. H., TRUDELL, J. R. & COHEN, E. N. 1976. The compression-ordering and solubility-disordering effects of high pressure gases on phospholipid bilayers. *Life Sciences,* 18**,** 489-497.

CHO, K., WANG, X., NIE, S., CHEN, Z. & SHIN, D. M. 2008. Therapeutic nanoparticles for drug delivery in cancer. *Clinical Cancer Research,* 14**,** 1310-1316.

CHUNG, T.-W., YANG, M.-C. & TSAI, W.-J. 2006. A fibrin encapsulated liposomes-in-chitosan matrix (FLCM) for delivering water-soluble drugs: Influences of the surface properties of liposomes and the crosslinked fibrin network. *International Journal of Pharmaceutics,* 311**,** 122-129.

CORREIA, R. C., JOZALA, A. F., MARTINS, K. F., PENNA, T. C. V., DUEK, E. A. D. R., RANGEL-YAGUI, C. D. O. & LOPES, A. M. 2015. Poly(lactic-co-glycolic acid) matrix incorporated with nisin as a novel antimicrobial biomaterial. *World Journal of Microbiology and Biotechnology,* 31**,** 649-659.

CROMMELIN, D. J. A. & FLORENCE, A. T. 2013. Towards more effective advanced drug delivery systems. *International Journal of Pharmaceutics,* 454**,** 496–511.

CUKIERMAN, E. & KHAN, D. R. 2010. The benefits and challenges associated with the use of drug delivery systems in cancer therapy. *Biochemical Pharmacology,* 80**,** 762-770.

D'AMBROSIO, L., CENTIS, R., SOTGIU, G., PONTALI, E., SPANEVELLO, A. & MIGLIORI, G. B. 2015. New anti-tuberculosis drugs and regimens: 2015 update. *European Respiratory Journal Open Research,* 1**,** 1-15.

DANHIER, F., ANSORENA, E., SILVA, J. M., COCO, R., LE BRETON, A. & PRÉAT, V. 2012. PLGA-based nanoparticles: An overview of biomedical applications. *Journal of Controlled Release,* 161**,** 505-522.

DEOL, P. & KHULLER, G. K. 1997. Lung specific stealth liposomes: stability, biodistribution and toxicity of liposomal antitubercular drugs in mice. *Biochimica et Biophysica Acta (BBA) - General Subjects,* 1334**,** 161-172.

DEOL, P., KHULLER, G. K. & JOSHI, K. 1997. Therapeutic efficacies of isoniazid and rifampin encapsulated in lung-specific stealth liposomes against Mycobacterium tuberculosis infection induced in mice. *Antimicrobial Agents and Chemotherapy,* 41**,** 1211-1214.

DESAI, M., LABHASETWAR, V., WALTER, E., LEVY, R. & AMIDON, G. 1997. The mechanism of uptake of biodegradable microparticles in Caco-2 cells is size dependent. *Pharmaceutical Research,* 14**,** 1568-1573.

DRUGBANK. 2005a. *Ethambutol* [Online]. Canadian Institutes of Health Research and The Metabolomics Innovation Centre (TMIC), . Available: http://www.drugbank.ca/drugs/DB00330 (Date accessed 29 February 2016).

DRUGBANK. 2005b. *Isoniazid* [Online]. Canadian Institutes of Health Research and The Metabolomics Innovation Centre (TMIC). Available: http://www.drugbank.ca/drugs/DB00951 (Date accessed 29 February 2016).

DRUGBANK. 2005c. *Pyrazinamide* [Online]. Canadian Institutes of Health Research and The Metabolomics Innovation Centre (TMIC). Available: http://www.drugbank.ca/drugs/DB00339 (Date accessed 29 February 2016).

DRUGBANK. 2005d. *Rifampicin* [Online]. Available: http://www.drugbank.ca/drugs/DB01045 (Date accessed 29 February 2016).

DU TOIT, L., PILLAY, V. & DANCKWERTS, M. 2006. Tuberculosis chemotherapy: current drug delivery approaches. *Respiratory Research,* 7**,** 1-18.

DUTT, M. & KHULLER, G. K. 2001. Liposomes and PLG microparticles as sustained release antitubercular drug carriers—an in vitro–in vivo study. *International Journal of Antimicrobial Agents,* 18**,** 245-252.

ENSIGN, L. M., CONE, R. & HANES, J. 2012. Oral drug delivery with polymeric nanoparticles: The gastrointestinal mucus barriers. *Advanced Drug Delivery Reviews,* 64**,** 557-570.

FAHY, E., SUBRAMANIAM, S., BROWN, H. A., GLASS, C. K., MERRILL, A. H., MURPHY, R. C., RAETZ, C. R. H., RUSSELL, D. W., SEYAMA, Y., SHAW, W., SHIMIZU, T., SPENER, F., VAN MEER, G., VANNIEUWENHZE, M. S., WHITE, S. H., WITZTUM, J. L. & DENNIS, E. A. 2005. A comprehensive classification system for lipids. *Journal of Lipid Research,* 46**,** 839-862.

FAROKHZAD, O. C. & LANGER, R. 2009. Impact of Nanotechnology on Drug Delivery. *ACS Nano,* 3**,** 16-20.

FLYNN, G. 1982. Considerations in controlled release drug delivery system. *Pharmaceutical Technology,* 6**,** 33-39.

GAMBOA, J. M. & LEONG, K. W. 2013. In vitro and in vivo models for the study of oral delivery of nanoparticles. *Advanced Drug Delivery Reviews,* 65**,** 800-810.

GAMUCCI, O., BERTERO, A., GAGLIARDI, M. & BARDI, G. 2014. Biomedical nanoparticles: Overview of their surface immune-compatibility. *Coatings,* 4**,** 139-159.

GAO, W., ZHANG, Y., ZHANG, Q. & ZHANG, L. 2016. Nanoparticle-Hydrogel: A hybrid biomaterial system for localized drug delivery. *Annals of Biomedical Engineering***,** 1-13.

GELDERBLOM, H., VERWEIJ, J., NOOTER, K. & SPARREBOOM, A. 2001. Cremophor EL: The drawbacks and advantages of vehicle selection for drug formulation. *European Journal of Cancer,* 37**,** 1590-1598.

GENTILE, P., CHIONO, V., CARMAGNOLA, I. & HATTON, P. 2014. An overview of poly(lactic-co-glycolic) acid (PLGA)-based biomaterials for bone tissue engineering. *International Journal of Molecular Sciences,* 15**,** 3640-3659.

GIL, E. S. & HUDSON, S. M. 2004. Stimuli-reponsive polymers and their bioconjugates. *Progress in Polymer Science,* 29**,** 1173-1222.

GIRI, T. K., CHOUDHARY, C., AJAZUDDIN, ALEXANDER, A., BADWAIK, H. & TRIPATHI, D. K. 2013. Prospects of pharmaceuticals and biopharmaceuticals loaded microparticles prepared by double emulsion technique for controlled delivery. *Saudi Pharmaceutical Journal,* 21**,** 125-141.

GITTINGS, M. R. & SAVILLE, D. A. 1998. The determination of hydrodynamic size and zeta potential from electrophoretic mobility and light scattering measurements. *Colloids and Surfaces A: Physicochemical and Engineering Aspects,* 141**,** 111-117.

GRABNAR, P. A. & KRISTL, J. 2011. The manufacturing techniques of drug-loaded polymeric nanoparticles from preformed polymers. *Journal of Microencapsulation,* 28**,** 323-335.

GROBLER, A. F. 2009. *Pharmaceutical applications of Pheroid™ technology.* Doctor of Philosophy in Pharmaceutics, North-West University. https://dspace.nwu.ac.za/handle/10394/6701 (Date accessed: 22 August 2013).

GROBLER, L. 2014. *The effect of Pheroid® technology on the bioavailability of artemisone in primates.* North-West University. https://dspace.nwu.ac.za/handle/10394/12241 (Date accessed: 02 February 2015).

HADINOTO, K., SUNDARESAN, A. & CHEOW, W. S. 2013. Lipid–polymer hybrid nanoparticles as a new generation therapeutic delivery platform: A review. *European Journal of Pharmaceutics and Biopharmaceutics,* 85**,** 427-443.

HALLAN, S. S., KAUR, P., KAUR, V., MISHRA, N. & VAIDYA, B. 2016. Lipid polymer hybrid as emerging tool in nanocarriers for oral drug delivery. *Artificial Cells, Nanomedicine, and Biotechnology,* 44**,** 334-349.

HANS, M. & LOWMAN, A. 2002. Biodegradable nanoparticles for drug delivery and targeting. *Current Opinion in Solid State and Materials Science,* 6**,** 319-327.

HARA, M. & MIYAKE, J. 2001. Calcium alginate gel-entrapped liposomes. *Materials Science and Engineering: C,* 17**,** 101-105.

HARI, B. N. V., CHITRA, K. P., BHIMAVARAPU, R., KARUNAKARAN, P., MUTHUKRISHNAN, N. & RANI, B. S. 2010. Novel technologies: A weapon against tuberculosis. *Indian Journal of Pharmacology,* 42**,** 338-44.

HAYESHI, R., SEMETE, B., KALOMBO, L., KATATA, L., LEMMER, Y., MELARIRI, P., NYAMBOLI, B. & SWAI, H. 2012. Nanomedicine in the Development of Drugs for Poverty-Related Diseases. *In:* CHIBALE, K., DAVIES-COLEMAN, M. & MASIMIREMBWA, C. (eds.) *Drug Discovery in Africa.* Springer Berlin Heidelberg. 407-429.

HOFFMAN, A. S. 2008. The origins and evolution of "controlled" drug delivery systems. *Journal of Controlled Release,* 132**,** 153-163.

HONARY, S. & ZAHIR, F. 2013. Effect of zeta potential on the properties of nano-drug delivery systems-a review (Part 2). *Tropical Journal of Pharmaceutical Research,* 12**,** 265-273.

HU, C.-M. J., KAUSHAL, S., CAO, H. S. T., ARYAL, S., SARTOR, M., ESENER, S., BOUVET, M. & ZHANG, L. 2010. Half-antibody functionalized lipid−polymer hybrid nanoparticles for targeted drug delivery to carcinoembryonic antigen presenting pancreatic cancer cells. *Molecular Pharmaceutics,* 7**,** 914-920.

IMMORDINO, M. L., DOSIO, F. & CATTEL, L. 2006. Stealth liposomes: Review of the basic science, rationale, and clinical applications, existing and potential. *International Journal of Nanomedicine* 1**,** 297-315.

JAIN, K. 2008. Drug delivery systems - An overview. *In:* JAIN, K. (ed.) *Drug Delivery Systems.* Humana Press.

JAIN, S., JAIN, V. & MAHAJAN, S. C. 2014. Lipid based vesicular drug delivery systems. *Advances in Pharmaceutics,* 2014, 12 Pages.

JANIN, Y. L. 2007. Antituberculosis drugs: Ten years of research. *Bioorganic & Medicinal Chemistry,* 15**,** 2479–2513.

JIA, L. 2005. Nanoparticle formulation increases oral bioavailability of poorly soluble drugs: Approaches experimental evidences and theory. *Current Nanoscience,* 1**,** 237-243.

JOKERST, J. V., LOBOVKINA, T., ZARE, R. N. & GAMBHIR, S. S. 2011. Nanoparticle PEGylation for imaging and therapy. *Nanomedicine (London, England),* 6**,** 715-728.

KALOMBO, L. 2011. *Nanoparticle carriers for drug administration and process for producing same*. US Patent 2011/0033550 A1.

KAUR, R. & KAUR, S. 2014. Role of polymers in drug delivery. *Journal of Drug Delivery and Therapeutics,* 4**,** 32-36.

KELES, H., NAYLOR, A., CLEGG, F. & SAMMON, C. 2015. Investigation of factors influencing the hydrolytic degradation of single PLGA microparticles. *Polymer Degradation and Stability,* 119, 228-241.

KENT, J. S., LEWIS, D. H., SANDERS, L. M. & TICE, T. R. 1987. *Microencapsulation of water soluble active polypeptides*. US Patents 1987/4675189 A.

KIM, B. Y. S., RUTKA, J. T. & CHAN, W. C. W. 2010. Nanomedicine. *New England Journal of Medicine,* 363**,** 2434-2443.

KING JR, A. D. & COAN, C. 1971. Solubility of water in compressed carbon dioxide, nitrous oxide, and ethane. Evidence for hydration of carbon dioxide and nitrous oxide in the gas phase. *Journal of the American Chemical Society,* 93**,** 1857-1862.

KISICH, K. O., GELPERINA, S., HIGGINS, M. P., WILSON, S., SHIPULO, E., OGANESYAN, E. & HEIFETS, L. 2007. Encapsulation of moxifloxacin within poly(butyl cyanoacrylate) nanoparticles enhances efficacy against intracellular Mycobacterium tuberculosis. *International Journal of Pharmaceutics,* 345**,** 154-162.

KISS, L., WALTER, F. R., BOCSIK, A., VESZELKA, S., ÓZSVÁRI, B., PUSKÁS, L. G., SZABÓ-RÉVÉSZ, P. & DELI, M. A. 2013. Kinetic analysis of the toxicity of pharmaceutical excipients Cremophor EL and RH40 on endothelial and epithelial cells. *Journal of Pharmaceutical Sciences,* 102**,** 1173-1181.

KOLATE, A., BARADIA, D., PATIL, S., VHORA, I., KORE, G. & MISRA, A. 2014. PEG — A versatile conjugating ligand for drugs and drug delivery systems. *Journal of Controlled Release,* 192**,** 67-81.

KOLYVA, A. S. & KARAKOUSIS, P. C. 2012. Old and new TB drugs: Mechanisms of action and resistance (Chapter 9). *Understanding Tuberculosis – New Approaches to Fighting Against Drug Resistance* InTech, 209-233.

KOPEČEK, J. 2013. Polymer-drug conjugates: Origins, progress to date and future directions. *Advanced Drug Delivery Reviews,* 65**,** 49-59.

KREUTER, J. 2007. Nanoparticles—a historical perspective. *International Journal of Pharmaceutics,* 331**,** 1-10.

KU, M. S. 2008. Use of the biopharmaceutical classification system in early drug development. *The AAPS Journal,* 10**,** 208-212.

KUMARI, A., YADAV, S. K. & YADAV, S. C. 2010. Biodegradable polymeric nanoparticles based drug delivery systems. *Colloids and Surfaces B: Biointerfaces,* 75**,** 1-18.

KWON, Y.-S., JEONG, B.-H. & KOH, W.-J. 2014. Tuberculosis: clinical trials and new drug regimens. *Current Opinion in Pulmonary Medicine,* 20**,** 280-286.

LAMPRECHT, A., UBRICH, N., HOMBREIRO PÉREZ, M., LEHR, C. M., HOFFMAN, M. & MAINCENT, P. 1999. Biodegradable monodispersed nanoparticles prepared by pressure homogenization-emulsification. *International Journal of Pharmaceutics,* 184**,** 97-105.

LAURENT, S., PARIMALA, B. & MARIA, N. E. 2011. Dynamics of dissolution and diffusion-controlled drug release systems. *Current Drug Delivery,* 8**,** 144-151.

LI, C. J., LI, Y., GADA, K. & DAI, X. 2016. *Biodegradable and Clinically-Compatible Nanoparticles As Drug Delivery Carriers*. US Patent 2016/0046936 A1.

LI, J., WANG, X., ZHANG, T., WANG, C., HUANG, Z., LUO, X. & DENG, Y. 2015. A review on phospholipids and their main applications in drug delivery systems. *Asian Journal of Pharmaceutical Sciences,* 10**,** 81-98.

LIAN, T. & HO, R. J. Y. 2001. Trends and developments in liposome drug delivery systems. *Journal of Pharmaceutical Sciences,* 90**,** 667-680.

LIECHTY, W. B., KRYSCIO, D. R., SLAUGHTER, B. V. & PEPPAS, N. A. 2010. Polymers for drug delivery systems. *Annual Review of Chemical and Biomolecular Engineering,* 1**,** 149–173.

LIU, Y., LI, K., PAN, J., LIU, B. & FENG, S.-S. 2010a. Folic acid conjugated nanoparticles of mixed lipid monolayer shell and biodegradable polymer core for targeted delivery of Docetaxel. *Biomaterials,* 31**,** 330-338.

LIU, Y., PAN, J. & FENG, S.-S. 2010b. Nanoparticles of lipid monolayer shell and biodegradable polymer core for controlled release of paclitaxel: Effects of surfactants on particles size, characteristics and in vitro performance. *International Journal of Pharmaceutics,* 395**,** 243-250.

LUDICK, C. E. 2014. *The development of an oral single dose emulgel formulation for Pheroid® technology.* Doctor of Philosophy in Pharmaceutics, North-West University. https://dspace.nwu.ac.za/handle/10394/12246 (Date accessed: 05 May 2016).

MAKADIA, H. K. & SIEGEL, S. J. 2011. Poly lactic-co-glycolic acid (PLGA) as biodegradable controlled drug delivery carrier. *Polymers,* 3**,** 1377-1397.

MALVERNINSTRUMENTS 2004. *Malvern, Zetasizer Nano Series User Manual*.

MANDAL, B., BHATTACHARJEE, H., MITTAL, N., SAH, H., BALABATHULA, P., THOMA, L. A. & WOOD, G. C. 2013. Core–shell-type lipid-polymer hybrid nanoparticles as a drug delivery platform. *Nanomedicine: Nanotechnology, Biology and Medicine,* 9**,** 474-491.

MATTHEE, L. I. 2007. *A preclinical evaluation of the possible enhancement of the efficacy of antituberculosis drugs by Pheroid™ technology.* Master of Science, North-West University. https://dspace.nwu.ac.za/handle/10394/1805 (Date accessed: 28 April 2014)

MELZAK, K. A., MELZAK, S. A., GIZELI, E. & TOCA-HERRERA, J. L. 2012. Cholesterol organization in phosphatidylcholine liposomes: a surface plasmon resonance study. *Materials,* 5**,** 2306-2325.

MOGHIMI, S. M., HUNTER, A. C. & MURRAY, J. C. 2005. Nanomedicine: current status and future prospects. *The FASEB Journal,* 19**,** 311-330.

MOHAN, A., KUMAR, D. P., HARIKRISHNA, J. & MURUGANATHAN, A. 2013. Newer anti-TB drugs and drug delivery systems (Chapter 86). *Therapeutics,* 388-392. *Jaypee Brothers Medical Publishers*

MOHANRAJ, V. J. & CHEN, Y. 2006. Nanoparticles - A review. *Tropical Journal of Pharmaceutical Research,* 5**,** 561-573.

MORNET, S., LAMBERT, O., DUGUET, E. & BRISSON, A. 2004. The formation of supported lipid bilayers on silica nanoparticles revealed by cryoelectron microscopy. *Nano Letters,* 5**,** 281-285.

MUFAMADI, M. S., PILLAY, V., CHOONARA, Y. E., DU TOIT, L. C., MODI, G., NAIDOO, D. & NDESENDO, V. M. K. 2011. A review on composite liposomal technologies for specialized drug delivery. *Journal of Drug Delivery,* 2011, 19 Pages.

MULLER, R. H. & KECK, C. M. 2004. Challenges and solutions for the delivery of biotech drugs – a review of drug nanocrystal technology and lipid nanoparticles. *Journal of Biotechnology,* 113**,** 151-170.

NAIR, L. S. & LAURENCIN, C. T. 2006. Polymers as biomaterials for tissue engineering and controlled drug delivery. *Advances in Biochemical Engineering/Biotechnology,* 102**,** 47-90.

NASIRUDDIN, M., NEYAZ, M. K. & DAS, S. 2017. Nanotechnology-based approach in tuberculosis treatment. *Tuberculosis Research and Treatment,* 2017, 12 Pages.

PANDEY, R. & KHULLER, G. K. 2004. Subcutaneous nanoparticle-based antitubercular chemotherapy in an experimental model. *Journal of Antimicrobial Chemotherapy,* 54**,** 266-268.

PANDEY, R., ZAHOOR, A., SHARMA, S. & KHULLER, G. K. 2003. Nanoparticle encapsulated antitubercular drugs as a potential oral drug delivery system against murine tuberculosis. *Tuberculosis,* 83**,** 373-378.

PARK, J. W. 2002. Liposome-based drug delivery in breast cancer treatment. *Breast Cancer Research,* 4**,** 95-99.

PARK, K. 2014. Controlled drug delivery systems: Past forward and future back. *Journal of Controlled Release,* 190**,** 3-8.

PARVEEN, S., MISRA, R. & SAHOO, S. K. 2012. Nanoparticles: a boon to drug delivery, therapeutics, diagnostics and imaging. *Nanomedicine: Nanotechnology, Biology and Medicine,* 8**,** 147-166.

PEPPAS, N. A., BURES, P., LEOBANDUNG, W. & ICHIKAWA, H. 2000. Hydrogels in pharmaceutical formulations. *European Journal of Pharmaceutics and Biopharmaceutics,* 50**,** 27-46.

PFEIFFER, C., REHBOCK, C., HÜHN, D., CARRILLO-CARRION, C., DE ABERASTURI, D. J., MERK, V., BARCIKOWSKI, S. & PARAK, W. J. 2014. Interaction of colloidal nanoparticles with their local environment: the (ionic) nanoenvironment around nanoparticles is different from bulk and determines the physico-chemical properties of the nanoparticles. *Journal of the Royal Society Interface,* 11**,** 20130931.

PIETERS, J. 2008. Mycobacterium tuberculosis and the macrophage: Maintaining a balance. *Cell Host & Microbe,* 3**,** 399-407.

PINHEIRO, M., LÚCIO, M., LIMA, J. L. F. C. & REIS, S. 2011. Liposomes as drug delivery systems for the treatment of TB. *Nanomedicine,* 6**,** 1413-1428.

RAEMDONCK, K., BRAECKMANS, K., DEMEESTER, J. & DE SMEDT, S. C. 2013. Merging the best of both worlds: hybrid lipid-enveloped matrix nanocomposites in drug delivery. *Chemical Society Reviews,* 43**,** 444-472.

RANADE, V. V., HOLLINGER, M. A. & CANNON, J. B. 2003. *Drug Delivery Systems,* CRC Press, 3-114.

REIS, C. P., NEUFELD, R. J., RIBEIRO, J., A. & VEIGA, F. 2005. Nanoencapsulation I. Methods for preparation of drug-loaded polymeric nanoparticles. *Nanomedicine: Nanotechnology, Biology and Medicine,* 2**,** 8-21.

RUBINS, J. B. 2003. Alveolar Macrophages. *American Journal of Respiratory and Critical Care Medicine,* 167**,** 103-104.

SACKS, L. V. & BEHRMAN, R. E. 2009. Challenges, successes and hopes in the development of novel TB therapeutics. *Future Medicinal Chemistry,* 1**,** 749-756.

SADOH 2014. National Tuberculosis Management Guidelines. *In:* HEALTH (ed.). *South Africa TB DOTS Strategy Coordination,* National Department of Health, 8-83.

SAROJ, S., DONEY ALEX BABY & M, S. 2012. Current trends in lipid based delivery systems and it's applications in drug delivery. *Asian Journal of Pharmaceutical and Clinical Research,* 5**,** 4-9.

SCHLUGER, N. W. 2005. The Pathogenesis of Tuberculosis. *American Journal of Respiratory Cell and Molecular Biology,* 32**,** 251-256.

SEMETE, B., BOOYSEN, L., LEMMER, Y., KALOMBO, L., KATATA, L., VERSCHOOR, J. & SWAI, H. S. 2010. In vivo evaluation of the biodistribution and safety of PLGA nanoparticles as drug delivery systems. *Nanomedicine: Nanotechnology, Biology and Medicine,* 6**,** 662-671.

SENGUPTA, S., EAVARONE, D., CAPILA, I., ZHAO, G., WATSON, N., KIZILTEPE, T. & SASISEKHARAN, R. 2005. Temporal targeting of tumour cells and neovasculature with a nanoscale delivery system. *Nature,* 436**,** 568-572.

SERCOMBE, L., VEERATI, T., MOHEIMANI, F., WU, S. Y., SOOD, A. K. & HUA, S. 2015. Advances and Challenges of Liposome Assisted Drug Delivery. *Frontiers in Pharmacology,* 6, 13 Pages.

SHAJI, J. & BHATIA, V. 2013. Proliposomes: a brief overview of novel delivery system. *International Journal of Pharmacy and Biological Sciences,* 4**,** 150-60.

SHARMA, A. & SHARMA, U. S. 1997. Liposomes in drug delivery: progress and limitations. *International Journal of Pharmaceutics,* 154**,** 123-140.

SHARMA, N. & PATANKAR, N. A. 2004. Direct numerical simulation of the Brownian motion of particles by using fluctuating hydrodynamic equations. *Journal of Computational Physics,* 201**,** 466-486.

SHEEN, G. 2010. *Stability of anti-tuberculosis actives in the Pheroid™ delivery system.* Master of Science (MSc), North-West University. https://dspace.nwu.ac.za/bitstream/handle/10394/4882/Sheen_G.pdf?sequence=2 (accessed: 13 October 2013).

SHISHOO, C. J., SHAH, S. A., RATHOD, I. S., SAVALE, S. S. & VORA, M. J. 2001. Impaired bioavailability of rifampicin in presence of isoniazid from fixed dose combination (FDC) formulation. *International Journal of Pharmaceutics,* 228**,** 53-67.

SHRESTHA, H., BALA, R. & ARORA, S. 2014. Lipid-Based Drug Delivery Systems. *Journal of Pharmaceutics,* 2014, 10 Pages.

SINGH, A. R. & SINGH, S. A. 2008. Diseases of poverty and lifestyle, well-being and human development. *Mens Sana Monogr,* 6**,** 187-225.

SMITH, I. 2003. Mycobacterium tuberculosis Pathogenesis and Molecular Determinants of Virulence. *Clinical Microbiology Reviews,* 16**,** 463-496.

SOSNIK, A., CARCABOSO, Á. M., GLISONI, R. J., MORETTON, M. A. & CHIAPPETTA, D. A. 2010. New old challenges in tuberculosis: Potentially effective nanotechnologies in drug delivery. *Advanced Drug Delivery Reviews,* 62**,** 547-559.

SOSNIK, A., SEREMETA, K. P., IMPERIALE, J. C. & CHIAPPETTA, D. A. 2012. Novel formulation and drug delivery strategies for the treatment of pediatric poverty-related diseases. *Expert Opinion on Drug Delivery,* 9**,** 303-323.

SRIVASTAVA, A., YADAV, T., SHARMA, S., NAYAK, A., KUMARI, A. A. & MISHRA, N. 2016. Polymers in drug delivery. *Journal of Biosciences and Medicines,* 4**,** 69-84.

STENEKES, R. H., LOEBIS, A., FERNANDES, C., CROMMELIN, D. A. & HENNINK, W. 2000. Controlled release of liposomes from biodegradable dextran microspheres: A novel delivery concept. *Pharmaceutical Research,* 17**,** 664-669.

STEYN, J. D., WIESNER, L., DU PLESSIS, L. H., GROBLER, A. F., SMITH, P. J., CHAN, W.-C., HAYNES, R. K. & KOTZÉ, A. F. 2011. Absorption of the novel artemisinin derivatives artemisone and artemiside: Potential application of Pheroid™ technology. *International Journal of Pharmaceutics,* 414**,** 260-266.

TAKEUCHI, H., THONGBORISUTE, J., MATSUI, Y., SUGIHARA, H., YAMAMOTO, H. & KAWASHIMA, Y. 2005. Novel mucoadhesion tests for polymers and polymer-coated particles to design optimal mucoadhesive drug delivery systems. *Advanced Drug Delivery Reviews,* 57**,** 1583-1594.

THEVENOT, J., TROUTIER, A.-L., DAVID, L., DELAIR, T. & LADAVIÈRE, C. 2007. Steric stabilization of lipid/polymer particle assemblies by poly(ethylene glycol)-lipids. *Biomacromolecules,* 8**,** 3651-3660.

TIWARI, G., TIWARI, R., SRIWASTAWA, B., BHATI, L., PANDEY, S., PANDEY, P. & BANNERJEE, S. K. 2012. Drug delivery systems: An updated review. *International Journal of Pharmaceutical Investigation,* 2**,** 2-11.

TORCHILIN, V. P. 2005. Recent advances with liposomes as pharmaceutical carriers. *Nature Reviews Drug Discovery,* 4**,** 145-160.

TROUILLER, P., OLLIARO, P., TORREELE, E., ORBINSKI, J., LAING, R. & FORD, N. 2002. Drug development for neglected diseases: a deficient market and a public-health policy failure. *The Lancet,* 359**,** 2188-2194.

TROUTIER, A.-L., DELAIR, T., PICHOT, C. & LADAVIÈRE, C. 2005a. Physicochemical and interfacial investigation of lipid/polymer particle assemblies. *Langmuir,* 21**,** 1305-1313.

TROUTIER, A.-L., VÉRON, L., DELAIR, T., PICHOT, C. & LADAVIÈRE, C. 2005b. New insights into self-organization of a model lipid mixture and quantification of its adsorption on spherical polymer particles. *Langmuir,* 21**,** 9901-9910.

UCHEGBU, I. F. & DUNCAN, R. 1997. Niosomes containing N-(2-hydroxypropyl) methacrylamide copolymer-doxorubicin (PK1): Effect of method of preparation and choice of surfactant on niosome characteristics and a preliminary study of body distribution. *International Journal of Pharmaceutics,* 155**,** 7-17.

UNAIDS 2014. Ending the AIDS epidemic. *In:* REPORT, T. U. G. (ed.) *The UNAIDS GAP Report.* Geneva Switzerland: The joint United Nations programme on HIV/AIDS (UNAIDS) http://www.unaids.org/en/resources/documents/2014/20140716_UNAIDS_gap_report (Date accessed: 25 July 2016).

UYS, C. E. 2006. *Preparation and characterization of Pheroids.* Master of Science, North-west University. https://dspace.nwu.ac.za/handle/10394/1669 (Date accessed: 25 April 2013).

VALENCIA, P. M., BASTO, P. A., ZHANG, L., RHEE, M., LANGER, R., FAROKHZAD, O. C. & KARNIK, R. 2010. Single-step assembly of homogenous lipid−polymeric and

lipid−quantum dot nanoparticles enabled by microfluidic rapid mixing. *ACS Nano,* 4**,** 1671-1679.

VIJAYKUMAR, N., NATARAJAN, V. & GURU, V. B. 2015. Proliposomes for oral delivery: Progress and challenges. *Current Pharmaceutical Biotechnology,* 16**,** 303-312.

VILAR, G., TULLA-PUCHE, J. & ALBERICIO, F. 2012. Polymers and drug delivery systems. *Current Drug Delivery,* 9**,** 367-394.

VOGELSON, C. T. 2001. Innovative pharmaceutical treatments require innovative methods of administration. *Advances in drug delivery systems,* 4**,** 49-52.

WANG, A. Z., YUET, K., ZHANG, L., GU, F. X., HUYNH-LE, M., RADOVIC-MORENO, A. F., KANTOFF, P. W., BANDER, N. H., LANGER, R. & FAROKHZAD, O. C. 2010. ChemoRad nanoparticles: a novel multifunctional nanoparticle platform for targeted delivery of concurrent chemoradiation. *Nanomedicine (London, England),* 5**,** 361-368.

WANG, K., YUAN, A., YU, J., WU, J. & HU, Y. 2016. One-step self-assembling method to prepare dual-functional transferrin nanoparticles for antitumor drug delivery. *Journal of Pharmaceutical Sciences,* 105**,** 1269-1276.

WANG, R., BILLONE, P. S. & MULLETT, W. M. 2013. Nanomedicine in action: An overview of cancer nanomedicine on the market and in clinical trials. *Journal of Nanomaterials,* 2013, 12 Pages.

WANG, X. & QUINN, P. J. 2002. The interaction of α-tocopherol with bilayers of 1-palmitoyl-2-oleoyl-phosphatidylcholine. *Biochimica et Biophysica Acta (BBA) - Biomembranes,* 1567**,** 6-12.

WANG, Y., KHO, K., CHEOW, W. S. & HADINOTO, K. 2012. A comparison between spray drying and spray freeze drying for dry powder inhaler formulation of drug-loaded lipid-polymer hybrid nanoparticles. *International Journal of Pharmaceutics,* 424**,** 98-106.

WHO 2013. *Global Tuberculosis Report,* World Health Organization. (Geneva, Switzerland) http://apps.who.int/iris/handle/10665/91355 (Accessed:25 July 2014).

WHO 2015. *Global tuberculosis report,* World Health Organization. (Geneva, Switzerland) http://www.who.int/topics/tuberculosis/en/ (Accessed:15 August 2016).

WILSON, K. D., RANEY, S. G., SEKIROV, L., CHIKH, G., DEJONG, S. D., CULLIS, P. R. & TAM, Y. K. 2007. Effects of intravenous and subcutaneous administration on the pharmacokinetics, biodistribution, cellular uptake and immunostimulatory activity of CpG ODN encapsulated in liposomal nanoparticles. *International Immunopharmacology,* 7**,** 1064-1075.

WONG, H., RAUTH, A., BENDAYAN, R., MANIAS, J., RAMASWAMY, M., LIU, Z., ERHAN, S. & WU, X. 2006a. A new polymer-lipid hybrid nanoparticle system increases cytotoxicity of doxorubicin against multidrug-resistant human breast cancer cells. *Pharmaceutical Research,* 23**,** 1574-1585.

WONG, H. L., BENDAYAN, R., RAUTH, A. M. & WU, X. Y. 2006b. Simultaneous delivery of doxorubicin and GG918 (Elacridar) by new polymer-lipid hybrid nanoparticles (PLN) for enhanced treatment of multidrug-resistant breast cancer. *Journal of Controlled Release,* 116**,** 275-284.

WONG, H. L., BENDAYAN, R., RAUTH, A. M., XUE, H. Y., BABAKHANIAN, K. & WU, X. Y. 2006c. A mechanistic study of enhanced doxorubicin uptake and retention in multidrug resistant breast cancer cells using a polymer-lipid hybrid nanoparticle system. *Journal of Pharmacology and Experimental Therapeutics,* 317**,** 1372-1381.

YUN, Y. H., LEE, B. K. & PARK, K. 2015. Controlled drug delivery: Historical perspective for the next generation. *Journal of Controlled Release,* 219**,** 2-7.

ZENG, L., XIN, X. & ZHANG, Y. 2017. Development and characterization of promising Cremophor EL-stabilized o/w nanoemulsions containing short-chain alcohols as a cosurfactant. *RSC Advances,* 7**,** 19815-19827.

ZHANG, L., CHAN, J. M., GU, F. X., RHEE, J.-W., WANG, A. Z., RADOVIC-MORENO, A. F., ALEXIS, F., LANGER, R. & FAROKHZAD, O. C. 2008. Self-assembled lipid−polymer hybrid nanoparticles: A robust drug delivery platform. *ACS Nano,* 2**,** 1696-1702.

ZHANG, L., ZHU, D., DONG, X., SUN, H., SONG, C., WANG, C. & KONG, D. 2015. Folate-modified lipid-polymer hybrid nanoparticles for targeted paclitaxel delivery. *International Journal of Nanomedicine,* 10**,** 2101-2114.

ZHAO, P., WANG, H., YU, M., LIAO, Z., WANG, X., ZHANG, F., JI, W., WU, B., HAN, J., ZHANG, H., WANG, H., CHANG, J. & NIU, R. 2012. Paclitaxel loaded folic acid targeted nanoparticles of mixed lipid-shell and polymer-core: In vitro and in vivo evaluation. *European Journal of Pharmaceutics and Biopharmaceutics,* 81**,** 248-256.

CHAPTER 3

This chapter covers the preparation and characterisation of the nanoparticles, Pheroid® vesicles and the NP-Pheroid hybrid system. This work was accepted and published in the peer reviewed journal, *Journal of Material Science*. See the following cover page. The guidelines for authors for this journal are given in annexure B of this thesis.

The aims of this chapter were:

a) To explore various methods of preparing the NP-Pheroid® hybrid system.

b) To determine the physicochemical properties of the NP-Pheroid® hybrid system using various techniques.

The fabrication and characterization of a PLGA nanoparticle–Pheroid® combined drug delivery system

Madichaba P. Chelopo, Lonji Kalombo, James Wesley-Smith, Anne Grobler & Rose Hayeshi

Journal of Materials Science
Full Set - Includes `Journal of Materials Science Letters'

ISSN 0022-2461
Volume 52
Number 6

J Mater Sci (2017) 52:3133-3145
DOI 10.1007/s10853-016-0602-4

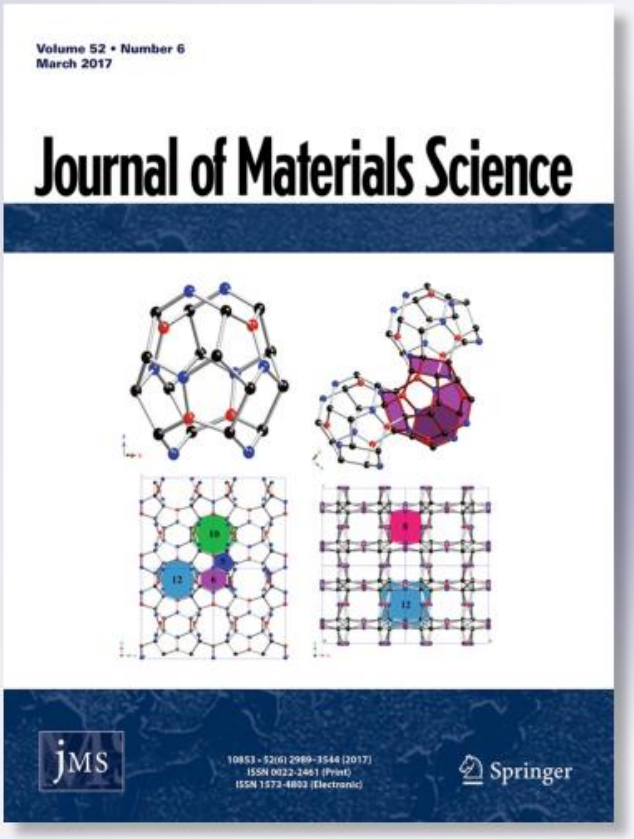

Springer

CHAPTER 3: THE FABRICATION AND CHARACTERIZATION OF PLGA NANOPARTICLE-PHEROID® COMBINED DRUG DELIVERY SYSTEM

Journal: *Journal of Material Science (JMSC-D-16-05272)*

Madichaba P Chelopo[a,b*], Lonji Kalombo[a], James Wesley-Smith[c], Anne Grobler[b], Rose Hayeshi[b]

[a] Council for Scientific and Industrial Research, Materials Science and Manufacturing, Polymers and Composites, PO Box 395, Pretoria, 0001, (South Africa)

[b] North-West University, DST/NWU Preclinical Drug Development Platform, Potchefstroom, 2520

[c] Council for Scientific and Industrial Research, DST/CSIR National Centre for Nanostructured Materials, PO Box 395, Pretoria, 0001

* Corresponding author: MChelopo@csir.co.za; Tel: +27 12 841 4603†

1. Abstract

The combination of polymeric nanoparticles (NPs) as a core, and lipid vesicles as a shell has emerged to be a robust and promising drug delivery strategy. This study explores the development of a novel combined delivery system where poly *d,l,* lactic-*co*-glycolic acid (PLGA) NPs are entrapped within Pheroid® drug delivery system. The solid NPs were combined with the Pheroid® vesicles using two different methods: pre-mix and post-mix. The surface properties of the PLGA NPs were altered through the inclusion (pos-NPs) and exclusion (neg-NPs) of chitosan (CT) and polyethylene glycol (PEG), to evaluate their interaction with the Pheroid® vesicles. The average particle size of the novel NP–Pheroid® combined system ranged from approximately 1990 nm to 2450 nm while the zeta potential (ZP) ranged from -18 to -30 mV, measured using dynamic light scattering (DLS) and electrophoretic velocity techniques, respectively. The NP/Pheroid® mixing ratio experiment indicated that a maximum of 2.5 % (w/v) NPs can be optimally added to the Pheroid® vesicles without compromising the structure and the stability of the NP- Pheroid® combined system. Visual analysis of this system was done through transmission electron microscopy (TEM), cryogenic (cryo) TEM and confocal laser scanning microscopy (CLSM) techniques to obtain adequate information of this novel combined drug delivery system which includes the localization of the PLGA NPs with the Pheroid® vesicles.

2. Introduction

The recent emergence of combined drug delivery systems has become an attractive approach in transporting various therapeutic actives. This strategy allows one to get the most out of the unique attributes that each delivery technology provides. The integration of lipid-based and polymeric nanoparticle (NP) systems, where a drug-loaded polymeric NP is entrapped within a lipid shell system to form lipid-polymeric NPs hybrid (LPNH) systems, has been widely investigated (Zhang *et al*., 2008, Raemdonck *et al*., 2013). Biodegradable poly *d*,*l*-lactic-co-glycolic acid (PLGA) is a common type of polymeric material used in these systems while liposomes are usually used as the lipid component of these LPNH systems (Hadinoto *et al*., 2013, Raemdonck *et al.*, 2013). Unlike previous studies, a lipid-based Pheroid® technology will be explored in this study instead of the conventional liposomes. This technology has been shown to have some superior properties compared to liposomes (Saroj *et al.*, 2012, Uys, 2006). For example, Pheroid® particles consist of essential fatty acids which can easily be metabolised by the cell rather than synthetic or modified lipids and have also shown the ability to enhance the absorption and efficacy of various drugs (Grobler, 2008). In a comparison study, Slabbert *et al*., showed that Pheroid® vesicles are more stable than liposomes and that their membrane is stably maintained without the addition of cholesterol (Slabbert *et al*., 2011). The stability of the Pheroid® is confirmed by the fact that it can deliver drugs through various administration routes including the most preferable oral route, which widens its applications, while most lipid-based systems are generally taken intravenously (Uys, 2006).

Previous research has indicated that the entrapment of orally administered drugs in Pheroid® vesicles improved their pharmacokinetic properties (Grobler, 2008, Nieuwoudt, 2009). However, drugs encapsulated within PLGA NPs resulted in their slow release which led to reduction of drug dosage for an improved disease therapy (Pandey *et al*., 2003, Semete *et al*., 2012). Thus, the combination of these two unique systems can result in increased gastrointestinal uptake of PLGA NPs, attributed by Pheroid® vesicles and this can then be followed by a prolonged release of drugs owing to a slow kinetic of degradation of PLGA. This strategy will ultimately amplify the pharmacokinetic properties of the drug with better curing rate. Researchers have stressed that while polymeric NPs are structurally more stable and are able to slowly release drugs (Soppimath *et al*., 2001, Hans and Lowman, 2002), lipid systems are known to be more biocompatible in the body due to their similarities with biological membranes (Torchilin, 2005). The LPNH systems already reported have shown

remarkable properties because of the combined effect of the two unique systems and have therefore resulted in improved efficacy of the encapsulated drug compared to those within the individual systems (Zhang *et al*., 2008, Mufamadi *et al*., 2011). However the combined PLGA NP-Pheroid® system possesses a structural difference to the LPNH in that instead of an individual PLGA NP, multiple PLGA NPs form the hydrophobic polymeric core covered by the Pheroid® lipid layer.

In this study, the feasibility of entrapment of PLGA NPs in lipid-based Pheroid® vesicles was explored as a potential basis for a novel drug delivery system. The physicochemical characterization of this combined system will be covered similar to some previous studies that have demonstrated the physical properties of combining gold NPs with liposomes as a useful tool for potential drug delivery (Park *et al*., 2006, Sau *et al*., 2009). The efficiency of combining the NPs with the Pheroid® vesicles was investigated by altering the surface charge of the NP using a cationic and mucoadhesive polymer, chitosan (CT), as well as the stealth polymer, polyethylene glycol (PEG). This provided the opportunity to explore the mechanism of interaction and the optimal method of combining the two systems to potentially develop a novel combined drug delivery system. The successful entrapment of the NPs within the Pheroid® was determined using physicochemical characterization which includes various microscopy analyses.

3. Experimental

3.1. Materials

All chemicals and solvents were obtained from Sigma-Aldrich Products (South Africa) except for the following: Pluronic® F127 and Kolliphor were from BASF AG (Ludwigshafen, Germany), stearic acid from Merck (South Africa); Surfynol 104 PG 50 was obtained from Air Products (Kempton Park, South Africa); chitosan was purchased from Fluka Air Products (South Africa). Vitamin F ethyl ester was obtained from Chemisches Laboratorium (Germany); *d,l*-α-Tocopherol was supplied by Chempure (Germiston, South Africa) and medicinal nitrous oxide (N_2O) was from Afrox, (Klerksdorp, South Africa).

3.2. Preparation of PLGA NPs

PLGA (*d,l* 50:50) was dissolved in ethyl acetate (EA) at a concentration of 15 mg/ml, a drop of Surfynol and 0.2% stearic acid (in EA) were added as soon as PLGA dissolved. The resulting solution was mixed with 1% (w/v) Pluronic® F127 in deionised water and homogenised on ice for 3 min at 5000 rpm using a high-speed Silverson L4R homogeniser (Silverson Machines Limited, Buckinghamshire, United Kingdom). The resulting water-in-oil (w/o) emulsion was added to an aqueous solution composed of 2% (w/v) polyvinyl alcohol (PVA) and 5% (w/v) lactose monohydrate for negatively charged nanoparticles (neg-NPs), whereas for positively charged nanoparticles (pos-NPs), the aqueous solution contained 0.3% (w/v) CT and 1% (w/v) PEG in addition to PVA and lactose. The mixture was further homogenised for 5 min on ice at 8000 rpm. This water-in-oil-in-water (w/o/w) double emulsion was fed into a Bench top Buchi Mini B-290 spray dryer (BÜCHI Labortechnik AG, Flawil, Switzerland) to produce solid NPs. Fluorescently labelled PLGA NPs were also prepared by adding coumarin 6 (C6) to the solution of PLGA in EA solution followed by the above procedure. The excess C6 on the outer layer of the NPs was removed by washing these NPs prior to the combination with the Pheroid® vesicles to avoid any possible leakage. These NPs were washed and freeze-dried before use.

3.3. Preparation of Pheroid® vesicles

Water phase saturated with N_2O was heated to 70 °C. The oil phase composed of 2.8% (w/w) Vitamin F ethyl ester and 1% (w/w) Kolliphor, was also heated to 70 °C. The oil phase constituents were cooled to 55 °C and 0.2% (w/w) *d,l*-α-Tocopherol was added. The oil phase was added to the water phase and immediately homogenised using a Heidolph Diax 600 homogenizer, (Heidolph, Germany) set at 13 500 rpm for 4 min while monitoring the temperature to a minimum of 40 °C. The batch was then shaken overnight on an orbital shaker at a speed of 150 rpm at room temperature.

3.4. Combination of PLGA NPs with Pheroid® vesicles

Two methods, pre-mix and post-mix, were explored for combining the polymeric PLGA NPs and the lipid-based Pheroid® vesicles. The same procedure for manufacturing Pheroid® vesicles was followed in both instances. The amount of NPs in the Pheroid® vesicles was kept constant at 1% (w/v) (10 mg/ml) for these combination experiments. In the post-mix method,

the preformed PLGA NPs and preformed Pheroid® vesicles were combined using a low-energy vortex approach, to obtain the NP-Pheroid® mixture (Figure 1A). The pre-mix method involved the addition of NPs to the oil-phase, which was subsequently added to the N_2O-gassed water and both phases mixed through the homogenisation process (Figure 1B). The mixtures obtained from both methods were shaken overnight at room temperature at a speed of 150 rpm to give NP-Pheroid® combined system.

3.5. NP/Pheroid® mixing Ratio

The NP/Pheroid® mixing ratio was investigated by varying the amount of NPs between 10 and 100 mg/ml (1-10 % w/v) to Pheroid® vesicles using the post-mix approach to prepare NP–Pheroid® vesicles.

3.6. Size, distribution, and zeta potential measurements

The hydrodynamic size and polydispersity index (PDI) of the solid NPs were determined using dynamic light scattering (DLS) while their zeta potential (ZP) was measured by the electrophoretic mobility (laser Doppler velocity) method, both using a Zetasizer Nano ZS (Malvern Instruments Ltd., United Kingdom). To determine the size, PDI and ZP measurement, the NPs were dispersed in distilled water at approximately 5 mg/ml. The free Pheroid® and NP-Pheroid® vesicles were diluted 100 times in distilled water and were analysed for size and distribution using a laser diffraction technique on a Mastersizer (Malvern Instruments Ltd., United Kingdom).

3.7. Microscopy

A field emission scanning electron microscope (Zeiss Auriga FEG SEM, Germany) was used to evaluate the morphology of the NPs. Pos-NPs were thinly placed on conductive carbon tape and subsequently coated with gold to ensure proper grounding to avoid charging artefacts.

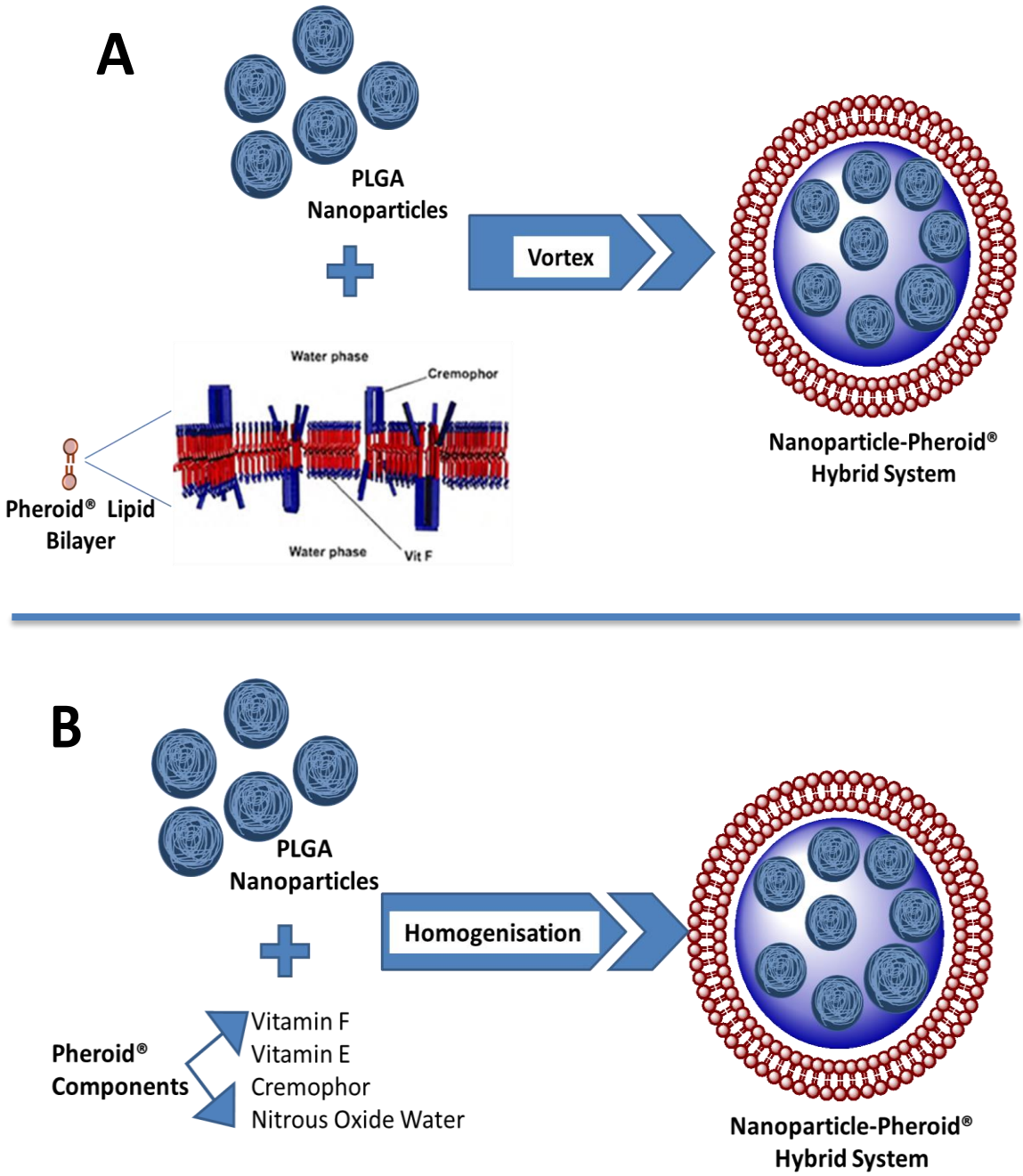

Figure 1: The illustration of two combination methods for Pheroid® and NPs and the hypothetical structure of the NP-Pheroid® combined system. (A) Post-mix method, where preformed Pheroid® lipid vesicles are combined with the preformed PLGA NPs through vortex. (B) Pre-mix method, the pre-formed NPs are added to the oil phase constituents of the Pheroid® and the N_2O saturated water though homogenisation.

Confocal laser scanning microscopy (CLSM) images were taken using a Nikon D-Eclipse C1 system (Nikon, Japan). Nile Red (5 µl) was added to 50 µl of the free-Pheroid® or C6 NP–

Pheroid® vesicles. The mixture was briefly vortexed and then stored in the dark for 5 min. A drop of the mixture was mounted on glass slides with a cover slip and imaged.

Transmission electron microscopy (TEM) was used to characterise free-Pheroid® and NP–Pheroid® vesicles using a JEOL JEM 2100 microscope (JAPAN). Several sample preparation variables were explored, to optimise contrast and identify possible drying artefacts. In a cryo-TEM approach, samples stained with 2% (w/v) uranyl acetate (UA) were thinly spread on carbon-coated grids, rapidly plunged into liquid nitrogen (LN_2)-cooled propane, and imaged at ≤ 140°C using a cryogenic-holder. In an alternate procedure, the samples on the grids were imaged at a room temperature (RT TEM) after subjection to air drying. Two methods of increasing contrast were explored on the RT TEM: samples were either negatively stained with 2% (w/v) uranyl acetate (UA) or exposed to 0.5% (w/v) osmium tetroxide (OsO4). In both instances, excess solution was immediately blotted dry to remove excess stain and rapidly air-dried prior to imaging.

4. Results

4.1. Preparation and characterization of PLGA NP and Pheroid® individual systems

The nanoparticle (NP) surface charge was varied by including or excluding CT and polyethene glycol (PEG). Neg-NPs (exclude PEG and CT), had smaller particle sizes compared to the pos-NPs (include PEG and CT). Both NPs had a similar size distribution (PDI) of approximately 0.250. Their zeta potentials (ZP) were consistent with their expected surface charge of -22 and +26 mV for the neg-NP and pos-NP respectively (Table 1). Unlike PLGA NPs, free Pheroid® vesicles naturally possess a negative ZP that averaged -22 mV and their wide range of sizes was denoted by the large PDI value (> 0.75) with an average size of about 2280 nm (Table 2 and 3). This average size of the Pheroid® system is the volume-weighted mean, calculated from three main size populations ranges of d (0.1) at ≈300 nm, d (0.5) at ≈1500 nm and d (0.9) at ≈4000 nm, where d (0.1), d (0.5) and d (0.9) indicate the 10^{th}, 50^{th} and 90^{th} percentile of the Pheroid® vesicles confirming the large-size distribution (Grobler *et al*., 2014).

Table 1: The average size, polydispersity index (PDI) and zeta potential (ZP) of the negatively (Neg-NPs) and positively charged NPs (Pos NPs).

	Neg-NPs	Pos-NPs
Average Size (nm)	214 ± 2	301 ± 7
Polydispersity Index	0.247 ± 0.02	0.263 ± 0.03
Zeta Potential (mV)	-22 ± 3	26 ± 2

4.2. Preparation and characterization of combined PLGA NP-Pheroid® system

The size and zeta potential (ZP) of the NP-Pheroid® combined systems were compared with the free Pheroid® vesicles. Table 2 shows the sizes and ZP of the neg-NPs (1% w/v) entrapped within the Pheroid® using both the pre-mix and the post-mix method. The average size of the NP-Pheroid® vesicles did not deviate significantly ($P > 0.05$) from the free Pheroid® vesicles when combined with neg-NPs using either the pre-mix or post-mix methods (Table 2). The negative ZP of this system also remained constantly higher (-24 mV) on addition of the neg-NPs using the pre-mix method; however, in the post-mix method, the value shifted to a relatively less negative value (-20.7 mV) from the free vesicles (-23 mV). On the other hand, the combination of pos-NPs (1% w/v) with the Pheroid® vesicles using either the pre-mix or post-mix methods resulted in a significant ($P < 0.05$) particle size increase from the free Pheroid® vesicle size (Table 3). The average size of free Pheroid® increased from 2120 nm to 2500 nm when pre-mix method was used and to 2800 nm when the post-mix method was used. The absolute ZP was lowered using the post-mix method, from -22 to -18 mV while for pre-mix method it slightly dropped to -20.6 mV.

Table 2: The average size, polydispersity index (PDI) and zeta potential (ZP) of the free Pheroid® and NP-Pheroid® system. The pre-mix and post-mix combination methods were used to prepare NP-Pheroid® combined system using 1% (w/v) neg-NPs (without CT and PEG).

Combination Method	Sample	Average Size (nm)	Polydispersity Index	Zeta Potential (mV)
	Free Pheroid®	2280 ± 54	0.764 ± 0.07	-23.7 ± 1.6
Pre-Mix	**NP - Pheroid®**	2314 ± 27	0.868 ± 0.05	-24.6 ± 1.4
Post - Mix	**NP - Pheroid®**	2324 ± 185	0.814 ± 0.14	-20.7 ± 4

Table 3: The average size, polydispersity index (PDI) and zeta potential (ZP) of the free Pheroid® and NP-Pheroid® system. The pre-mix and post-mix combination methods were used to prepare NP-Pheroid® combined system using 1% (w/v) pos-NPs (with CT and PEG).

Combination Method	Sample	Average size (nm)	Polydispersity Index	Zeta Potential (mV)
	Free Pheroid®	2120 ± 103	0.782 ± 0.05	-22.6 ± 0.6
Pre-Mix	**NP – Pheroid®**	2517 ± 74	0.787 ± 0.04	-20.6 ± 0.3
Post-Mix	**NP – Pheroid®**	2858 ± 141	0.963 ± 0.16	-18.1 ± 0.5

4.3. Microscopy

Prior to combination, the individual systems were characterised through microscopy (Figure 2). Both SEM and TEM, (Figures 2A and 2B, respectively) illustrate the morphology of the solid NPs. Figure 2C indicates the wide size range of Pheroid® vesicles in their native state observed under optical light microscopy. The TEM images of free Pheroid® vesicles will be shown in the following section in comparison with the combined system.

The entrapment of the NPs within Pheroid® vesicles was demonstrated through confocal laser scanning microscopy (CLSM). The Pheroid® vesicles were stained with Nile red (excitation

488 nm emission 515 nm), which emits red fluorescence, while coumarin 6 (C6) (excitation 485 nm, emission 612 nm), encapsulated in the NPs, fluoresces in the green range. Control Pheroid® vesicles images did not exhibit any fluorescence in the green channel (Figure 3A), while there was vivid green fluorescence co-localised with the Pheroid® vesicles for the C6 NP-Pheroid® sample (Figure 3B). There was no green fluorescence observed outside the Pheroid® vesicles which indicates that leakage of the NPs was very unlikely at this mixing ratio. The combination of the red and green channels resulted in orange colour, which further provides evidence for the co-localization of C6 NPs with the Pheroid® vesicles while the colour remained red for the control vesicles.

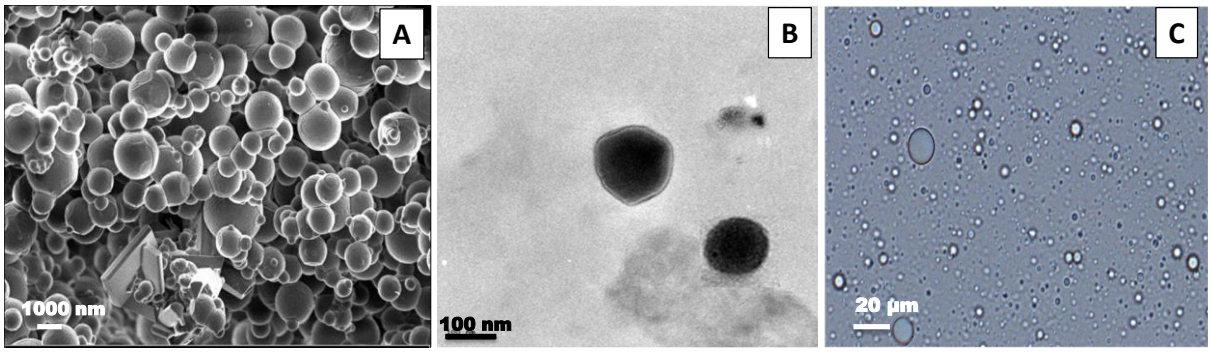

Figure 2: Typical micrographs of PLGA NPs shown by (A) SEM (scale bar= 1 µm) and (B) TEM (scale bar= 0.1 µm). The image of Pheroid® vesicles was viewed using (C) light microscope (scale bar = 20 µm).

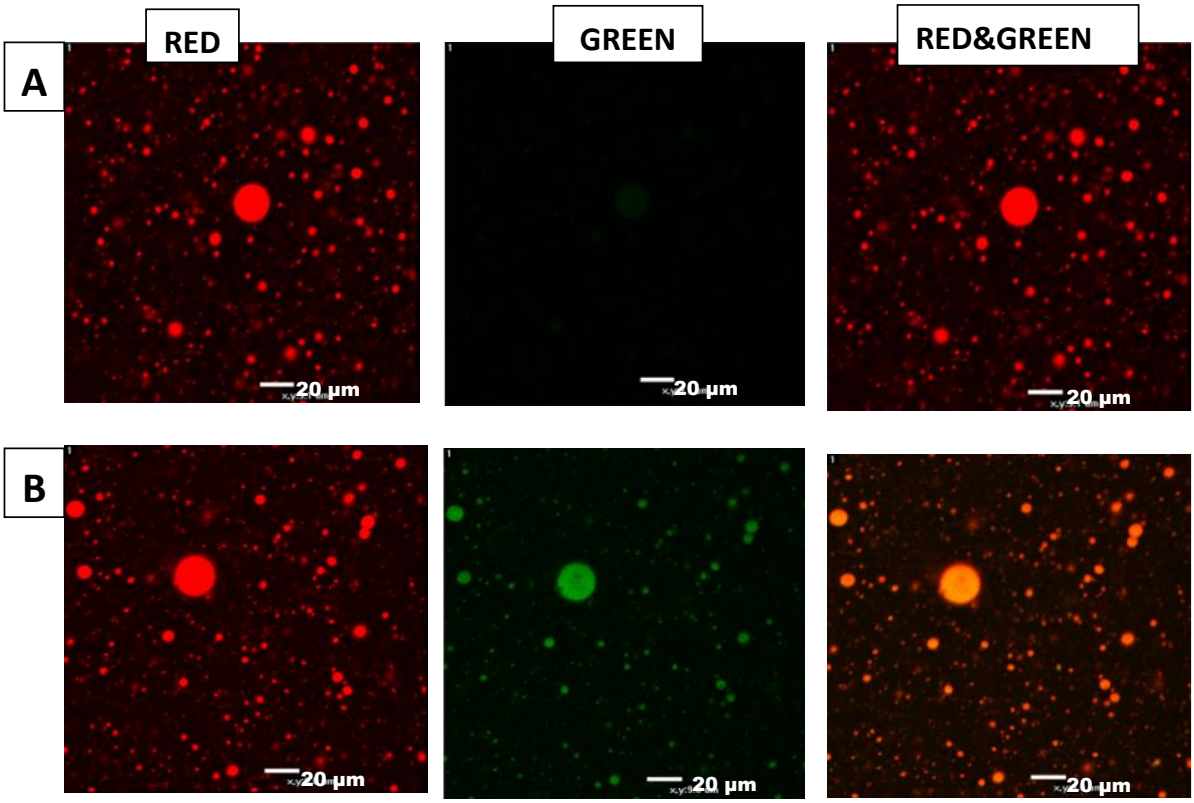

Figure 3: Confocal Images of 1% (w/v) C6 NP (Pos-NPs) combined with Pheroid® vesicles (stained with Nile red) by pre-mix method. Row A: Control Pheroid® vesicles shown in the Red and Green channels and Row B, C6 NP - Pheroid® Vesicles shown in the Red, Green and Red and Green channels. (Scale bars = 20 µm).

In addition to the illumination of optical and laser light to the view the free Pheroid® and the combined NP- Pheroid® system, the TEM techniques were used to visualise them through their interaction with beam of electrons. Cryo-TEM has been extensively used in literature to characterise other liquid-based combined systems (Mandal *et al*., 2013, Hadinoto *et al*., 2013). This method reportedly immobilises liquid emulsions into an electron-transparent vitreous film that minimises the risk of morphological changes that could happen during air drying (Ruozi *et al*., 2011, Bershteyn *et al*., 2008). A typical cryo-TEM image in Figure 4A reflects the wide size range as shown by the Mastersizer technique, optical light and confocal microscopy. However, the contrast between the vesicles and the surrounding area was low and the PLGA NPs could not be seen co-localising with the Pheroid® vesicles. A comparison of cryo-TEM images with air-dried counterparts showed similar Pheroid® size distribution (albeit wide), validating the use of air-drying and RT TEM (Figure 4B). RT TEM generally revealed large free Pheroid® vesicles containing or co-localised with smaller vesicles. OsO_4 predictably

increased the electron opacity of all membranes, as it revealed a thick layer in the lipid membrane of the Pheroid® vesicles (Figure 5B), but occasionally at the expense of visibility (Figure 5A). Negatively-stained (UA stained) Pheroid® vesicles appeared to be more consistent in appearance, and is proposed here to be a superior method to OsO_4 staining (Figure 5C). The combined system visualised after UA staining method resulted in high contrasted images and provided evidence of co-localization of NPs, electron-dense spots, with some of the Pheroid® vesicles (Figure 5D – F).

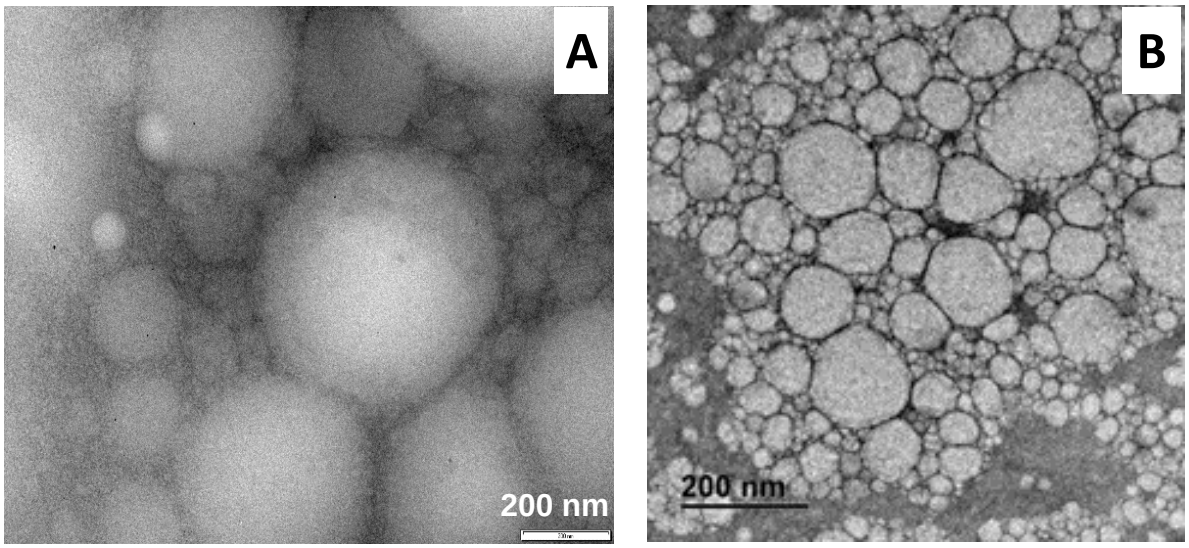

Figure 4: TEM images of free Pheroid® vesicles obtained after (A) Cryogenic method (cryo-TEM) and (B) air dried method (RT TEM). All samples were negatively stained using uranyl acetate (UA) (scale bar = 0.2 μm).

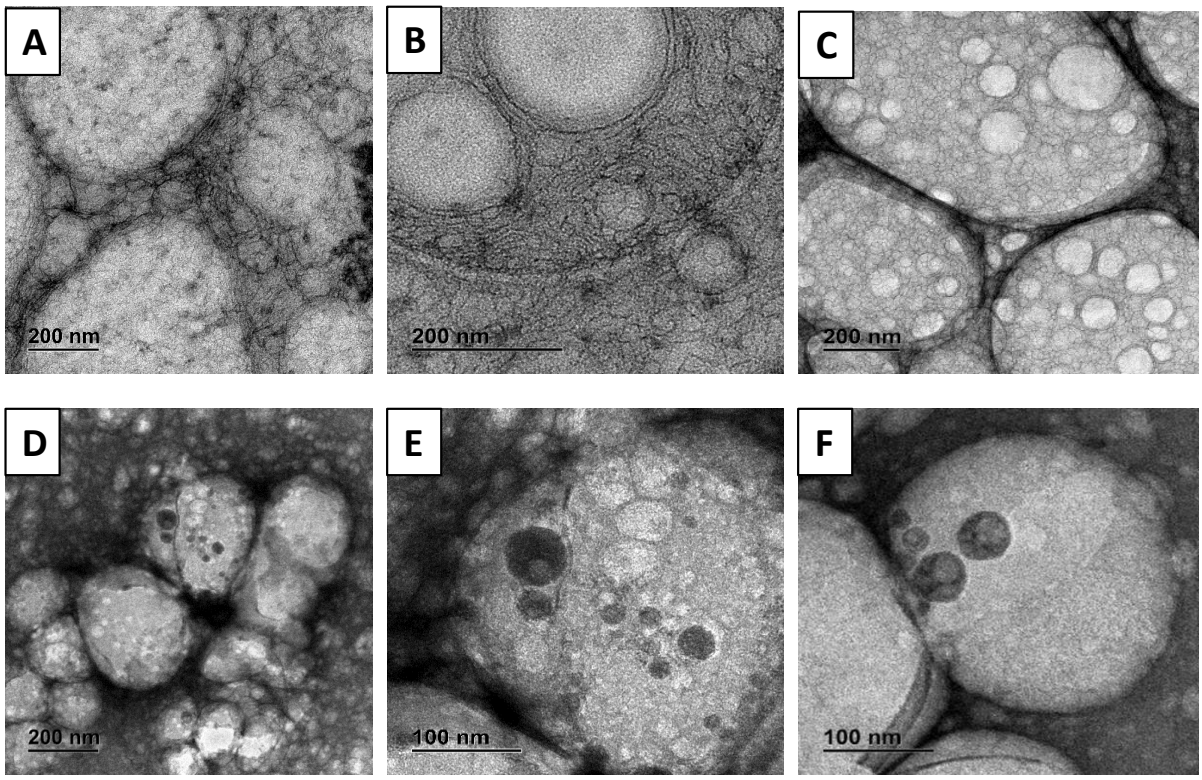

Figure 5: TEM images of neat Pheroid® vesicles: (A-B) Osmium tetraoxide (OsO_4) and (C) Uranyl acetate (UA). The second row images display NP-Pheroid® system (D-F) stained with uranyl acetate (UA) and were prepared using pre-mix method at 1% (w/v) NP (Pos NP).

4.4. NP/Pheroid® mixing Ratio

The increase in the ratio of pos-NPs to Pheroid® vesicles was observed to have an effect on the size and the ZP shown by the column graphs in Figure 6. These pos-NP resulted in the increasing trend of the average size (from approximately 2000 to 14000 nm) while the absolute ZP remained negative with a steady drop from -20 mV of the free Pheroid® vesicles to about -15 mV of the 10% (w/v) NP/Pheroid® ratio. Increasing the ratios of neg-NPs to Pheroid® led to no effect in the size, however, a similar trend in the change of ZP to that of the pos-NPs was observed. The Mastersizer distribution curves shown in Figure 8A illustrate that the distinct change occurs above 2.5% (w/v) of pos-NPs to Pheroid® vesicle with a wider and bi-modal size distribution compared to the free Pheroid® vesicles. The NP/Pheroid® ratio using C6 pos-NPs enabled the visualisation of the effect of varying the NP/Pheroid® ratio on the morphology of the vesicle through confocal microscopy. The confocal images revealed aggregation of vesicles as the ratio increased, from 5% to 10% (w/v) of NP/Pheroid® ratio (Figure 8B). There was also an observed phase separation of Pheroid® vesicles at this high mixing ratio (5% - 10% w/v) which confirmed the instability of the combined system.

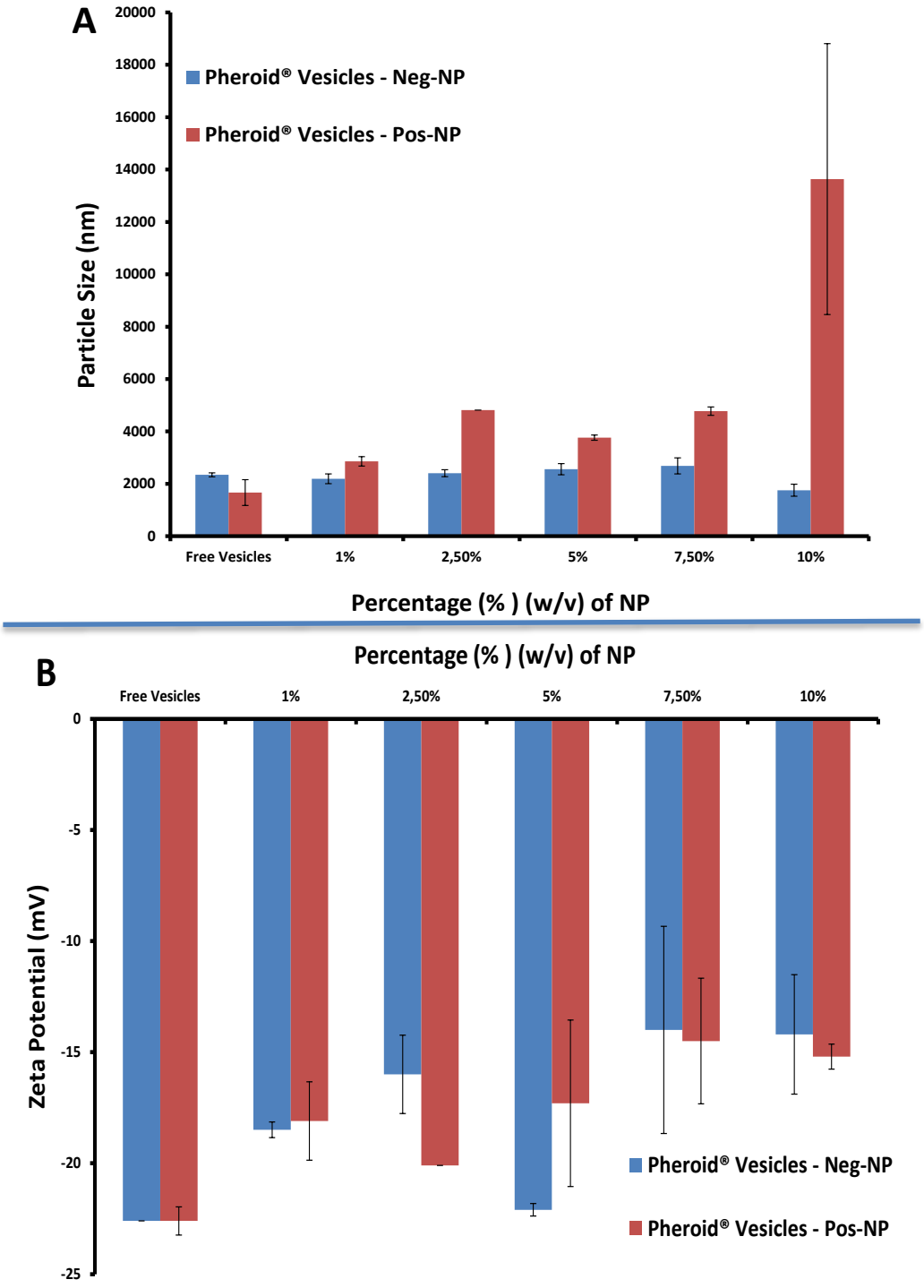

Figure 6: Graphs showing the effect when varying NP/Pheroid® mixing ratio using neg-NPs (without CT and PEG) and pos-NPs (with CT and PEG) on the (A) Particle size and (B) Zeta Potential (ZP).

5. Discussion

5.1. Preparation and characterization of PLGA NPs and Pheroid® individual systems

PLGA NPs were prepared using a modified double-emulsion method and were subsequently dried using a spray drying technique. This method is known to yield reproducible and high-quality NPs (Sollohub and Cal, 2009). The variation of the excipients in the NP formulations was done to produce either pos-NPs or neg-NPs in the anticipation of understanding their mechanism of interaction with the Pheroid® vesicles. The pos-NPs had a larger particle size (301 nm ± 7) than the neg-NPs (214 nm ± 2) due to the additional coating of the CT and PEG excipients onto the surface of these NPs leading to a general positive ZP of the NPs. The biological advantage of using PEG in the formulation is to increase the *in vivo* residence time of NPs. CT is a cationic mucoadhesive polysaccharide polymer which helps to enhance the uptake of the NPs through the gastrointestinal tract and to further increase their circulation time (Bernkop-Schnürch and Dünnhaupt, 2012). Both CT and PEG have been previously reported to confer a positive ZP to various NPs (Maldiney *et al*., 2011, Chen *et al*., 2013). The spherical shape of the solid NPs, revealed through SEM and TEM imaging (Figure 1A and 1B), is a crucial element that can influence both the *in vivo* pharmacokinetics and cell uptake (Truong *et al*., 2015). However, the average size of NPs on SEM images was observed to be about 1 μm, which does not correlate with the hydrodynamic size, obtained using the DLS method. This larger size has been postulated to be due to the presence of the lactose component on the non-dispersed solid NPs, previously reported to prevent the dimpling of the NPs and shown to contribute to the drying of the NPs (Semete *et al*., 2012). The DLS method measures only the hydrodynamic diameter of the water-dispersed NPs, which is the inner sphere of the polymeric particle, suggesting that the lactose hydration layer has dissolved. The NPs were dispersed in water before TEM characterization, which dissolved the lactose layer, showing the electron-dense, spherically shaped particles, in Figure 1B, that correlated to the NP sizes obtained in the DLS method.

The size measurements method of NP and Pheroid® vesicles were different, because the two systems vary significantly in their size range. The solid NPs (<350 nm) were measured using the dynamic light scattering (DLS) which gave irreproducible results when measuring the Pheroid® vesicles (maximum size of ≈ 4000 nm). The reason for this could be because in the size calculation in DLS, all particles are assumed to be spherical (Klang and Valenta, 2011),

which may not always be the case for Pheroid® system with a PDI that ranged from 0.7 to 0.9. According to Klang *et al.,* a low PDI indicates the property of the system' s resistance to destabilisation (Klang and Valenta, 2011). Although the Pheroid® vesicles have large PDI, they have been established to be more stable compared to some known lipid-based system like liposomes (Uys, 2006). The image in Figure 1C shows that Pheroid® can be large enough to be viewed at low magnification such as optical light microscopy and their wide size range was confirmed by the laser diffraction and the confocal imaging results.

5.2. Preparation and characterisation of the combined PLGA NP-Pheroid® system

In the two methods explored to prepare the combined delivery systems, the post-mix method has traditionally been used, and it is similar to the described two-step method in literature, where the two systems are formed separately and mixed together (Thevenot *et al*., 2007). This method assumes that the lipid bilayer membranes are dynamic in that they engulf the preformed NPs and self-assemble. On the other hand, in the pre-mix method, the preformed solid NPs are assumed to be entrapped within the Pheroid® vesicles simultaneously with the formation of the lipid membrane. This pre-mix method is a combination method similar the reported single-step method, which involves the simultaneous formation of the polymeric NPs with the liposomes in one-step process (Hadinoto *et al*., 2013), with slight modification.

The observed trends in the change of average size and ZP when combining various NPs with Pheroid® (Table 1 and 2) are converted into percentage change (Δ) illustrated in Figure 7. The NP- Pheroid® combined systems with neg-NPs prepared using either pre- or post-mix led to statistically non-significant change in size ($P > 0.05$) from the free Pheroid® vesicles. Pos-NPs led to statistically significant increase in the size of the combined system prepared using both the pre-mix ($P = 0.005$) and post-mix ($P = 0.001$) methods at 95% confidence intervals using an unpaired Students *t*-test.

An increase in size of the control Pheroid® vesicles could suggest successful incorporation of the NPs within the vesicle, or optimal combination of these two systems. Interestingly, the minimal or no change in size observed when neg-NPs are added to the Pheroid® (which are also negatively charged) suggests that the two systems are not adhering optimally to form the NP-Pheroid® combined system. The observed difference in size change between the neg-NPs and pos-NPs may also suggest that electrostatic forces could influence the interaction between Pheroid® and NPs. We furthermore stipulate that a vesicle entrapping positive NPs could be

the centre of electrostatic attraction of oppositely charged vesicles in its vicinity leading therefore to a possible fusion of few droplets that could result in the observed increase of particles size. The combination of the Pheroid® vesicles (-22 mV), with the pos-NPs, (+26 mV) resulted in a general negative ZP (-19 mV) of the combined system. The ZP is highly negative enough to impart an electrostatic repulsion between Pheroid® vesicles to prevent their aggregation. This may imply that the positively charged NPs have been entrapped within the Pheroid® and that the combined system remains relatively stable. Therefore for all the microscopy experiments, pos-NPs (1% w/v) were combined with the Pheroid® vesicles using the pre-mix method. It has been reported that such a method leads to an increased encapsulation of the NPs which makes it more efficient than the two-step method (Mandal *et al*., 2013). However, the same trend of change (Δ) for both the pre-mix and the post-mix method was observed when, mixed with pos-NPs, although the post-mix attributed to the larger change in size (39%) and ZP (18%). Therefore, the post-mix method was used for the NP/Pheroid® mixing ratio experiment, because of its practical flexibility for use at small-scale.

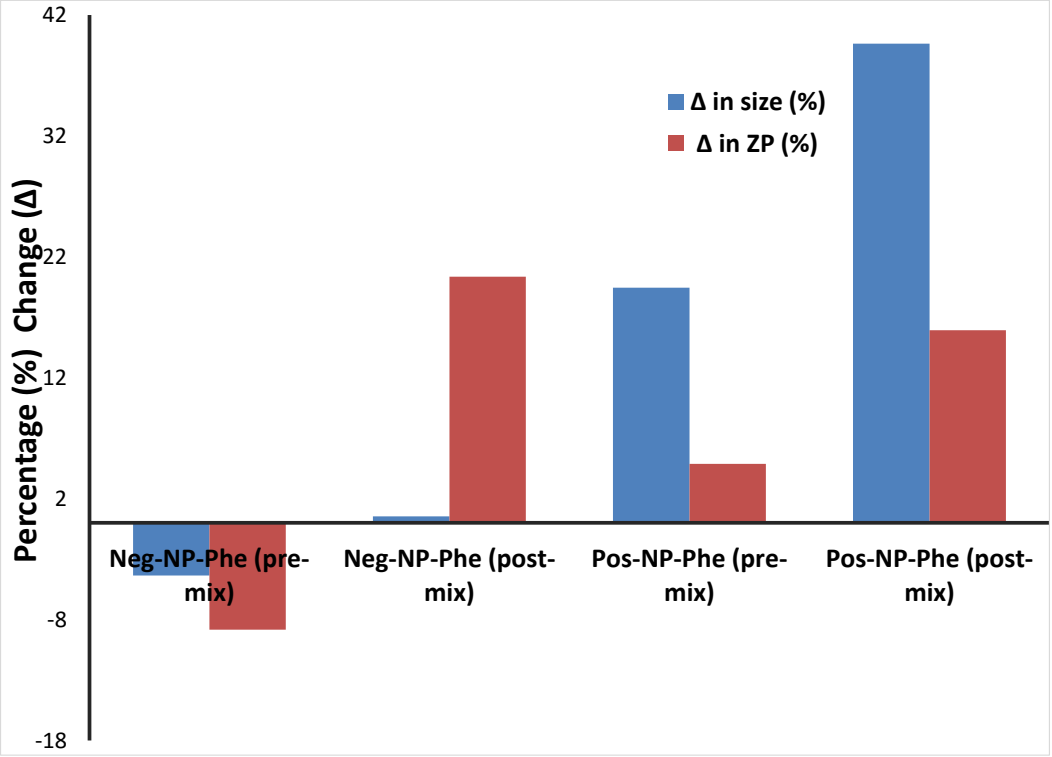

Figure 7: The percentage change in Size and ZP when 1% (w/v) of neg-NPs and pos-NPs are used to form the combined system.

5.3. Microscopy analysis

The CLSM technique showed the co-localization of the green fluorescent C6 NPs with the Nile red-stained Pheroid® vesicles, further suggesting that NPs could be entrapped within the vesicles (Figure 5). This observation is unlike the findings by Ruozi *et al.* who demonstrated that a fluorescent dye, rhodamine 123, was localised in the bilayer structures providing more detailed architecture of the liposomes (Ruozi *et al*., 2011). The only drawback with confocal microscopy in this study is that it did not provide the organisational details of the lipid at the particles surface because of its optical resolution limitations. However, it provided valuable information on the morphology of the Pheroid® in its native nature without exposure to the electron beam in EM technique.

Given that this is a novel combined drug delivery system, it was crucial to obtain sufficient information about its physicochemical properties and its stability. Another essential microscopically analysis of the combined system with pos-NPs was done through an electron optical technique (TEM). Due to the wide range of size of the Pheroid®, it was aimed that Pheroid® vesicles in the size range of >500 nm where NPs (≈300 nm) can potentially occupy and be visualised. However, it was difficult locating these polymeric NPs within the low contrasted images of the vesicles obtained from the cryo-TEM method. Some previous work on lipid-NP combined systems analysed using cyro-TEM have portrayed perfectly enveloped NPs within a lipid shell which were more uniform sized (Bershteyn *et al*., 2008, Mornet *et al*., 2004).

The poor contrast of the typical cryo-TEM images with dark field area at the top left of the image indicating the boarder of illumination caused by the varying intensity of the electron beam (Figure 4A), was postulated to either result from instrumental method set up or errors in sample preparation. The high electron acceleration voltage of 200 kV was used in order to provide high resolution of the images however according to Kuntsche *et al*, a high voltage has been found to lead to poor contrast because of low electron scattering (Kuntsche *et al*., 2011). The other reason could have been the inadequate thickness of the vitrified sample film during preparation, which is said to be greatly difficult to obtain (Belkoura *et al*., 2004). Friedrich *et al.,* also reported a similar image that was obtained with a low-intensity electron beam to remove a hexagonal ice in an image that appears as a particulate material (Friedrich *et al*., 2010, Bouchet-Marquis and Hoenger, 2011). With all these mentioned cryo-TEM artefacts, this method provided a new visual perspective regarding the morphology of Pheroid® vesicles at the microscopic level which has not been done before.

Conventional RT TEM is not a popular method to view lipid-based emulsion samples due to the air-drying step during sample preparation that could potentially compromise morphology of the lipids membrane structure. However, Klang *et al.,* has demonstrated that this technique can be used as an essential tool to characterise nanoemulsions (Klang and Valenta, 2011), which is not common in literature. In the present study, Pheroid® morphology was similar following cryo-TEM and RT TEM imaging, justifying the use of RT imaging as a more convenient and artefact-free option, Figure 4A-B. The overall appearance of the uranyl acetate negative staining was preferable to OsO_4 as a contrasting procedure. In the UA staining method, it is likely that the high affinity of uranyl ions to carboxyl groups of glycoproteins lipids in the vesicle membrane may have contributed to the high contrast attained (Leica, 2013). However, OsO_4 is known to interact with the double bond of the unsaturated fatty acid (Vitamin F) making up the vesicle membrane (StainFile, 2015). The images of vesicles from this OsO_4 method gave a deeper insight into the membrane bilayer of the Pheroid® vesicle. The broader width of the membrane observed could convey that there is more than one lipid bilayer of the vesicles (Figure 5B). However, this visible thick membrane seen from this staining method could also be a possible artefact caused by the loss of water from the Pheroid® during the air-drying step of the sample preparation.

Another shortcoming to this staining method was that the NPs could not be located in the obtained NP-Pheroid® images. Given the fact that these electron micrographs for this novel NP/Pheroid® combined system are the first to be reported it was important to show all the various qualities of the images from each technique to show its potential as well as its limitations. Images in Figure 5D-F show the magnified image of Pheroid® vesicles stained using UA, populated with a number of electron-dense particulates that are spherically shaped which appears to be PLGA NPs, with reference to Figure 2B. While the sizes of the NPs localised with the Pheroid® vesicles in TEM appear to be smaller than measurements obtained from DLS, one must bear in mind that in the latter a far greater number of vesicles are sampled compared to microscopy. The direct comparison of particle sizes obtained from DLS and TEM is sometimes not recommended due to the complexity of sample preparation in TEM which may result in the various sizes (Klang and Valenta, 2011). This therefore implies a possible co-localization of NPs with some large Pheroid® vesicle sizes, with a clear contrast between the two structures that can be clearly demonstrated through conventional RT TEM.

5.4. NP/Pheroid® mixing Ratio

This experiment was done to study the effect of varying the NP/Pheroid® ratio on the size and the ZP of the combined system. Since the pre- and post-mix methods gave comparable trends when combining 1% (w/v) of the pos-NPs to the Pheroid® vesicles, the post-mix method was chosen due to its flexibility and the capability to allow small-scale experiments set up unlike the pre-mix method. Figure 6A shows that the average size of vesicles remained relatively constant when increasing the ratio of neg-NPs to Pheroid®, while the size increased when the pos-NPs were added confirming the trend as illustrated in Figure 7. This observed change according to the NP surface charge suggest that the inclusion of CT and PEG in the NPs' formulation alters their interaction with the Pheroid® vesicles in this combined system. This increase in the NP/Pheroid® ratio leads to a steady drop in absolute ZP for both the neg-NPs and pos-NPs to Pheroid® vesicles supporting the decrease in stability of the combined system at high mixing ratios (Figure 6B). Bershteyn *et al.*, has previously reported the effect of varying the lipid-polymer mixing ratio by changing the amount of lipid rather than the amount of the NPs (Bershteyn *et al*., 2008). They demonstrated that increasing the amount of the lipid component led to multilamellar stacks of lipid surrounding the polymer and these stacks of lipid differed in their morphology depending on the lipid charge using cryo-TEM (Bershteyn *et al*., 2008). The described change in the arrangement of lipids structure implied some degree of influence on the stability of the combined system which can then be compared to the effect of changing the amount of NPs with various charges (neg-/pos-) to the Pheroid® vesicles.

CLSM images in Figure 8A show agglomeration of the vesicles from 5% (w/v) of pos-NPs to Pheroid® ratio, and that the agglomeration increased at 10% (w/v) ratio. This agglomeration can be attributed to the loss of stability. Increasing the NP/Pheroid® ratio using pos-NPs resulted in wider size distribution curves, with a notable population in the 200-400 nm size range corresponding to free excess NPs. This effect is also visible from 5% to 10 % (w/v) NP/Pheroid® ratio, confirming the CLSM results. Therefore the Mastersizer distribution curves and confocal images both indicate that a maximum of 2.5 % (w/v) NPs can be optimally added to the Pheroid® vesicles without compromising the structure and the stability of the NP-Pheroid® combined system. For future studies, it would be worth exploring how one can increase the amount of NPs, beyond the 2.5% w/v ratio, but still maintain the stability of the combined system.

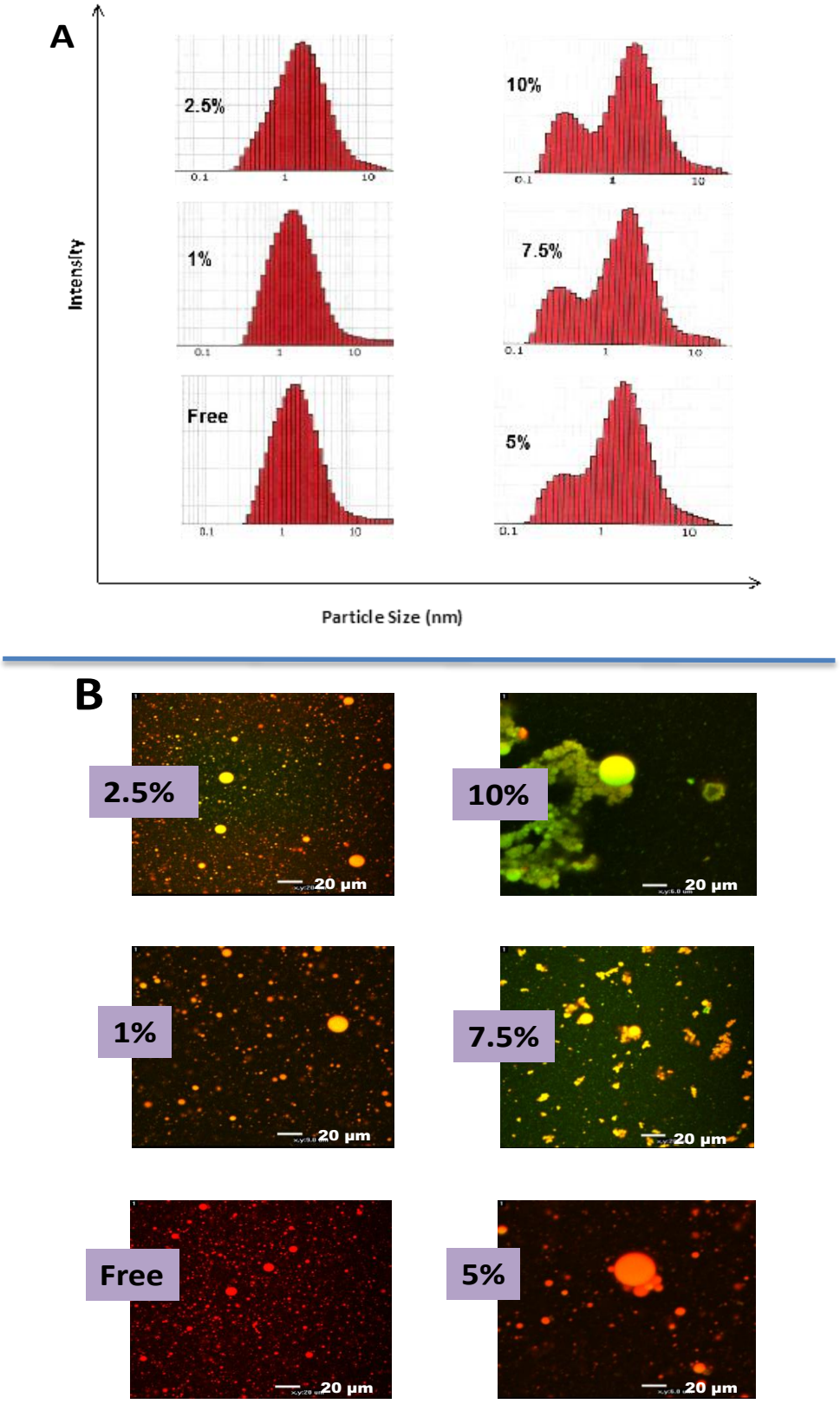

Figure 8: (A) The size distribution curves of the Pheroid® vesicles with an increasing amount of pos NPs in percentages (% w/v) and (B) The confocal images of Pheroid® vesicles with varying ratios of C6 pos-NPs (Scale bars = 20 µm).

6. Conclusions

The fabrication of a novel PLGA NP-Pheroid® delivery system where the NP core is entrapped within the Pheroid® vesicle shell proved to be successful, through visual analysis using both TEM and confocal microscopy. The combination of the pos-NPs and Pheroid® vesicles lead to an observed increase in the particle size of the vesicles, which suggests that electrostatic forces can be responsible for the interaction of the two systems. The combined system remains stable with a highly negative ZP, suggesting that the inclusion of CT in the PLGA NPs formulation has a positive effect on its interaction to with the Pheroid® vesicles. RT TEM technique showed no visible signs of drying artefacts compared with cryo-TEM, becoming the imaging method of choice and providing in-depth structural information of the Pheroid® vesicles and the novel combined NP-Pheroid® used in this study. The maximum mixing ratio was determined to be 2.5% (w/v) of NPs to Pheroid®, as beyond this ratio the particle size distribution increased due to non-entrapped NPs as well as morphological disruption of the Pheroid® vesicles observed through confocal imaging, which was also confirmed by the decrease in the ZP in the combined system. These results gave us evidence that the stability of the combined systems is compromised when increasing the amount of NPs to Pheroid® vesicles beyond 5% (w/v) NP/Pheroid® mixing ratio.

6.1. Acknowledgements

The authors would like to thank the National Research Foundation (NRF) and the Department of Science and Technology (DST) for financial support. The authors also thank Dr Matthew Glyn for his technical assistance with the CLSM.

7. References

BELKOURA, L., STUBENRAUCH, C. & STREY, R. 2004. Freeze Fracture Direct Imaging: A New Freeze Fracture Method for Specimen Preparation in Cryo-Transmission Electron Microscopy. *Langmuir,* 20**,** 4391-4399.

BERNKOP-SCHNÜRCH, A. & DÜNNHAUPT, S. 2012. Chitosan-based drug delivery systems. *European Journal of Pharmaceutics and Biopharmaceutics,* 81**,** 463-469.

BERSHTEYN, A., CHAPARRO, J., YAU, R., KIM, M., REINHERZ, E., FERREIRA-MOITA, L. & IRVINE, D. J. 2008. Polymer-supported lipid shells, onions, and flowers. *Soft Matter,* 4**,** 1787-1791.

BOUCHET-MARQUIS, C. & HOENGER, A. 2011. Cryo-electron tomography on vitrified sections: A critical analysis of benefits and limitations for structural cell biology. *Micron,* 42**,** 152-162.

CHEN, M.-C., MI, F.-L., LIAO, Z.-X., HSIAO, C.-W., SONAJE, K., CHUNG, M.-F., HSU, L.-W. & SUNG, H.-W. 2013. Recent Advances in Chitosan-based Nanoparticles for Oral Delivery of Macromolecules. *Advanced Drug Delivery Reviews,* 65**,** 865-879.

FRIEDRICH, H., FREDERIK, P. M., DE WITH, G. & SOMMERDIJK, N. A. 2010. Imaging of Self-Assembled Structures: Interpretation of TEM and Cryo-TEM Images. *Angewandte Chemie International Edition,* 49**,** 7850-7858.

GROBLER, A. F. 2008. *Pharmaceutical applications of Pheroid™ technology.* Doctor of Philosophy in Pharmaceutics, North-West University. https://dspace.nwu.ac.za/handle/10394/6701

GROBLER, L., GROBLER, A., HAYNES, R., MASIMIREMBWA, C., THELINGWANI, R., STEENKAMP, P. & STEYN, H. S. 2014. The effect of the Pheroid delivery system on the in vitro metabolism and in vivo pharmacokinetics of artemisone. *Expert Opinion on Drug Metabolism & Toxicology* 10**,** 313-25.

HADINOTO, K., SUNDARESAN, A. & CHEOW, W. S. 2013. Lipid–polymer hybrid nanoparticles as a new generation therapeutic delivery platform: A review. *European Journal of Pharmaceutics and Biopharmaceutics,* 85**,** 427-443.

HANS, M. & LOWMAN, A. 2002. Biodegradable nanoparticles for drug delivery and targeting. *Current Opinion in Solid State and Materials Science,* 6**,** 319-327.

KLANG, V. & VALENTA, C. 2011. Lecithin-based nanoemulsions. *Journal of Drug Delivery Science and Technology,* 21**,** 55-76.

KUNTSCHE, J., HORST, J. C. & BUNJES, H. 2011. Cryogenic transmission electron microscopy (cryo-TEM) for studying the morphology of colloidal drug delivery systems. *International Journal of Pharmaceutics,* 417**,** 120-137.

LEICA. 2013. EM Sample Preparation Contrasting. Available: www.leica-microsystems.com.

MALDINEY, T., RICHARD, C., SEGUIN, J., WATTIER, N., BESSODES, M. & SCHERMAN, D. 2011. Effect of Core Diameter, Surface Coating, and PEG Chain Length on the Biodistribution of Persistent Luminescence Nanoparticles in Mice. *ACS Nano,* 5**,** 854-862.

MANDAL, B., BHATTACHARJEE, H., MITTAL, N., SAH, H., BALABATHULA, P., THOMA, L. A. & WOOD, G. C. 2013. Core–shell-type lipid-polymer hybrid nanoparticles as a drug delivery platform. *Nanomedicine: Nanotechnology, Biology and Medicine,* 9**,** 474-491.

MORNET, S., LAMBERT, O., DUGUET, E. & BRISSON, A. 2004. The Formation of Supported Lipid Bilayers on Silica Nanoparticles Revealed by Cryoelectron Microscopy. *Nano Letters,* 5**,** 281-285.

MUFAMADI, M. S., PILLAY, V., CHOONARA, Y. E., DU TOIT, L. C., MODI, G., NAIDOO, D. & NDESENDO, V. M. K. 2011. A Review on Composite Liposomal Technologies for Specialized Drug Delivery. *Journal of Drug Delivery,* 2011, 19 Pages.

NIEUWOUDT, L.-M. 2009. *The impact of PheroidTM technology on the bioavailability and efficacy of anti-tuberculosis drugs in an animal model/L. Nieuwoudt.* North-West University. https://dspace.nwu.ac.za/handle/10394/4316

PANDEY, R., ZAHOOR, A., SHARMA, S. & KHULLER, G. K. 2003. Nanoparticle encapsulated antitubercular drugs as a potential oral drug delivery system against murine tuberculosis. *Tuberculosis,* 83**,** 373-378.

PARK, S.-H., OH, S.-G., MUN, J.-Y. & HAN, S.-S. 2006. Loading of gold nanoparticles inside the DPPC bilayers of liposome and their effects on membrane fluidities. *Colloids and Surfaces B: Biointerfaces,* 48**,** 112-118.

RAEMDONCK, K., BRAECKMANS, K., DEMEESTER, J. & DE SMEDT, S. C. 2013. Merging the best of both worlds: hybrid lipid-enveloped matrix nanocomposites in drug delivery. *Chemical Society Reviews,* 43**,** 444-472.

RUOZI, B., BELLETTI, D., TOMBESI, A., TOSI, G., BONDIOLI, L., FORNI, F. & VANDELLI, M. A. 2011. AFM, ESEM, TEM, and CLSM in liposomal characterization: a comparative study. *International Journal of Nanomedicine,* 6**,** 557-563.

SAROJ, S., DONEY ALEX BABY & M, S. 2012. Current trends in liipid based delivery systems and its applications in drug delivery. *Asian Journal of Pharmaceutical and Clinical Research,* 5**,** 4-9.

SAU, T. K., URBAN, A. S., DONDAPATI, S. K., FEDORUK, M., HORTON, M. R., ROGACH, A. L., STEFANI, F. D., RÄDLER, J. O. & FELDMANN, J. 2009. Controlling loading and optical properties of gold nanoparticles on liposome membranes. *Colloids and Surfaces A: Physicochemical and Engineering Aspects,* 342**,** 92-96.

SEMETE, B., KALOMBO, L., KATATA, L., CHELULE, P., BOOYSEN, L. I. J., LEMMER, Y., NAIDOO, S., RAMALAPA, B., HAYESHI, R. & SWAI, H. 2012. Potential of Improving the Treatment of Tuberculosis Through Nanomedicine. *Molecular Crystals and Liquid Crystals,* 556**,** 317-330.

SLABBERT, C., DU PLESSIS, L. H. & KOTZÉ, A. F. 2011. Evaluation of the physical properties and stability of two lipid drug delivery systems containing mefloquine. *International Journal of Pharmaceutics,* 409**,** 209-215.

SOLLOHUB, K. & CAL, K. 2009. Spray Drying Technique: II. Current Applications in Pharmaceutical Technology. *Journal of Pharmaceutical Sciences,* 9999**,** 1-11.

SOPPIMATH, K. S., AMINABHAVI, T. M., KULKARNI, A. R. & RUDZINSKI, W. E. 2001. Biodegradable polymeric nanoparticles as drug delivery devices. *Journal of Controlled Release,* 70**,** 1-20.

STAINFILE. 2015. *Osmium Tetroxide* [Online]. Available: http://stainsfile.info/StainsFile/prepare/fix/agents/osmium_tetroxide.htm [Accessed 14 December 2015 2015].

THEVENOT, J., TROUTIER, A.-L., DAVID, L., DELAIR, T. & LADAVIÈRE, C. 2007. Steric Stabilization of Lipid/Polymer Particle Assemblies by Poly(ethylene glycol)-Lipids. *Biomacromolecules,* 8**,** 3651-3660.

TORCHILIN, V. P. 2005. Recent advances with liposomes as pharmaceutical carriers. *Nature Reviews Drug Discovery,* 4**,** 145-160.

TRUONG, N. P., WHITTAKER, M. R., MAK, C. W. & DAVIS, T. P. 2015. The importance of nanoparticle shape in cancer drug delivery. *Expert Opin Drug Deliv,* 12**,** 129-42.

UYS, C. E. 2006. *Preparation and characterization of Pheroids.* Master of Science, North-west University. https://dspace.nwu.ac.za/handle/10394/1669

ZHANG, L., CHAN, J. M., GU, F. X., RHEE, J.-W., WANG, A. Z., RADOVIC-MORENO, A. F., ALEXIS, F., LANGER, R. & FAROKHZAD, O. C. 2008. Self-Assembled Lipid−Polymer Hybrid Nanoparticles: A Robust Drug Delivery Platform. *ACS Nano,* 2**,** 1696-1702.

CHAPTER 4

This chapter consists of the *in vitro* work experiments done on Caco-2 cells. The objectives of this chapter were:

c) To determine the appropriate concentration of the NP, Pheroid and NP-Pheroid to use on the Caco-2 cells.

d) To find out the effect of these three formulations on the cell permeability and intracellular uptake of Coumarin 6

CHAPTER 4: THE EFFECT OF THE NP-PHEROID® HYBRID SYSTEM ON THE VIABILITY OF AND TRANSPORT ACROSS CACO-2 CELLS

Madichaba P Chelopo[a,b], Lonji Kalombo[a], Pascaline N. Fonteh[c], Anne Grobler[b], Rose Hayeshi[b*]

[a] Materials Science and Manufacturing, Polymers and Composites, Council for Scientific and Industrial Research, PO Box 395, Pretoria, 0001, South Africa

[b] DST/NWU Preclinical Drug Development Platform, North-West University, Potchefstroom, 2520, South Africa

[c] Department of Biochemistry, University of Pretoria, Hatfield Campus, Pretoria 0002, South Africa

[*] Corresponding author: Rose.Hayeshi@nwu.ac.za

1. Abstract

The use of an *in vitro* cell model to predict permeability of orally administered drugs plays a significant role in the drug development process. Drug candidates encapsulated within drug delivery systems (DDS) have previously shown improved intracellular permeability and uptake and thereby present a potential for enhanced oral bioavailability. The *in vitro* experiments described here were aimed at investigating the effect of the hybrid DDS composed of poly (DL-lactic-*co*-glycolic acid) (PLGA) nanoparticles (NP) and Pheroid® vesicles on the permeability of a fluorescent marker compound, coumarin 6 (C6), using the Caco-2 cell model. A suitable concentration of the delivery system to apply for the trans-cellular assay was evaluated through trypan blue exclusion test, MTT assay and the real-time cell analysis (RTCA) xCELLigence® system. The trans-epithelial electrical resistance (TEER) and the passage of lucifer yellow (LY) were used to examine the Caco-2 cell monolayer integrity during the transport studies. One thousand times diluted Pheroid® vesicles (0.004% v/v) and a maximum of 1% w/v for NP were considered safe for use in the Caco-2 trans-cellular assay. The free C6 was found to be impermeable through the Caco-2 cell monolayer; however, its permeability was improved when encapsulated in NP, Pheroid® or NP-Pheroid® systems with apparent permeability (P_{app}) values of less than 3 x10^{-6} cm/sec. The apparent uptake of the C6 from all the formulations (free, NP Pheroid® and NP-Pheroid®) was speculated to mostly be the association of the C6 with the cell membranes and this constituted approximately 1.3 µg/ml of the 2 µg/ml C6 initially added. Future studies should focus on ways to optimise the PLGA NP–Pheroid® hybrid DDS and evaluate the permeability and uptake enhancing properties for a range of hydrophilic and hydrophobic model drugs on Caco-2 cells.

2. Introduction

Oral drug administration remains the most convenient and comfortable route of drug administration, thus promoting patient compliance. The intestinal epithelium tissue functions as a crucial passage through which oral medicine enters the systemic circulation. This epithelium is formed by a monolayer of enterocytes with a large surface area maximising the absorption of many compounds or drugs into the systemic circulation (Gustafson and Bradshaw-Pierce, 2011, Meunier *et al.,* 1995). Caco-2 cells are a secondary cell line derived from human colorectal adenocarcinoma cells that were obtained from a 72-year-old Caucasian adult male (ATCC, 2016). Caco-2 cells undergo spontaneous differentiation into an enterocyte cell-like monolayer expressing several morphological and functional characteristics of the small intestinal enterocytes (Natoli *et al.,* 2012, Sambuy *et al.,* 2005). The characteristics of differentiated Caco-2 cells include mosaic expression of brush-border enzymes such as sucrose-isomaltase and polarised expression of nutrient transporters (e.g., glucose transporters) (Sambuy *et al.,* 2005) and various drug uptake and efflux transporters in the cell membrane. The functional similarity of the Caco-2 cells to the intestinal epithelium has resulted in their extensive use by the pharmaceutical industry for the prediction of the absorption and permeability of orally administered drugs as well as in the determination of transport pathways of medicines (Awortwe *et al.*, 2014, SGS, 2011, Sevin *et al.*, 2013, Sun and Pang, 2008, Maubon et al.., 2007). As such, Caco-2 cells have been listed by the USA Food and Drug Administration (FDA) as an acceptable *in vitro* model for new drug candidates screening (FDA, 2012). Additionally, they influence the Biopharmaceutics Classification System (BCS) of drugs through their use in the prediction of solubility and permeability (Awortwe *et al.*, 2014, O'Hagan and Kell, 2015).

The permeability or uptake experiments are done using a differentiated Caco-2 monolayer that has been cultured on a polycarbonate membrane in a trans-well plate (SGS, 2011). Test drug diluted in a culture medium or buffer is added on the apical side of the monolayer, while fresh medium goes to the basal side. Samples of the culture medium are collected from the basal side for quantification of the test drug at specified incubation time. At the completion of the experiment, apparent drug permeability (P_{app}) across the Caco-2 cells is calculated using data from the collected samples ,and this P_{app} can then be correlated to the oral drug absorption in humans (Hubatsch *et al.,* 2007, Obringer *et al.,* 2016).

Drug delivery systems (DDS) can be used to enhance the permeability of orally administered drugs across the intestinal epithelium and to protect the drugs against degradation in the gastrointestinal tract, (Ensign *et al.*, 2012). Polymeric nanoparticles (NP) and lipid-based particles are the most popular drug delivery systems (Raemdonck *et al.*, 2013). The combination of these two classes of DDS can lead to additional attractive properties. For example, a hybrid DDS between poly (DL-lactide-*co*-glycolide) (PLGA) NP, which offers stability and leads to controlled release of the drugs (Danhier *et al.*., 2012), and the lipid-based Pheroid® system that has the capability to increase the absorption rate of the entrapped compounds (Grobler, 2009), could lead to a DDS that enhances drug absorption and maintains sustained release of the drug.

As alluded to earlier, the Caco-2 cell line would be an ideal model to investigate, *in vitro*, the permeability enhancing effects of hybrid DDS. However, the assay may be limited by the concentration-dependent cell viability disruption by the drug carriers (Rastogi *et al.*, 2013). It is, therefore, important to ensure that the DDS are at suitable concentrations *in vitro* for the accurate determination of their effect on the permeability of the drugs they encapsulate.

Cell viability assays are based on measuring a cellular response to certain stimuli or a cellular activity associated with viability such as enzyme activity, signal transduction events, receptor binding and much more (Riss *et al.*, 2013). The trypan blue method, also known as the exclusion test, is a popular, quick and simple assay based on the principle that non-viable cells take up the trypan blue dye resulting in stained cytoplasm, while viable cells with an intact membrane do not take up the dye and hence the cytoplasm remains unstained (Strober, 2001, Katsares *et al.*, 2009, Masson-Meyers *et al.*, 2016). The 3-(4, 5-dimethylthiazolyl-2)-2, 5-diphenyltetrazolium bromide (MTT) reduction method is another widely adapted assay for cell viability testing (Masson-Meyers *et al.*, 2016, Stockert *et al.*, 2012). The yellow MTT dye (also known as tetrazolium salt) is metabolically reduced in viable cells by the action of dehydrogenase enzymes in the mitochondria, to generate an insoluble purple formazan crystal. The crystal is then solubilised and quantified colourimetrically to determine the number of viable cells (Riss *et al.*, 2013).

Recently, real-time cell analysis (RTCA) systems have been used to monitor cellular processes such as cell attachment, adhesion degree, viability, proliferation, motility and morphology (Teng *et al*., 2013). These systems fall under the field of biosensors as they transform a cellular response stimulus to a measurable signal (Fang, 2011). A biotechnology company, ACEA Biosciences, has developed the xCELLigence® RTCA system which uses micro-electronic

biosensor technology to measure numerous cell events (Abassi, 2009). This dynamic, label-free and non-invasive analysis, uses E-Plates that are equipped with gold microelectrodes and can be connected to a computer that quantifies the impedance in an electrical circuit built within each well (Martinez-Serra *et al.*, 2014). The impedance is then converted into a parameter named the cell index (CI), a dimensionless value that quantifies the cellular status influenced by several factors for a real-time study (Sun *et al.*, 2012). RTCA is a possible solution to mitigate the issues of inaccuracies that occur with the use of other traditional cell-based viability assays such as interference with the measurement of colour in the MTT assay (Boyd *et al.*, 2008). This analytical technique has been applied for assessing DDS induced cytotoxicity (Moe *et al.*, 2013, Boodhia, 2013).

This study aims to determine the effect of the Pheroid®, PLGA NP and the NP-Pheroid® hybrid formulation on the permeability and uptake of coumarin 6 (C6) in Caco-2 cells. Coumarin 6 is a highly fluorescent compound and a derivative of the hydrophobic benzopyrone chemical class of coumarins and was used as a model drug to monitor the DDS, see Figure 1. To ensure the validity of the permeability experiments, the effect of each of the three formulations on Caco-2 cell viability was first investigated.

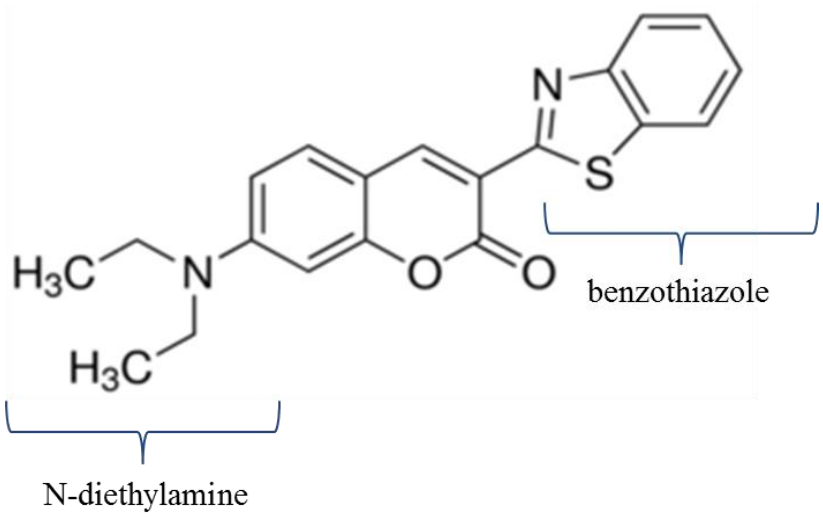

Figure 1: The chemical structure of coumarin 6 (C6), composed of hydrophobic benzopyrone backbone and N-diethylamine or benzothiazole substituents.

3. Materials and methods

3.1. Materials

Caco-2 cells were purchased from the American Type Culture Collection (ATCC, Manassas, United States); Dulbecco's Modified Eagle's Medium (DMEM); penicillin/streptomycin; Hanks' Balanced Salt Solution (HBSS), 0.5 % trypsin (with 1 mM ethylenediaminetetraacetic acid (EDTA)), fungizone and amphotericin were purchased from Gibco (Life Technologies, CA United States). Foetal bovine serum (FBS) was purchased from Biochrom AG (The Scientific Group, Midrand, South Africa). N-2-hydroxyethylpiperazine-N-2-ethane sulfonic acid (HEPES) was purchased from Duchefa Biochemie (Haarlem, The Netherlands). Trypan blue solution, sodium hydroxide (NaOH), coumarin 6 (C6) and MTT assay reagents were purchased from Sigma Aldrich (Johannesburg, South Africa). E-plates were purchased from ACEA Biosciences (CA, USA), while 96 well plates, cell culture flasks were purchased from Corning (New York, USA). The 6 well plates and trans-well polycarbonate: HTS well inserts (surface area = 0.33 cm^2, pore size = 0.4 μm, diameter = 30 mm) were purchased from Millipore (Merck Millipore, NY, USA). The formulations used in this study were prepared as shown in chapter 3 of this thesis (Chelopo *et al.*, 2017) and the test sample dilutions are shown in section 3.2.3 below.

3.2. Methods

3.2.1. Cell culture

Caco-2 cells were resuscitated and seeded in a 25 cm^2 flask and fed with complete DMEM (cDMEM) that is, DMEM supplemented with 10% FBS and 1% penicillin/streptomycin (100 IU/mL / 100 μg/ml). They were grown in a humidified atmosphere of 5% CO_2 at 37 ºC. The medium was replaced with fresh cDMEM every 2 days (d) until the cells reached 75-85% confluency, at which point they were trypsinised using 6 ml of trypsin. The Caco-2 cells were then seeded in a 75 cm^2 flask at a density of 1.5×10^6 cell/ml in cDMEM. They reached confluency after 5-7 d (the medium was replaced every 2 d) of incubation and were subcultured and maintained in a 75 cm^2 flask until the required number of cells was obtained for the studies described below. The passage number used ranged from 15 to 18.

3.2.2. Trypan blue assay

The cytotoxicity of different dilutions of Pheroid® vesicles was first determined using the trypan blue assay. Caco-2 cells were seeded in 6 well plates (1 x 10^4 cells/ml) and allowed to differentiate for 21 d. The cells were then incubated with Pheroid® vesicles in duplicates at concentrations ranging from 0.004% to 4% in cDMEM for 3 hours (h) at 37 °C. The Pheroid® vesicles are composed of 4% of the oil phase with 96% being the aqueous phase. Therefore, the undiluted Pheroid® vesicles are regarded as 4%. To obtain 1% (v/v) of the Pheroid® vesicles, 1 ml of undiluted Pheroid® is added to a total of 4ml solution (1:4); 1 ml of the undiluted Pheroid® vesicles in 10 ml (1:10) solution gives us 0.4% (v/v) of the Pheroid®; The 1000 times diluted Pheroid® (1:1000) are interpreted as 0.004% (v/v) in the text. The cells were then trypsinised with 200 µl of trypsin to obtain a cell suspension and 20 µl was removed and mixed with 20 µl of 0.4% (v/v) trypan blue in phosphate-buffered saline (PBS) and allowed to stand for 5 minutes (min) at room temperature. The cell mixture was then loaded onto a hemocytometer and the cells were observed under a light microscope. The number of viable (clear) and non-viable cells (stained blue) were counted from the 5 x 5 squares at the centre of the hemocytometer. The cell count was established by using the following formula (Equation 4.1).

$$Cell\ Count = No.of\ Cells\ x\ Dilution\ Factor\ x\ 10^4\ \left(\frac{cells}{ml}\right) \qquad \text{(Equation 4.1)}$$

3.2.3. MTT assay

Caco-2 cells were seeded at 5 x 10^4 cells/ml in a 96 well plate with 200 µl cDMEM. The cells were supplied with fresh medium every 2 d until the monolayer was confluent and cells were incubated for a period of 8 d to allow differentiation, as determined previously (Sun *et al.*, 2012). The sample concentrations (in cDMEM) of Pheroid® vesicles, NP and the hybrid system (NP-Pheroid®) used for this assay are shown in Table 1. The NP suspended in the aqueous phase, where 5 mg NP in 100 ml water are referred to as 5% (w/v) of the NP and 0.5mg in 100 ml are 0.5% (w/v). All samples and controls were pre-warmed in a 37 °C water bath before adding them to cells. The 96 well plate with cells was removed from the incubator; old media was aspirated from the plated cells which were then rinsed with fresh cDMEM. Each

well of cells was treated with 200 µl of appropriate samples in duplicate. Duplicate sets of treatments in two separate 96 well plates were set up for two different study periods of at 3 h and 24 (h) in a humidified atmosphere of 5% CO_2 at 37 ºC. At the appropriate time point (3 or 24 h) each plate was removed from the incubator into a laminar flow hood to add 20 µl of reconstituted MTT solution (5mg/mL) with 180 µl cDMEM to all the wells. The plate was returned to the incubator. After 3 h, the plates were centrifuged using a Swing-bucket Allegra 64R Centrifuge (Beckman Coulter, IN, USA) at 1500 rpm for 5 min and 150 µl of the MTT solution was carefully removed and replaced with 150 µl solubilisation reagent (1M hydrochloric acid (HCl) in propanol 1:9). After 30 min at room temperature, the solution in each well was homogenised using a pipette to ensure complete solubilisation of the formazan crystal. The absorbance of the resultant solution was measured at 550nm using a Multiskan Ascent® V1.24 spectrophotometer (Labsystems, Helsinki, Finland). Percentage viability of the cells was determined according to the following equation (4.2):

$$\% \text{ Viability} = \frac{\text{Absorbance}_{Sample}}{\text{Absorbance}_{Control}} x\ 100 \qquad \text{(Equation 4.2)}$$

Table 1: The sample concentrations or dilutions for each formulation of NP, Pheroid® and NP-Pheroid® used for the MTT assay. The samples used for the xCELLigence® assay are indicated by an asterisk (*).

Pheroid® Vesicle- % (v/v)	**NP - % (w/v)**	**NP-Pheroid® vesicles**		
		0.4% Pheroid® and NP % (w/v)	0.04% Pheroid® and NP % (w/v)	0.004% Pheroid® and NP % (w/v)
1% (1:4)	*5%	*5%	*5%	5%
*0.4% (1:10)	3.5%	3.5%	3.5%	3.5%
*0.04% (1:100)	*2.5%	*2.5%	*2.5%	*2.5%
*0.004% (1:1000)	*1%	*1%	*1%	*1%
0.002% (1:2000)	0.5%	0.5%	0.5%	0.5%

3.2.4. Real-time cell analysis (RTCA)

An xCELLigence® real-time cell analyser (ACEA Biosciences, CA, USA) was used to monitor the proliferation of Caco-2 cells in 16 well E-plates. The E-plates were placed on the device station located in a 37 °C incubator equipped with the xCELLigence® system. The plate has a sensor electrode that enables the monitoring of adherent cells in each well. The presence and adherence of cells in each well leads to an increase in electronic impedance. The impedance detected by the system analyser was reported as cell index (CI) which is determined according to the following mathematical formula (Sun *et al.*, 2012).

$$CI = \max_{i-1,\dots N} \left(\frac{R_{cell}(fi)}{R_b(fi)} - 1 \right) \qquad \text{(Equation 4.3)}$$

N is the number of the frequency points where impedance gets measured. R_{cell}(fi) and R_b(fi) are the electrode resistances with cells and without cells respectively (Sun *et al.*, 2012).

A normalised CI at a particular time point is acquired by dividing the CI value by a specific value at a reference time point (Sun *et al.*, 2012). The seeding titration experiment was set up in duplicates for cell density ranging from 0.1 x 10^4 to 3.2 x 10^4 cells/ml in the E-plates wells. Figure 2 shows the first 2 d and last 2 d cell monitoring of the 8 d period prior to treatment. The optimal time or the best period for the cell treatment is when the cells are still proliferating (Kho *et al.*, 2015). As shown in Figure 2, the higher cell densities had a CI that plateaued too quickly, indicating that the cells had reached their maximum growth in a well and were not in the best conditions to be treated with any compounds. The optimum cell density of the Caco-2 cells in the E-plates was first determined to be 0.25 x 10^4 cells/ml, see Figure 2. For the viability assay Caco-2 cells were then plated at 2.5 x 10^3 cells/ml in 16 well E-Plates and cultured for a period of 8 d, as previously done by Sun *et al.*, (2012). Test sample (NP, Pheroid® and NP-Pheroid®) concentrations used were the same as for the MTT assay shown in Table 1, however only selected sample concentrations (indicated by * in Table 1), were used to treat the cells in duplicate for the RTCA because of a limited number of wells on the E-Plate.

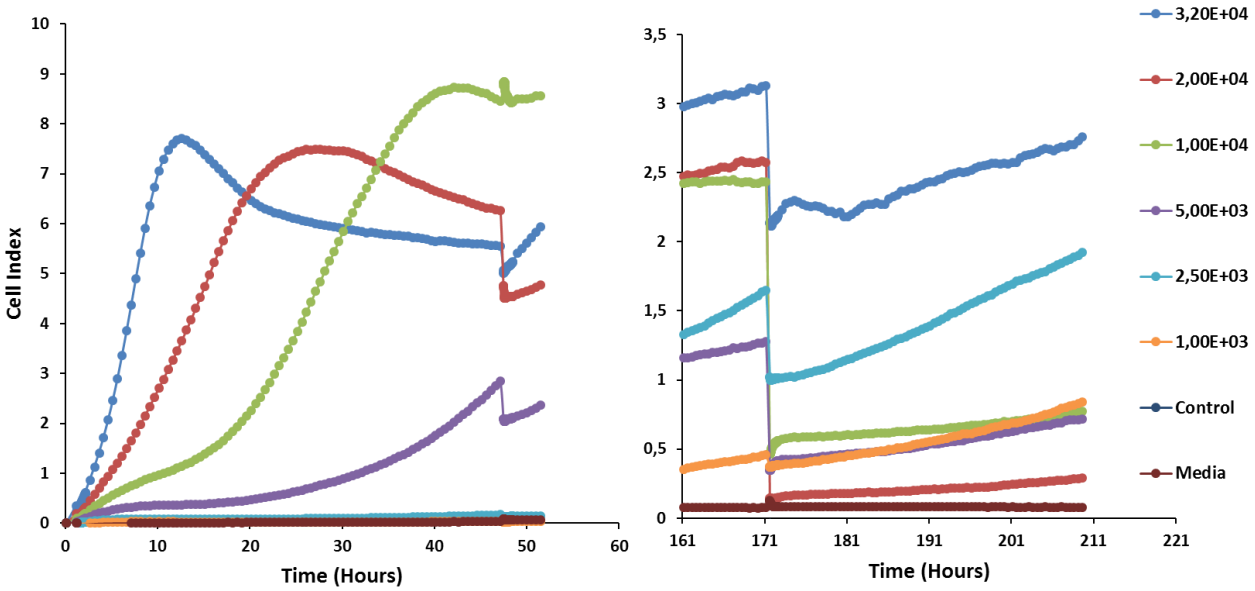

Figure 2: The titration of Caco-2 cell density in the xCELLigence® E-plate wells to identify the ideal seeding density. The optimum density that was suitable for treatment, where the cells were slowly proliferating, was determined to be 2.5 x 10^3. (n=2).

3.2.5. Permeability and uptake studies

Permeability and uptake were determined through a Caco-2 trans-cellular experiment for C6 (2 µg/ml) entrapped in NP, Pheroid® and NP-Pheroid®. The preparation of these formulations is described in Chapter 3 of this thesis (Chelopo *et al.*, 2017). Caco-2 cells were seeded at 1 x 10^4 cells/ml (am optimum cell density determined) in a six well plate on polycarbonate-treated filter trans-well membrane inserts and supplied with fresh cDMEM containing 1% fungizone every 2 d. The cells were thus maintained for a period of 21 d to allow development of a differentiated cell monolayer. The integrity of the Caco-2 cell monolayer was monitored through cell visualisation under the microscope and weekly measurements of the transepithelial electrical resistance (TEER) over 21 d until an acceptable reading was observed (>250 ohms). The TEER readings were measured with a Millicell®-ERS meter (Microsep (Pty) Ltd, Johannesburg, South Africa). Cells were used for the transport and uptake studies between 21 d and 25 d post seeding. The cells were washed with 37 °C pre-warmed assay buffer containing HBSS supplemented with 25 mM HEPES. The assay buffer was adjusted to a pH of 7.4 using 1 M sodium hydroxide (NaOH) solution. The assay buffer was added to both the apical (1000 µl) and basolateral (2000 µl) compartments of the trans-well plated cells which were then pre-

incubated for 15 min at 37 °C in a Thermo-incubator orbital shaker at 450 rpm (Thermostar, BMG LaboTech, Offenburg, Germany) after which TEER measurements were taken. The buffer was then removed from the apical compartment and replaced with 1000 µl of test samples, 2 µg/ml of free C6, C6 in NP, C6 in Pheroid® and C6 in NP-Pheroid®. These samples were maintained at 37 °C through the experiment. Each sample treatment was done in triplicate. Permeability was then measured by collecting 200 µl samples from the basolateral compartment at specified time points (30, 60, 90, 120 and 180 min) and replacing the collected sample with the same volume of pre-warmed assay buffer. The fluorescence of the collected samples was recorded using an Infinite F500 spectrofluorometer (Tecan Group Ltd, Männedorf, SC) at excitation and emission wavelengths of 458 nm and 540 nm, respectively. The permeability of free C6 was compared to that of C6 NP, C6 Pheroid® and C6 NP-Pheroid®. The P_{app} values (cm/s) were calculated using equation 4.4. Where dQ/dt is the increase in the concentration of drug in the receiver compartment over time or the drug permeation rate (µg/ml s), A represents the monolayer surface area (cm^2) and C_0 stands for the initial concentration of the test compound added to the donor compartment (µg/ ml) (Tangyuenyongwatana *et al.*, 2009).

$$P_{app}\left(\frac{cm}{s}\right) = \frac{dQ}{dt}\ X\ \left(\frac{1}{AC0}\right) \qquad \text{(Equation 4.4)}$$

TEER was measured again at the end of the experiment to determine whether the test substances affected the integrity of the cell monolayer. The final TEER values were calculated using equation 4.5.

$$\text{TEER } (\Omega) = \text{TEER}_{(\text{with cells})} - \text{TEER}_{(\text{without cells})} \qquad \text{(Equation 4.5)}$$

The integrity of the cell monolayer was further confirmed using a marker compound, 100 µM lucifer yellow (LY), prepared with the assay buffer or 1000x time diluted Pheroid®. The LY rejection was calculated as shown in equation 4.6 where the relative fluorescence units (RFU) of LY (measured at 485/535 nm) in the basolateral compartment was compared with the apical compartment, measured at the 60 min time point of the experiments.

$$\% \text{ LY Rejection} = 100\,[1 - RFU_{basolateral} / RFU_{apical}] \qquad \text{(Equation 4.6)}$$

Cellular uptake was determined by temperature shock cell lysis. After exposure of the cells to the test samples for 3 h, the cells were cooled to -80 °C for more than 1 h and then added 250 µl assay at room temperature. The ruptured cells were vortexed in assay buffer and centrifuged at room temperature at 2500 rpm, and the fluorescence of the supernatant was measured using an Infinite F500 spectrofluorometer (Tecan Group Ltd, Männedorf, SC) at excitation and emission wavelengths of 458 nm and 540 nm, respectively.

4. Results and discussion

4.1. *In vitro* viability - Trypan blue

The trypan blue exclusion test was applied to rapidly assess the viability of Caco-2 cells 3 h post-treatment with Pheroid® vesicles at concentrations ranging from 0.004% to 4% (v/v), see Figure 3. The undiluted (4%) Pheroid® vesicles resulted in the highest cytotoxicity (100%). Pheroid® vesicle dilutions between 0.4% and 2% were also found to be highly cytotoxic. The 0.04% and 0.004% samples had the least cytotoxicity which was a little higher than 40 %. However, this may be neglected because of the 70% viability recorded for the negative control sample. The results obtained here are supported by a recent study which determined the cytotoxicity of the Pheroid® system on Caco-2 cells using a live/dead viability method through calcein AM (acetoxymethyl) and ethidium homodimer-1 reagents (Grobler, 2014). It was deduced that the high concentration of Pheroid® causes the onset of apoptosis and it was also confirmed that the 0.01 to 0.001% (100x to 1000x dilutions) Pheroid® concentration did not have any cytotoxic effect. The 30% reduction in viability in the control cells could have been due to the 5 min incubation time of the trypsinisation step used to get the cells in suspension before the addition of trypan blue reagent. Trypsin is a proteolytic enzyme which cleaves peptide chains to detach cells from the vessel (Zhang *et al.*, 2012). However, it is known to affect the cell membrane integrity and cell viability when in contact with cells for an extended time. It has been shown that trypsin induces necrosis of chondrocytes over prolonged exposure with its concentration influencing the cytotoxicity (Sutradhar *et al.*, 2010).

In general, the trypan blue exclusion assay is a simple and conventional viability test, however there is proven experimental variability in the counting of cells using hemocytometer readings (Szabo *et al.*., 2004). The inaccuracy of this method can also be associated with the small sample volume of the cell suspension that leads to less confidence in the results (Katsares *et al.*, 2009). The results obtained in this study indicated that there was concentration-dependent cytotoxicity from the Pheroid® vesicles toward the Caco-2 cells.

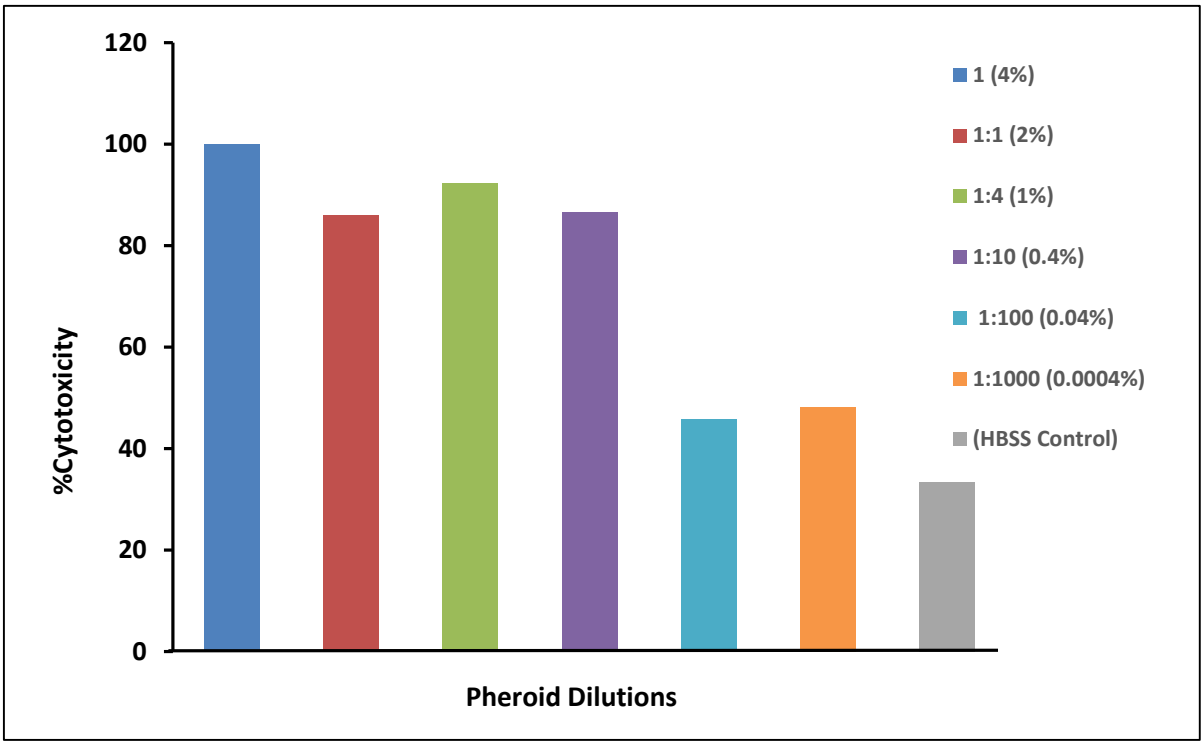

Figure 3: Cytotoxicity of various Pheroid® concentrations in Caco-2 cells determined using the trypan blue assay. A Pheroid® concentration-dependent response is indicated. (The Pheroid % depict w/v; n=2).

4.2. *In vitro* viability - MTT and xCELLigence® assay

To further confirm the best concentration of Pheroid® as well as NP suitable for the Caco-2 cell permeability studies, the MTT and xCELLigence® viability assays were performed. These assays were aimed at determining the cell viability after exposure to various concentrations of NP, Pheroid® and NP-Pheroid® formulations. Five concentrations of each formulation were

tested in the MTT assay at two time points, 3 and 24 h, while only three or fewer concentrations of samples were used for the real-time study due to the limited number of E-plate wells, as shown in Table 1 (section 3.2.3). Background plates containing compound only, without cells, were set up for the MTT assay to enable background subtraction of any signal that could interfere with the results.

The results obtained from the trypan blue cell exclusion test helped determine the appropriate concentrations of Pheroid® vesicles to use in these two assays, where the most cytotoxic Pheroid® concentrations (2% – 4%) were eliminated, to reduce the number of wells required. The cell response to the Pheroid® was analysed from a maximum concentration of 1% (v/v) to a minimum concentration of 0.004% (v/v) in the MTT assay. However, the cellular response to Pheroid® treatment in the MTT assay was unclear and was postulated to be due to the interaction of the Pheroid® solution with the MTT reagent. The purple colour was more intense at higher Pheroid® concentrations (1%), which was very unlikely to be caused by viable cells and therefore it was concluded that Pheroid® interfered with the colourimetric measurement of the formazan. For instance, increased cell viability was observed at higher Pheroid® concentrations (1%) than at lower concentrations (0.04%) and this was not correlating with the preliminary trypan blue exclusion test results as well as previous study results from Grobler, (2014). Even so, subtracting the background plate absorbance values did not help correct the interference by the Pheroid®. This suggested that there were factors in the Pheroid® sample matrix that were non-enzymatically reducing the MTT reagent to form the purple colour. Therefore, the MTT data for both the Pheroid® vesicle and NP-Pheroid® hybrid formulation could not be presented due to the interference which invalidated the results. However, the MTT data for NP is discussed below.

A number of compounds including sulfhydryl-containing compounds (glutathione), vitamin A, ascorbic acid and dicoumarol are known to be reducing compounds that disrupt the accurate determination of viability in the MTT assay (Riss *et al.*, 2013). Although the real MTT reduction mechanism has not been well established, according to Riss *et.al*, (2013) the reduction of the tetrazolium salt to formazan may involve nicotinamide adenine dinucleotide phosphate (NADPH) dependent mitochondrial dehydrogenase enzyme transfer of electrons to the MTT (Riss *et al.*, 2013, Marshall *et al.*, 1995). Various MTT interfering compounds may use a different mechanism to reduce the MTT; for example vitamin A (retinol) has been found to be a reductase that catalyses MTT reduction using vitamin C (ascorbic acid) as an electron donor (Chakrabarti *et al.*, 2001), while a naturally occurring anti-coagulant dicoumarol is

known to uncouple the electron transport from oxidative phosphorylation of ATP, therefore reducing the MTT (Collier and Pritsos, 2003). The reducing capability of the MTT by Pheroid®, was previously suggested to be caused by the presence of vitamin E in the Pheroid® ingredients (Botha, 2008). This current study serves to confirm the Pheroid® MTT interference and proves that the combination with NP to make a NP-Pheroid® hybrid system does not have any effect on the interaction of the Pheroid® with the MTT reagent.

The dynamic indication of cell viability was obtained by measuring the impedance data from the RTCA xCELLigence® method. The optimum cell density plated in the E-plate was chosen to be 2.5 x 10^3 cell/ml according to the cell density titration graph in Figure 2 (section 3.2.4). The titration of the cell density is considered to be a vital step in running a successful study without the risk of reduced growth of the cells (Tukulula *et al.*, 2015). Kho *et al.*, strongly recommended cell density titration for all cell types used on the xCELLigence® not only because it reveals the optimal seeding density but also the length of time that cells can be cultured without compromise and can define the best period to treat the cells (Kho *et al.*, 2015). The adhesion and the proliferation of the Caco-2 cells were successfully monitored for the full culturing period of 8 d with a subsequent change of the cell media. During this growing period, the cell index (CI) gradually increased toward the 8 d culturing period, indicating that the Caco-2 cells were healthy before treatment.

4.2.1. Effect of the NP on Caco-2 cells (MTT and xCELLigence®)

The cell viability, measured by the MTT assay, after treatment with NP for 24 h resulted in a dose-response profile, Figure 4. The results after the 3 h treatment period of the cells with the NP were inconclusive (results not shown). NP have no interference with the MTT reduction reaction, therefore well to well experimental errors could have compromised the latter results. The highest concentration of NP (5% w/v) resulted in decreased viability while 90-98% viability was measured after exposure to the lower NP concentration (0.5%-1% w/v) for 24 h, see Figure 4.

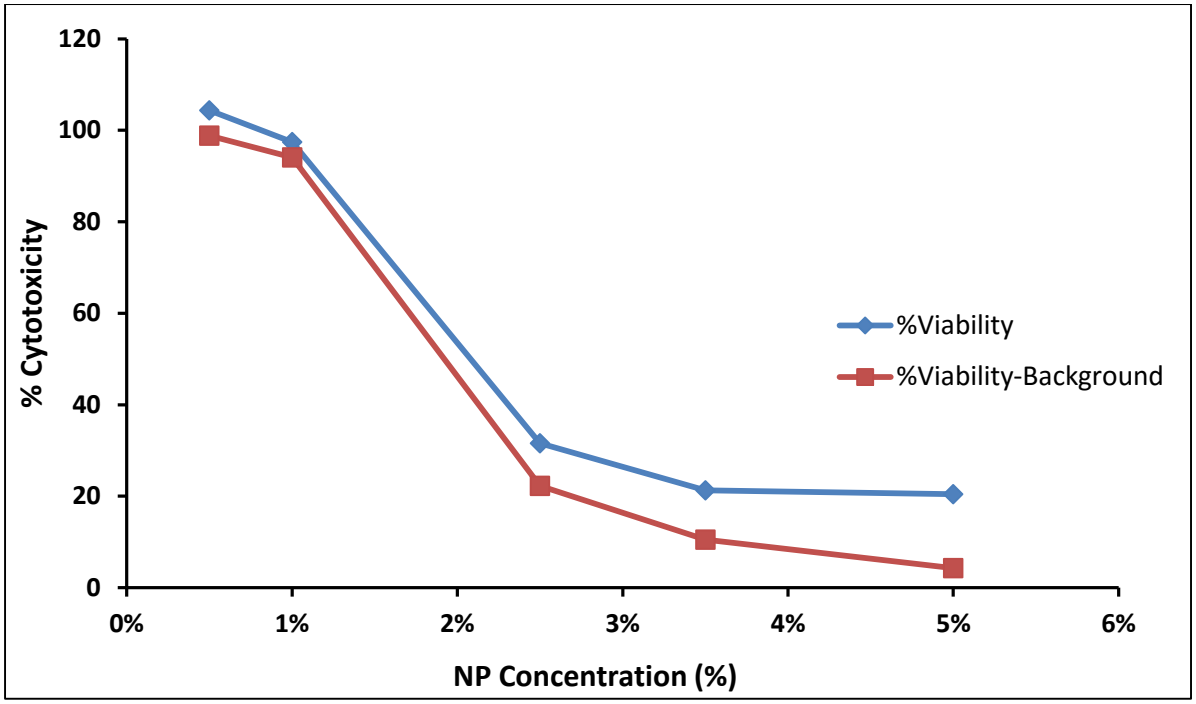

Figure 4: MTT cell viability response to nanoparticles (NP) after 24 h. The curve shows a dose-dependent decrease in cell viability. (The NP % depict w/v; n=2).

The effect of the NP was also confirmed by an immediate decrease of the CI on the xCELLigence® curve shown in Figure 5, when the cells were treated with 5% w/v NP and a constant CI when treated with 1% w/v of the NP over 24 h, see Figure 5. The low cell viability after exposure to high NP concentrations (2.5% - 5% w/v) was assumed to be caused by sedimentation of the NP on the cells. Tukulula *et al.*, (2015) study has shown that increasing PLGA NP concentrations to 0.2 mg/ml did not have any effect on Caco-2 cell viability as measured by the MTT assay and Semete *et al.*, (2010a) demonstrated no cytotoxicity toward Caco-2 cells, at NP concentration ranging between 0.001 and 0.1 mg/ml. In this current study, the high NP concentrations ranging between 0.5-5% (w/v) which is equivalent to 5-50 mg/ml, were chosen based on the NP-Pheroid® mixing ratio experiment reported in chapter 3 of this thesis (Chelopo *et al.*, 2017). The 0.5% (w/v) NP concentration, which is equivalent to 5 mg/ml, was non-cytotoxic according to the MTT studies, see Figure 4, however it was excluded from the xCELLigence® assay due to a limited number of wells on the E-plate. The results from both the MTT and the xCELLigence® curves (Figure 4 and 5) illustrate that 1% (w/v) NP, equivalent to 10 mg/ml, also induced no cytotoxicity, which makes this study the first to report the highest PLGA NP concentration used on Caco-2 cells without affecting the cell viability. Previous studies have demonstrated that PLGA NP were non-cytotoxic toward Caco-2 cells

when treated with a maximum concentration of 5.8 mg/ml using an MTS assay, which produces a soluble formazan product (Nkabinde *et al*., 2014). It was then concluded that intact PLGA NP could be transported across the intestinal epithelium without affecting the cell monolayer post oral administration. However, 5 mg/ml PLGA NP has been indicated to induce about 20% toxicity on another epithelial cell line (Calu-3) derived from the human airway (Mura *et al.*, 2011). Caco-2 cells have a more robust barrier capacity toward the movement of NP and their cell morphology as well as the absence of the mucus have been indicated to differ considerably with Calu-3 cell lines (Vllasaliu *et al.*, 2011), which may explain why they are not susceptible to NP toxicity.

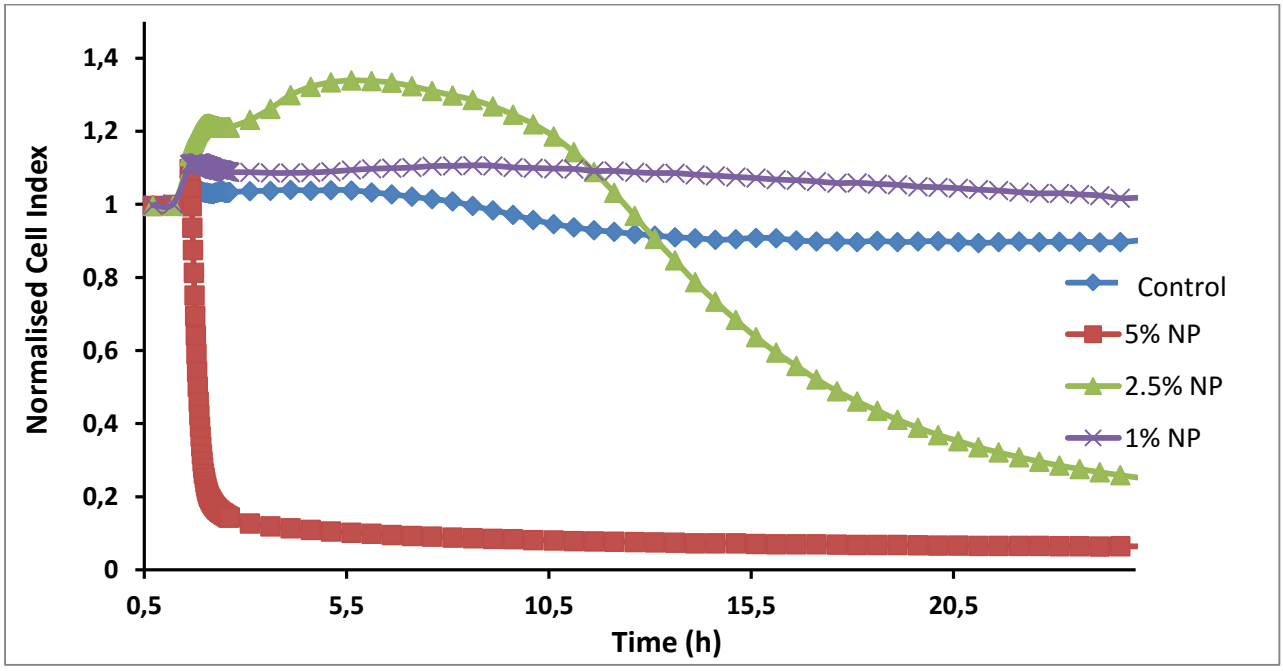

Figure 5: The RTCA profiles of the cells after treatment with PLGA NP over 24 h. The 5% NP resulted in cell death immediately upon treatment. (The NP % depict w/v; n=2).

4.2.2. Effect of the Pheroid® vesicles on Caco-2 cells (xCELLigence®)

The real-time xCELLigence® curve extracted at the 3 h time point post-treatment with various concentrations of Pheroid® vesicles showed a minor dose-response relation, Figure 6. The 3 h time of analysis was necessary for indicating the effect of the DDS on Caco-2 cells because the permeability studies were to be conducted for a period of 3 h. As observed with the trypan blue assay, both the 0.04% and 0.004% Pheroid treatments were non-cytotoxic after 3 h, see Figure 6. After 24 h, the 0.004% Pheroid® vesicles treatment still showed no cytotoxicity as evidenced by the CI value that was comparable to that of the untreated Caco-2 cells control. A previous study conducted by Grobler, (2014) confirmed that 1000 times (0.004% v/v) dilution of the Pheroid® is the safest to use in the Caco-2 cells. Interestingly, 0.04% Pheroid® led to a CI higher than the control cells but eventually stabilised back to a CI of one at the 24 h time point, see Figure 7. However, it was concluded that 0.04% Pheroid® was non-cytotoxic while treatment with 0.4% Pheroid led to an immediate decrease in CI, indicating cytotoxicity.

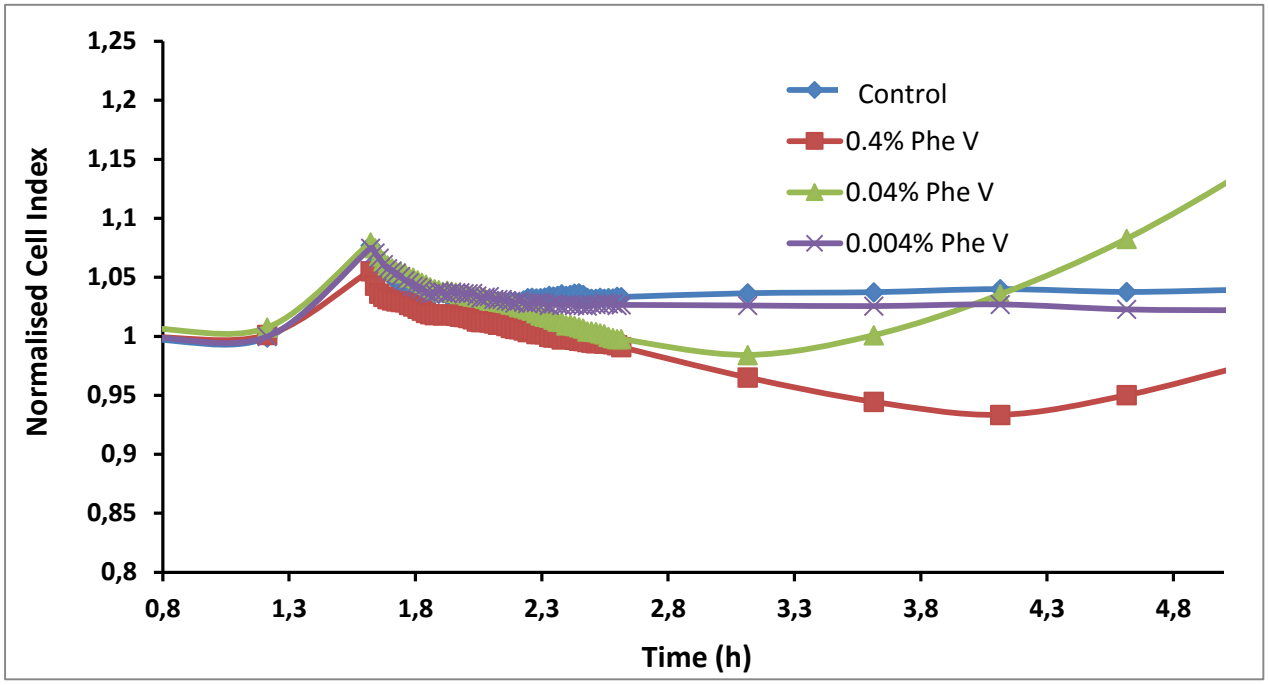

Figure 6: The RTCA profiles of the cells after treatment with Pheroid® vesicles (Phe V) over 3 h, showing no evidence of decreased cell viability. (The Phe V % depict v/v; n=2).

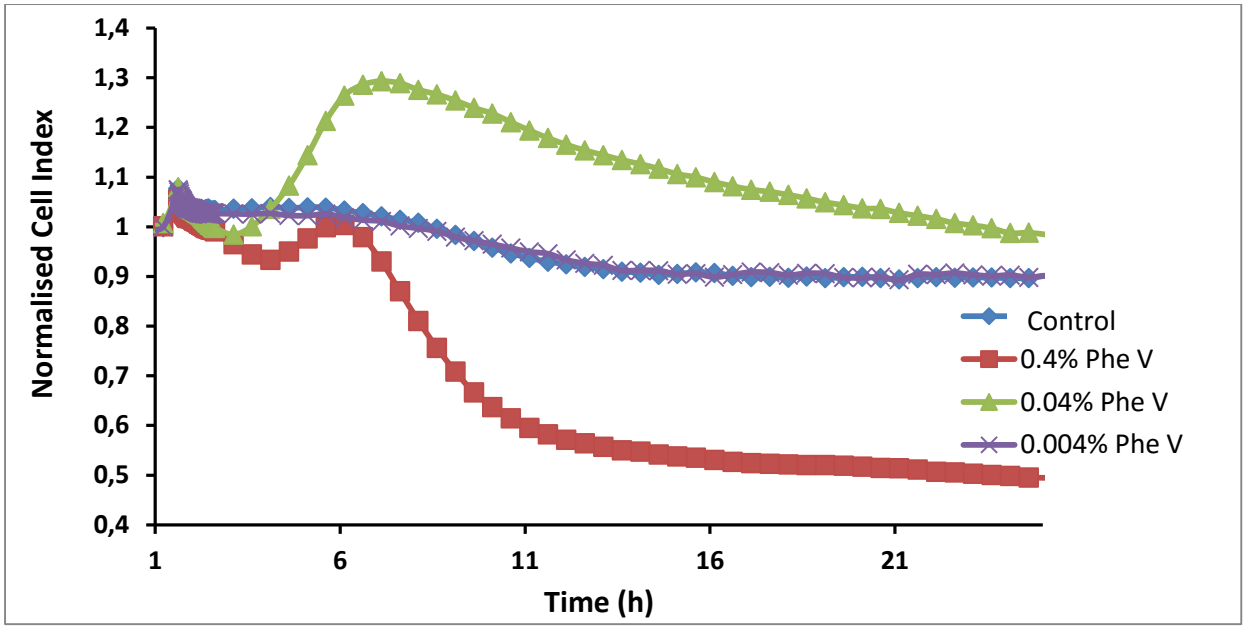

Figure 7: The RTCA profiles of the cells after treatment by Pheroid® vesicles (Phe V) over 24 h. A dose-response relation is evident, where 0.4% Pheroid® vesicles were the most cytotoxic concentration. (The Phe V % depict v/v; n=2).

4.2.3. Effect of the NP-Pheroid® on Caco-2cells (xCELLigence)

In the determination of the effect of the hybrid system on cell viability, a rapid decrease in the CI was observed when various amounts of NP were combined with 0.4 % Pheroid®, see Figure 8. Similarly, 5% NP combined with 0.4 % (Figure 8) or 0.04 % Pheroid (Figure 9), led to an instantaneous decline of the CI. This indicates that the cytotoxicity was due to the 0.4% Pheroid® in the former case and due to the 5% NP in the latter case. The NP-Pheroid® hybrid system composed of 0.04% Pheroid® with either 2.5% or 1% NP also led to reduced cell viability, see Figure 9. However, as highlighted in the previous section, exposure of the cells to only 0.04% Pheroid® did not result in reduced viability, but a transient increase in the CI to above that of the control cells was also observed, see Figure 7. This transient increase in CI (resulting in a "bump") could be associated with the effect of the pattern in which the adherent cells spread (McGrath, 2007). The dynamic monitoring of cell adhesion studies through the measurement of cell impedance has shown that changes in the morphology of the cells during and after the cell spreading can cause fluctuations in the CI or resistance (Heijink *et al.*, 2010, Luong *et al.*, 2001). Kho *et al.*, (2015) found that the bump in the xCELLigence® curve

resulting from the increase in the CI above the control cells, was associated with exposure of the cells to pro-inflammatory cytokines which led to the swelling (or increase in the size) of the cells, which could be associated with compound uptake. There is no evidence in literature on the immunological response from Pheroid®, however the effect of PLGA NP on the secretion of pro-inflammatory cytokines *in vivo* was found to be insignificant, with induction of anti-inflammatory cytokines at a relatively smaller extent (Semete *et al.*, 2010b). Another deduced mechanism in the fluctuations of the CI, referred to as 'spoon-shaped' profiles, is suggested to be caused by the regulation of the intracellular calcium ion (Ca^{2+}) concentration, which has been indicated to cause changes in cell morphology (Denelavas *et al.*, 2011, Tukulula *et al.*, 2015). There is also a possibility that NP could interfere with the xCELLigence® signal as shown in a study of carbon nanotubes, which when precipitated were found to hamper the impedance measurements, leading to the underestimation of their cytotoxicity (Meindl *et al.*, 2013). However, this latter possibility cannot be compared to this current study as the PLGA NP provided a dose-response relation implying a reliable estimation of their cytotoxicity.

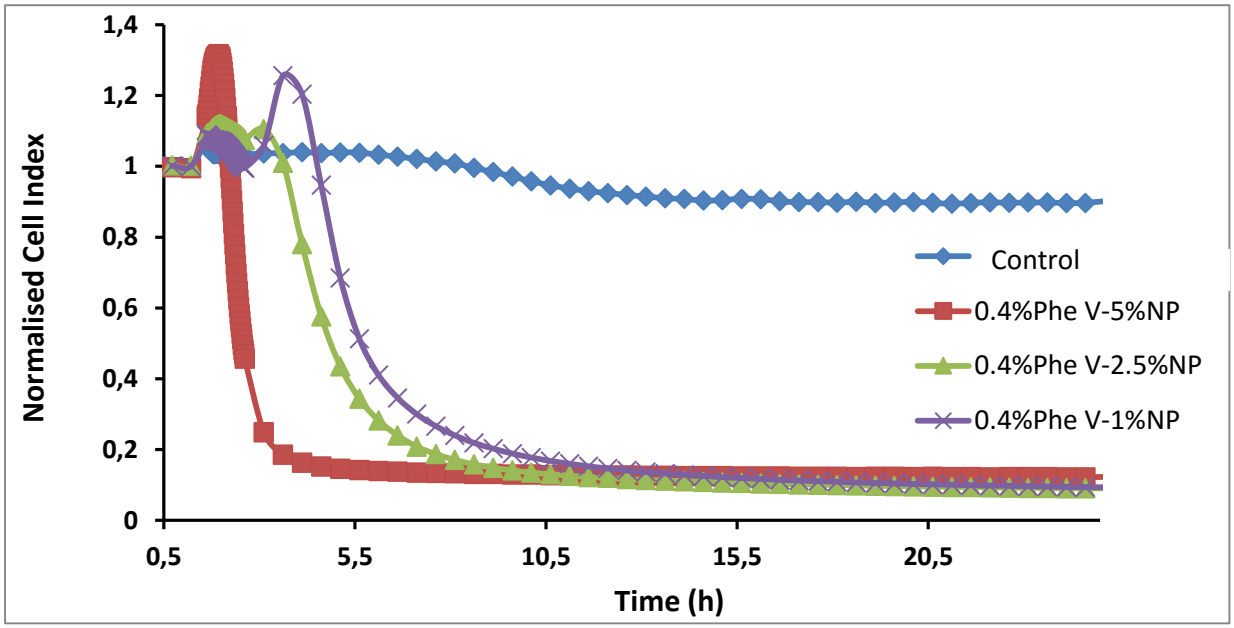

Figure 8: xCELLigence® plot of cell response to 0.4% (v/v) Pheroid® vesicles (Phe V) combined with various NP concentrations over 24 h period. All combinations lead to an acute decline in the CI. (The Phe V % depict v/v; NP % depict w/v; n=2).

The transcellular studies were done within 3 h so any cytotoxic effect observed after this time should not have any impact on these studies. For example, there was no observed cytotoxic effect from 0.04% Pheroid® combined with either 2.5% or 1% NP by the 3 h time point, see Figure 9. The increase in CI to above that of the control after 4 h, from the 0.04% Pheroid® treatment, Figure 7, is then assumed to have been a compromised cell condition or change in the cell morphology which became susceptible to rapid reduction of the CI when combined with the 1% of NP, see Figure 9, shown to be non-cytotoxic when used individually, see Figure 5. Therefore the NP-Pheroid® ratio which proved to have no negative effect on the viability of the Caco-2 cells for the most prolonged time duration was the 1% NP:0.004% Pheroid® vesicles, with no deviation from the CI of the control cells, see Figure 10. It was concluded from the RTCA experiments that 1% NP:0.004% Pheroid® formulation was the best option to use for the permeability and uptake experiments.

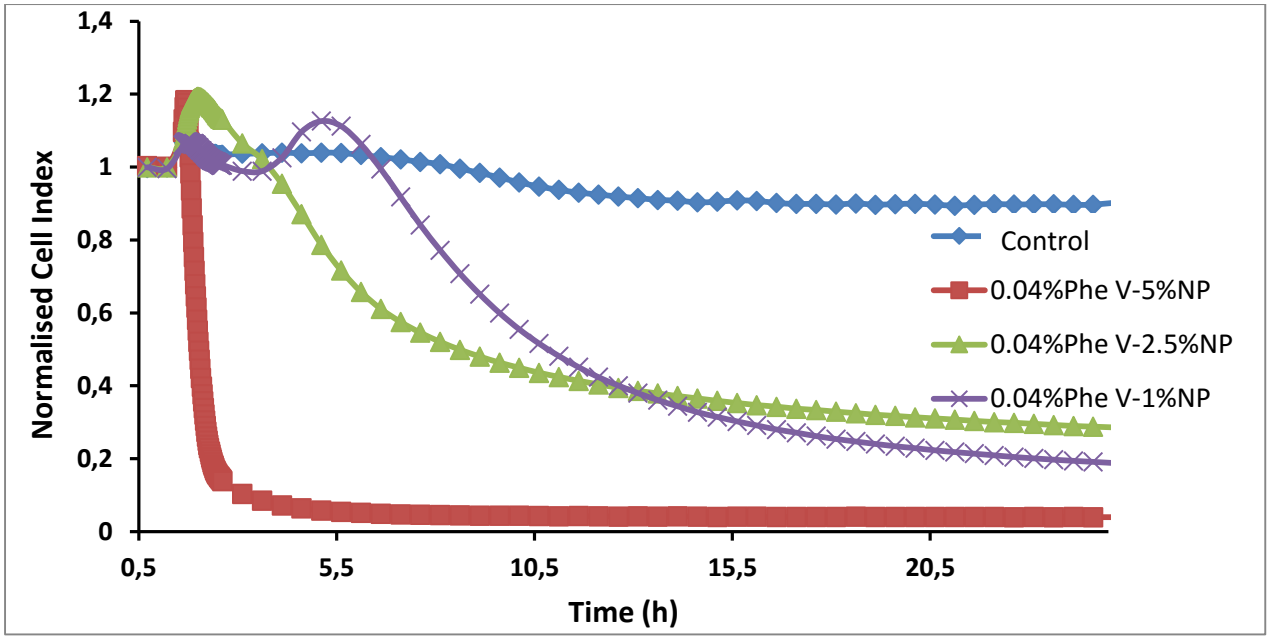

Figure 9: xCELLigence® plot of cell response to 0.04% (v/v) Pheroid® vesicles (Phe V) combined with various NP concentrations over 24 h period. A delayed decline in the CI is observed at the lowest NP concentration (1%) combined with the 0.04% Pheroid® vesicles. (The Phe V % depict v/v; NP % depict w/v; n=2).

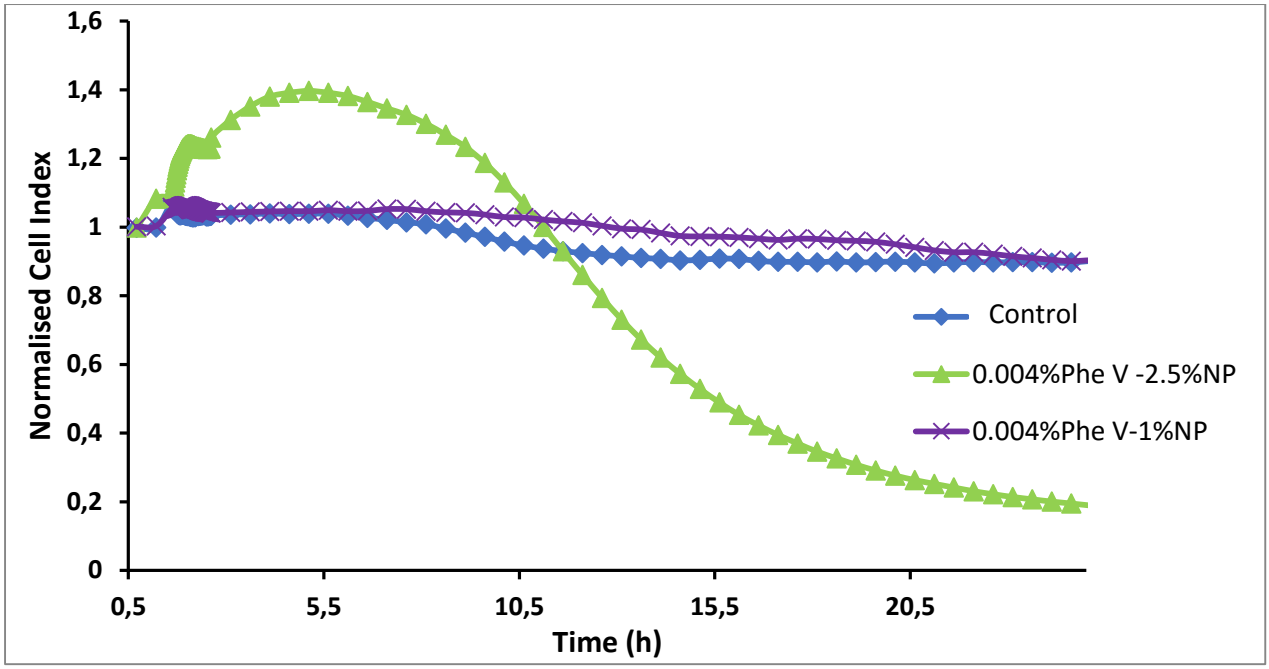

Figure 10: xCELLigence® plot of cell response to 0.004% (v/v) Pheroid® vesicles (Phe V) combined with various NP concentrations over 24 h period. The 0.004% Phe V:1% NP ratio was not cytotoxic. (The Phe V % depict v/v; NP % depict w/v; n=2).

This study has confirmed previous studies by providing evidence that the viability data obtained from the RTCA is more trustworthy than the MTT assay which is prone to drawbacks such as the interference with the colourimetric measurement of formazan (Teng *et al.*, 2013, Martinez-Serra *et al.*, 2014, Haselsberger *et al.*, 1996). Therefore, a direct comparison of the cytotoxicity results from these two assays was not possible except the similar cell response to NP shown in Figure 4 and 5. Similarly, other published studies could not correlate the MTT viability with the xCELLigence® due to the experimental errors from the MTT assay (Fonteh *et al.*, 2011, Róka *et al.*, 2015). The xCELLigence® technique was therefore more reliable in determining the Caco-2 cell viability in this study.

It should be taken into consideration that the cytotoxicity of the high concentrations of Pheroid® vesicles toward the Caco-2 cells is not the ultimate standard of determining their safety *in vivo.* The reason for the observed cytotoxicity of Pheroid® toward the Caco-2 cells was due to the lack of nutrients and gas exchange of the cells with the media caused by the lipophilic Pheroid® oil phase forming on top of the cells. Therefore, less concentrated Pheroid® allows the interaction of the medium with the cells ensuring their viability, and it does not affect the thermodynamics and the effectiveness of the Pheroid® in the *in vitro* system (Grobler, 2014).

Undiluted Pheroid® has been used in the *in vivo* system and has been shown to improve the absorption of anti-TB and anti-malarial drugs without any evidence of toxicity (Grobler, 2009, Matthee, 2007). The mechanism of absorption enhancement has been associated with permeation enhancing properties, which has been compared to N-trimethyl chitosan chloride (TMC) (Bruyn, 2006). It has been demonstrated that most permeation enhancers require use at low concentrations for *in vitro* Caco-2 studies to reduce their risk of damaging the cell monolayer (Rastogi *et al.*, 2013), which supports the purpose of the experiments done in this work to adjust Pheroid® concentration for the Caco-2 permeability study. The concentration-dependent toxic effect of permeation enhancers in cells can often be misinterpreted (Rastogi *et al.*, 2013), as it may not be a representation of the *in vivo* environment.

4.3. *In vitro* permeability and uptake study

4.3.1. Cell monolayer integrity

The growth of Caco-2 cells over the 21 d of culture was monitored by observation under the light microscope and a weekly record of TEER measurements. On the day of the experiment, both LY and TEER readings were used to determine the integrity of the differentiated cell monolayer. LY is a hydrophobic compound used as paracellular transport marker (Hanani, 2012). The LY rejection values were calculated from the two sample preparation media, *i.e.*, the assay buffer and the 1000x diluted Pheroid®, to determine their effect on the cell integrity. The LY rejection values in HBSS and Pheroid® buffered solutions obtained at the 60 min experimental time point were 97% and 95% respectively. These values were comparable to values obtained in a similar study where even after 60 min the LY rejection remained above 90% (Nkabinde *et al.*, 2012). The TEER reading measurements also remained constantly above 300 Ω, before and after the experiment, Figure 11. Any slight changes observed in TEER and %LY rejection were negligible as they were within the reference recommended values for Caco-2 cells and are similar to those obtained in a similar study (Artursson *et al.*, 2001). This indicates that the test samples did not compromise the integrity of the cell monolayer.

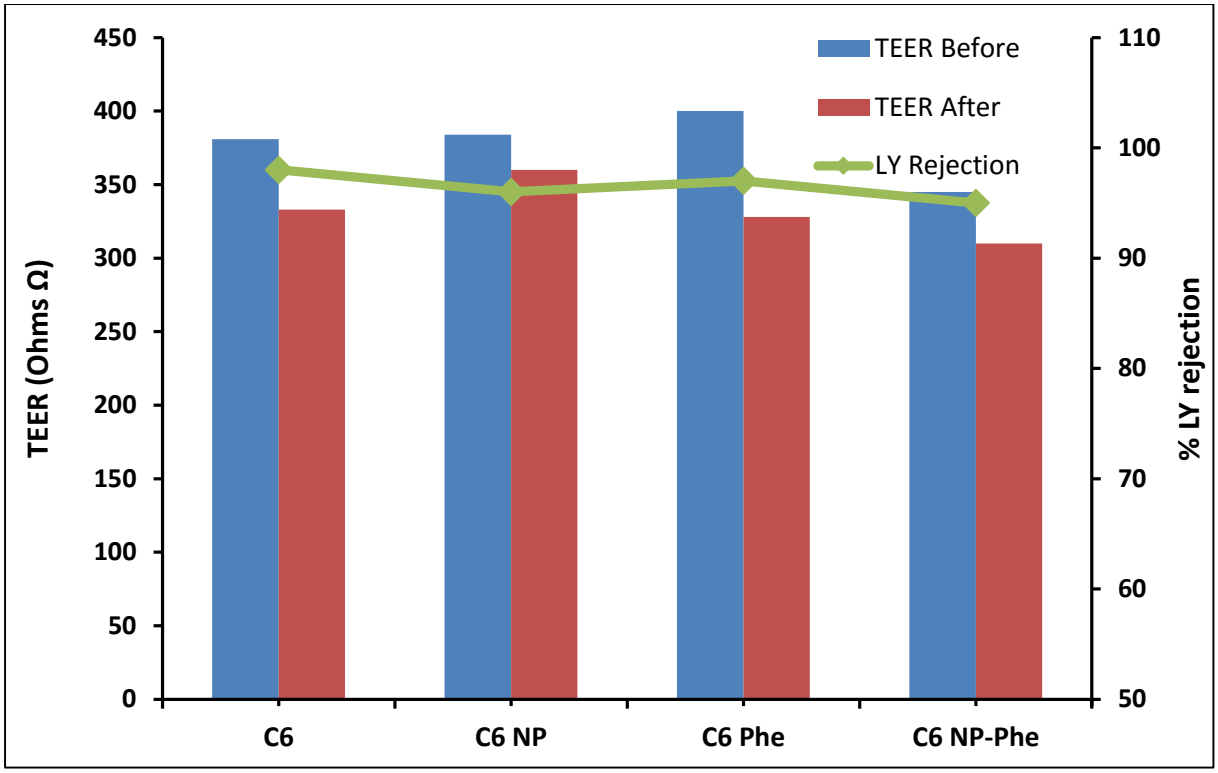

Figure 11: Before and after experiment TEER values and the % LY rejection for the Caco-2 cell monolayer. The TEER values were obtained from three wells before the experiment and two wells after the experiment. Each TEER value was subtracted from TEER without cells = 190 Ω. All Pheroid® (Phe) samples were 1000x dilutions. (n=2).

4.3.2. Cell permeability

A uni-directional study, apical to basal (A → B), was conducted on differentiated Caco-2 cells, to assess the effect of the hybrid NP-Pheroid® system on the uptake and permeability of C6. The fluorescence of C6 detected in the basal compartment, was used to calculate the difference in the permeability of free C6, C6 NP, C6 Pheroid® and C6 NP-Pheroid®. Coumarin 6 in the basal compartment after exposure of the cells to free C6 could not be quantified implying that it could not permeate through the cell monolayer. The apparent permeability coefficient (P_{app}) could only be calculated after exposure of the cells to C6 encapsulated within NP, Pheroid® or the NP-Pheroid® systems. These formulations resulted in P_{app} ranging from 1.5 x 10^{-6} cm/sec to 3.5 x 10^{-6} cm/sec, see Figure 12, implying improvement of the permeability of C6. Statistical evaluation using the student's *t*-test showed that these P_{app} values of the three formulations were not significantly different from each other at a 95% confidence interval ($P > 0.05$);

therefore, the effect of the hybrid system on C6 permeability could not be differentiated from the individual NP and Pheroid® systems.

The NP enhancing permeability results obtained in this study can be compared to the previously reported improvement of *in vitro* permeability of drug encapsulated in PLGA NP in comparison to free drug (Nkabinde *et al.*, 2012). The permeability obtained in this current work can be considered moderate ($P_{app} < 3.5 \times 10^{-6}$ cm/sec) in accordance with the published classifications, whereby low permeability P_{app} is represented by values $< 0.5 \times 10^{-6}$ cm/sec; moderate permeability P_{app} ranges between 0.5 and5 $\times 10^{-6}$ cm/sec; while high permeability P_{app} values are $> 10 \times 10^{-6}$ cm/sec (Balimane *et al.*, 2006, Peng *et al.*, 2014). The Caco-2 cell permeability of various derivatives of coumarins was shown to be high with $P_{app} > 4 \times 10^{-5}$ cm/sec (Galkin *et al.*, 2009). The studied coumarin derivatives in Galkin *et al.*, (2009) mainly had hydroxyl (OH) and methoxy (OCH_3) substituents on the benzopyrone, whereas the C6, used in this study, possesses N-diethylamine and benzothiazole substituents on position 3 and 7 of the benzopyrone backbone, as shown in Figure 1. It is thus speculated that the C6 substituents make it more hydrophobic and account for its low permeability compared to the coumarins used by Galkin *et al.* (2009). The other difference to the Galkin *et al.*, (2009) study was that they used high initial concentrations of their coumarins (250 µM), which is equivalent to 87.5 µg/ml of C6 and they used chromatographic methods to quantify them to determine their permeability. In this study, only 2 µg/ml of C6 was used and was adequate to be quantified through fluorescence. This study has demonstrated the improved permeability of C6 through Caco-2 cells by entrapping it in PLGA NP, Pheroid® and NP-Pheroid® hybrid, which has not been previously reported.

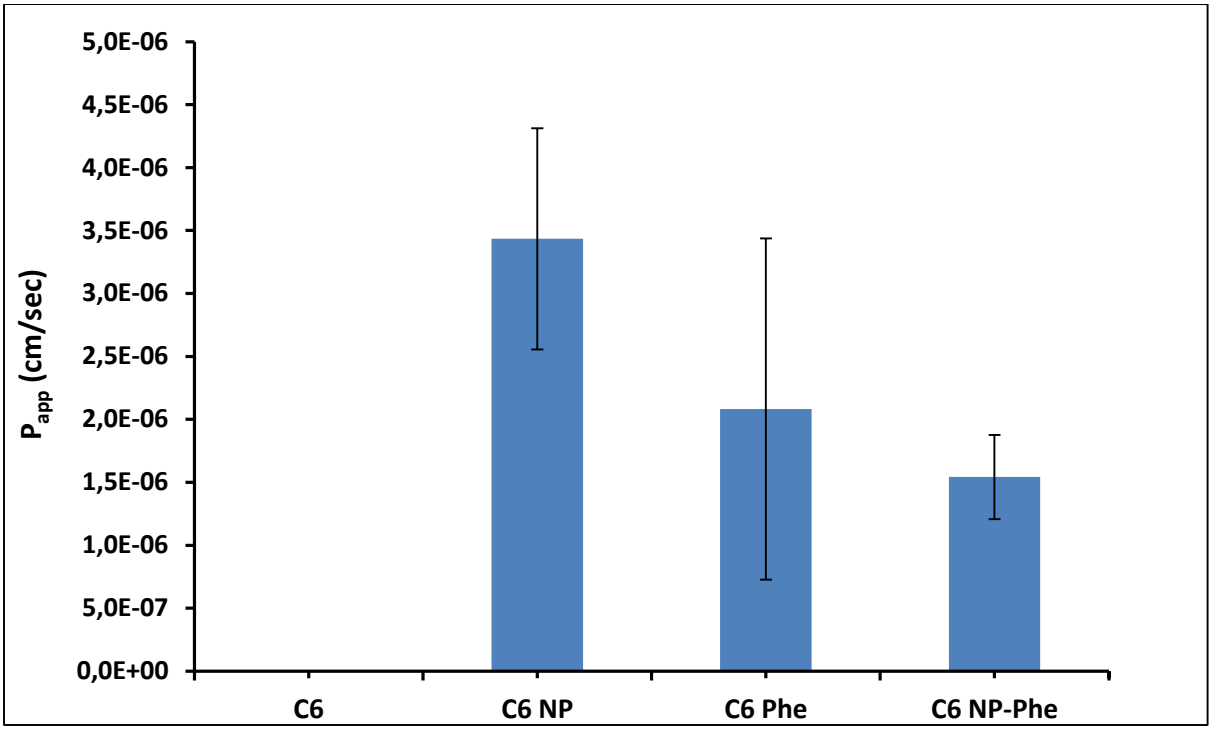

Figure 12: The permeability of C6 (at 2µg/ml) in apical-to-basolateral (A→B) directions. The P_{app} values are an average of three wells, and the error bars represent SD from the average P_{app}. (n=3).

4.3.3. Cell uptake

The confocal images in Figure 13 show the visualisation of C6 in a C6 NP, C6 Pheroid® and C6 NP-Pheroid® formulation within the Caco-2 cells. The green fluorescence of C6 seems to be mostly localised in the intercellular spaces of the cells rather than in the cytoplasm. Therefore the quantified C6 is more likely to be associated with the cell membrane rather than cell uptake, indicating the high affinity of all the C6 formulations to the lipid regions of the cells. The lysis of the cells 3 h after treatment) resulted in C6 concentrations ranging from 1.1 to 1.38 µg/ml among all the formulations, Figure 14, where the initial concentration of 2 µg/ml C6 was used. The difference in C6 concentration from the three formulations was also found to be statistically insignificant ($P > 0.05$). Therefore, the entrapment of C6 in the individual or hybrid system had no significant effect on the association of C6 with the Caco-2 cells.

The PLGA NP as an individual system has previously been indicated to be internalised intact within the cytoplasm through endocytosis. Nkabinde *et al.*, (2014) demonstrated that the PLGA NP labelled with an alternative fluorescence molecule, rhodamine-6G, were not only adsorbed onto the cell membrane but were internalised within the Caco-2 cells transcellularly

and were co-localised with the cytoplasmic lysosomes, which encloses degradative enzymes (Nkabinde *et al*., 2014). The observed uptake of rhodamine-6G NP could have been influenced by the relatively higher aqueous solubility of the rhodamine-6G in comparison with C6 that was used in this current study. Therefore, it is assumed that the entrapped rhodamine-6G fluorophore may have changed the surface chemistry of the NP (*i.e.*, surface charge and the degree of hydrophobicity) thus affecting its intracellular pathway. The use of C6 has been demonstrated to provide more stable lifetimes in comparison to other fluorophores (Kristoffersen *et al.*, 2014). In a previous study that used C6 at 50 μg/ml (3.42 μM), an enhanced cellular uptake was demonstrated through fluorescence microscopy upon encapsulation within solid lipid NP, using A30, HEK and COS-7 cell lines (Rivolta *et al*., 2011). The confocal images recently presented by Miao *et al.*, (2015) indicated that the uptake of C6 at 0.3 μg/ml (0.86 nM) within the cytoplasm of MDCK cells was moderately assisted by its solubilisation with Tween 80 (0.2%) and the C6 uptake was significantly increased by its complexation with cucurbit[7]uril while free C6 in HBSS could not be taken up into the cells. In contrast to both Rivolta *et al*., (2011) and Miao *et al.*, (2015) studies, in this current study neither the individual DDS (NP and Pheroid®) nor the NP-Pheroid® hybrid DDS improved the apparent uptake of C6 within the Caco-2 cell monolayer.

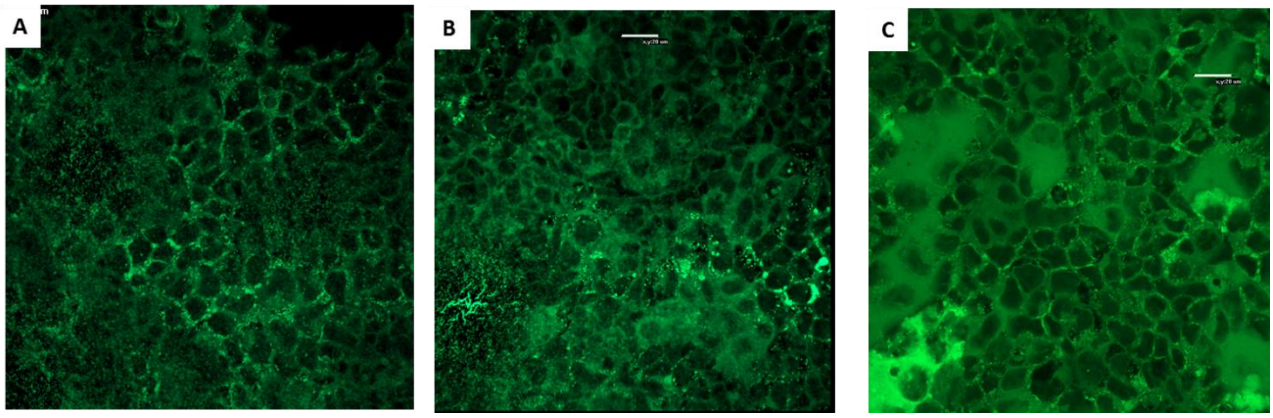

Figure 13: Confocal images of Caco-2 cells after 3 h treatment with C6 NP (A), C6 Pheroid® (B) and C6 NP-Pheroid® (C) formulations, showing the association of C6 with the cells.

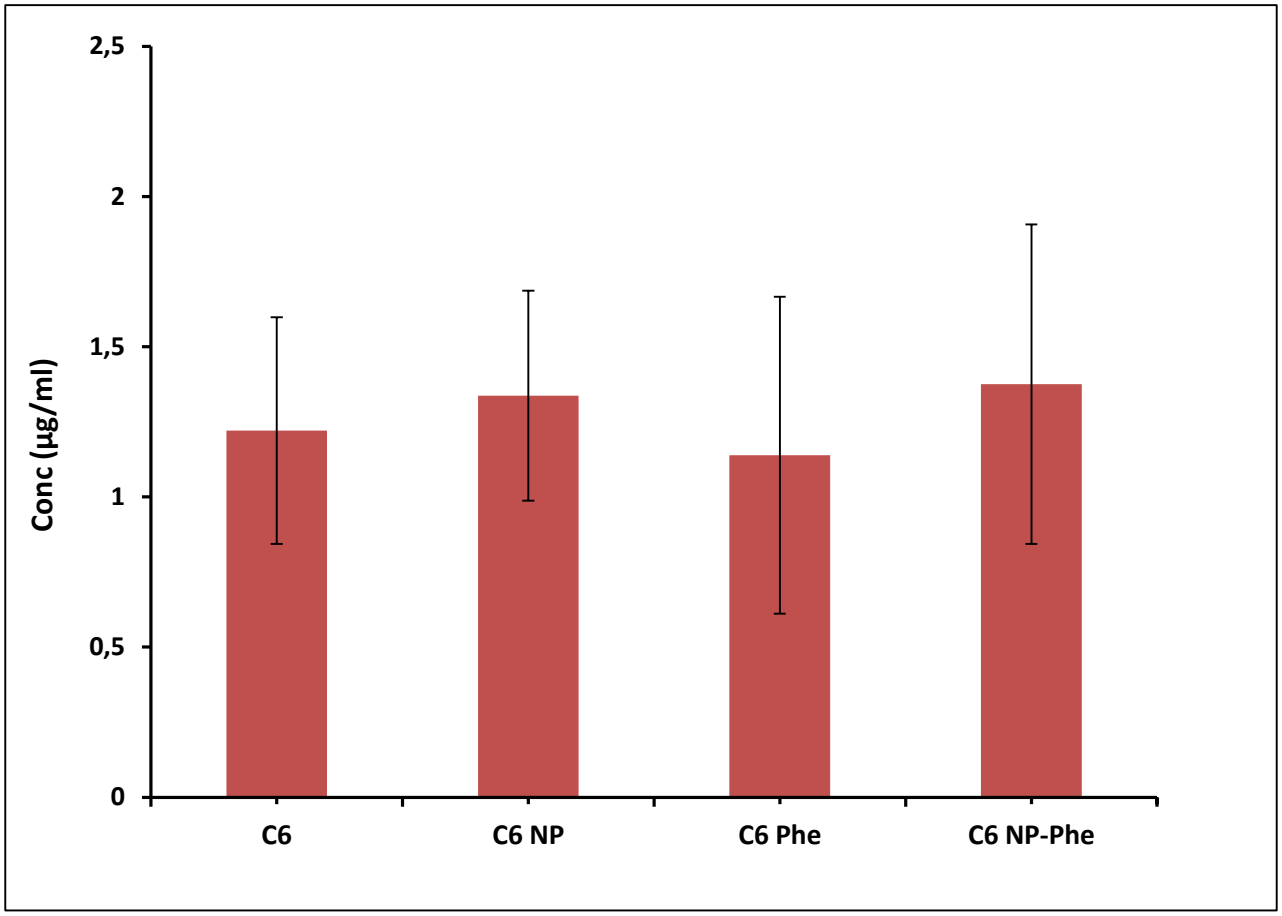

Figure 14: The association of C6 (at 2µg/ml) in Caco-2 cells. Average concentrations (Conc) were calculated from three wells, and the error bars represent as SD from the average concentration. (n=3).

5. Conclusion

The viability assays were carried out to determine the appropriate concentrations of the individual and hybrid DDS to use in the *in vitro* permeability study with the Caco-2 cell model. The use of Pheroid® in a cell culture environment has previously been shown to prevent the exchange of gas and nutrients between the media and cells, and therefore it is imperative to dilute it for optimal *in vitro* cell experiment outcomes. The trypan blue test indicated the Pheroid® vesicle concentrations that did not compromise the cell viability over the 3 h period ranged between 0.04 and 0.004% (v/v). The MTT assay could not be used to determine the effect of both the Pheroid® and NP-Pheroid® on cell viability due to the interference of Pheroid® with the purple formazan absorption signal. This interference has been assumed to be caused by the vitamin E component in the Pheroid®. Cell impedance measured using the xCELLigence® system gave more accurate and reproducible viability results than the MTT assay. The appropriate dilutions that showed prolonged safety for the Caco-2 cells over a period of 24 h using the RTCA were confirmed to be 0.004% (v/v) of the Pheroid® vesicles and the maximum of 1% (w/v) for the NP. The permeability of the green fluorescent marker, C6 entrapped in individual delivery systems of NP and Pheroid® vesicles, as well as the NP-Pheroid® hybrid system, was significantly enhanced to a maximum $P_{app} = 3.5 \times 10^{-6}$ cm/sec over the Caco-2 cell monolayer. However, none of the formulations altered the apparent Caco-2 uptake of C6.

5.1. Acknowledgements

Miss Abongile Ndamase for her help in some of the cell culture experiments during her internship at Polymers and Composites, CSIR; The National Research Foundation and the Department of Science and Technology for the funding.

6. References

ABASSI, Y. 2009. Dynamic monitoring of cell adhesion and spreading. *Cell,* 6000**,** 17-19.

ARTURSSON, P., PALM, K. & LUTHMAN, K. 2001. Caco-2 monolayers in experimental and theoretical predictions of drug transport 1. *Advanced Drug Delivery Reviews,* 46**,** 27-43.

ATCC 2016. Caco2 (ATCC® HTB37™). *In:* ATCC (ed.) *Product Sheet.* Manassas, VA 20108 USA American Type Culture Collection (ATCC).

AWORTWE, C., FASINU, P. S. & ROSENKRANZ, B. 2014. Application of Caco-2 cell line in herb-drug interaction studies: Current approaches and challenges. *Journal of Pharmacy & Pharmaceutical Sciences,* 17**,** 1-19.

BALIMANE, P. V., HAN, Y.-H. & CHONG, S. 2006. Current industrial practices of assessing permeability and P-glycoprotein interaction. *The American Association of Pharmaceutical Scientists Journal,* 8**,** E1-E13.

BOODHIA, K. 2013. *Assessing the potential toxicity of gold nanoparticle carrier systems conjugated with therapeutic peptides.* Master of Science in Biochemistry, University of Johannesburg. http://www.netd.ac.za/portal/?action=view&identifier=oai%3Aunion.ndltd.org%3Auj%2Fuj%3A11604 (Date accessed: 15 June 2016).

BOTHA, M. M. 2007. *Pre-clinical evaluation of the possible enhancement of the efficacy of antiretroviral drugs by pheroid technology.* North-West University. https://www.researchgate.net/publication/26988859_Preclinical_evaluation_of_the_possible_enhancement_of_the_efficacy_of_antiretroviral_drugs_by_pheroid_technology_MM_Botha (Date accessed: 15 May 2017).

BOYD, J. M., HUANG, L., XIE, L., MOE, B., GABOS, S. & LI, X.-F. 2008. A cell-microelectronic sensing technique for profiling cytotoxicity of chemicals. *Analytica Chimica Acta,* 615**,** 80-87.

BRUYN, T. D. 2006. *Nasal delivery of insulin with Pheroid® technology.* Master of Science, North-West University. https://dspace.nwu.ac.za/handle/10394/730 (Date accessed: 22 July 2013).

CHAKRABARTI, R., KUNDU, S., KUMAR, S. & CHAKRABARTI, R. 2001. Vitamin A as an enzyme that catalyzes the reduction of MTT to formazan by vitamin C. *Journal of Cellular Biochemistry,* 80**,** 133-138.

CHELOPO, M. P., KALOMBO, L., WESLEY-SMITH, J., GROBLER, A. & HAYESHI, R. 2017. The fabrication and characterization of a PLGA nanoparticle–Pheroid® combined drug delivery system. *Journal of Materials Science,* 52**,** 3133-3145.

COLLIER, A. C. & PRITSOS, C. A. 2003. The mitochondrial uncoupler dicumarol disrupts the MTT assay. *Biochemical Pharmacology,* 66**,** 281-287.

DANHIER, F., ANSORENA, E., SILVA, J. M., COCO, R., LE BRETON, A. & PRÉAT, V. 2012. PLGA-based nanoparticles: An overview of biomedical applications. *Journal of Controlled Release,* 161**,** 505-522.

DENELAVAS, A., WEIBEL, F., PRUMMER, M., IMBACH, A., CLERC, R. G., APFEL, C. M. & HERTEL, C. 2011. Real-time cellular impedance measurements detect Ca^{2+} channel-dependent oscillations of morphology in human H295R adrenoma cells. *Biochimica et Biophysica Acta (BBA) - Molecular Cell Research,* 1813**,** 754-762.

ENSIGN, L. M., CONE, R. & HANES, J. 2012. Oral drug delivery with polymeric nanoparticles: The gastrointestinal mucus barriers. *Advanced Drug Delivery Reviews,* 64**,** 557-570.

FANG, Y. 2011. Label-free biosensors for cell biology. *International Journal of Electrochemistry,* 2011**,** 1-16.

FDA 2012. Drug interaction studies — study design, data analysis, implications for dosing, and labeling recommendations *Guidance for Industry.* Febuary 2012 ed. Rockville, MD Food and Drug Administration.

FONTEH, P. N., KETER, F. K. & MEYER, D. 2011. New bis(thiosemicarbazonate) gold(III) complexes inhibit HIV replication at cytostatic concentrations: Potential for incorporation into virostatic cocktails. *Journal of Inorganic Biochemistry,* 105**,** 1173-1180.

GALKIN, A., FALLARERO, A. & VUORELA, P. M. 2009. Coumarins permeability in Caco-2 cell model. *Journal of Pharmacy and Pharmacology,* 61**,** 177-184.

GROBLER, A. F. 2009. *Pharmaceutical applications of Pheroid™ technology.* Doctor of Philosophy in Pharmaceutics, North-West University. https://dspace.nwu.ac.za/handle/10394/6701 (Date accessed: 22 August 2013).

GROBLER, L. 2014. *The effect of Pheroid® technology on the bioavailability of artemisone in primates.* North-West University. https://dspace.nwu.ac.za/handle/10394/12241 (Date accessed : 02 February 2015).

GUSTAFSON, D. L. & BRADSHAW-PIERCE, E. L. 2011. Fundamental Concepts in Clinical Pharmacology. *In:* SPRINGER (ed.) *Principles of Anticancer Drug Development.* Springer. Page 37-62.

HANANI, M. 2012. Lucifer yellow – an angel rather than the devil. *Journal of Cellular and Molecular Medicine,* 16**,** 22-31.

HASELSBERGER, K., PETERSON, D. C., THOMAS, D. G. & DARLING, J. L. 1996. Assay of anticancer drugs in tissue culture: Comparison of a tetrazolium-based assay and a protein binding dye assay in short-term cultures derived from human malignant glioma. *Anticancer Drugs,* 7**,** 331-338.

HEIJINK, I. H., BRANDENBURG, S. M., NOORDHOEK, J. A., POSTMA, D. S., SLEBOS, D.-J. & VAN OOSTERHOUT, A. J. M. 2010. Characterisation of cell adhesion in airway epithelial cell types using electric cell–substrate impedance sensing. *European Respiratory Journal,* 35**,** 894-903.

HUBATSCH, I., RAGNARSSON, E. G. & ARTURSSON, P. 2007. Determination of drug permeability and prediction of drug absorption in Caco-2 monolayers. *Nature Protocols* 2**,** 2111-2119.

KATSARES, V., PETSA, A., FELESAKIS, A., PAPARIDIS, Z., NIKOLAIDOU, E., GARGANI, S., KARVOUNIDOU, I., ARDELEAN, K.-A., GRIGORIADIS, N. & GRIGORIADIS, J. 2009. A rapid and accurate method for the stem cell viability evaluation: The Case of the thawed umbilical cord blood. *Laboratory Medicine,* 40**,** 557-560.

KHO, D., MACDONALD, C., JOHNSON, R., UNSWORTH, C. P., O'CARROLL, S. J., MEZ, E. D., ANGEL, C. E. & GRAHAM, E. S. 2015. Application of xCELLigence RTCA biosensor technology for revealing the profile and window of drug responsiveness in real time. *Biosensors,* 5**,** 199-222.

KRISTOFFERSEN, A. S., ERGA, S. R., HAMRE, B. & FRETTE, Ø. 2014. Testing fluorescence lifetime standards using two-photon excitation and time-domain instrumentation: Rhodamine B, Coumarin 6 and Lucifer Yellow. *Journal of Fluorescence,* 24, 1015-1024.

LUONG, J. H., HABIBI-REZAEI, M., MEGHROUS, J., XIAO, C., MALE, K. B. & KAMEN, A. 2001. Monitoring motility, spreading, and mortality of adherent insect cells using an impedance sensor. *Analytical Chemistry,* 73**,** 1844-1848.

MARSHALL, N. J., GOODWIN, C. J. & HOLT, S. J. 1995. A critical assessment of the use of microculture tetrazolium assays to measure cell growth and function. *Growth Regulation,* 5**,** 69-84.

MARTINEZ-SERRA, J., GUTIERREZ, A., MUÑOZ-CAPÓ, S., NAVARRO-PALOU, M., ROS, T., AMAT, J. C., LOPEZ, B., MARCUS, T. F., FUEYO, L., SUQUIA, A. G., GINES, J., RUBIO, F., RAMOS, R. & BESALDUCH, J. 2014. xCELLigence system for real-time label-free monitoring of growth and viability of cell lines from hematological malignancies. *OncoTargets and Therapy,* 7**,** 985-994.

MASSON-MEYERS, D. S., BUMAH, V. V. & ENWEMEKA, C. S. 2016. A comparison of four methods for determining viability in human dermal fibroblasts irradiated with blue light. *Journal of Pharmacological and Toxicological Methods,* 79**,** 15-22.

MATTHEE, L. I. 2007. *A preclinical evaluation of the possible enhancement of the efficacy of antituberculosis drugs by Pheroid™ technology*. Master of Science, North-West University. https://dspace.nwu.ac.za/handle/10394/1805 (Date accessed: 28 April 2014).

MAUBON, N., LE VEE, M., FOSSATI, L., AUDRY, M., LE FERREC, E., BOLZE, S. & FARDEL, O. 2007. Analysis of drug transporter expression in human intestinal Caco-2 cells by real-time PCR. *Fundamental & Clinical Pharmacology,* 21**,** 659-663.

MCGRATH, J. L. 2007. Cell spreading: the power to simplify. *Current Biology,* 17**,** R357-R358.

MEINDL, C., ABSENGER, M., ROBLEGG, E. & FROHLICH, E. 2013. Suitability of cell-based label-free detection for cytotoxicity screening of carbon nanotubes. *BioMed Research International,* 2013, 13 Pages.

MEUNIER, V., BOURRIE, M., BERGER, Y. & FABRE, G. 1995. The human intestinal epithelial cell line Caco-2; pharmacological and pharmacokinetic applications. *Cell Biology and Toxicology,* 11**,** 187-194.

MIAO, X., LI, Y., WYMAN, I., LEE, S. M. Y., MACARTNEY, D. H., ZHENG, Y. & WANG, R. 2015. Enhanced in vitro and in vivo uptake of a hydrophobic model drug coumarin-6 in the presence of cucurbit[7]uril. *Medicinal Chemical Communications,* 6**,** 1370-1374.

MOE, B., GABOS, S. & LI, X.-F. 2013. Real-time cell-microelectronic sensing of nanoparticle-induced cytotoxic effects. *Analytica Chimica Acta,* 789**,** 83-90.

MURA, S., HILLAIREAU, H., NICOLAS, J., LE DROUMAGUET, B., GUEUTIN, C., ZANNA, S., TSAPIS, N. & FATTAL, E. 2011. Influence of surface charge on the potential toxicity of PLGA nanoparticles towards Calu-3 cells. *International Journal of Nanomedicine,* 6**,** 2591-2605.

NATOLI, M., LEONI, B. D., D'AGNANO, I., ZUCCO, F. & FELSANI, A. 2012. Good Caco-2 cell culture practices. *Toxicology In Vitro,* 26**,** 1243-1246.

NKABINDE, L. A., SHOBA-ZIKHALI, L. N. N., SEMETE-MAKOKOTLELA, B., KALOMBO, L., SWAI, H. S., HAYESHI, R., NAICKER, B., HILLIE, T. K. & HAMMAN, J. H. 2012. Permeation of PLGA nanoparticles across different in vitro models. *Current Drug Delivery,* 9**,** 617-627.

NKABINDE, L., SHOBA-ZIKHALI, L., SEMETE-MAKOKOTLELA, B., GROBLER, A. & HAMMAN, J. 2014. Poly (D, L-lactide-co-glycolide) nanoparticles: Uptake by epithelial cells and cytotoxicity. *eXPRESS Polymer Letters* 8, 197-206O'HAGAN, S. & KELL, D. B. 2015. The apparent permeabilities of Caco-2 cells to marketed drugs: magnitude, and independence from both biophysical properties and endogenite similarities. *PeerJ,* 3**,** e1405, 17 Pages.

OBRINGER, C., MANWARING, J., GOEBEL, C., HEWITT, N. J. & ROTHE, H. 2016. Suitability of the in vitro Caco-2 assay to predict the oral absorption of aromatic amine hair dyes. *Toxicology in Vitro,* 32**,** 1-7.

PENG, Y., YADAVA, P., HEIKKINEN, A. T., PARROTT, N. & RAILKAR, A. 2014. Applications of a 7-day Caco-2 cell model in drug discovery and development. *European Journal of Pharmaceutical Sciences,* 56**,** 120-130.

RAEMDONCK, K., BRAECKMANS, K., DEMEESTER, J. & DE SMEDT, S. C. 2013. Merging the best of both worlds: Hybrid lipid-enveloped matrix nanocomposites in drug delivery. *Chemical Society Reviews,* 43**,** 444-472.

RASTOGI, H., PINJARI, J., HONRAO, P., PRABAND, S. & SOMANI, R. 2013. The impact of permeability enhancers on assessment for monolayer of colon adenocarcinoma cell line (CACO-2) used in in vitro permeability assay. *Journal of Drug Delivery and Therapeutics,* 3**,** 20-29.

RISS, T. L., MORAVEC, R. A., NILES, A. L., BENINK, H. A., WORZELLA, T. J., MINOR, L., STORTS, D. & REID, Y. 2013. Cell Viability Assays. *In:* SITTAMPALAM GS, COUSSENS NP & NELSON H (eds.) *Assay Guidance Manual* Bethesda (MD): Eli Lilly & Company and the National Center for Advancing Translational Sciences.

RIVOLTA, I., PANARITI, A., LETTIERO, B., SESANA, S., GASCO, P., GASCO, M., MASSERINI, M. & MISEROCCHI, G. 2011. Cellular uptake of coumarin-6 as a model drug loaded in solid lipid nanoparticles. *Journal of Physiology and Pharmacology,* 62**,** 45.

RÓKA, E., UJHELYI, Z., DELI, M., BOCSIK, A., FENYVESI, É., SZENTE, L., FENYVESI, F., VECSERNYÉS, M., VÁRADI, J., FEHÉR, P., GESZTELYI, R., FÉLIX, C., PERRET, F. & BÁCSKAY, I. 2015. Evaluation of the cytotoxicity of α-cyclodextrin derivatives on the Caco-2 cell line and Human Erythrocytes. *Molecules,* 20**,** 20269–20285.

SAMBUY, Y., DE ANGELIS, I., RANALDI, G., SCARINO, M., STAMMATI, A. & ZUCCO, F. 2005. The Caco-2 cell line as a model of the intestinal barrier: influence of cell and culture-related factors on Caco-2 cell functional characteristics. *Cell Biology and Toxicology,* 21**,** 1-26.

SEMETE, B., BOOYSEN, L., LEMMER, Y., KALOMBO, L., KATATA, L., VERSCHOOR, J. & SWAI, H. S. 2010a. In vivo evaluation of the biodistribution and safety of PLGA nanoparticles as drug delivery systems. *Nanomedicine: Nanotechnology, Biology and Medicine,* 6**,** 662-671.

SEMETE, B., BOOYSEN, L. I. J., KALOMBO, L., VENTER, J. D., KATATA, L., RAMALAPA, B., VERSCHOOR, J. A. & SWAI, H. 2010b. In vivo uptake and acute immune response to orally administered chitosan and PEG coated PLGA nanoparticles. *Toxicology and Applied Pharmacology,* 249**,** 158-165.

SEVIN, E., DEHOUCK, L., FABULAS-DA COSTA, A., CECCHELLI, R., DEHOUCK, M. P., LUNDQUIST, S. & CULOT, M. 2013. Accelerated Caco-2 cell permeability model for drug discovery. *Journal of Pharmacological and Toxicological Methods,* 68**,** 334-339.

SGS 2011. Caco-2 cellular system: An overview. *In:* SERVICE, S. S. L. S. (ed.). SGS Life Science - Technical Bulletin.

STOCKERT, J. C., BLÁZQUEZ-CASTRO, A., CAÑETE, M., HOROBIN, R. W. & VILLANUEVA, Á. 2012. MTT assay for cell viability: Intracellular localization of the formazan product is in lipid droplets. *Acta Histochemica,* 114**,** 785-796.

STROBER, W. 2001. Trypan blue exclusion test of cell viability. *Current Protocols in Immunology.* John Wiley & Sons, Inc. 21, A.3B.1–A.3B.2.

SUN, H. & PANG, K. S. 2008. Permeability, Transport, and Metabolism of Solutes in Caco-2 Cell Monolayers: A Theoretical Study. *Drug Metabolism and Disposition,* 36**,** 102-123.

SUN, M., FU, H., CHENG, H., CAO, Q., ZHAO, Y., MOU, X., ZHANG, X., LIU, X. & KE, Y. 2012. A dynamic real-time method for monitoring epithelial barrier function in vitro. *Analytical Biochemistry,* 425**,** 96-103.

SUTRADHAR, B., PARK, J., HONG, G., CHOI, S. & KIM, G. 2010. Effects of trypsinization on viability of equine chondrocytes in cell culture. *Pakistan Veterinary Journal* 30**,** 232-238.

SZABO, S. E., MONROE, S. L., FIORINO, S., BITZAN, J. & LOPER, K. 2004. Evaluation of an automated instrument for viability and concentration measurements of cryopreserved hematopoietic cells. *Laboratory Hematology,* 10**,** 109-111.

TANGYUENYONGWATANA, P., KOWAPRADIT, J., OPANASOPIT, P. & GRITSANAPAN, W. 2009. Cellular transport of anti-inflammatory pro-drugs originated from a herbal formulation of Zingiber cassumunar and Nigella sativa. *Chinese Medicine,* 4**,** 19, 5 Pages.

TENG, Z., KUANG, X., WANG, J. & ZHANG, X. 2013. Real-time cell analysis – A new method for dynamic, quantitative measurement of infectious viruses and antiserum neutralizing activity. *Journal of Virological Methods,* 193**,** 364-370.

TUKULULA, M., HAYESHI, R., FONTEH, P., MEYER, D., NDAMASE, A., MADZIVA, M., KHUMALO, V., LUBUSCHAGNE, P., NAICKER, B., SWAI, H. & DUBE, A. 2015. Curdlan-conjugated PLGA nanoparticles possess macrophage stimulant activity and drug delivery capabilities. *Pharmaceutical Research,* 32**,** 2713-2726.

VLLASALIU, D., FOWLER, R., GARNETT, M., EATON, M. & STOLNIK, S. 2011. Barrier characteristics of epithelial cultures modelling the airway and intestinal mucosa: A comparison. *Biochemical and Biophysical Research Communications,* 415**,** 579-585.

ZHANG, B., SHAN, H., LI, D., LI, Z. R., ZHU, K. S., JIANG, Z. B. & HUANG, M. S. 2012. Different methods of detaching adherent cells significantly affect the detection of TRAIL receptors. *Tumori,* 98**,** 800-3.

CHAPTER 5

This chapter comprises all the *in vivo* work done using BALB/c mice to determine the effect of the NP-Pheroid® hybrid drug delivery system on the pharmacokinetics of anti-TB drugs. The work covered in this chapter will make up a full-length article to be submitted to the "*International Journal of Pharmaceutics*". The author guidelines for this journal are given in Annexure B of this thesis.

The aims of this chapter were:

a) To study how the hybrid DDS affects the plasma levels of isoniazid and rifampicin in mice.
b) To determine the effect of the hybrid system on organ distribution of these two anti-TB drugs.

CHAPTER 5: PHARMACOKINETIC EVALUATION OF ANTI-TB DRUGS IN A NP – PHEROID® HYBRID DRUG DELIVERY SYSTEM

Madichaba P Chelopo[a,b], Lonji Kalombo[a], Brendon Naicker[a], Anne Grobler[b], Rose Hayeshi[b*]

[a] Council for Scientific and Industrial Research, Materials Science and Manufacturing, Polymers and Composites, PO Box 395, Pretoria, 0001, South Africa

[b] North-West University, DST/NWU Preclinical Drug development Platform, Potchefstroom, 2520, South Africa

[*] Corresponding author: Rose.Hayeshi@nwu.ac.za

1. Abstract

Hybrid drug delivery systems (DDS) have recently emerged as robust vehicles with the potential for improving the pharmacokinetic (PK) properties of several drugs. In this study, *in vivo* evaluation was carried out to investigate the potential of a PLGA NP-Pheroid® hybrid formulation to improve the PK properties of loaded anti-tuberculosis drugs in comparison with the free drugs and with drug-loaded NP. BALB/c female mice were used to study the effect of the hybrid formulation on the PK of two major anti-TB drugs, rifampicin (RIF) and isoniazid (INH), in both plasma and selected organs. Statistical comparison between the three formulations did not indicate any significant difference with respect to plasma PK parameters on a 5% confidence level ($P > 0.05$). INH could not be detected in any of the harvested organs, while RIF was widely distributed to all the harvested organs with its highest accumulation detected in the liver. The significant effect observed from the hybrid formulation was reduced time to reach maximum concentration (T_{max}) as well as prolonged circulation of RIF in the lungs in comparison with the free RIF and RIF NP.

2. Introduction

Tuberculosis (TB) is a chronic, highly contagious airborne infection that is caused by a rod-shaped bacillus called *Mycobacterium tuberculosis* (*M.tb*) and it is one of the major causes of death from infectious diseases worldwide. South Africa is ranked amongst the top 22 high burden countries which account for 83% of all TB incidence globally (WHO, 2015). The occurrence of TB among people living with human immunodeficiency virus (HIV) infection is

highest in most poverty-stricken countries in the African region and South Africa alone has reported more than 50% of HIV-TB co-infected patients in 2014 (UNAIDS, 2014). The current treatment for TB, requires a fixed dose combination (FDC) of the four potent drugs:, rifampicin (RIF), isoniazid (INH), pyrazinamide (PYZ) and ethambutol (ETB), to be taken daily for a period of up to six months (D'Ambrosio *et al.*, 2015). The long duration of this therapy, as well as the development of side effects, causes patients to be less compliant to the scheduled administration which has led to the development of multidrug-resistant TB (MDR-TB) strains subsequently resulting in multiple challenges in the treatment of this infectious disease (Hari *et al.*, 2010, D'Ambrosio *et al.*, 2015). The emergence of *M.tb* resistant strains to the current broad range of drugs in the FDC has led to the exploration of various avenues to improve the current TB therapy. These avenues include a search for novel compounds that are active against *M.tb* as well as the design of innovative drug delivery systems (DDS) to enhance the pharmacokinetic (PK) properties of the current drugs.

PK involves the kinetics of absorption, distribution, metabolism and elimination of an investigated drug in animal models, in preclinical studies; or human subjects, in clinical studies (Urso *et al*., 2002). The amount of the administered drug that reaches the systemic circulation for bioactivity represents the drug's bioavailability. Quantifying the levels or concentrations of a drug in body fluids or tissues at various time points provides an insight into the pathway that a drug follows from entering the body until it gets to the target site as well as a calculated estimation of the drug effect. A single PK profile can be represented using the following parameters: maximum concentration (C_{max}), time to reach maximum concentration (T_{max}), drug half-life ($t_{1/2}$) and area under the curve (AUC) among others (Urso *et al*., 2002). C_{max} refers to the peak concentration that the drug reaches in blood plasma or a specified organ in the body after administration; T_{max} is the time at which the C_{max} occurs; $t_{1/2}$ indicates the time required for the drug to reach half of its original concentration and AUC represents the index of drug exposure to the body (plasma levels) or a specified organ. The PK parameters of currently used anti-TB drugs differ, and a comprehensive understanding of the current TB treatment such as the function, dose, and efficacy is required for the rational design of new agents, dosage form or drug delivery vehicle (Davies and Nuermberger, 2008, du Toit *et al.*, 2006).

Out of the four drugs in the FDC, INH and RIF are considered to be the most effective drugs in TB chemotherapy (Somasundaram *et al.*, 2014). INH is a hydrophilic drug, and its bactericidal activity involves the inhibition of the mycolic acid biosynthesis, which is essential for the *M.tb* bacterial cell wall (Kolyva and Karakousis, 2012). Although INH has been

reported to be quickly absorbed, its elimination is influenced by the rate of its metabolism by *N*-acetyltransferase, which leads to differences in its half-life amongst human subjects (Wang *et al.*, 2016, Arbex *et al.*, 2010, McIlleron *et al.*, 2006). RIF, on the other hand, is a highly lipophilic drug that acts by preventing the activity of DNA-dependent RNA polymerase and therefore inhibiting bacterial cell division (Kolyva and Karakousis, 2012). A large percentage of RIF is metabolised through microsomal enzymes found in the liver and high oral bioavailability of RIF has been demonstrated, however, RIF can be further deacylated into a less absorbable metabolite (Agrawal and Panchagnula, 2005, Arbex *et al.*, 2010, McIlleron *et al.*, 2006). The use of animal models such as mice to study the PK properties of drugs in various formulations or delivery vehicle is a crucial step to ensure optimisation of TB therapy (Davies and Nuermberger, 2008).

The encapsulation of anti-TB drugs within DDS presents the potential to improve the therapy for this life-threatening disease (Wang *et al.*, 2013, Basavaraj and Betageri, 2014). DDS have demonstrated the capability to enhance the PK of anti-TB drugs (Swai *et al.*, 2009, Pinheiro *et al.*, 2011). The preparation and the *in vivo* evaluation of poly(DL-lactic-*co*-glycolic acid) (PLGA) nanoparticles (NP), encapsulating anti-TB drugs have been reported in several studies (Pandey *et al.*, 2003a, du Toit *et al.*, 2006, Semete *et al.*, 2010). These NP formulations were found to improve several PK parameters of the anti-TB drugs, due to their slow release as the PLGA gradually biodegrades in the body. Lipid-based DDS have also been used to transport anti-TB drugs *in vivo* for the improvement of TB therapy (Singh *et al.*, 2013, Bhandari and Kaur, 2013, Pinheiro *et al.*, 2011). The Pheroid® system is a lipid-based emulsion, that has also been investigated for delivery of anti-TB drugs *in vivo* and has demonstrated rapid absorption and increased drug plasma levels of these drugs (Grobler, 2009, Nieuwoudt, 2009). The pro-Pheroid® is a stable precursor of the Pheroid ® system composed of a free-flowing oil phase saturated with nitrous oxide, which spontaneously forms vesicles when in contact with an aqueous phase (Grobler *et al.*, 2014, Matthee, 2007).

Hybrid DDS have emerged as an innovative delivery platform with better potential than individual DDS, for improving the PK properties of several drugs (Wong *et al.*, 2006, Zhang *et al.*, 2008, Hadinoto *et al.*, 2013). For example, lipid-based DDS have been combined with polymeric NP leading to a more robust hybrid delivery technology, in attempts to improve cancer therapy (Raemdonck *et al.*, 2013). This research study aims to evaluate a novel hybrid DDS, composed of PLGA NP and Pheroid® system, see Figure 1, for its potential to improve the PK properties of INH and RIF. The *in vivo* study in mice was designed to determine the

effect of entrapping INH and RIF in the NP-Pheroid® hybrid DDS, on the PK of the anti-TB drugs through the measurements of:

- The plasma levels of the drugs from the hybrid system in comparison with the free drugs and drug-loaded NP over a period of 14 days.
- The biodistribution of these drugs across the liver, kidneys, lungs and intestines

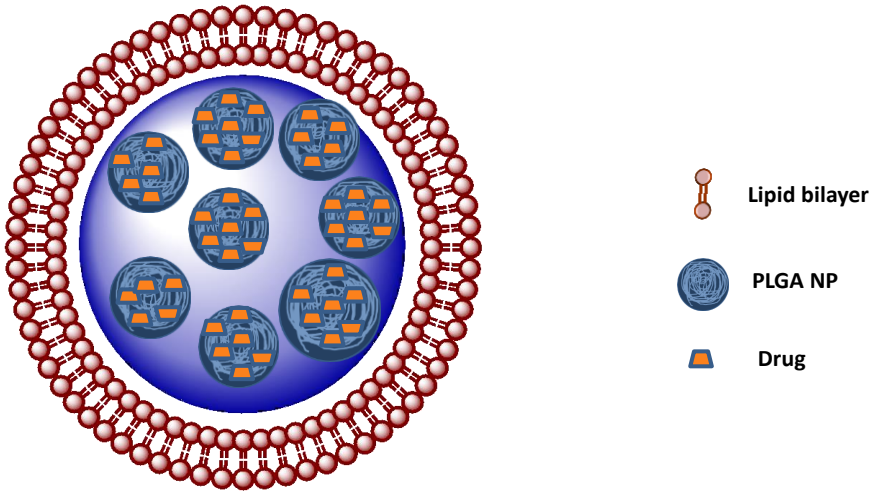

Figure 1: The hypothetical structure of drug-loaded NP-Pheroid® hybrid drug delivery system (DDS). This image illustrates the drug loaded-PLGA NP core enveloped by a Pheroid® lipid bilayer shell.

3. Materials and methods

3.1. Materials

All chemicals and solvents were purchased from Sigma Aldrich Products (Johannesburg, South Africa) unless otherwise stated. Pluronic® F127 and Kolliphor EL were obtained from BASF AG (Ludwigshafen, Germany), stearic acid from Merck (Sandton, South Africa); Surfynol 104 PG 50 was purchased from Air Products (Kempton Park, South Africa); chitosan was purchased from Fluka Air Products (Emalahleni, South Africa). Vitamin F ethyl ester was obtained from Chemisches Laboratorium (Berlin, Germany); Butylated hydroxyanisole (BHA), butylated hydroxytoluene (BHT), polyethylene glycol (PEG 400) and D/L-α-Tocopherol was supplied by Chempure (Germiston, South Africa). Sterile water was purchased from SABAX (Johannesburg, South Africa) and medicinal nitrous oxide (N_2O) was

from Afrox, (Klerksdorp, South Africa). HPLC grade acetonitrile (ACN) was purchased from Merck. Rifampicin (RIF) and isoniazid (INH) were supplied by DB fine Chemicals (Woodmead, Johannesburg).

3.2. Methods

3.2.1. Preparation and characterisation of drug- loaded NP–Pheroid®

The drug-loaded NP were produced as previously described (Chelopo *et al.*, 2017). The INH NP were prepared by dissolving PLGA in ethyl acetate (EA) at a concentration of 15 mg/ml; a drop of Surfynoyl and 0.2% (w/v) stearic acid (in EA) were added as soon as the PLGA dissolved. A solution of INH (110 mg/ml) in 1% (w/v) Pluronic® F127 (in water) was homogenised (High Speed Homogenizer, Silverson L4R) at 5000 rpm with the above PLGA solution on ice for 3 minutes (min) to make a water-in-oil (w/o) emulsion. The RIF NP were produced by dissolving RIF (10 mg/ml) and PLGA (12.5 mg/ml) in EA and the first w/o emulsion was formed by homogenisation at 5000 rpm with a solution of 1% Pluronic® F127 in an aqueous medium. The w/o emulsions of the two drugs were individually homogenised on ice again at 8000 rpm in an aqueous mixture composed of 0.3% (w/v) chitosan (CT), 1% (w/v) polyethylene glycol (PEG), 2% (w/v) polyvinyl alcohol (PVA) and 5% (w/v) lactose monohydrate for 5 min to form a double emulsion (w/o/w). This emulsion was then fed into a bench top Buchi Mini B-290 spray dryer (BÜCHI Labortechnik AG, Flawil, Switzerland) at the following conditions: aspirator = 100%; pump = 2; pressure = 6 – 7 bars, inlet temperature = 96 °C and outlet temperature = 70 °C. Both INH- and RIF- loaded NP produced were in the form of solid, free-flowing powder.

To combine the drug loaded NP with the Pheroid® system, a pro-Pheroid® formulation was first prepared using a previously reported method (Grobler *et al.*, 2014). A mixture of 4.9% (w/w) PEG 400, 66.4% (w/w) Vitamin F ethyl ester, 0.01% (w/w) BHA and 0.01% (w/w) BHT was heated to 70 °C while Kolliphor EL, 27.7% (w/w), was heated to 120 °C. The mixture was then combined with the Kolliphor EL and cooled to 55 °C followed by the addition of 1% (w/w) D/L-α-tocopherol. INH NP and RIF NP were first exposed to UV light for 10 min for sterilisation, and the appropriate amount of each was then added to the pro-Pheroid® mixture. INH NP were added to a portion of the pro-Pheroid® constituents such that the final dose of INH to mice would be 5 mg/kg, while the RIF NP were added to result in a dose of 10 mg/kg of RIF when administered to mice. The combined pro-Pheroid® and drug-loaded NP were

placed in a small pressure vessel located inside a laminar flow hood and gassed with N_2O under the pressure of 200 kPa for 4 days. Sterile water saturated with N_2O was added to the pro-Pheroid®, to instantaneously form the Pheroid® vesicles immediately prior to administration to mice. The amount of water added was calculated from the number of mice to be treated ensuring that the dose remains constant.

In order to determine the size, the drug-free pro-Pheroid® and drug-loaded NP pro-Pheroid® were added to an aqueous solution with 1% (v/v) 0.1 N hydrochloric acid (HCl), to simulate the stomach environment and analysed for size and size distribution using a laser diffraction technique on a Hydro Mastersizer 2000MU (Malvern Instruments Ltd., United Kingdom). The zeta potential (ζ-potential) was determined through electrophoretic mobility using a Zetasizer Nano ZS (Malvern Instruments Ltd., United Kingdom). Visual analysis was done through confocal laser scanning microscopy (CLSM, Nikon D-Eclipse C1, Netherlands) as illustrated in Chapter 3 of this thesis, by staining the Pheroid® with Nile red (Chelopo *et al.*, 2017).

3.2.2. Drug loading and encapsulation efficiency determination

The percentage drug loading (DL) and encapsulation efficiency (EE) of INH and RIF were determined from the drug-loaded PLGA NP formulation using the following direct methods. The DL determined from the PLGA NP were assumed to be equal to those in Pheroid-NP hybrid system. INH NP were hydrolysed in 0.05 M NaOH solution overnight and then neutralised to pH 6-7 using 0.1 M HCl solution. INH standard solutions, with a concentration range of 1-50 µg/ml, were prepared simultaneously with the INH NP samples using the same procedure. The loading of RIF in the NP was determined using a previously reported procedure (Tukulula *et al.*, 2015). RIF NP were weighed and dissolved in acetonitrile, which made up 40% of the final solution, through sonication. Phosphate buffer (pH 6.64) making up the remaining 60% was then added, and the mixture was centrifuged at 10 000 g for 10 min at room temperature, using a Sigma 3K30 Centrifuge (United Kingdom), and the supernatant was collected for high-performance liquid chromatography (HPLC) analysis. RIF standard solutions, with a concentration range of 1-50 µg/ml, were also prepared simultaneously with the RIF NP samples using the same procedure. All INH NP and RIF NP samples were diluted ten times in 40:60 ACN:phosphate buffer (pH 6.64), to match the HPLC mobile phase.

Both the standard solutions and diluted samples were analysed using an HPLC coupled to an SPD Diode array detector, with a CTO-10AS VP column oven (Shimadzu Prominence HPLC

series, Shimadzu Corporation, Kyoto, Japan). INH and RIF were eluted under isocratic conditions using the above specified mobile phase. The maximum HPLC back pressure during the run ranged from 1815 to 1845 psi. Injection volume was set at 20 µl, and the drugs were each eluted at a flow rate of 1 ml/min at 268 nm and 254 nm detection wavelengths for INH and RIF, respectively. The DL and EE were calculated using the following equations:

$$\text{DL (\%)} = \frac{Actual\ Amount\ (mass)\ of\ RIF\ or\ INH\ encapsulated}{Amount\ (mass)\ of\ the\ nanoparticle\ weighed} \times 100$$

(Equation 5.1)

$$\text{EE (\%)} = \frac{Total\ Mass\ of\ RIF\ or\ INH\ used\ in\ the\ \ formulation - Mass\ of\ RIF\ unencapsulated}{Initial\ Amount\ (mass) of\ RIF\ or\ INH\ added} \times 100$$

(Equation 5.2)

3.2.3. Experimental animals

The animal species mostly used for the preclinical development of anti-TB drugs are mice, especially BALB/c strain, due to their susceptibility to being infected by *M. tuberculosis* (De Groote *et al.*, 2011). Inbred, specified pathogen-free, BALB/c mice were obtained from the University of KwaZulu-Natal. Female mice, 6-7 weeks old with an average weight of 20 g were used. Female BALB/c mice were chosen to avoid the aggressive interaction that usually occurs between male mice that may compromise the well-being of other mice and could lead to invalid experimental results (Van Loo *et al.*, 2003). Ethics approval for this study was obtained from the North-West University (NWU) research ethics committee (Ethics approval number: NWU-00128-11-A5.). The study was conducted at the Vivaruim of the NWU, Potchefstroom Campus. The mice were housed in individually ventilated cages with sterilised dust free wood bedding, under controlled temperature of 22 ± 1ºC, relative humidity of 55% (± 10%), a light/dark cycle of 12 h, and ventilation of 20 air changes per h under positive pressure. Mice were randomly assigned to experimental groups with eight mice per group. Sufficient care for the mice was ensured by cleaning of cages and animal rooms every third day by well-trained animal caretakers. Mice were allowed to acclimatise for one week and a

half before the commencement of the experiments. They were provided with standard pellet diet as well as sterile water ad libitum.

3.2.4. Administration of the formulations to the mice and sample collection

The total number of 480 mice was divided into six test groups, each with 80 animals, as shown in Table 1. Test formulations were orally administered and from each test group, eight mice were euthanised at ten different time points (6 groups x 10 time points x 8 mice = 480 mice).

Table 1: Test group assignment of the mice (INH was given at 5 mg/kg and RIF at 10 mg/kg)

Group code	Test Formulations
G1A	Pure Isoniazid (INH) dissolved in water
G2A	Isoniazid (INH) NP suspended in water
G3A	Isoniazid (INH) NP entrapped in Pheroid® vesicles
G1B	Pure Rifampicin (RIF) sonicated in water
G2B	Rifampicin (RIF) NP suspended in water
G3B	Rifampicin (RIF) NP entrapped in Pheroid® vesicles

Each mouse was firmly restrained using the double handed manual restraint method shown in the diagrams in Figure 2. Each mouse was picked up by holding the end of the tail and placed on the lid of the cage for gripping (1). The base of the tail was placed between the index finger and thumb of the right hand while the remaining three fingers were placed gently but firmly on the back of the mouse (2). Subsequently, the skin of the neck (as close to the ears as possible) was pulled between the thumb and index finger of the left hand, the mouse was lifted to get the mouth, pharynx and stomach in a straight line - vertical position (3). The needle was carefully inserted through the oesophageal orifice and 200 µl directly injected into the stomach (4). Each treated mouse was numbered through ear punching for identification.

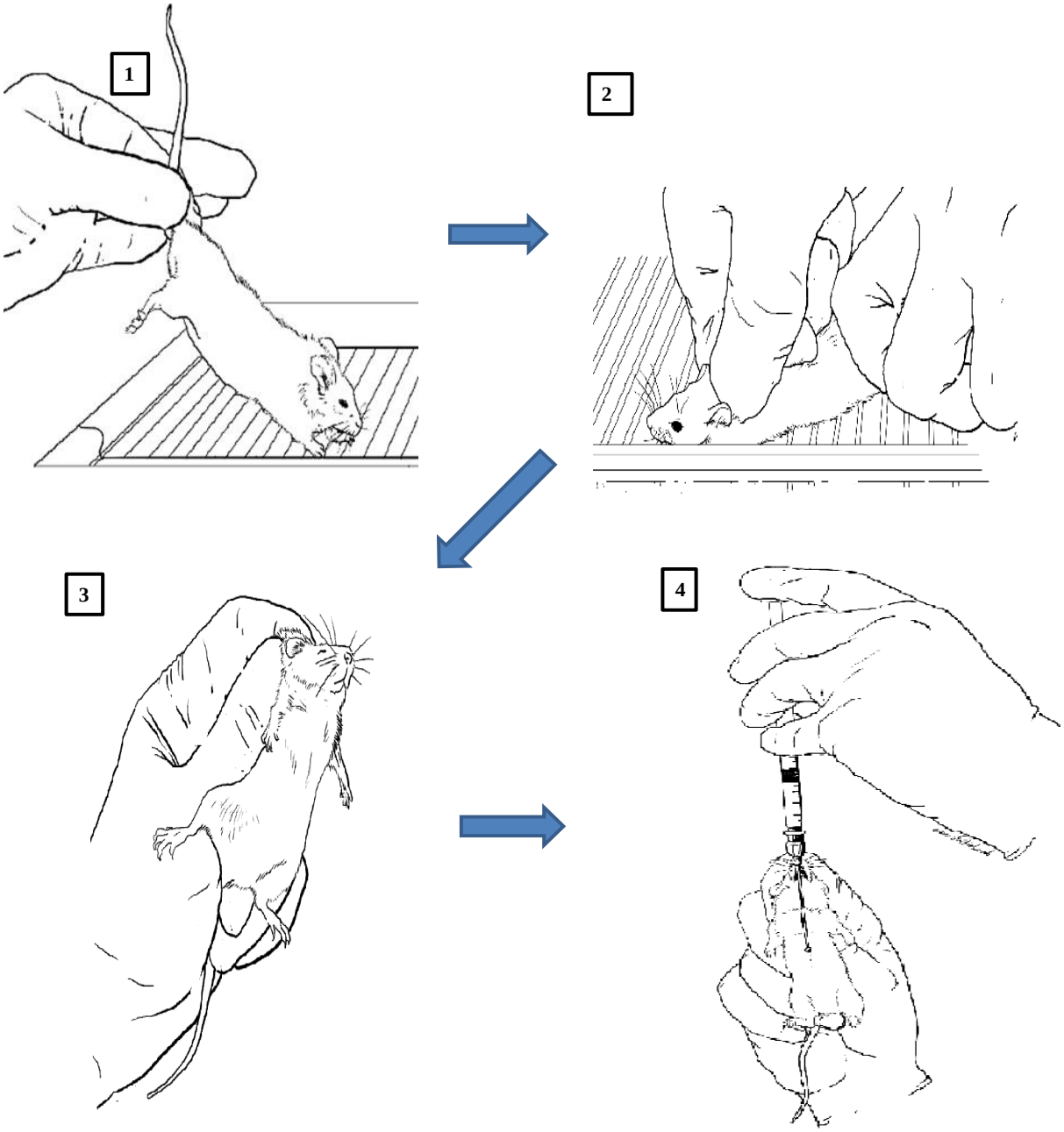

Figure 2: The illustration of four steps taken in handling and restraining a mouse for an oral gavage administration of drugs, Images obtained with permission from UIC, (2014).

A single dose of either 5 mg/kg INH or 10 mg/kg RIF, formulated in three test formulation (free drug; drug loaded NP and drug loaded NP-Pheroid®), was administered to mice in a volume of 200 µl via oral gavage. . The drug-loaded Pheroid® group was excluded, due to limited resources and thus relied on the fact that the study was previously conducted using the

same dose of RIF and INH (Nieuwoudt, 2009). Each formulation was administered to a group of eight mice at a time, which were then euthanised at 2 hours (h), 4 h, 8 h, 12 h, 24 h, 3 days (d), 5 d, 7 d and 14 d. Mice that were euthanised without receiving formulation formed the blank (0h time point) samples. Whole blood was drawn from the heart, via cardiac puncture, and was collected into Eppendorf™ tubes that already contained heparin to prevent the coagulation of the blood. The blood plasma was obtained as a supernatant after centrifuging the whole blood at 5000 rpm for 5 min and was collected into cryovials that were snap-frozen in liquid nitrogen. Organs (liver, lungs, kidneys and intestines) were also simultaneously collected from each mouse in cryovials and were snap frozen in liquid nitrogen. Both the plasma and organ samples were stored at -80ºC until analysis by liquid chromatography-tandem mass spectrometry (LC-MS/MS).

3.2.5. Plasma sample preparation

Liquid-liquid sample extraction was used to extract INH and RIF from the plasma. INH plasma (10 µl) samples were diluted five times using an extraction solvent (50 µl), made of 50% acetonitrile (ACN) in deionised water with 0.03% (v/v) formic acid (FA) and 100 µl of 1µg/ml 6-aminonicotinic acid (6-ANA) as internal standard (IS). RIF plasma samples (10 µl) were also diluted five times using a solution mixture of 1µg/ml rifabutin (RIB) as internal standard (IS) and pure acetonitrile (ACN) with 0.03% (v/v) FA as extraction solvent. The samples were vortex mixed for 1 min and centrifuged at 10 000 g at 16 °C for 15 min, using Sigma 3K30 Centrifuge (United Kingdom). The supernatant was transferred into inserts placed in labelled HPLC vials for LC-MS/MS analysis.

3.2.6. Organ (liver, lungs, kidneys and intestines) sample preparation

The organs were slowly thawed on ice, separately weighed into round bottomed tubes where 4 ml of IS (1µg/ml) was added (RIB for RIF samples and 6-ANA for INH samples) and 1 ml of the extraction solvent (ACN for RIF samples and 50% ACN for INH samples). All samples were thoroughly homogenised using a micro homogeniser, Stuart SHM1 (Bibby Scientific, United Kingdom), at 35 000 rpm, followed by a water-bath sonication for about 5 min. The homogenates were then centrifuged at 20 000 g for 15 min at 16 °C, using Sigma 3K30 Centrifuge (United Kingdom). The supernatant (500 µl) was transferred into Eppendorf™ tubes and centrifuged once again at 15 000 g at 16 °C for 15 min. The final supernatant was added to inserts in labelled HPLC vials for analysis.

3.2.7. Calibration curves

The stock solution of INH (100 μg/ml) and its IS, 6-ANA (100 μg/ml), were prepared in extraction solvent made of 50% ACN in deionised water with 0.03% (v/v) FA while the stock solution of RIF (100 μg/ml) and RIB (100 μg/ml) were prepared in 100% ACN with 0.03% FA. The linearity was established by constructing a standard curve of both RIF and INH separately with a concentration range of 0.1 to 50 μg/ml, through serial dilution. The IS (RIB or 6-ANA) were diluted to a final concentration of 1 μg/ml with 0.03% FA, which was kept constant in all samples.

Blank plasma (50 μl) was spiked with standard solutions of either RIF or INH. Each sample was further diluted in Eppendorf™ tubes by adding a 1 μg/ml of internal standard (100 μl) and an extraction solvent (50 μl). All standards and samples (RIF and INH) were mixed through vortex, then centrifuged and analysed the same way as the plasma samples. Standards for organ samples (at the same concentration range as for the plasma) were prepared by spiking a known weight of blank organ homogenate with 4 ml of 1 μg/ml internal standard and 1 ml of RIF or INH standard solutions. These samples were homogenised, centrifuged and analysed similarly to the organ samples. The plasma and organ spiking with the addition of IS to all samples compensated for any matrix effects.

3.2.8. LC-MS/MS method

The levels of INH and RIF in the plasma and organs were determined on a Shimadzu Prominence Ultra-Fast LC (UFLC) series system (Shimadzu Corporation, Kyoto, Japan) coupled to an ABSciex 3200 Q-Trap Triple Quadrupole Tandem Mass Spectrometer (ABSciex, Massachusetts, USA). Quantification was achieved by multiple reaction monitoring (MRM) in positive electrospray ionisation (ESI) mode. Compound optimisation of each drug yielded major fragmentation ions as follows: RIF 824→792; RIB 848→816; INH 138→121; 6-ANA 139→93, see Figure 3. The sample injection volume used was 10 μl, and the chromatographic separation was achieved using a Phenomenex Gemini 5μ C18 110Å column 250 x 4.6mm for INH analysis and a Phenomenex Kinetex 2.6μ C18 100Å 50 x 2.1mm column for RIF analysis. Gradient elution was implemented using varying composition of the mobile phase from 50% to 95% ACN in deionised water while 0.03% FA remained constant. The flow rate was 0.5 ml/min for INH and 0.75 ml/min for RIF. The inclusion of the IS in all steps of the extraction method compensated for any matrix effects.

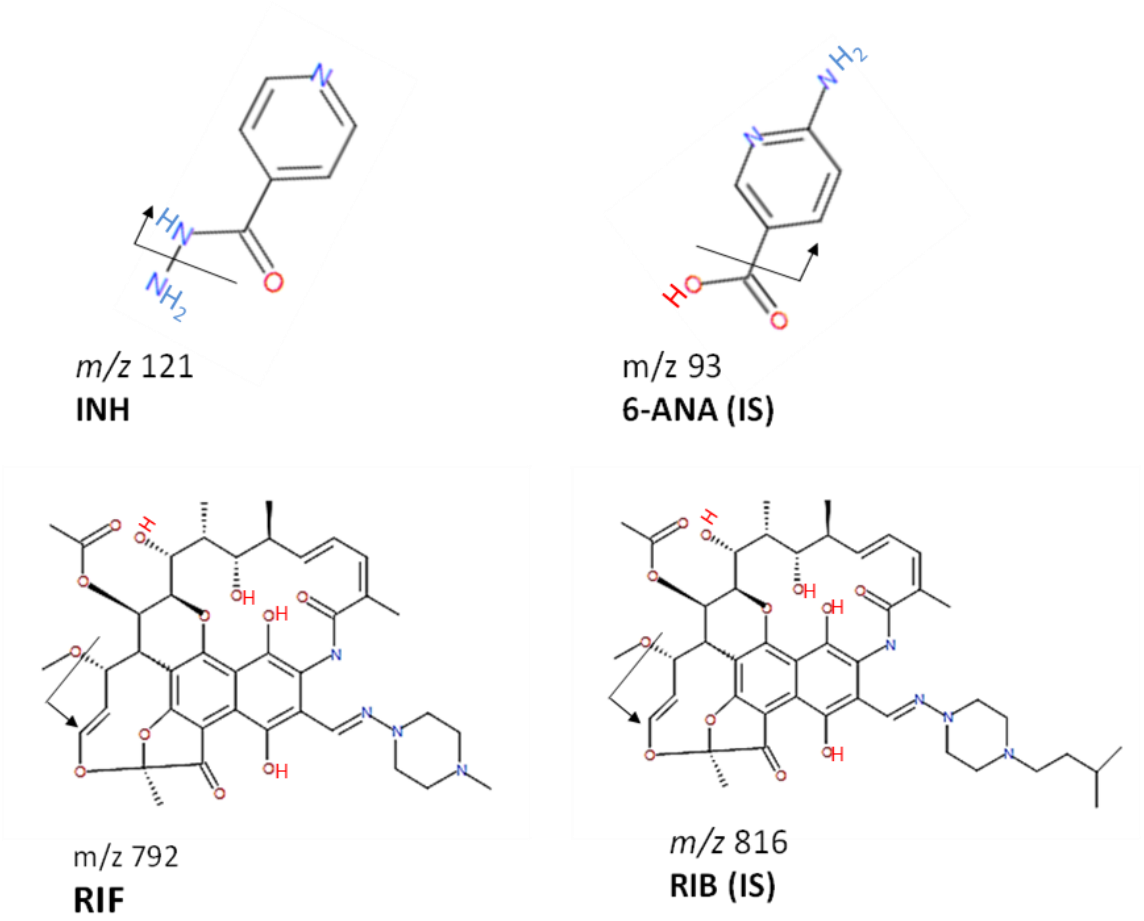

Figure 3: Chemical structures and the mass-to-charge ratio (m/z) of the two anti-TB drugs, INH and RIF, as well as their internal standards (IS), RIB and 6-ANA. The arrow shows the anticipated points of fragmentation to form major ions for detection.

3.2.9. Data analysis

The PK parameters of RIF and INH in the plasma and organs of the mice were calculated from the individual concentration-time curves of each mouse, by using non-compartmental methods. The PK parameters, AUC, C_{max}, T_{max} and $t_{1/2}$ were determined using SAS software (SAS Institute Inc. 2016). One-way analysis of variance (ANOVA) was applied in comparing the differences in the PK parameters between the free drug, NP and NP-Pheroid® formulations. The Kruskal-Wallis post-test was also applied to compare the treatments. Descriptive statistics

for the three types of formulation groups are given as mean ± standard deviation (SD). STATISTICA software (StatSoft, Inc. version 12 (2014)) was used to perform statistical analysis at the significance level of 5% ($p < 0.05$).

4. Results and discussion

4.1. Characterisation of the drug-loaded NP-Pheroid® hybrid system

The preparation of drug (RIF or INH)-loaded NP-Pheroid® system involved the use of pro-Pheroid®, which only consists of the oil phase saturated with N_2O gas, as it is a more suitable formulation for the stability of RIF and INH than in a liquid form for PK studies with mice (Grobler, 2008, Nieuwoudt, 2009, Grobler *et al.*, 2014). Using pro-Pheroid® can be compared to the use of pro-liposomes, as a stable alternative for the oral delivery of drugs for *in vivo* evaluation, rather than normal liposomes, which are unstable for oral delivery (Chu *et al.*, 2011). The pro-Pheroid® formulations were prepared by adding the appropriate amount of the drug-loaded NP to the pro-Pheroid® oil phase constituents. The NP-Pheroid® vesicles were spontaneously formed by adding sterile N_2O-saturated water to the pro-Pheroid® before administration to the mice. The particle size and ζ-potential of the formed vesicle were measured by adding 0.1 N HCl aqueous solution to mimic the stomach conditions, as previously done (Nieuwoudt, 2009, Grobler *et al.*, 2014) and the results are shown in Table 2.

Table 2: The particle size, polydispersity index (PDI) and zeta potential of the Pheroid® vesicles prepared from the pro- Pheroid® and their combination to INH/RIF-loaded NP (<1% w/v). (n=2).

	d(0.1) /µm	d(0.5) /µm	d(0.9) /µm	Mean Particle Size /µm	PDI / Uniformity	Zeta Potential /mV
Free Pheroid®	1.14	36.02	87.35	40.17	0.76	-21.25
INH NP-Pheroid®	0.65	9.36	68.07	23.37	2.23	-17.56
RIF NP-Pheroid®	0.65	7.54	62.21	28.54	3.51	-11.02

The vesicles formed from pro-Pheroid® formulation displayed a wide size distribution. The mean particle size and broad distribution range obtained are comparable to those obtained by Grobler *et al.* (2014), who characterised their Pheroid® formulations in a similar way to this current study. However, they reported the span value, which is an alternative demonstration of the size distribution calculated from the d(0.1), d(0.5) and d(0.9) percentile, instead of the PDI value. The pro-Pheroid® vesicles obtained in this study had relatively high negative ζ-potential (-11 to -21 mV) compared to those reported by Grobler *et al.,* (2014), which were almost in the neutral ranges (1-3 mV). Their low zeta potential was deemed to be due to the presence of PEG 400 in the pro-Pheroid® formulation; however this constituent was also included in this current study and yet the lowest ζ-potential obtained was -11 mV from the RIF NP-Pheroid® vesicles. The difference between the ζ-potential obtained in this study and that by Grobler *et al*., (2014) could have been influenced by the use of different instrument used for ζ-potential measurements. A Malvern 2000 Zetasizer was used in the Grobler *et al.,* (2014) study while a Malvern Zetasizer Nano ZS was used in this current research and these two techniques use different principles in the determination of ζ-potential. Although ζ-potential is a crucial parameter in establishing particle stability, the Pheroid® vesicles produced from pro- Pheroid® may have a relatively low ζ-potential but the system remains stable as the aggregation of the vesicles is inhibited by the steric hindrance between the vesicles caused by the presence of PEG molecules (Grobler *et al*., 2014, Jokerst *et al.,* 2011). The Pheroid® vesicles formed from pro-Pheroid® are well separated spherical particles, which are shown in the CLSM image in Figure 4.

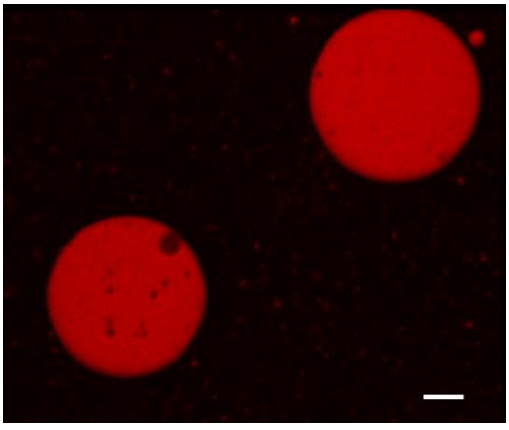

Figure 4: The CLSM images of Pheroid® vesicles produced from pro-Pheroid®, stained using Nile Red. (*Scale bar = 8.9 µm.*)

4.1.1. Drug loading (DL) and encapsulation efficiency (EE)

INH and RIF from the NP were detected at UV wavelengths of 259 and 254 nm respectively. Calibration curves of absorbance peak area *versus* (*vs*) concentration with linearity over the range of 1 to 50 µg/ml ($R^2 \geq 0.99$) were used to quantify the INH and RIF extracted from the NP. The average EE was 45% (w/w) for the INH NP and 43% (w/w) for the RIF NP. These %EE values were relatively lower compared to an average of 55% and 68% for INH NP and RIF NP respectively obtained from previous work (Semete *et al.*, 2012, Booysen *et al.*, 2013). The difference could have been caused by the slight variation in the preparation method and composition of the NP between the previous studies and the method described here. Both Semete *et al.*, (2012) and Booysen *et al*., (2013) used phosphate buffered saline (PBS) as an aqueous phase, for the first emulsion (w/o) and added 1% PVA as a stabiliser for the second emulsion (w/o/w), instead of Pluronic® and 2% PVA, respectively used in this study. EE denotes the ratio of the weight of drug entrapped into a carrier system to the total drug added (Equation 5.2). It illustrates the proficiency of the NP production process to contain the given drug within the NP as it takes into account the initial amount of the drug used. DL refers to the ratio of drug to the weight of the total DDS, which entails the actual amount of the drug contained within the NP (Equation 5.1). This parameter was used to determine the exact amount of the drug in the NP and NP-Pheroid® formulation. The %DL of the INH in the NP was an average of 12% (w/w), while the loading of RIF in the NP was found to be about 5% (w/w), see Table 3. The RIF DL is relatively higher compared to the 1% DL obtained in previous work that used the same DL method of analysis on RIF NP (Tukulula *et al.*, 2015). The difference may have also been caused by the fact that only 2 mg/ml of RIF was used to prepare the RIF NP in Tukulula *et al*., (2015) while in this current method 10 mg/ml of RIF was used. The weight of the NP administered to the mice in a 200 µl suspension was calculated using equation 5.3 and 5.4, depending on the % DL, see Table 3.

$$Ratio\ of\ drug\ in\ NP = \frac{100}{\%\ DL} \qquad \text{(Equation 5.3)}$$

$$\textit{Weight of administered NP} = Ratio\ of\ Drug\ in\ NPs \times Dose \times Mouse\ Weight$$

(Equation 5.4)

Table 3: The amount of formulation calculated to be administered to mice. The weight of NP was calculated from the %DL. The %EE and %DL are presented as mean values. (n=2)

	%EE (w/w)	%DL (w/w)	Dose /(mg/kg)	Ave. Mice Weight (kg)	Administered Volume / µl	Weight of Administered /mg
INH	-	-	5	0.02	200	0.10
INH NP	45.48	11.92	5	0.02	200	0.84
RIF	-	-	10	0.02	200	0.20
RIF NP	43.93	5.22	10	0.02	200	3.85

4.2. LC-MS/MS detection and quantification of INH and RIF

The LC-MS/MS method used for detecting and quantifying INH and RIF was developed and assessed for its sensitivity. Linear calibration curves for both INH and RIF were obtained in the measured concentration range of standard solution (0.1 - 50 µg/ml) with high co-efficient of determination values (R^2) > 0.98, in both plasma and organs as shown in Table 4. INH eluted at 7.20 min while its internal standard, 6-ANA (IS), eluted at 5.77 min, see Figure 5. The RIF detection is shown by the representative chromatograms in Figure 6, where the elution times of RIF and RIB parent ions were 2.99 and 3.05 min, respectively. RIF and RIB have very close elution times, and their peaks could overlap on the chromatogram. However, the method that we used to quantify RIF from the samples was optimised to be sensitive enough to separate the peaks.

Table 4: The linear equations and coefficient of determination (R^2) values for each drug. (n=3).

Sample	Concentration Range (µg/ml)	INH		RIF	
		Equation	R^2	Equation	R^2

Plasma	0.1 – 50	y = 0.533x + 0.0121	0.9946	y = 0.216x	0.9984
Liver	0.1 – 50	y = 0.0517x - 0.0141	0.9520	y = 0.254x + 0.239	0.9981
Kidneys	0.1 – 50	y = 0.0594x + 0.0797	0.9958	y = 0.301x + 0.541	0.9871
Lungs	0.1 – 50	y = 0.0674x + 0.0262	0.9975	y = 0.29x + -0.029	0.9993
Intestines	0.1 – 50	y = 0.065x - 0.0541	0.9620	y = 0.354 + 0.0667	0.9970

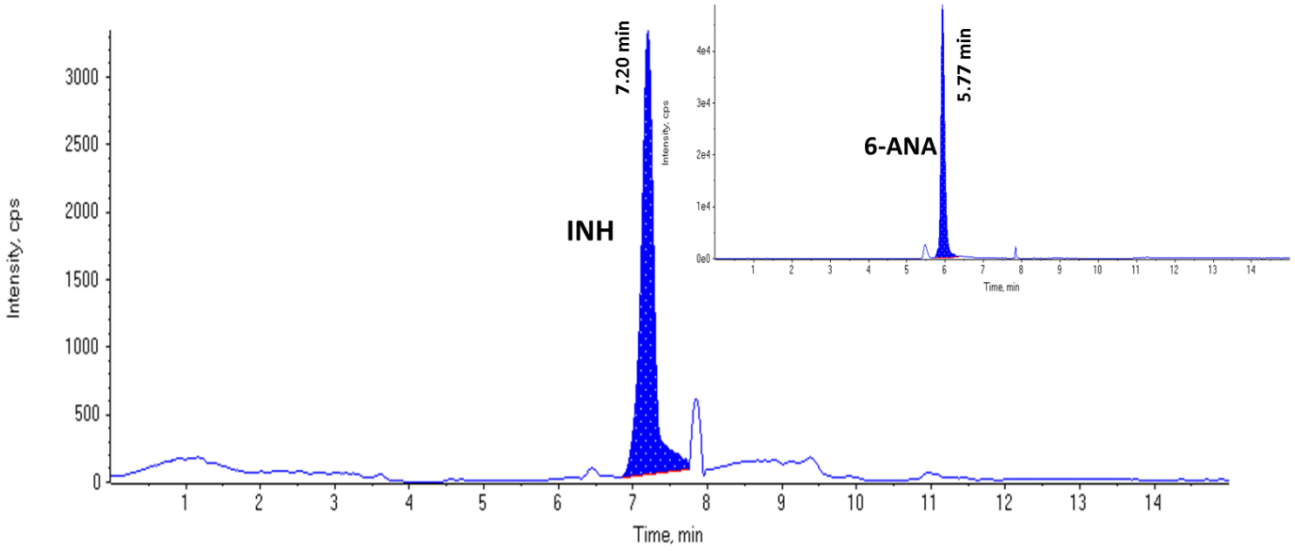

Figure 5: Typical LC-MS/MS chromatograms of INH and 6-ANA (Insert).

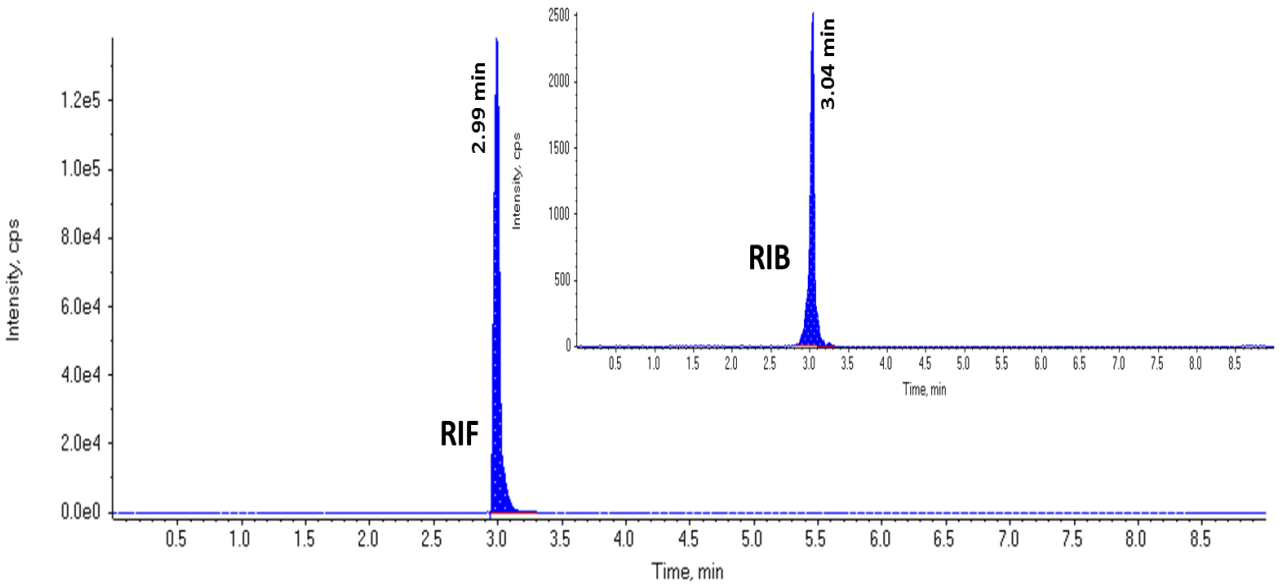

Figure 6: Typical LC-MS/MS chromatograms of RIF and RIB (Insert)

4.3. PK analysis of INH and RIF in mouse plasma

Single doses of 5 mg/kg and 10 mg/kg for INH and RIF were respectively administered to healthy female BALB/c mice as free drug, drug in NP or drug in NP-Pheroid®. These doses were selected to match the efficacious daily dosage given to TB patients according to the standard treatment guidelines (WHO, 2010, SADOH, 2014, CDC, 2003). This study excluded drug entrapped in Pheroid® as a control, due to limited resources and relied on previously conducted studies in mice at the same drug doses although the study was conducted over 4 h only (Nieuwoudt, 2009). Nieuwoudt (2009) reported an increase in AUC of INH and RIF as a result of their entrapment in Pheroid® and a corresponding enhancement of the bioavailability by 17.1% for INH and 26.4% for RIF, see Table 5. In this current study, the determined drug levels in plasma per time point are demonstrated in the concentration *vs* time curves in Figure 7 and Figure 8, for INH and RIF respectively. From both these curves, it can be seen that RIF in all three formulations was detected up to 72 h (5 d) and INH was cleared within 12 h in mice.

Table 5: Summary of PK parameters previously obtained comparing free INH or Free RIF to Pheroid® formulation. Data extracted from Nieuwoudt, (2009).

	$AUC_{0\text{-}t}$ (µg/ml. min)	C_{max} (µg/ml)	T_{max} (min)	$t_{1/2}$ (h)
Free INH	190	2.33	10	0.99
INH-Phe V	225	1.71	45	1.13
Free RIF	580	3.63	240	Not reported-
RIF-Phe V	700	5.16	60	1.56

4.3.1. Plasma PK of INH

The INH from NP-Pheroid® hybrid formulation was detectable up to 12 h while the INH as free drug and in NP formulation, was cleared by the 8 h time point, see Figure 7. This observation may suggest that the hybrid system was prolonging the INH circulation, however the PK calculations indicate that there is no significant difference in the three formulation groups with 95% confidence intervals ($p > 0.05$), see Table 6. This implies that neither the INH NP nor INH NP-Pheroid® hybrid formulation had any effect on the INH PK as was initially hypothesised. The NP formulation in the plasma neither provided the expected prolonged INH release nor improved the PK as reported in some previous studies (Pandey *et al.*, 2003b, Semete *et al.*, 2010). However, some of the PK results from the NP formulation in this study are comparable to the results reported by Booysen *et al*., (2013), where INH NP had no significant effect on the AUC, C_{max} and T_{max} of INH when given to mice orally. This latter study only indicated that the effect of the NP in their study was the significant improvement of the INH $t_{1/2}$ and the prolonged detection of INH in the plasma up to 3 d, compared to 8 h clearance of the free INH (Booysen *et al.*, 2013). The difference in their results to this current work may have been influenced by their use of a higher INH dose of 150 mg/kg, compared to the 5 mg/kg in this study, which could have led to higher levels and more extended circulation of INH in the mouse plasma.

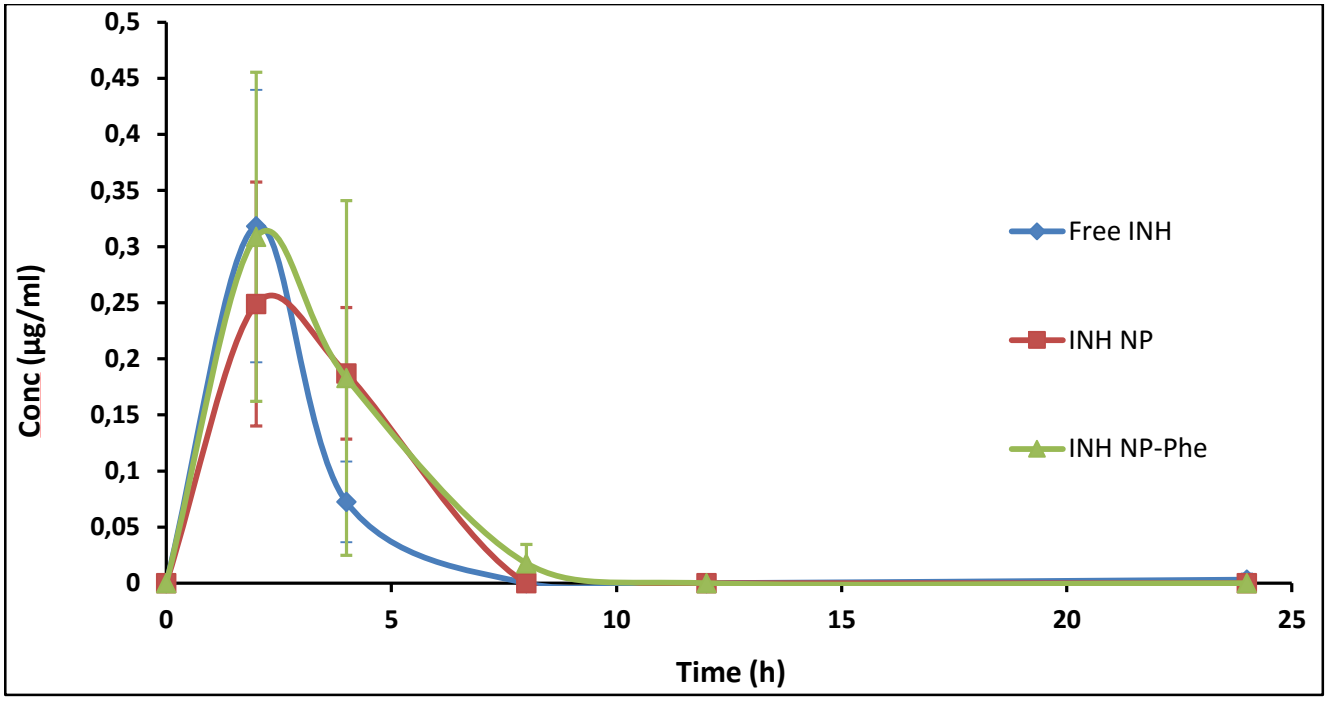

Figure 7: Concentration (Conc) of INH detected in mice plasma from free, NP and NP-Pheroid® formulations. All INH formulations were administered at a dose of 5 mg/kg. The error bars indicate the SD obtained from n=8 samples. (Phe = Pheroid®).

In this current study, the rapid clearance of INH resulted in a maximum of three data points at 2, 4 and 8 h, with the highest C_{max} and T_{max} of 0.33 µg/ml and 2 h, respectively. In comparison, Nieuwoudt, (2009) obtained relatively higher C_{max} (2 µg/ml) and reduced T_{max} (0.75 h) after 5 mg/kg was orally administered to mice regardless of the INH formulation. It is therefore speculated that for future INH PK studies, a significant increase in the INH dose could be considered (Lenaerts *et al*., 2005) or the inclusion of several INH sampling time points before 2 h when the 5 mg/kg dose is administered to mice. These strategies could help in measuring the maximum INH levels in the plasma and eliminate the possibility of few data points due to the rapid INH clearance from all formulations as observed in this study.

Table 6: The average mouse plasma PK parameters (T_{max}, C_{max}, AUC and $t_{1/2}$) for free INH, INH NP and INH NP-Pheroid®, presented as mean ± SD. INH was given at 5 mg/kg dose (n=8). (Phe = Pheroid®).

	***AUC*$_{0-t}$ (µg/ml. min)**	***C*$_{max}$ (µg/ml)**	***T*$_{max}$ (h)**	***t*$_{1/2}$ (h)**
Free INH	0.95 ± 0.40	0.33 ± 0.13	2.00 ± 0.61	2.55 ± 2.53
INH NP	1.66 ± 1.29	0.28 ± 0.05	2.50 ± 0.62	2.12 ± 0.79
INH NP-Phe	1.45 ± 1.22	0.33 ± 0.16	2.25 ± 1.10	1.52 ± 0.79

4.3.2. Plasma PK of RIF

The statistical comparison of RIF PK parameters from the plasma data showed no significant difference ($P > 0.05$) amongst the three formulation groups, see Figure 8 and Table 7. The elevated peak observed on the concentration *vs* time curve of the RIF NP formulation, with C_{max} of 11 µg/ml, reached at the lowest T_{max} of 4 h, is assumed to be caused by the burst release of RIF. This early release of RIF had no ultimate effect on the PK parameters of the RIF NP, although it was not observed in the other two formulations. Booysen *et al.*, (2013) reported a significantly reduced T_{max} of 2 h by RIF NP compared to 8 h obtained from free RIF following the dose of 60 mg/kg. In comparison to a published mouse PK study (De Groote *et al.*, 2010) whereby the same dose of RIF was used, the T_{max} and AUC of free RIF obtained in this study were relatively higher: 6.5 h *vs* 1.6 h and 145 µg/ml.h *vs* 97.46 µg/ml.h, respectively. However, their C_{max} of free RIF (11 µg/ml) is comparable to this current study (9.65 µg/ml). Rosenthal *et al.*, (2012) reported an AUC (142 µg/ml.h) of free RIF, which is similar to the 145 µg/ml.h obtained in this current study, using the same dose of 10 mg/kg in BALB/c mice. Their $t_{1/2}$ of free RIF at the same dose level was however 2.35 h, which was also lower than that obtained in this study for all formulations (11 – 13 h).

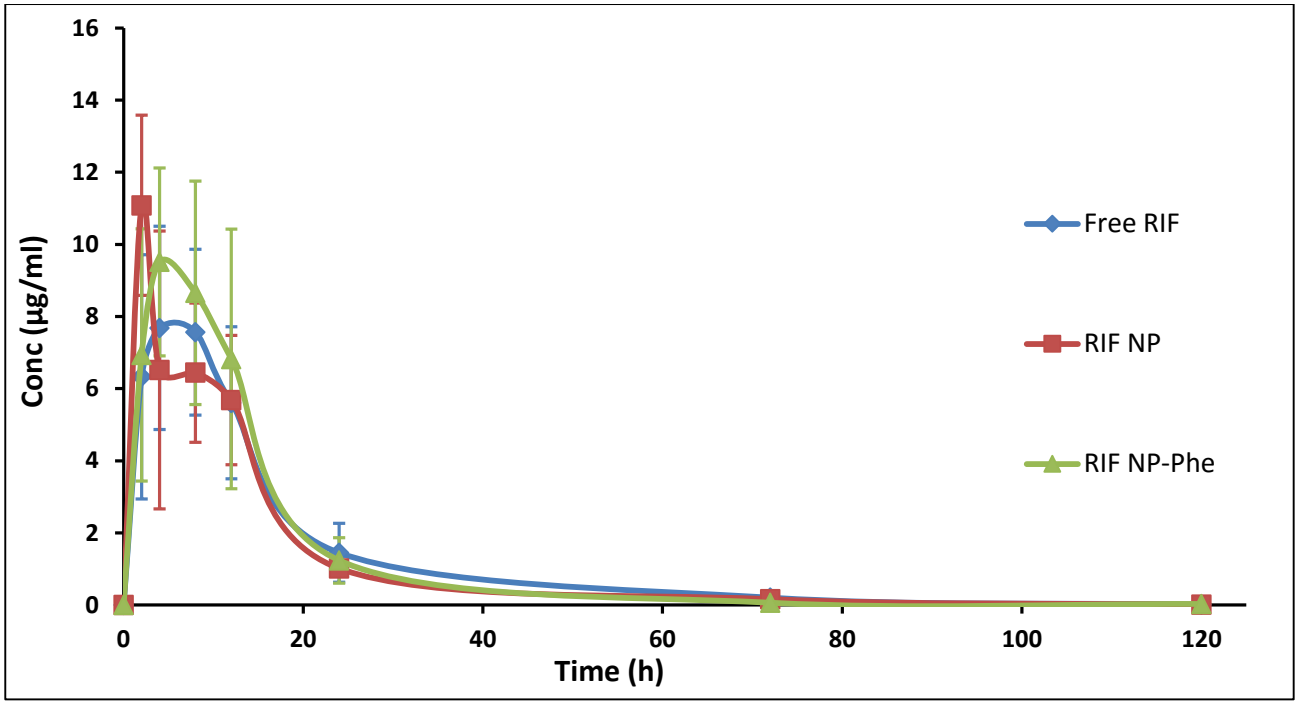

Figure 8: Concentration (Conc) of RIF detected in mouse plasma from free, NP and NP-Pheroid® formulations. All RIF formulations were administered at a dose of 10 mg/kg. The error bars indicate the SD obtained from n=8 samples. (Phe = Pheroid®).

Table 7: The average mouse plasma PK parameters (T_{max}, C_{max}, AUC and $t_{1/2}$) for free RIF, RIF NP and RIF NP-Pheroid® (Phe), presented as mean ± SD. RIF was given at 10 mg/kg dose (n=8).

	***AUC*$_{0-t}$ (µg/ml h)**	***C*$_{max}$ (µg/ml)**	***T*$_{max}$ (h)**	***t*$_{1/2}$ (h)**
Free RIF	145.30 ± 35.52	9.65 ± 1.57	6.50 ± 3.51	12.65 ± 1.77
RIF NP	157.49 ± 23.53	11.43 ± 1.92	4.29 ± 2.93	11.03 ± 1.82
RIF NP-Phe	172.10 ± 44.01	11.01 ± 2.14	7.50 ± 3.34	11.91 ± 3.29

As previously mentioned, entrapment of RIF in Pheroid® resulted in a reduction in T_{max} and increase in both the AUC and C_{max} of RIF, ultimately resulting in improved bioavailability of RIF, see Table 5 (Grobler, 2009, Nieuwoudt, 2009). With regard to encapsulation of RIF in NP, the RIF PK plasma data reported by Booysen *et al.*, (2013), showed the effect of RIF NP, which significantly reduced T_{max} from 8 h to 2 h following a dose of 60 mg/kg. However, they

also indicated that the encapsulation of RIF in NP enhanced neither the AUC nor the C_{max} of RIF, in fact, the AUC of free RIF (1057 μg/ml.min) was two times higher than the NP encapsulated RIF (Booysen *et al.*, 2013). Their results are comparable to this current study in that the RIF NP had no effect on the free RIF PK. The main objective of this study was to evaluate the effect of the hybrid NP-Pheroid® formulation on the bioavailability of RIF and as mentioned above the difference between the three treatments was not substantial. Therefore the results reported in this thesis suggest that the hybrid formulation did not affect the PK parameters of RIF in the plasma.

4.3.3. C_{max}/AUC ratio of INH and RIF

The plasma C_{max} and AUC indicate the highest drug concentration reached, total drug exposure as well as the efficiency of the system to eliminate a drug (Urso, 2002, Gustafson and Bradshaw-Pierce, 2011). The ratio of these highly correlated parameters provides a more precise measure of drug absorption rate, and it is a better demonstration, than C_{max} alone, of the bioequivalence in clinical studies (Endrenyi *et al.*, 1991, Lacey *et al.*, 1994). Bioequivalence is a state where the same drug existing in various formulations can be equally absorbed in the body producing a similar physiological effect. The graph in Figure 9, shows the C_{max}/AUC ratios for this study, to further demonstrate any possible difference in the plasma bioavailability data amongst the three formulations. All INH formulations had average C_{max}/AUC ratios ranging from 0.22 to 0.35 and RIF formulations ratios were less than 0.08. The difference between the C_{max}/AUC ratios of both drugs for the three formulations was not significant. This outcome once again provides evidence that the NP-Pheroid® hybrid formulation had no effect on the absorption rate of neither RIF nor INH in the plasma. The C_{max}/AUC PK ratio parameter implies that both INH and RIF in all three formulations are bioequivalent. This observation does not support the hypothesis put forth for this study that the NP and NP-Pheroid® would enhance the plasma PK of these two drugs.

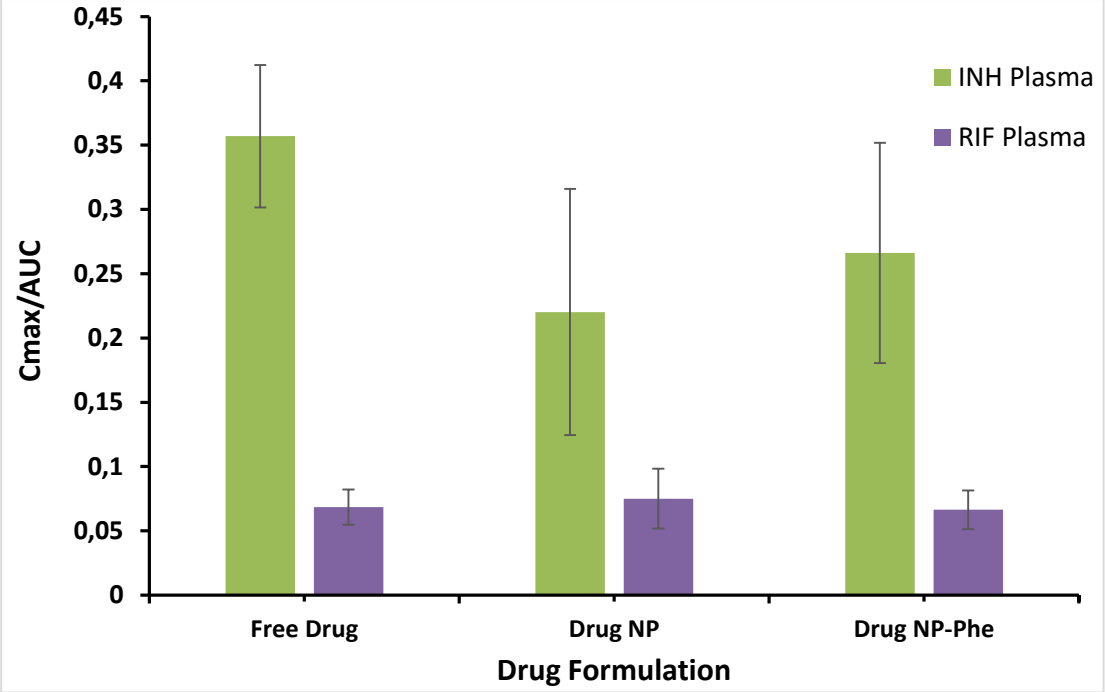

Figure 9: The C_{max}/AUC ratio of INH and RIF in plasma from free drug, drug in NP and drug in NP-Pheroid® post oral administration. INH dose = 5 mg/kg and RIF dose = 10 mg/kg/.

4.4. The distribution of INH and RIF in the organs of the mice

The PK processes such as absorption and distribution of drugs through body fluids and organs as well as drug elimination in a living system can be demonstrated in Figure 10 (Urso *et al*., 2002). A fraction of the blood that passes through organs is in parallel, excluding the lungs that are reached by all blood. Drug elimination can occur from kidneys, intestines and liver; however drug metabolites from the liver may enter the body circulation. The difference in organ distribution between drugs is mainly influenced by the blood flow to tissues, tissue affinity and the physicochemical properties of the drug such as the lipophilicity (Budha *et al*., 2008). The method of analysing the amount of INH and RIF in the organs was evaluated for its capacity to extract the drug by spiking blank organ homogenates with the free drugs to determine whether both drugs could be detected. Both drugs were extracted and measured from all the spiked organs with high recovery values.

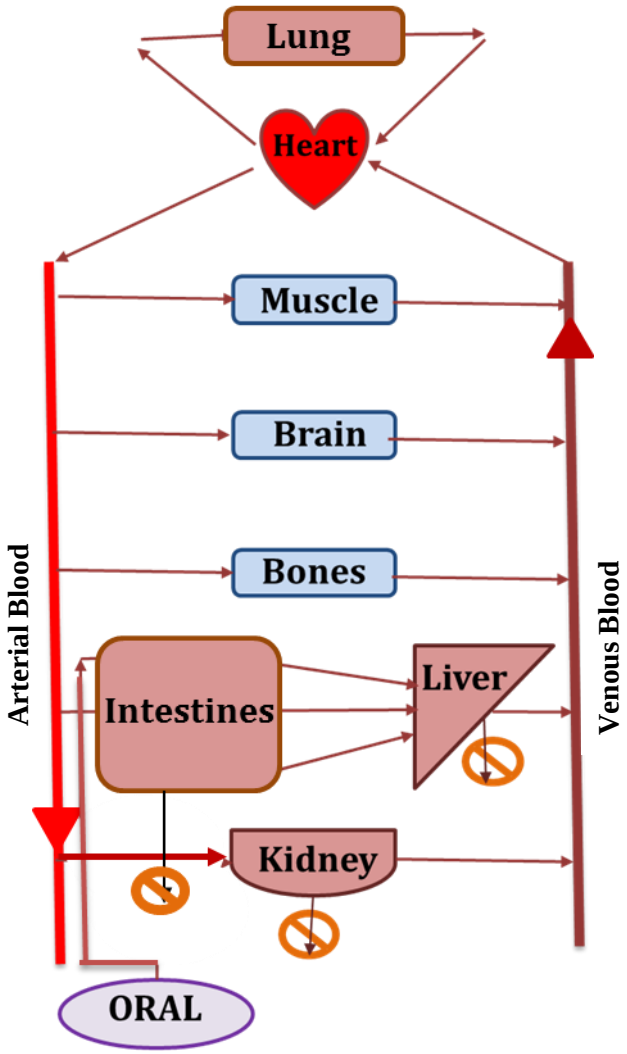

Figure 10: Blood circulation and passage through tissues. Reprinted with permission from Shin *et al*., (2016).

4.4.1. INH detection in the organs

Although INH could be measured in the spiked organ matrix, it could not be detected in any of the harvested organ samples. The possible reasons for this observation include the following: the level of INH might have been below the instrument's limit of detection; there was rapid metabolism of the INH in the mice, or the INH was not distributed to the organs (Li *et al.*, 2004, Bhandari and Kaur, 2013). INH has been shown to undergo rapid and extensive hepatic first-pass metabolism (Metushi *et al*., 2011, Maryam *et al*., 2010), which could limit its distribution to other organs. The extent of INH metabolism, measured by the presence of its main metabolite acetyl isoniazid, has been shown to significantly reduce the concentration of

INH, leading to the low-level detection of INH and its metabolites in rat plasma and organs (Ng *et al*., 2007, Bhandari and Kaur, 2013). The method of INH analysis used in this current study was not optimised to allow the detection of any INH metabolites. Other efforts to study the INH organ distribution without any interferences in the measurements was by the in-tissue derivatisation of INH to enhance the sensitivity of the detection techniques which was either matrix-assisted laser desorption/ionisation (MALDI) or HPLC-MS/MS (Manier *et al.*, 2011).

Similarly, Booysen *et al.*, (2013), reported that both INH from free INH and PLGA INH NP, administered to mice at 150 mg/kg could not be detected in the kidneys and liver, however, they did detect it in the lungs. In contrast, a study by Bhandari and Kaur, (2013) reported improved plasma and brain bioavailability of INH at the same dose (5 mg/kg) as used in this current study due to the encapsulation of INH in solid lipid NP (SLNs) which was found to minimise the rapid metabolism of INH. Encapsulation of INH in alginate NP has also been shown to result in improved INH distribution to various organs when a higher, therapeutically recommended dose (60 mg/kg) was administered to guinea pigs (Ahmad *et al.*, 2009). Therefore, future studies could help enhance the detection of INH in organs as well as investigate the effect of its encapsulation within NP and NP-Pheroid® formulations. These investigations include: the increase of the administered INH dose, the optimisation of the detection method for both INH and its metabolites and the derivatisation of INH in the organs.

4.4.2. Organ PK of RIF

The difference in the drug distribution between INH and RIF is influenced by their various physicochemical properties where INH is a hydrophilic drug with proven low permeability (Mariappan and Singh, 2003) while RIF is lipophilic and thus can easily cross biological membranes (Budha *et al.*, 2008). The detection of RIF, in all the organs investigated, from the free RIF formulation was beyond 24 h which did not correlate with previous studies where RIF was cleared within 24 h from organs (Semete *et al.*, 2012, Ahmad *et al.*, 2009). These studies reported improved circulation of RIF which was detected in the system up to 7 or 15 d when encapsulated in NP, however, in this current study, RIF was detected in all the harvested organs to a maximum of 3–5 d from all formulations.

The highest levels of RIF were measured in the liver (> 295 µg/g) compared to any other organ (< 100 µg/g), see Figure 11. The total circulation or residence time of RIF in each organ was interpreted as the last time point RIF was detected in the specified organ. The C_{max} and AUC

values were significantly larger in the liver than in any other organ, see Figure 11 and Table 8. These observations are likely influenced by the fact that the liver is regarded as the prime organ where the first pass metabolism of RIF occurs (Arbex *et al*., 2010). RIF undergoes deacetylation in liver hepatocytes by hepatic microsomal enzymes to produce deacetylrifampicin, a metabolic derivative which is more polar and known to be more microbiologically active than RIF (Benedetti and Dostert, 1994, Chen *et al*., 2006). It is therefore expected that RIF accumulates more in the liver than in any other organ. There have been assumptions that RIF could induce toxicity to the liver (Tung-Yuan *et al.*, 2013), however other studies demonstrated that RIF was the least likely drug to cause hepatotoxicity among all the other four anti-TB drugs used to treat TB patients with chronic liver dysfunctions (Dhiman *et al.*, 2012, Wang *et al*., 2016).

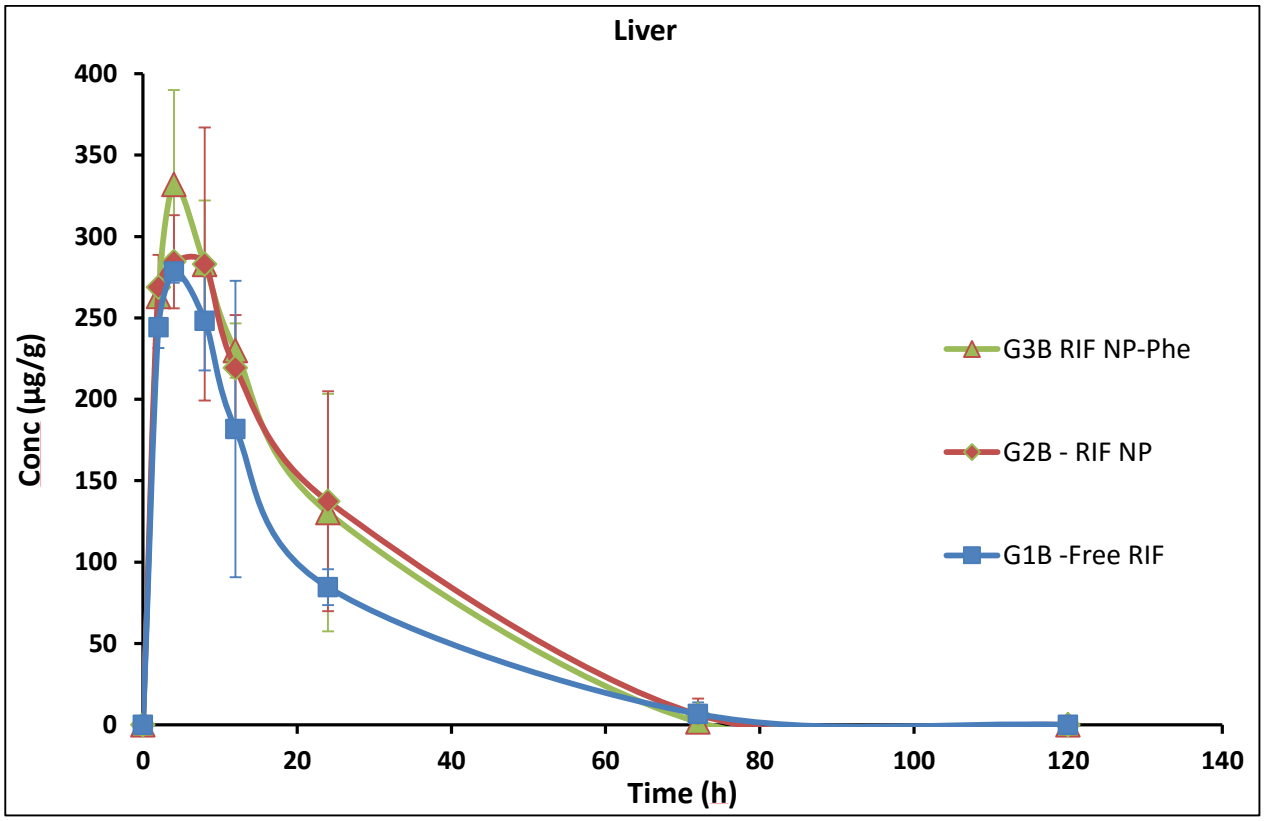

Figure 11: The tissue concentration (Conc) of RIF in the liver following oral administration of free RIF (G1B), RIF NP (G2B) and RIF NP-Pheroid® (G3B). The dose level of RIF was 10 mg/kg in each formulation. The error bars indicate SD from the mean concentration that was obtained from n=8 samples. (Phe = Pheroid®).

Statistical analysis showed no significant difference, on a 5% level, among three liver PK parameters, AUC, T_{max} and $t_{1/2,}$ of free RIF and RIF NP and RIF NP-Pheroid®, see Table 8. However, free RIF had a significantly higher C_{max} in the liver than the RIF NP (p = 0.042) while the C_{max} from RIF NP-Pheroid® hybrid formulation was insignificantly different to both formulations (p > 0.05). Therefore, the encapsulation of RIF in NP-Pheroid® did not alter its distribution while NP lowered the amount of RIF in the liver. The difference between the RIF C_{max} of the free drug and the NP is assumed to be due to the release mechanism of the drug from the NPs. The encapsulation of RIF in the NP is controlling its release while free RIF readily accumulates in the liver. However, the effect of NP on the distribution of RIF to the liver has previously been demonstrated to improve the levels of RIF detected (Semete *et al*., 2012). Booysen *et al*., (2013) reported that PLGA NP improved the residence time of RIF in the liver, which was detected for 10 d while free RIF could only be quantified until 7 d, however, they used higher doses of RIF. The latter study results are comparable to those of this current work in that free RIF was not cleared within the 24 h as other studies have shown but after 3 d, but they used higher doses of RIF and their PLGA NP improved the residence time of RIF in the liver.

Table 8: The average mouse liver PK parameters (T_{max}, C_{max}, AUC and $t_{1/2}$) for free RIF, RIF NP and RIF NP-Pheroid®, presented as mean ± SD. RIF was given at 10 mg/kg dose (n=8). (Phe = Pheroid®).

	***AUC*$_{0-t}$ (µg/g.h)**	***C*$_{max}$ (µg/g)**	***T*$_{max}$ (h)**	***t*$_{1/2}$ (h)**
Free RIF	8293.56 ± 2086.92	414.29* ± 146.51	6.00 ± 4.14	16.15 ± 14.03
RIF NP	7273.37 ± 2344.07	298.87* ± 50.55	3.25 ± 2.12	13.28 ± 5.06
RIF NP-Phe	6379.96 ± 2371.79	308.06 ± 43.79	6.25 ± 2.49	10.37 ± 5.92

*Significant difference in the C_{max}, ***P* -value = 0.0420** (free RIF and RIF NP).

RIF from all formulations was retained the longest in the lungs in comparison to any other organ, see Figure 12. Interestingly, the hybrid formulation seemed to improve the duration of

RIF in the lungs from 3 d (by free RIF and RIF NP) to a maximum period of 5 d (172 h) with a significantly reduced T_{max} of 4.25 h (P = 0.0420), see Figure12, Figure13 and Table 9. This observation could imply that the clinical use of the NP-Pheroid® hybrid formulation for the delivery of anti-TB drugs would be useful for the most common form of active TB, pulmonary TB, as the TB pathogen is known to mostly reside in the lung alveoli cells (Smith, 2003). Although the RIF C_{max} from the hybrid formulation seemed higher (50 µg/g), it was insignificantly different to other formulations (P > 0.05). In contrast, Booysen *et al.*, (2013) showed that RIF NP had no effect on the distribution of RIF to the lungs, which was only detected for 2 d.

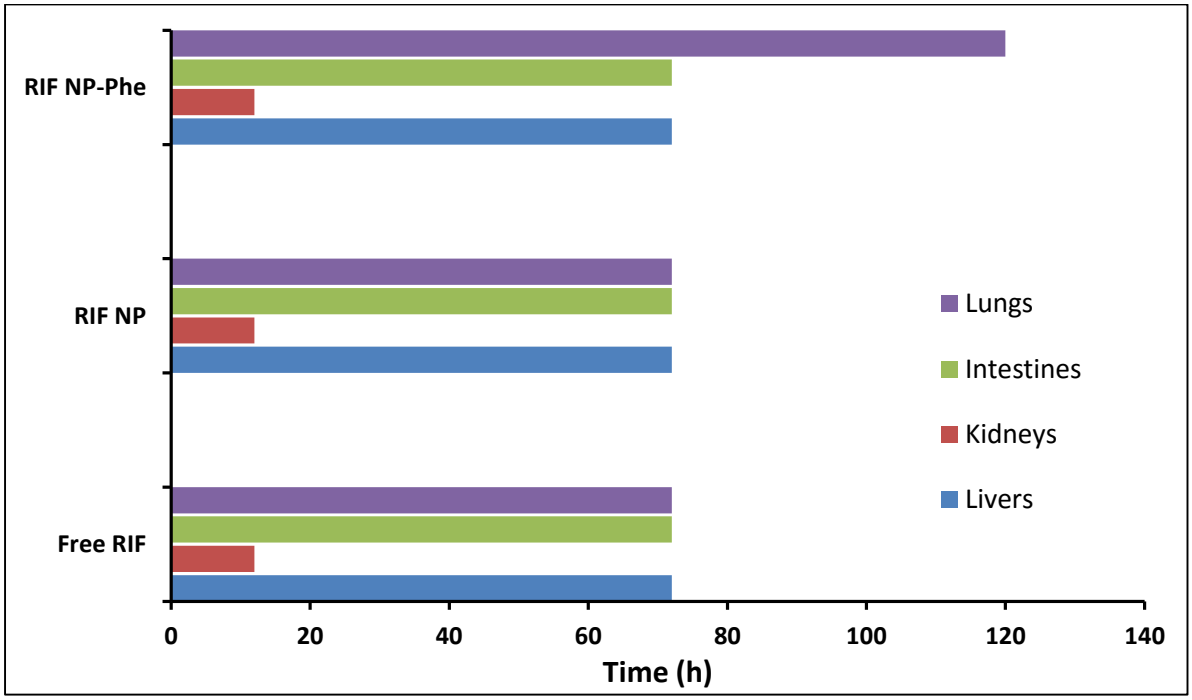

Figure 12: The circulation time of RIF in lungs, intestines, kidneys and liver from Free RIF, RIF NP and RIF NP-Pheroid® after oral administration. RIF dose = 10 mg/kg.

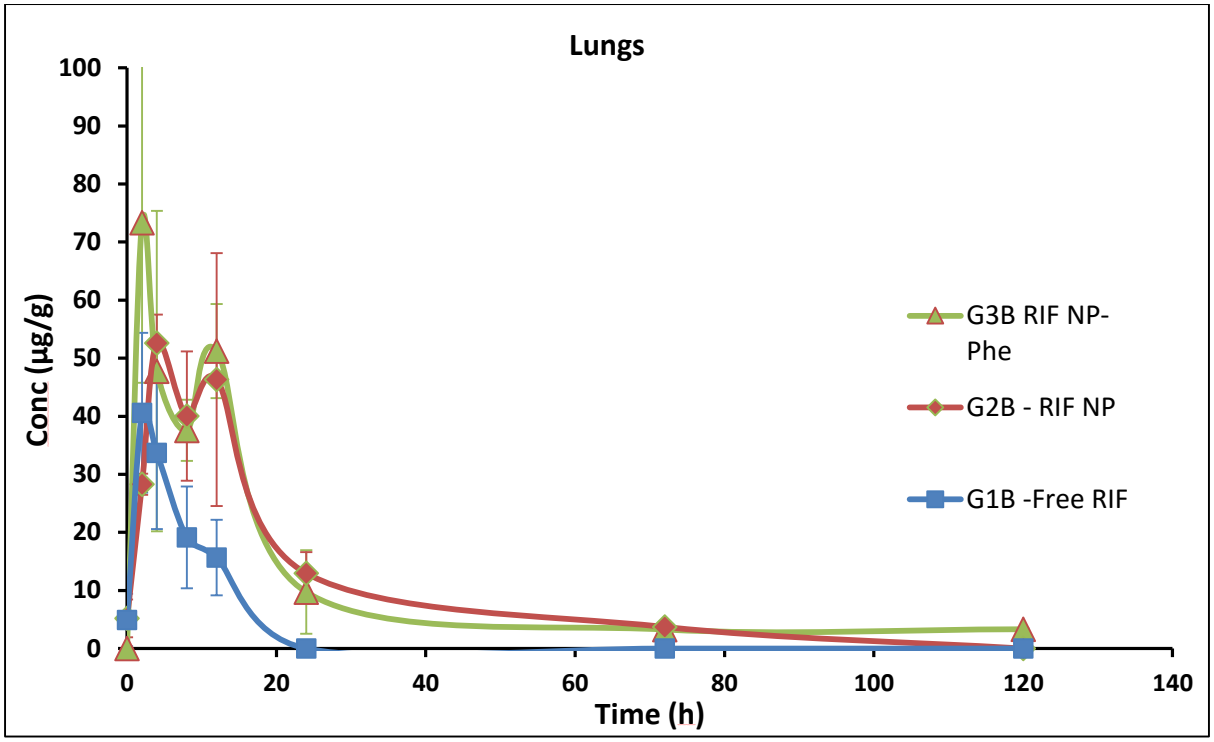

Figure 13: The tissue concentration (Conc) of RIF in the lungs following oral administration of free RIF (G1B), RIF NP (G2B) and RIF NP-Pheroid® (G3B). The dose level of RIF was 10 mg/kg in each formulation. The error bars indicate SD from the mean concentration that was obtained from n=8 samples. (Phe = Pheroid®).

Table 9: The average mouse lung PK Parameters (T_{max}, C_{max}, AUC and $t_{1/2}$) for free RIF, RIF NP and RIF NP-Pheroid®, presented as Mean ± SD. RIF was given at 10 mg/kg dose (n=8). (Phe = Pheroid®).

	***AUC*$_{0-t}$ (µg/g.h)**	***C*$_{max}$ (µg/g)**	***T*$_{max}$ (h)**	***t*$_{1/2}$ (h)**
Free RIF	634.44 ± 535.33	37.10 ± 13.95	4.50 ± 2.32	58.72 ± 114.13
RIF NP	1283.40 ± 1401.82	40.72 ± 14.39	11.00* ± 8.21	20.51 ± 30.03
RIF NP-Phe	695.83 ± 643.35	49.84 ± 28.61	4.250* ± 3.77	10.70 ± 13.91

*Significant difference in the T_{max}, ***P* -value = 0.020** (RIF NP and RIF NP-Pheroid®)

In contrast to the extended retention in the lungs, RIF was only detected for a maximum period of 24 h in the kidneys from all three formulations, which was the shortest residence time amongst all the organs investigated, Figure 12. Booysen *et al.*, (2013) reported the detection of RIF in the kidneys up to 48 h from free RIF and 24 h from RIF NP. Figure 14 illustrates the concentration *vs* time curves of all formulations in the kidneys and Table 10 shows that the difference between C_{max}, T_{max} and AUC was not significant amongst all the RIF formulations. However, there was a substantial increase in the RIF $t_{1/2}$ caused by the NP-Pheroid® hybrid formulation from about 4 h for free RIF to about 16 h (*P*-value = 0.0425). This increased $t_{1/2}$ could imply that the hybrid DDS has high affinity to the kidneys cells, therefore resulting in an enhanced residence time of the substance it is delivering. The evidence of both RIF and its metabolite (des-acetyl RIF) detected in urine has been reported (Vree *et al.*, 1992, Agrawal *et al.*, 2004), however the long retention of RIF in the kidneys is usually not ideal, especially since RIF-induced renal toxicity in animals and humans has been shown (Shabana *et al*., 2012, Beebe *et al*., 2015, Agrawal *et al*., 2016). Nonetheless, studies can be conducted to determine if the NP-Pheroid® hybrid DDS formulation can be used for targeted renal delivery of appropriate drugs because there is a need for novel DDS directed to kidney cells to enhance the therapy of renal diseases (Dolman *et al.*, 2010, Zhou *et al*., 2014).

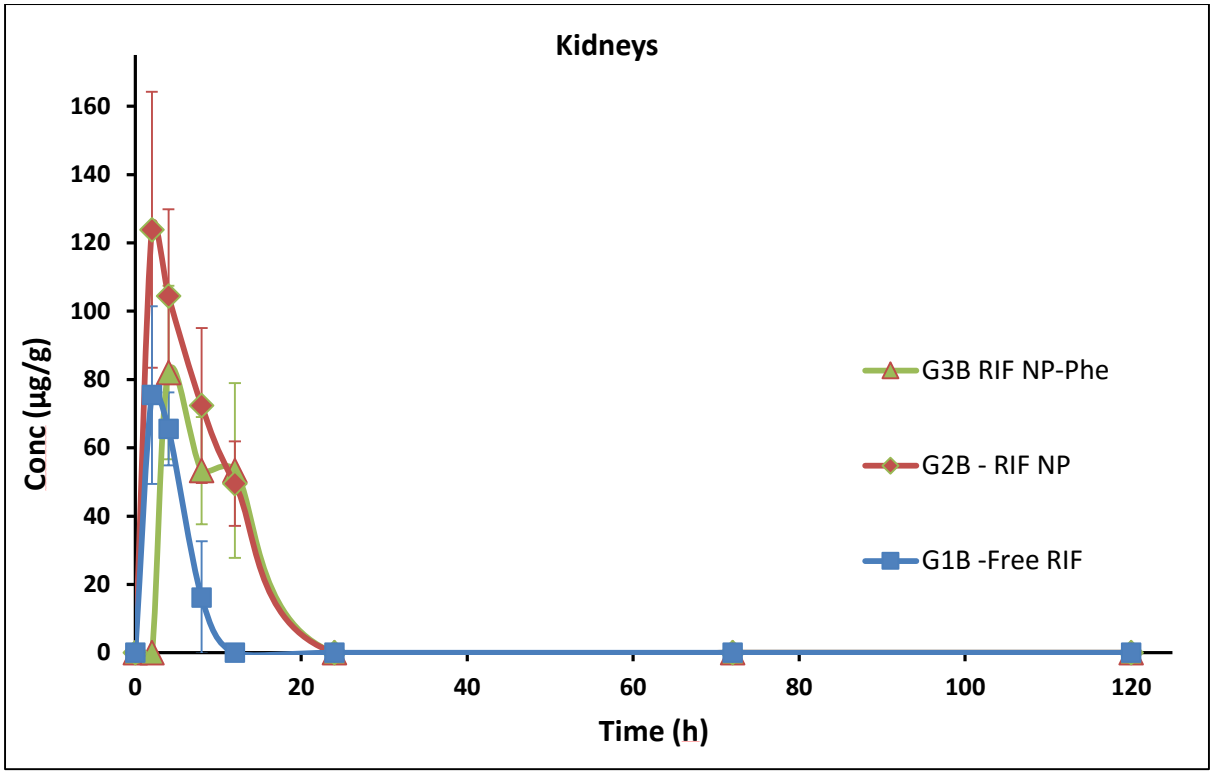

Figure 14: The tissue concentration (Conc) of RIF in the kidneys following oral administration of free RIF (G1B), RIF NP (G2B)) and RIF NP-Pheroid® (G3B). The dose level of RIF was 10 mg/kg in each formulation. The error bars indicate SD from the mean concentration that was obtained from n=8 samples. (Phe = Pheroid®).

Table 10: The average mouse kidney PK Parameters (T_{max}, C_{max}, AUC and $t_{1/2}$) for free RIF, RIF NP and RIF NP-Pheroid®, presented as Mean ± SD. RIF was given at 10 mg/kg dose (n=8). (Phe = Pheroid®).

	***AUC*$_{0-t}$ (µg/g.h)**	***C*$_{max}$ (µg/g)**	***T*$_{max}$ (h)**	***t*$_{1/2}$ (h)**
Free RIF	627.789 ± 539.77	65.66 ± 19.02	2.75 ± 1.03	3.947* ± 1.68
RIF NP	808.83 ± 392.43	81.15 ± 50.26	3.50 ± 2.07	6.55 ± 3.59
RIF NP-Phe	586.64 ± 310.26	55.21 ± 26.58	4.50 ± 2.33	15.73* ± 13.64

*Significant difference in the $t_{1/2}$, ***P* -value = 0.0425** (free RIF and RIF NP-Pheroid®)

The intestine is a vital organ as it regulates the extent of absorption of oral drugs (Pang, 2003). Figure 12 and 15 show that the levels of RIF in the intestines were cleared almost at the same time as from the liver and plasma (72 h) in all formulations. The free RIF had the highest C_{max} in the intestines which was significantly different from the RIF NP and RIF NP-Pheroid® (P = 0.02), see Table 11. These results could indicate that NP and NP-Pheroid® may have resulted in more rapid absorption of RIF from the intestines into the circulation, which resulted in low levels of intestinal RIF from these formulations. Similar to kidneys there is limited literature on RIF distribution to the intestines. However, Semete *et al.*, (2010) demonstrated histopathology images of fluorescently labelled PLGA NP in the intestines in mice, indicating the possible enhancement of anti-TB drug distribution by these NP when administered via the oral route.

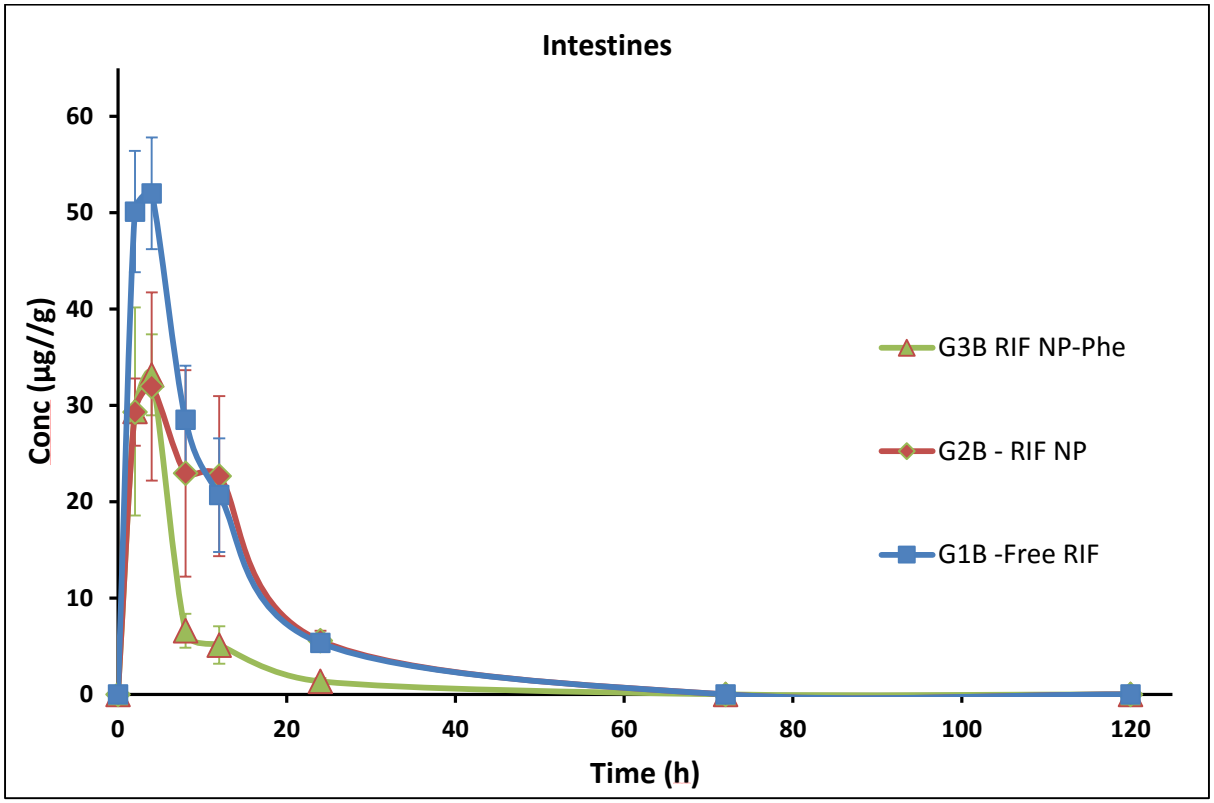

Figure 15: The tissue concentration (Conc) of RIF in the intestines following oral administration of free RIF (G1B), RIF NP (G2B)) and RIF NP-Pheroid® (G3B). The dose level of RIF was 10 mg/kg in each formulation. The error bars indicate SD from the mean concentration that was obtained from n=8 samples. (Phe = Pheroid®).

Table 11: The average mouse intestine PK Parameters (T_{max}, C_{max}, AUC and $t_{1/2}$) for free RIF, RIF NP and RIF NP-Pheroid®, presented as Mean ± SD. RIF was given at 10 mg/kg dose (n=8). (Phe = Pheroid®).

	***AUC*$_{0-t}$ (µg/g.h)**	***C*max (µg/g)**	***T*max (h)**	***t*$_{1/2}$ (h)**
Free RIF	743.95 ± 218.29	66.17* ± 29.32	3.00 ± 1.07	17.73 ± 17.03
RIF NP	716.03 ± 138.94	44.50* ± 13.49	4.50 ± 2.98	14.42 ± 7.57
RIF NP-Phe	583.99 ± 271.99	43.78 ± 11.46	4.25 ± 2.49	8.47 ± 4.73

*Significant difference with in the C_{max}, ***P*-value = 0.0255** (free RIF and RIF NP)

Organ to plasma ratios have been used in literature to demonstrate the overall organ distribution and penetration of drugs from plasma (Damle *et al.*, 2008). The AUC ratio is an indication of how correlated an individual plasma AUC is to its corresponding individual tissue AUC. The AUC ratios, shown in Figure 16, allowed the absolute comparison of RIF distribution from the plasma to the organs. This graph validates that RIF was distributed from plasma to the liver in significantly greater amounts than to other organs. Although the AUC ratio in the liver for free RIF (58) is higher compared to both the RIF NP (43) and RIF NP-Pheroid® (37), they are insignificantly different ($P > 0.05$). Therefore, this ratio also indicates that RIF was distributed to the liver in all formulations at a higher concentration than in the plasma. A higher organ/plasma ratio of RIF to the liver as found in this study has previously been reported (Bruzzese *et al.*, 2000). An AUC lung/AUC plasma ratio of RIF obtained in this study (4.37) is comparable to a ratio of 3.5 ± 1.5 that was reported by Kjellsson *et al.*, (2012).

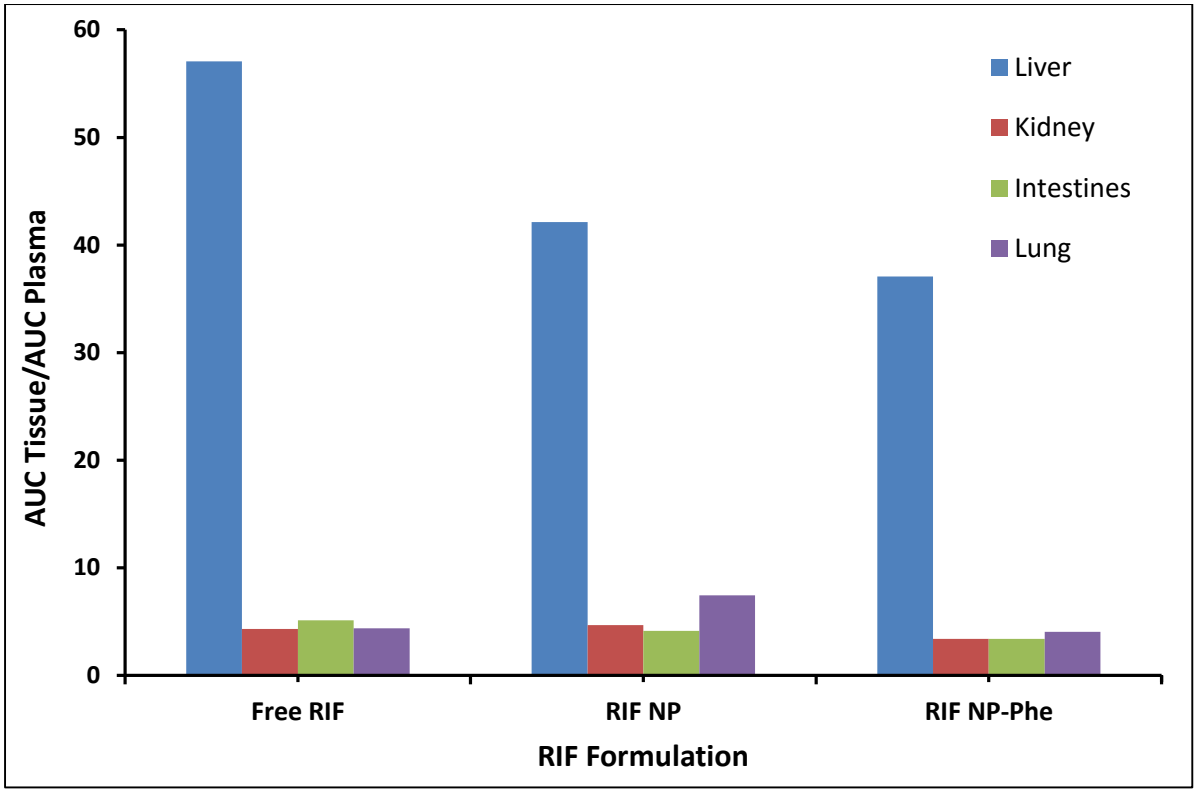

Figure 16: The AUC organ/AUC plasma ratio of RIF in lungs, intestines, kidneys and liver from free RIF, RIF NP and RIF NP-Pheroid® after oral administration. RIF dose = 10 mg/kg.

5. Conclusion

The effect of a novel NP-Pheroid® hybrid DDS on the plasma drug levels and organ distribution of INH and RIF was determined in mice. The plasma data for both drugs did not provide evidence of an effect of this hybrid formulation as the PK parameters did not change when compared with either free drug or drug-loaded NP. INH was detected in the plasma up to a maximum of 8 h, however it was not detected in any of the harvested organs. RIF was detected in all the organs harvested up to a period of 3 to 5 d, with the highest accumulation and organ penetration in the liver (high C_{max}; AUC and organ/plasma AUC ratio). The PLGA NP did not demonstrate enhanced circulation of RIF as reported in previous studies (Semete *et al.,* 2010 and Pandey *et al.,* 2003). However the RIF NP results acquired in this current work were comparable with the results reported by Booysen *et al.,* (2013). Statistical analysis showed that the difference between the AUC and the C_{max} of RIF NP-Pheroid® hybrid formulation in all the harvested organs was not significant when compared to free RIF and RIF NP at 95% confidence interval. However, the C_{max} of free RIF was significantly higher than that of RIF NP in the liver and intestines (P = 0.0420 and 0.025). The effect on RIF distribution by the NP-Pheroid® hybrid formulation was a significant reduction of T_{max} (4 h) compared to the NP (11 h). The hybrid formulation also increased the RIF retention time in the lungs up to a period of 5 d, compared to 3 d from free RIF and RIF NP. In the distribution of RIF to the kidneys, the NP-Pheroid® hybrid formulation also resulted in a significant increase of RIF $t_{1/2}$ (16 h) in comparison to the free RIF with $t_{1/2}$ of 4 h (P = 0.0425). Although it cannot be concluded that the hybrid formulation improved the overall PK parameters of the two anti-TB drugs in the plasma, it displayed significant effects on the biodistribution of RIF to the lungs and kidneys.

5.1. Acknowledgements

The authors would like to thank the following:

Prof Steyn for the all the statistical evaluations done for the ethical application as well as data analysis of results obtained from the mice; Liezl-Marie Scholtz for assistance in planning the animal studies; Antoinette Fick and Hylton Buntting for the technical support during the animal experiments; Abongile Ndamase, Nontokozo Magwaza and Lungile Thwala for their assistance in sample preparation for LC- MS/MS sample analysis.

6. References

AGRAWAL, A., AGARWAL, S. K., KALEEKAL, T. & GUPTA, Y. K. 2016. Rifampicin and anti-hypertensive drugs in chronic kidney disease: Pharmacokinetic interactions and their clinical impact. *Indian Journal of Nephrology,* 26**,** 322-328.

AGRAWAL, S. & PANCHAGNULA, R. 2005. Implication of biopharmaceutics and pharmacokinetics of rifampicin in variable bioavailability from solid oral dosage forms. *Biopharmaceutics & Drug Disposition,* 26**,** 321-334.

AGRAWAL, S., SINGH, I., KAUR, K. J., BHADE, S. R., KAUL, C. L. & PANCHAGNULA, R. 2004. Comparative bioavailability of rifampicin, isoniazid and pyrazinamide from a four drug fixed dose combination with separate formulations at the same dose levels. *International Journal of Pharmaceutics,* 276**,** 41-49.

AHMAD, Z., KLINKENBERG, L. G., PINN, M. L., FRAIG, M. M., PELOQUIN, C. A., BISHAI, W. R., NUERMBERGER, E. L., GROSSET, J. H. & KARAKOUSIS, P. C. 2009. Biphasic Kill curve of isoniazid reveals the presence of drug-tolerant, not drug-resistant, mycobacterium tuberculosis in the guinea pig. *Journal of Infectious Diseases,* 200**,** 1136-1143.

ARBEX, M. A., VARELLA, M. D. C. L., SIQUEIRA, H. R. D. & MELLO, F. A. F. D. 2010. Antituberculosis drugs: Drug interactions, adverse effects, and use in special situations. Part 1: First-line drugs*. *Jornal Brasileiro de Pneumologia,* 36**,** 626-640.

BASAVARAJ, S. & BETAGERI, G. V. 2014. Can formulation and drug delivery reduce attrition during drug discovery and development—review of feasibility, benefits and challenges. *Acta Pharmaceutica Sinica B,* 4**,** 3-17.

BEEBE, A., SEAWORTH, B. & PATIL, N. 2015. Rifampicin-induced nephrotoxicity in a tuberculosis patient. *Journal of Clinical Tuberculosis and Other Mycobacterial Diseases,* 1**,** 13-15.

BENEDETTI, M. S. & DOSTERT, P. 1994. Induction and autoinduction properties of rifamycin derivatives: a review of animal and human studies. *Environmental Health Perspectives,* 102**,** 101-105.

BHANDARI, R. & KAUR, I. P. 2012. A sensitive hplc method for determination of isoniazid in rat plasma, brain, liver and kidney. *Journal of Chromatography & Separation Techniques,* 3**,** 1-5.

BHANDARI, R. & KAUR, I. P. 2013. Pharmacokinetics, tissue distribution and relative bioavailability of isoniazid-solid lipid nanoparticles. *International Journal of Pharmaceutics,* 441**,** 202-212.

BOOYSEN, L. L. I. J., KALOMBO, L., BROOKS, E., HANSEN, R., GILLILAND, J., GRUPPO, V., LUNGENHOFER, P., SEMETE-MAKOKOTLELA, B., SWAI, H. S., KOTZE, A. F., LENAERTS, A. & DU PLESSIS, L. H. 2013. In vivo/in vitro pharmacokinetic and pharmacodynamic study of spray-dried poly-(dl-lactic-co-glycolic) acid nanoparticles encapsulating rifampicin and isoniazid. *International Journal of Pharmaceutics,* 444**,** 10-17.

BRUZZESE, T., RIMAROLI, C., BONABELLO, A., MOZZI, G., AJAY, S. & COOVERJ, N. D. 2000. Pharmacokinetics and tissue distribution of rifametane, a new 3-azinomethyl-rifamycin derivative, in several animal species. *Arzneimittelforschung,* 50**,** 60-71.

BUDHA, N. R., LEE, R. E. & MEIBOHM, B. 2008. Biopharmaceutics, pharmacokinetics and pharmacodynamics of antituberculosis drugs. *Current Medicinal Chemistry,* 15**,** 809-825.

CDC 2003. Treatment of Tuberculosis, . *In:* AMERICAN THORACIC SOCIETY, C., AND INFECTIOUS DISEASES SOCIETY OF AMERICA. (ed.) *Morbidity and Mortality Weekly Report.* U.S. Department of Health and Human Services, Atlanta, GA 30333.: Centers for Disease Control and Prevention.

CHELOPO, M. P., KALOMBO, L., WESLEY-SMITH, J., GROBLER, A. & HAYESHI, R. 2017. The fabrication and characterization of a PLGA nanoparticle–Pheroid® combined drug delivery system. *Journal of Materials Science***,** 52, 3133-3145.

CHEN, J. & RAYMOND, K. 2006. Roles of rifampicin in drug-drug interactions: underlying molecular mechanisms involving the nuclear pregnane X receptor. *Annals of Clinical Microbiology and Antimicrobials,* 5, 3, 11 Pages.

CHEN, M.-L., SHAH, V., PATNAIK, R., ADAMS, W., HUSSAIN, A., CONNER, D., MEHTA, M., MALINOWSKI, H., LAZOR, J. & HUANG, S.-M. 2001. Bioavailability and bioequivalence: an FDA regulatory overview. *Pharmaceutical Research,* 18**,** 1645-1650.

CHU, C., TONG, S.-S., XU, Y., WANG, L., FU, M., GE, Y.-R., YU, J.-N. & XU, X.-M. 2011. Proliposomes for oral delivery of dehydrosilymarin: preparation and evaluation in vitro and in vivo. *Acta Pharmacologica Sinica,* 32**,** 973-980.

D'AMBROSIO, L., CENTIS, R., SOTGIU, G., PONTALI, E., SPANEVELLO, A. & MIGLIORI, G. B. 2015. New anti-tuberculosis drugs and regimens: 2015 update. *European Respiratory Journal Open Research,* 1**,** 1-15.

DAVIES, G. R. & NUERMBERGER, E. L. 2008. Pharmacokinetics and pharmacodynamics in the development of anti-tuberculosis drugs. *Tuberculosis,* 88**,** S65-S74.

DAMLE, B., STOGNIEW, M. & DOWELL, J. 2008. Pharmacokinetics and tissue distribution of anidulafungin in rats. *Antimicrobial Agents and Chemotherapy,* 52**,** 2673-2676.

DE GROOTE, M. A., GILLILAND, J. C., WELLS, C. L., BROOKS, E. J., WOOLHISER, L. K., GRUPPO, V., PELOQUIN, C. A., ORME, I. M. & LENAERTS, A. J. 2011. Comparative studies evaluating mouse models used for efficacy testing of experimental drugs against mycobacterium tuberculosis. *Antimicrobial Agents and Chemotherapy,* 55**,** 1237-1247.

DHIMAN, R. K., SARASWAT, V. A., RAJEKAR, H., REDDY, C. & CHAWLA, Y. K. 2012. A guide to the management of tuberculosis in patients with chronic liver disease. *Journal of Clinical and Experimental Hepatology,* 2**,** 260-270.

DOLMAN, M. E. M., HARMSEN, S., STORM, G., HENNINK, W. E. & KOK, R. J. 2010. Drug targeting to the kidney: Advances in the active targeting of therapeutics to proximal tubular cells. *Advanced Drug Delivery Reviews,* 62, 1344-1357.

DU TOIT, L., PILLAY, V. & DANCKWERTS, M. 2006. Tuberculosis chemotherapy: current drug delivery approaches. *Respiratory Research,* 7**,** 1-18.

ENDRENYI, L., FRITSCH, S. & YAN, W. 1991. Cmax/AUC is a clearer measure than Cmax for absorption rates in investigations of bioequivalence. *International Journal of Clinical Pharmacology, Therapy, and Toxicology,* 29**,** 394-399.

GROBLER, A. F. 2009. *Pharmaceutical applications of Pheroid™ technology.* Doctor of Philosophy in Pharmaceutics, North-West University. https://dspace.nwu.ac.za/handle/10394/6701 (Date accessed: 22 August 2013).

GROBLER, L., GROBLER, A., HAYNES, R., MASIMIREMBWA, C., THELINGWANI, R., STEENKAMP, P. & STEYN, H. S. 2014. The effect of the Pheroid delivery system on the in vitro metabolism and in vivo pharmacokinetics of artemisone. *Expert Opinion on Drug Metabolism & Toxicology,* 10**,** 313-25.

GUSTAFSON, D. L. & BRADSHAW-PIERCE, E. L. 2011. Fundamental concepts in clinical pharmacology. *In:* SPRINGER (ed.) *Principles of Anticancer Drug Development.* Springer.

HADINOTO, K., SUNDARESAN, A. & CHEOW, W. S. 2013. Lipid–polymer hybrid nanoparticles as a new generation therapeutic delivery platform: A review. *European Journal of Pharmaceutics and Biopharmaceutics,* 85**,** 427-443.

HARI, B. N. V., CHITRA, K. P., BHIMAVARAPU, R., KARUNAKARAN, P., MUTHUKRISHNAN, N. & RANI, B. S. 2010. Novel technologies: A weapon against tuberculosis. *Indian Journal of Pharmacology*, 42**,** 338-44.

JOKERST, J. V., LOBOVKINA, T., ZARE, R. N. & GAMBHIR, S. S. 2011. Nanoparticle PEGylation for imaging and therapy. *Nanomedicine (London, England),* 6**,** 715-728.

KJELLSSON, M. C., VIA, L. E., GOH, A., WEINER, D., LOW, K. M., KERN, S., PILLAI, G., BARRY, C. E. & DARTOIS, V. 2012. Pharmacokinetic evaluation of the penetration of antituberculosis agents in rabbit pulmonary lesions. *Antimicrobial Agents and Chemotherapy,* 56**,** 446-457.

KOLYVA, A. S. & KARAKOUSIS, P. C. 2012. Old and new tb drugs: mechanisms of action and resistance, *In:* Understanding tuberculosis – new approaches to fighting against drug resistance Intech, 209-233.

LACEY, L. F., KEENE, O. N., DUQUESNOY, C. & BYE, A. 1994. Evaluation of different indirect measures of rate of drug absorption in comparative pharmacokinetic studies. *Journal of Pharmaceutical Sciences,* 83**,** 212-215.

LENAERTS, A. J., JOHNSON, C. M., MARRIETA, K. S., GRUPPO, V. & ORME, I. M. 2005. Significant increases in the levels of liver enzymes in mice treated with anti-tuberculosis drugs. *International Journal of Antimicrobial Agents,* 26**,** 152-158

LI, A. C., JUNGA, H., SHOU, W. Z., BRYANT, M. S., JIANG, X.-Y. & NAIDONG, W. 2004. Direct injection of solid-phase extraction eluents onto silica columns for the analysis of polar compounds isoniazid and cetirizine in plasma using hydrophilic interaction chromatography with tandem mass spectrometry. *Rapid Communications in Mass Spectrometry,* 18**,** 2343-2350.

MANIER, M. L., REYZER, M. L., GOH, A., DARTOIS, V., VIA, L. E., BARRY, C. E. & CAPRIOLI, R. M. 2011. Reagent precoated targets for rapid in-tissue derivatization of the anti-tuberculosis drug isoniazid followed by maldi imaging mass spectrometry. *Journal of the American Society for Mass Spectrometry,* 22**,** 1409-1419.

MARIAPPAN, T. T. & SINGH, S. 2003. Regional gastrointestinal permeability of rifampicin and isoniazid (alone and their combination) in the rat. *The International Journal of Tuberculosis and Lung Disease,* 7**,** 797-803.

MARYAM, S., BHATTI, A. S. A. & SHAHZAD, A. W. 2010. Protective effects of silymarin in isoniazid induced hepatotoxicity in rabbits. *Annals of King Edward Medical University,* 16, 43-47.

MATTHEE, L. I. 2007. *A preclinical evaluation of the possible enhancement of the efficacy of antituberculosis drugs by Pheroid™ technology.* Master of Science North-West University. https://dspace.nwu.ac.za/handle/10394/1805 (Date accessed: 28 April 2014).

MCILLERON, H., WASH, P., BURGER, A., NORMAN, J., FOLB, P. I. & SMITH, P. 2006. Determinants of rifampin, isoniazid, pyrazinamide, and ethambutol pharmacokinetics in a cohort of tuberculosis patients. *Antimicrobial Agents and Chemotherapy,* 50**,** 1170-1177.

METUSHI, I. G., CAI, P., ZHU, X., NAKAGAWA, T. & UETRECHT, J. P. 2011. A fresh look at the mechanism of isoniazid-induced hepatotoxicity. *Clinical Pharmacology & Therapeutics,* 89, 911-914.

NIEUWOUDT, L. 2009. *The impact of Pheroid technology on the bioavailability and efficacy of anti-tuberculosis drugs in an animal model.* Master of Science (MSc), North-West University. https://dspace.nwu.ac.za/handle/10394/4316 (Date accessed: 13 January 2014).

PANDEY, R., SHARMA, A., ZAHOOR, A., SHARMA, S., KHULLER, G. K. & PRASAD, B. 2003a. Poly (dl-lactide-co-glycolide) nanoparticle-based inhalable sustained drug delivery system for experimental tuberculosis. *Journal of Antimicrobial Chemotherapy,* 52**,** 981-986.

PANDEY, R., ZAHOOR, A., SHARMA, S. & KHULLER, G. K. 2003b. Nanoparticle encapsulated antitubercular drugs as a potential oral drug delivery system against murine tuberculosis. *Tuberculosis,* 83**,** 373-378.

PANG, K. S. 2003. Modeling of intestinal drug absorption: roles of transporters and metabolic enzymes (for the gillette review series). *Drug Metabolism and Disposition,* 31**,** 1507-1519.

PINHEIRO, M., LÚCIO, M., LIMA, J. L. F. C. & REIS, S. 2011. Liposomes as drug delivery systems for the treatment of TB. *Nanomedicine,* 6**,** 1413-1428.

POGGESI, I. 2004. Predicting human pharmacokinetics from preclinical data. *Current Opinion in Drug Discovery and Development,* 7**,** 100-111.

REISFELD, B., METZLER, C. P., LYONS, M. A., MAYENO, A. N., BROOKS, E. J. & DEGROOTE, M. A. 2012. A physiologically based pharmacokinetic model for capreomycin. *Antimicrobial Agents and Chemotherapy,* 56**,** 926-934.

REMMER, H. 1970. The role of the liver in drug metabolism. *The American Journal of Medicine,* 49**,** 617-629.

ROSENTHAL, I. M., TASNEEN, R., PELOQUIN, C. A., ZHANG, M., ALMEIDA, D., MDLULI, K. E., KARAKOUSIS, P. C., GROSSET, J. H. & NUERMBERGER, E. L. 2012. Dose-ranging comparison of rifampin and rifapentine in two pathologically distinct murine models of tuberculosis. *Antimicrobial agents and chemotherapy,* 56**,** 4331-4340.

SADOH 2014. National Tuberculosisi management guidelines. *In:* HEALTH (ed.). South Africa TB DOTS strategy coordination, National Department of Health. .

SEMETE, B., BOOYSEN, L., LEMMER, Y., KALOMBO, L., KATATA, L., VERSCHOOR, J. & SWAI, H. S. 2010. In vivo evaluation of the biodistribution and safety of PLGA nanoparticles as drug delivery systems. *Nanomedicine: Nanotechnology, Biology and Medicine,* 6**,** 662-671.

SEMETE, B., KALOMBO, L., KATATA, L., CHELULE, P., BOOYSEN, L. I. J., LEMMER, Y., NAIDOO, S., RAMALAPA, B., HAYESHI, R. & SWAI, H. 2012. Potential of improving the treatment of tuberculosis through nanomedicine. *Molecular Crystals and Liquid Crystals,* 556**,** 317-330.

SHABANA, M. B., IBRAHIM, H. M., KHADRE, S. E. M. & ELEMAM, M. G. 2012. Influence of rifampicin and tetracycline administration on some biochemical and histological parameters in albino rats. *The Journal of Basic & Applied Zoology,* 65, 299-308.

SHIH, T.Y., HO, S.C., HSIONG, C.H., HUANG, T.Y. & YOA-PU HU, O. 2013. Selected pharmaceutical excipient prevent isoniazid and rifampicin induced hepatotoxicity. *Current Drug Metabolism,* 14**,** 720-728.SHIN, H. K., KANG, Y.-M. & NO, K. T. 2016. Predicting ADME Properties of Chemicals. *In:* LESZCZYNSKI, J. (ed.) *Handbook of Computational Chemistry.* Dordrecht: Springer Netherlands. 38 Pages.

SMITH, I. 2003. Mycobacterium tuberculosis pathogenesis and molecular determinants of virulence. *Clinical Microbiology Reviews,* 16**,** 463-496.

SOMASUNDARAM, S., RAM, A. & SANKARANARAYANAN, L. 2014. Isoniazid and Rifampicin as Therapeutic Regimen in the Current Era: A Review. *Journal of Tuberculosis Research,* 2**,** 40-51.

SWAI, H., SEMETE, B., KALOMBO, L., CHELULE, P., KISICH, K. & SIEVERS, B. 2009. Nanomedicine for respiratory diseases. *Wiley Interdisciplinary Reviews: Nanomedicine and Nanobiotechnology,* 1**,** 255-263.

TUKULULA, M., HAYESHI, R., FONTEH, P., MEYER, D., NDAMASE, A., MADZIVA, M., KHUMALO, V., LUBUSCHAGNE, P., NAICKER, B., SWAI, H. & DUBE, A. 2015. Curdlan-Conjugated PLGA Nanoparticles Possess Macrophage Stimulant Activity and Drug Delivery Capabilities. *Pharmaceutical Research,* 32**,** 2713-2726.

UIC. 2014. *The Laboratory Mouse* [Online]. Animals in biomedical research - University of Illinois. Available: https://www.brl.uic.edu/?q=node/18#resources (Date accessed 30 January 2016).

UNAIDS 2014. Ending the AIDS epidemic. *In:* REPORT, T. U. G. (ed.) *The UNAIDS GAP Report.* Geneva Switzerland: The joint united nations programme on HIV/AIDS (UNAIDS).

URSO, R., BLARDI, P. & GIORGI, G. 2002. A short introduction to pharmacokinetics. *European review for medical and pharmacological sciences,* 6**,** 33-44.

VAN LOO, P. L. P., VAN ZUTPHEN, L. & BAUMANS, V. 2003. Male management: coping with aggression problems in male laboratory mice. *Laboratory Animals,* 37**,** 300-313.

VREE, T. B., HEKSTER, Y. A. & ANDERSON, P. G. 1992. Contribution of the human kidney to the metabolic clearance of drugs. *Annals of Pharmacotherapy,* 26**,** 1421-1428.

WANG, R., BILLONE, P. S. & MULLETT, W. M. 2013. Nanomedicine in action: An overview of cancer nanomedicine on the market and in clinical trials. *Journal of Nanomaterials,* 2013**,** 12 Pages.

WANG, P., PRADHAN, K., ZHONG, X.-B. & MA, X. 2016. Isoniazid metabolism and hepatotoxicity. *Acta Pharmaceutica Sinica B,* 6**,** 384-392.

WHO 2010. *Treatment of tuberculosis: guidelines*, World Health Organization

WHO 2015. *Global Tuberculosis Report,* World Health Organization.

WONG, H., RAUTH, A., BENDAYAN, R., MANIAS, J., RAMASWAMY, M., LIU, Z., ERHAN, S. & WU, X. 2006. A new polymer–lipid hybrid nanoparticle system increases cytotoxicity of doxorubicin against multidrug-resistant human breast cancer cells. *Pharmaceutical Research,* 23**,** 1574-1585.

ZHANG, L., CHAN, J. M., GU, F. X., RHEE, J.-W., WANG, A. Z., RADOVIC-MORENO, A. F., ALEXIS, F., LANGER, R. & FAROKHZAD, O. C. 2008. Self-assembled lipid−polymer hybrid nanoparticles: A robust drug delivery platform. *ACS Nano,* 2**,** 1696-1702.

ZHOU, P., SUN, X. & ZHANG, Z. 2014. Kidney–targeted drug delivery systems. *Acta Pharmaceutica Sinica B,* 4, 37-42.

CHAPTER 6

This final chapter summarises the entire thesis, points out the contribution as well as the shortcomings of this current work and gives the direction for further research studies.

CHAPTER 6: THESIS SUMMARY

A novel PLGA NP-Pheroid® hybrid DDS was successfully developed and evaluated to determine its effect on improving the PK of selected anti-TB therapeutic drugs. The outcomes of this research project did not prove the initial hypothesis presented in chapter 1, however they resulted in an essential contribution of knowledge to this research field. A critical review article by Park (2016), alluded that hypotheses are developed with an increasing knowledge on any topic to establish certain theories, however it is not uncommon to disprove these theories (Park, 2016). This review mentioned frequent mistakes made by research scientists, and that is to take inconclusive experimental data to make conclusions such as the prediction of clinical outcomes. Nonetheless, the improvement of patient treatment is the fundamental purpose of the effort of the design of efficient DDS. Consequently, further extension of this research work is worth being considered before finalising conclusions on the effect of NP-Pheroid® hybrid DDS.

1. Thesis outcomes

This thesis introduced a hybrid DDS with the potential for multifunctional capability in both chapter 1 and 2. Previously studied hybrid systems have been proven to be more advantageous in comparison with the individual systems. Their design and application have been limited mainly to the improvement of cancer therapy, and therefore a gap in the scope of applying these hybrid DDS was identified to be in the potential to improve treatment for infectious diseases such as TB. The novel hybrid DDS developed in this study was aimed at combining the unique features of PLGA NP as the polymeric core with Pheroid® vesicles as the lipid shell. Chapter 3 of the thesis showed the optimum method of mixing the two DDS. The combination of NP with positive ζ-potential (pos–NP) with Pheroid® vesicles that naturally possess a negative ζ-potential resulted in a significant particle size increase of the Pheroid® vesicles suggesting successful entrapment of NP within the vesicles through electrostatic interaction, see Figure 1. The pre-mix preparation method resulted in a relatively higher ζ-potential which implied more stability and less aggregation of the hybrid system than using the post-mix method. Both CLSM and TEM images indicated the co-localisation of the NP with the Pheroid® vesicles. Chapter 3 also concluded that a maximum of 2.5% (w/v) of NP could be optimally added to the Pheroid® vesicle without compromising the Pheroid® vesicle morphology.

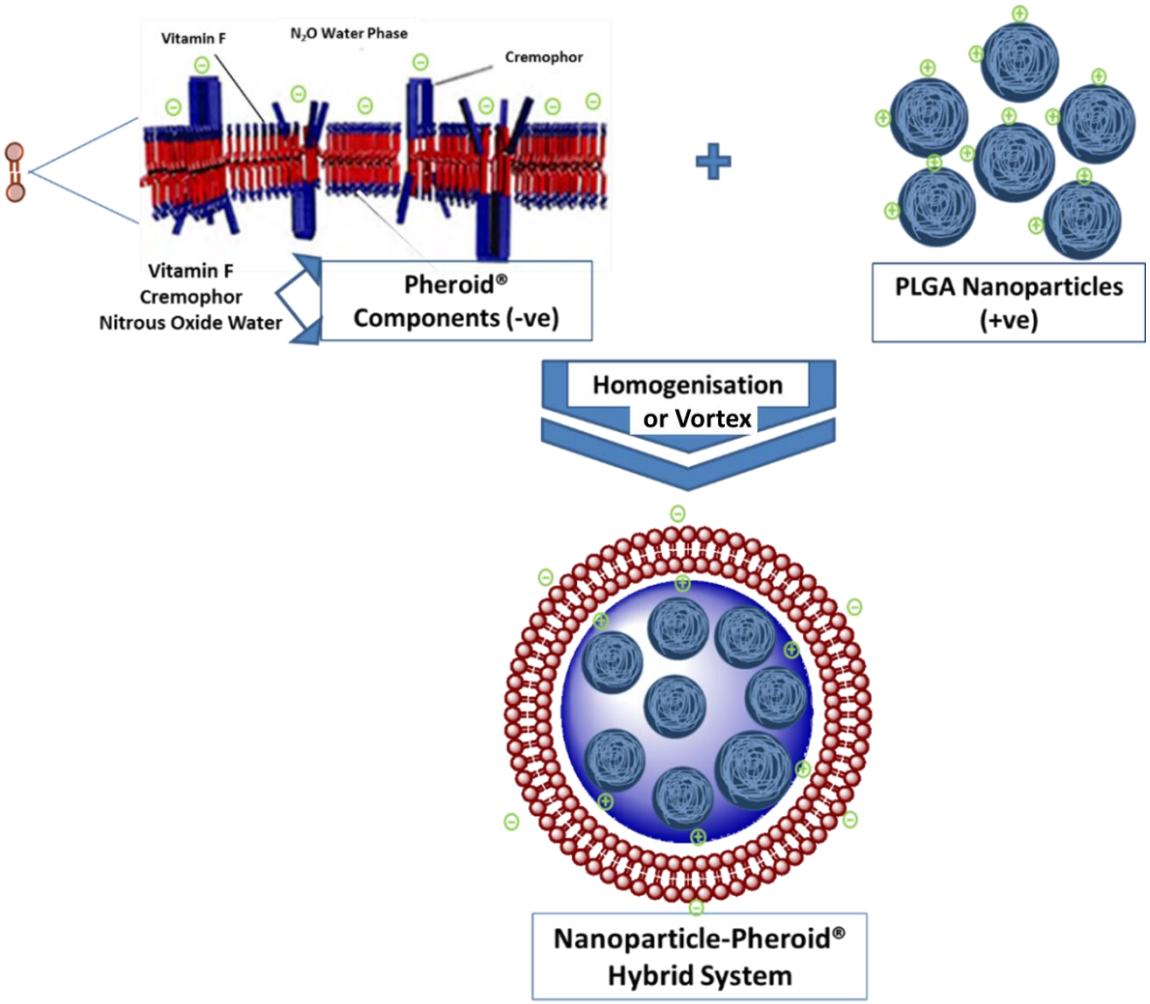

Figure 1: An illustration of the electrostatic interaction of Pheroid® vesicles (negative ζ-Potential) with nanoparticles (positive ζ-Potential) into a nanoparticle-Pheroid® hybrid system.

Chapter 4 covered the *in vitro* studies using Caco-2 cells. The appropriate concentrations of the NP, Pheroid® and NP-Pheroid® were determined for the *in vitro* permeability and uptake studies. Out of three viability assays used, the xCELLigence® RTCA gave more accurate and reproducible viability results than the MTT assay and trypan blue exclusion test. The maximum concentrations which showed no cytotoxic effects toward the Caco-2 cells over a period of 24 h were confirmed to be 0.004% (v/v) (1000 times dilution) of the Pheroid® vesicles and 1% (w/v) (10 mg/ml) for the NP, using RTCA. The permeability of the fluorescent hydrophobic model drug, C6, was significantly enhanced when entrapped in NP, Pheroid® vesicles as well as the NP-Pheroid® hybrid while free C6 could not permeate through the Caco-

2 cells. Interestingly, there was no significant improvement in the cell permeability of C6 in hybrid DDS in comparison to the individual NP and Pheroid® DDS as was initially hypothesised. C6 was shown to be more likely localised on the Caco-2 cell membrane rather than in the cytoplasm, and none of the DDS had an impact on this association of C6 with Caco-2 cells.

The case study of this research work involved the PK evaluation of two anti-TB drugs, INH and RIF, formulated as free drug, drug-loaded NP and NP-Pheroid®-entrapped drug. This work was conducted *in vivo* using female BALB/c mice and was covered in chapter 5. The plasma levels of both drugs did not provide convincing evidence that the NP-Pheroid® hybrid formulation has any effect on the PK of the anti-TB drugs. For the organ drug distribution, INH was assumed to have undergone rapid metabolism from all three formulations as it could not be detected in any of the harvested organs. On the other hand, RIF was detected in all the harvested organs up to a period of 3 to 5 d. The highest accumulation and organ penetration of RIF was found to be in the liver. Although the RIF NP-Pheroid® hybrid DDS did not affect either the AUC or the C_{max} of RIF in any of the harvested organs, it resulted in the significant reduction of $T_{max,}$ from 11 to 4 h in the lungs in comparison with the RIF NP ($P = 0.020$). The hybrid formulation also resulted in increased retention of RIF in the lungs up to a period of 5 d, compared to a maximum of 3 d for both free RIF and RIF NP. These observations could imply that the hybrid system could have increased affinity to the lungs which is the primary host organ for the TB bacilli. The NP-Pheroid® hybrid formulation also demonstrated a significant increase of the $t_{1/2}$ of RIF in the kidneys from 4 h to 16 h compared to free RIF ($P = 0.0425$). This observation may warrant further studies to determine if the hybrid formulation can be considered for targeted delivery for renal diseases.

2. Research contribution

2.1. The use of Pheroid® as a lipid component in hybrid DDS

As a central goal of this study, a novel hybrid DDS was developed, which is unique from those previously reported. To the best of our knowledge, this research work was the first to report the use of Pheroid® technology as the lipid component of the hybrid DDS instead of the commonly used liposome. It was also interesting to show evidence that there could be an electrostatic interaction between the positive NP, with Pheroid® vesicles, that naturally possess

a negative ζ-potential. Therefore, this work forms the basis for a new hybrid DDS with the possibility of broader applications. The objective of this work was driven by the urgent need to find a suitable system that can contribute towards the efficient delivery of anti-TB drugs based on the potential that the combined effect of the NP and the Pheroid® system could have.

2.2. The visualisation of Pheroid® and NP-Pheroid® hybrid system through TEM imaging

The previously reported visual analysis of Pheroid® was in their native state using CLSM. Cryogenic TEM is typically used to visualise liquid emulsions, however this study, regular room temperature TEM was used, even though the vesicles are made up of 96% water and had to be subjected to air-drying. The room temperature TEM images reported had satisfactory contrast and confirmed the co-localisation of electron dense NP within the Pheroid® vesicles. The visualisation of the Pheroid® vesicle was enabled by the negative staining of the Pheroid® vesicles lipid membrane.

2.3. High cell viability at the highest PLGA NP concentration on Caco-2 cell

The other important contribution from this study was that the highest PLGA NP concentration of 10 mg/ml (1% w/v) had no cytotoxic effects on the Caco-2 cells and this has not yet been reported in literature according to our knowledge.

2.4. Effect of the hybrid system on RIF distribution to the lungs and kidneys

Although there was no significant influence of the hybrid system on the mouse plasma PK for both the INH and RIF, there was an interesting effect on the organ distribution of RIF. The hybrid system enhanced residence of RIF and reduced its T_{max} in the lungs. There was also a significant increase of RIF $t_{1/2}$ in the kidneys by the NP-Pheroid® hybrid formulation in comparison to the free RIF. However, more studies are required to confirm the effect of this hybrid system.

3. Study limitations

3.1. The use of RT TEM rather than cryo-TEM for the liquid form of the hybrid DDS

The thick bilayer membrane of the Pheroid vesicles observed from the room temperature TEM images could have been a possible artefact due the drying process. Cryo-TEM has previously been used to view liquid state hybrid DDS. However, this project could not produce conclusive cryo-TEM images to assist with the location of NP within the Pheroid® vesicles due to the low contrast. The availability of cryo-TEM facilities and corresponding expertise would help characterise this novel system with high resolution as reported for other similar systems (Friedrich *et al.*, 2010, Bershteyn *et al.*, 2008).

3.2. The lack of the Pheroid® control in the *in vivo* studies

In this study excluded the INH/RIF entrapped in Pheroid® control formulation due to limited resources. This study, therefore, relied on previously obtained results of this drug-Pheroid® group in mice studies conducted at the same drug doses (Matthee, 2007, Nieuwoudt, 2009). However, this led to difficulties in the comparison studies, as this current study indicated no effect on the bioavailability of both drugs when formulated in either NP or NP-Pheroid® formulation, while the Pheroid® formulation from previous studies improved the bioavailability of both INH and RIF by large margins in comparison to the free drug formulation.

3.3. The inadequate data points for INH PK studies

In the plasma data, the INH could only be quantified at a maximum of three data points (out of 10-time points), that is at 2, 4 and 8 h, with the highest C_{max} and T_{max} of 0.33 µg/ml and 2 h, respectively. This is speculated to have resulted from the rapid clearance of INH from the system. However, the dose of INH (5 mg/kg) as well as the selected far apart time points for INH measurement could have resulted in the inadequate data points obtained from the plasma, in comparison to previous studies. For example, in Booysen *et al*., (2013) the highest INH C_{max} of 38 µg/ml at a T_{max} of 2 h was obtained after administering a higher dose of 150 mg/kg to mice. Nieuwoudt, (2009) had frequent measurement time points before the 2 h mark and achieved a C_{max} of 2 µg/ml at a T_{max} of 0.75 h after 5 mg/kg administration. It is therefore suggested the future INH PK mice studies include frequent early time points

4. Future recommendations

The direction that may be followed for further insight into the potential of this novel hybrid DDS could be the following:

4.1. Three-dimensional electron microscopy (3D EM) imaging

The use of powerful tools such as 3D EM would be an efficient method for characterising the novel hybrid system. This would be a quantitative way to precisely locate the position of the NP within Pheroid® vesicles and have more structural insight into the system. These imaging methods may provide unambiguous 3D images with distinguished parts as well as offer quantitative information of an object (Ersen *et al*., 2007, Tafti *et al.*, 2015).

4.2. Modelling of the novel DDS

Mathematical modelling presents several advantages in the design of an optimised DDS along with computer simulations. The use of appropriate computer/mathematical programs can lead to a reasonable estimation of the required components of a formulation and preparation procedures to obtain an ideal DDS. The overall benefits of these methods are reduced cost through the elimination of many experiments and a possible elucidation of drug release mechanisms from the DDS. Some researchers have advanced to use modelling as part of their designs of DDS (Ruell, 2003, Siepmann and Siepmann, 2008, Siepmann and Siepmann, 2012).

4.3. Optimisation of the NP-Pheroid® hybrid system.

The maximum 2.5% (w/v) NP in Pheroid® that lead to a stable hybrid system contains only a small amount of drugs that may not translate into acceptable pharmaceutical dosage size. The ideal optimised hybrid system would have increased drug loading in the NP and controlled release capability. It will also be worth pursuing how one can increase the stability of the hybrid system at higher NP/Pheroid® mixing ratios (> 5% w/v).

4.4. The use of alternative model drug for *in vitro* studies

This is based on the fact that in this current study, the apparent uptake of the lipophilic C6 was found to rather be an association with the cellular membranes. However, the use of alternative fluorescent compounds or UV active anti-TB drugs of interest should be considered to efficiently determine the effect of the hybrid system on cell permeability and uptake.

4.5. Detection of INH metabolites on the LC-MS/MS

Establishing a sensitive LC-MS/MS method for detecting parent ion of INH as well its metabolites would enable insight into and help determine the rate of INH metabolism in plasma and organs after exposure to the hybrid system (Zhou *et al*., 2010, Milán-Segovia *et al*., 2007).

5. References

BERSHTEYN, A., CHAPARRO, J., YAU, R., KIM, M., REINHERZ, E., FERREIRA-MOITA, L. & IRVINE, D. J. 2008. Polymer-supported lipid shells, onions, and flowers. *Soft Matter,* 4**,** 1787-1791.

BHANDARI, R. & KAUR, I. P. 2012. A Sensitive HPLC method for determination of isoniazid in rat plasma, brain, liver and kidney. *Journal of Chromatography & Separation Techniques,* 3**,** 1-5.

BOOYSEN, L. L. I. J., KALOMBO, L., BROOKS, E., HANSEN, R., GILLILAND, J., GRUPPO, V., LUNGENHOFER, P., SEMETE-MAKOKOTLELA, B., SWAI, H. S., KOTZE, A. F., LENAERTS, A. & DU PLESSIS, L. H. 2013. In vivo/in vitro pharmacokinetic and pharmacodynamic study of spray-dried poly-(dl-lactic-co-glycolic) acid nanoparticles encapsulating rifampicin and isoniazid. *International Journal of Pharmaceutics,* 444**,** 10-17.

ERSEN, O., HIRLIMANN, C., DRILLON, M., WERCKMANN, J., TIHAY, F., PHAM-HUU, C., CRUCIFIX, C. & SCHULTZ, P. 2007. 3D-TEM characterization of nanometric objects. *Solid State Sciences,* 9**,** 1088-1098.

FRIEDRICH, H., FREDERIK, P. M., DE WITH, G. & SOMMERDIJK, N. A. 2010. Imaging of self-assembled structures: Interpretation of TEM and cryo-TEM images. *Angewandte Chemie International Edition,* 49**,** 7850-7858.

GROBLER, L. 2014. *The effect of Pheroid® technology on the bioavailability of artemisone in primates.* North-West University. https://dspace.nwu.ac.za/handle/10394/12241 (Date accessed: 13 January 2014).

MATTHEE, L. I. 2007. *A preclinical evaluation of the possible enhancement of the efficacy of antituberculosis drugs by Pheroid™ technology.* Master of Science, North-West University. https://dspace.nwu.ac.za/handle/10394/1805 (Date accessed: 28 April 2014).

MILÁN-SEGOVIA, R., PÉREZ-FLORES, G., TORRES-TIRADO, J., HERMOSILLO-RAMÍREZ, X., VIGNA-PÉREZ, M. & ROMANO-MORENO, S. 2007. Simultaneous

HPLC determination of isoniazid and acetylisoniazid in plasma. *Acta Chromatographica,* 19**,** 110.

NIEUWOUDT, L. 2009. *The impact of Pheroid technology on the bioavailability and efficacy of anti-tuberculosis drugs in an animal model.* Master of Science (MSc), North-West University. https://dspace.nwu.ac.za/handle/10394/4316 (Date accessed: 13 January 2014).

PANDEY, R. & AHMAD, Z. 2011. Nanomedicine and experimental tuberculosis: facts, flaws, and future. *Nanomedicine: Nanotechnology, Biology and Medicine,* 7**,** 259-272.

PARK, K. 2016. Drug delivery of the future: Chasing the invisible gorilla. *Journal of Controlled Release,* 240**,** 2–8.

RAEMDONCK, K., BRAECKMANS, K., DEMEESTER, J. & DE SMEDT, S. C. 2013. Merging the best of both worlds: hybrid lipid-enveloped matrix nanocomposites in drug delivery. *Chemical Society Reviews,* 43**,** 444-472.

RUELL, J. 2003 Permeability assays and oral absorption modeling can make the difference between drugs and dregs. *Mordern Drug Discovery - American Chemical Society_thetoolbox***,** 28-30.

SEMETE, B., KALOMBO, L., KATATA, L., CHELULE, P., BOOYSEN, L. I. J., LEMMER, Y., NAIDOO, S., RAMALAPA, B., HAYESHI, R. & SWAI, H. 2012. Potential of Improving the Treatment of Tuberculosis Through Nanomedicine. *Molecular Crystals and Liquid Crystals,* 556**,** 317-330.

SIEPMANN, J. & SIEPMANN, F. 2008. Mathematical modeling of drug delivery. *International Journal of Pharmaceutics,* 364**,** 328-343.

SIEPMANN, J. & SIEPMANN, F. 2012. Modeling of diffusion controlled drug delivery. *Journal of Controlled Release,* 161**,** 351-362.

TAFTI, A. P., KIRKPATRICK, A. B., ALAVI, Z., OWEN, H. A. & YU, Z. 2015. Recent advances in 3D SEM surface reconstruction. *Micron,* 78**,** 54-66.

TUKULULA, M., HAYESHI, R., FONTEH, P., MEYER, D., NDAMASE, A., MADZIVA, M., KHUMALO, V., LUBUSCHAGNE, P., NAICKER, B., SWAI, H. & DUBE, A. 2015. Curdlan-conjugated PLGA nanoparticles possess macrophage stimulant activity and drug delivery capabilities. *Pharmaceutical Research,* 32**,** 2713-2726.

ZHOU, Z., CHEN, L., LIU, P., SHEN, M. & ZOU, F. 2010. Simultaneous Determination of Isoniazid, Pyrazinamide, Rifampicin and Acetylisoniazid in Human Plasma by High-Performance Liquid Chromatography. *Analytical Sciences,* 26**,** 1133-1138.

ANNEXURES

ANNEXURE A – Overall Flow of Experiments

The following diagram shows a summary of the experiments performed in this study.

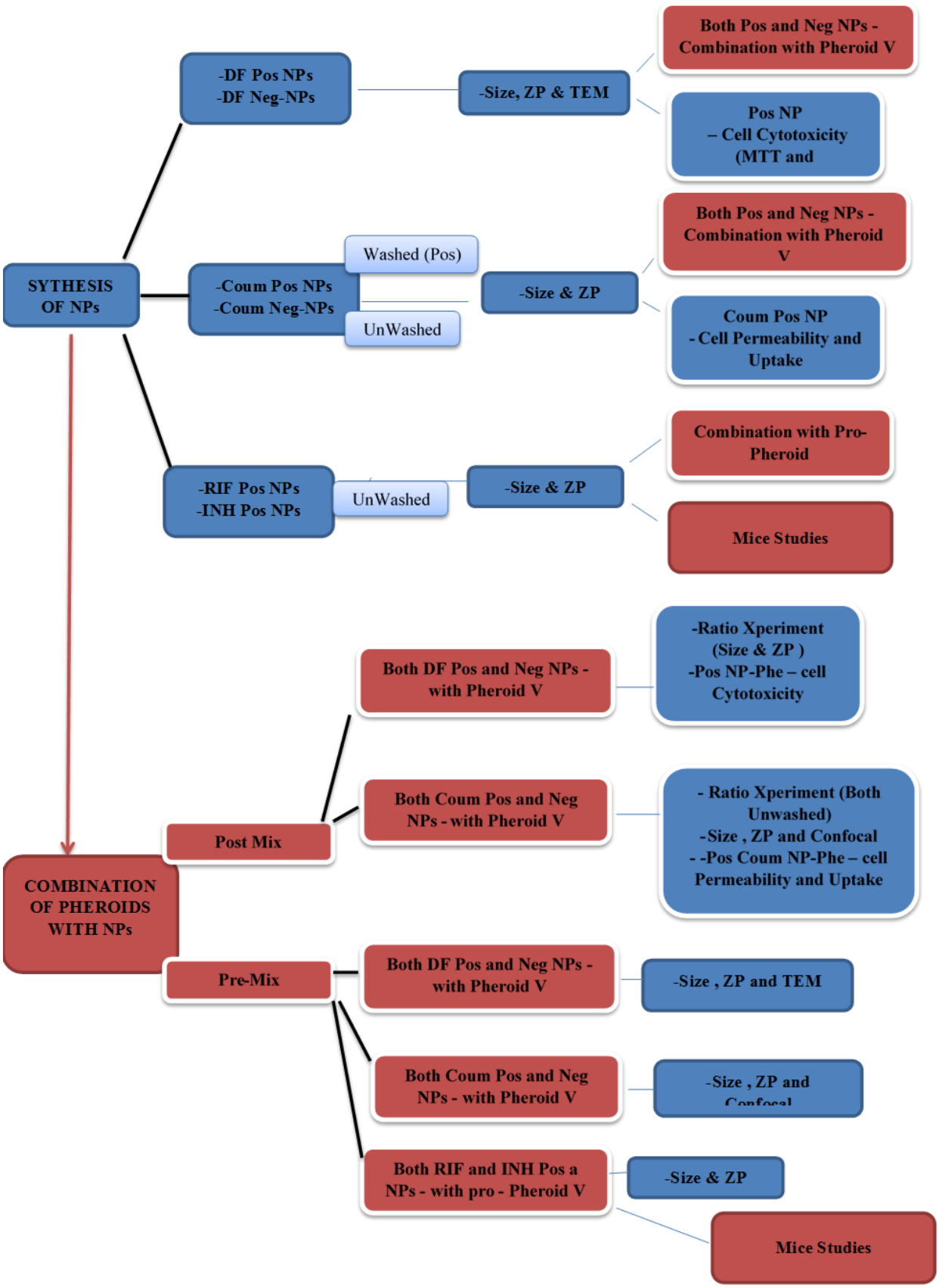
SYTHESIS OF NPs
-DF Pos NPs
-DF Neg-NPs
-Size, ZP & TEM
Both Pos and Neg NPs - Combination with Pheroid V
Pos NP – Cell Cytotoxicity (MTT and
-Coum Pos NPs
-Coum Neg-NPs
Washed (Pos)
UnWashed
-Size & ZP
Both Pos and Neg NPs - Combination with Pheroid V
Coum Pos NP - Cell Permeability and Uptake
-RIF Pos NPs
-INH Pos NPs
UnWashed
-Size & ZP
Combination with Pro-Pheroid
Mice Studies
COMBINATION OF PHEROIDS WITH NPs
Post Mix
Both DF Pos and Neg NPs - with Pheroid V
-Ratio Xperiment (Size & ZP)
-Pos NP-Phe – cell Cytotoxicity
Both Coum Pos and Neg NPs - with Pheroid V
- Ratio Xperiment (Both Unwashed)
-Size , ZP and Confocal
- -Pos Coum NP-Phe – cell Permeability and Uptake
Pre-Mix
Both DF Pos and Neg NPs - with Pheroid V
-Size , ZP and TEM
Both Coum Pos and Neg NPs - with Pheroid V
-Size , ZP and
Both RIF and INH Pos a NPs - with pro - Pheroid V
-Size & ZP
Mice Studies

ANNEXURE B - Journal Author Guidelines

Journal 1 – *Journal of Material Science*

Springer www.springer.com

Materials Home > Materials

Aims and Scope: Journal of Materials Science

The *Journal of Materials Science* is now firmly established as the leading source of primary communication for scientists investigating the structure and properties of all engineering materials. The *Journal of Materials Science* publishes reviews and full-length papers recording original research results on, or techniques for, studying the relationship between structure, properties, and uses of materials. Materials include metals, ceramics, glasses, polymers, energy materials, electrical materials, composite materials, fibers, nanostructured materials, nanocomposites, and biological and biomedical materials.

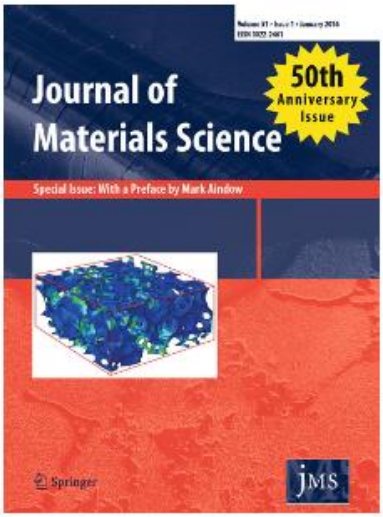

Journal of Materials Science
Editor-in-Chief: C. B. Carter
E-mail: cbcarter@gmail.com
ISSN: 0022-2461 (print version)
ISSN: 1573-4803 (electronic version)

The Journal of Materials Science publishes reviews and full-length papers recording original research on, or techniques for, studying the fundamental relationships between structure, processing, properties and performance of materials.

Instructions for authors

Please note that these Instructions include guidelines that are specific to the Journal of Materials Science. Where the Instructions differ from the generic Springer version found on Springer.com, the version given here takes precedence.

Manuscript submission

Author representations

Submission of a manuscript implies: that the work described has not been published before; that it is not under consideration for publication anywhere else; that its publication has been approved by all co-authors, if any, as well as by the responsible authorities — tacitly or explicitly — at the institute where the work has been carried out. The publisher will not be held legally responsible should there be any claims for compensation.

Permissions

Authors wishing to include figures, tables, or text passages that have already been published elsewhere are required to obtain permission from the copyright owner(s) for both the print and online format and to include evidence that such permission has been granted when submitting their papers. Any material received without such evidence will be assumed to originate from the authors.

Online submission

Authors must submit their manuscripts online via the Journal of Materials Science Editorial Manager website at: https://www.editorialmanager.com/jmsc/.

Article types

Regular articles

Regular articles report original research on, or techniques for studying, the fundamental relationships between structure, processing, properties and performance of materials.

Typical topics include, but are not limited to: metals, ceramics, glasses, polymers, electrical and electronic materials, composite materials, fibers, nanostructured materials, nanocomposites, and biological and biomedical materials.

The median typeset length for a regular research article published in the Journal in 2014 was nine pages.

Articles in special issues and themed sections

Special issues are collections of themed articles, sometimes arising from a conference, symposium or other notable event. Only full papers of the same standard as regular articles will be considered for publication in special issues.

Articles submitted to the Journal for inclusion in special issues are processed in the same manner as regular articles, but will typically involve a Guest Editor in addition to the normal Editorial Board.

Reviews

Review articles are intended to be comprehensive summaries of the state-of-the-art in a particular aspect of materials science. The median typeset length for a review article published in the Journal from 2013 to 2015 inclusive was 17 pages. The median number of references in these articles was 114.

Prospective authors of reviews should contact the Editor-in-Chief before preparing their articles.

Viewpoint articles

Viewpoint articles, introduced in 2016, are short personal perspectives on a topical area of general interest to the materials science community. Authors of Viewpoint articles are invited by the Editor-in-Chief. Suggestions for Viewpoint articles may be directed to the Editor-in-Chief.

Manuscript format

Cover letter

All submissions must include a cover letter that includes:

- A confirmation of author representations that: the work described has not been published before; it is not under consideration for publication anywhere else; and publication has been approved by all co-authors and the responsible authorities at the institute(s) where the work has been carried out.
- A statement of the novelty and significance of the work and the relevance to the mission of the Journal of Materials Science.
- Names, affiliations and email addresses of at least three suitable referees, together with a brief statement of why they are qualified to evaluate the manuscript. Referees should be selected from countries other than those where the authors reside.

Title page

The title page should include:

- The name(s) of the author(s), with symbols to link each name with that author's institutional affiliation and an asterisk to denote the corresponding author
- A concise and informative title
- The affiliation(s) and address(es) of the author(s)
- The e-mail addresses of all authors and the telephone number of the corresponding author

The use of abbreviations in titles is discouraged. These abbreviations can appear in the abstract and keywords to ensure the article is automatically indexed properly.

The author list should include only those who have made significant scientific contributions to the manuscript. These contributions must include conception and planning of the work that led to the manuscript or acquisition, analysis and interpretation of the data, or both; drafting or critical revision of the manuscript for important intellectual content, or both; and approval of the final submitted version of the manuscript. Others who have contributed to the work should be noted in the Acknowledgements.

Abstract

The abstract should be 150 to 250 words. The content should state the main purposes and research questions of the study, the methods used, the main results, and the key conclusions.

Keywords

Authors should provide 4 to 6 keywords, which can be used for indexing purposes.

Effective keywords include abbreviations or phrases that may not appear in the title or abstract and that link the work to wider fields of research.

Main body

Manuscripts describing original research will typically include the following sections:

- Introduction: a concise, up-to-date description of the background to provide a general reader of the Journal with enough context to understand the research being presented and its significance, as well as providing a clear statement of the research question and any hypotheses being explored.
- Materials and methods: techniques, materials and equipment described in sufficient detail for another trained researcher to be able to reproduce the experimental work reported. Methods that are identical to published procedures should still be summarized in brief and include a citation to the original work.
- Analysis: in submissions that have a significant theoretical or mathematical component, a description of the analytical procedures may be required.
- Results: a description of the analyses and measurements related to answering the central research questions.
- Discussion: the interpretation of the results, considering their significance, and putting them into a wider context through comparison to previously published research. The use of a combined "Results and Discussion" section is discouraged.
- Conclusions: a concise statement of the main conclusions drawn from the research reported in the manuscript.
- Acknowledgments: a list of people who contributed to the work in the manuscript but who are not named in the author list, and a list of funding sources that supported the research presented. The Acknowledgments should appear as a separate section before the reference list. The names of funding organizations should be written in full.
- Conflicts of interest: a statement that declares all relationships or interests of the manuscript's authors that could potentially influence or bias the submitted work. If no conflicts of interest exist, the authors must include a statement stating this. Details on potential conflicts of interest are included in the 'publishing ethics' section.
- Supplementary information: a brief description of any additional material omitted from the main body in the interest of presentation a clearer and more readable manuscript.

Text

Text formatting

Manuscripts should be submitted in Microsoft Word. PDF is *not* an acceptable format.

- Use a normal, plain font (e.g., 12-point Times Roman) for text.
- Use italics for emphasis.
- Use the automatic page numbering function to number the pages.
- Do not use field functions.
- Use tab stops or other commands for indents, not the space bar.
- Use the table function, not spreadsheets, to make tables.
- Use the equation editor or MathType for equations.
- Save your file in docx format (Word 2007 or higher) or doc format (older Word versions).

Manuscripts with mathematical content can also be submitted in LaTeX.

- A LaTeX macro package (zip, 182 kB) is available for download. Full instructions on preparing a TeX submission for our editorial manager system are available on the Editorial Manager site.

Headings

No more than three levels of displayed headings should be used.

Abbreviations

Abbreviations should be defined at the point of first use and be used consistently thereafter. Abbreviations defined in the abstract should be redefined in the main body of the submission.

Footnotes

Footnotes can be used to give additional information, which may include the citation of a reference included in the reference list. They should not consist solely of a reference citation, and they should never include the bibliographic details of a reference. They should also not contain any figures or tables.

Footnotes to the text are numbered consecutively; those to tables should be indicated by superscript lower-case letters (or asterisks for significance values and other statistical data). Footnotes to the title or the authors of the article are not given reference symbols.

Always use footnotes instead of endnotes.

Equations

Some equations entered using Microsoft Equation do not convert correctly when a submission written in Microsoft Word is converted into a PDF by Editorial Manager. Authors are encouraged to double-check all equations before final submission and to use Insert|Equation... for better compatibility.

Scientific style

- Internationally accepted signs and symbols for units (SI units) should be used throughout. Negative exponents should be used instead of a slash, e.g., m s^{-2} rather than m/s^2.
- Nomenclature: Insofar as possible, authors should use systematic names similar to those used by Chemical Abstracts Service or IUPAC.
- A decimal point (dot, full stop) should be used to mark the radix point instead of a comma, e.g., 0.5%.
- The following standard mathematical notation should be used for formulae, symbols, etc.:
  - Italics for single letters that denote mathematical constants, variables, and unknown quantities
  - Roman (upright) face for numerals, operators, and punctuation, and commonly defined functions or abbreviations, e.g., cos, det, e or exp, lim, log, max, min, sin, tan, d (for derivative)
  - Bold face for vectors, tensors, and matrices.

References

Citation

Reference citations in the text should be identified by numbers in square brackets; these should be placed before punctuation marks. Some examples:

1. This material is used in a wide variety of applications [3].
2. This result was later contradicted by Becker and Seligman [5].
3. This effect has been widely studied [1–3, 7].

Reference list

The list of references should only include works that are cited in the text and that have been published or accepted for publication. Personal communications and unpublished works should only be mentioned in the text. Do not use footnotes or endnotes as a substitute for a reference list.

The entries in the list should be numbered consecutively.

Journal article

[1] Hanaor DAH and Sorrell CC (2011) Review of the anatase to rutile phase transformation, J Mater Sci 46:855-874.

Ideally, the names of all authors should be provided, but the usage of "et al" in long author lists will also be accepted:

[2] Eichhorn SJ, Dufresne A, Aranguren M et al (2010) Review: current international research into cellulose nanofibres and nanocomposites, J Mater Sci 45:1-33.

Articles published online but not yet assigned page numbers may be cited using the DOI:

[3] Kaplan WD, Chatain D, Wynblatt P, Carter WC (2013) A review of wetting versus adsorption, complexions, and related phenomena: the Rosetta stone of wetting, J Mater Sci. doi: 10.1007/s10853-009-3874-0

Book

[4] Carter CB, Norton MG (2013) Ceramic Materials: Science and Engineering 2nd edn. Springer, New York

Book chapter

[5] Nieh TG (2007) Deformation Behavior. In: Miller MK, Liaw P (eds) Bulk Metallic Glasses. Springer, New York, pp 147-161

Online document

[6] Barthelmy D (2007) Cryptomelane. http://webmineral.com/data/Cryptomelane.shtml. Accessed 28 July 2013

Dissertation

[7] Blanford CF (2000) Synthesis and electron microscopy of inorganic and hybrid organic-inorganic mesoporous and macroporous materials. PhD Dissertation, University of Minnesota

Always use the standard abbreviation of a journal's name according to the ISSN List of Title Word Abbreviations, see www.issn.org/2-22661-LTWA-online.php

For authors using EndNote, Springer provides an output style that supports the formatting of in-text citations and reference list. EndNote style (zip, 2 kB)

For authors using Docear, Mendeley, Zotero or other citation-management software, a citation style language (CSL) version of this Journal's reference style can be downloaded from https://www.zotero.org/styles/journal-of-materials-science.

Authors preparing their manuscript in LaTeX can use the BibTeX file spbasic.bst, which is included in Springer's LaTeX macro package, or generate their file using pandoc with the argument --csl=journal-of-materials-science.csl.

Tables

- All tables are to be numbered using Arabic numerals.
- Tables should always be cited in text in consecutive numerical order.
- Each table must be accompanied by a table caption (title) explaining the components of the table.
- The original source of any previously published material is to be identified using a reference at the end of the table caption.
- Footnotes to tables should be indicated by superscript lower-case letters (or asterisks for significance values and other statistical data) and included beneath the table body.

Artwork and illustration guidelines

Electronic figure submission

- Supply all figures electronically.
- For vector graphics, the preferred format is EPS; for halftones, use TIFF format. Vector graphics file formats (e.g., EPS) must have fonts embedded in the file. MS Office files are also acceptable.
- Name your figure files with "Fig" and the figure number, e.g., Fig1.eps.

Line art

- Definition: Black and white graphic with no shading.
- Do not use faint lines and/or lettering and check that all lines and lettering within the figures are legible at final size.
- All lines should be at least 0.1 mm (0.3 pt) wide.
- Scanned line drawings and line drawings in bitmap format should have a minimum resolution of 1200 dpi.

Data plots

- Definition: Graphical representation of data to reveal relationships between variables.
- Plots should follow guidelines for line art in line width, font sizes and file resolution. All plots should use a white background.
- Simple geometric symbols (e.g., open and filled triangles, squares, circles, etc.) should be used for data points, with capped error bars to denote the precision of measurements.
- Axes should be labeled with the appropriate units included in parentheses.
- The use of Microsoft Excel to generate plots is strongly discouraged.

Halftone art

- Definition: Micrographs, photographs, drawings, or paintings with fine shading, etc. Magnifications should not be given (e.g., 1000×).
- If any magnification is used in the photographs, indicate this by using scale bars within the figures themselves. Microscope-generated scale bars, particularly "tick-mark" style ones, typically reproduce poorly and should be replaced by larger, more legible scale bars.
- The contrast in micrographs should be adjusted to fill the grey levels so long as it does lead to misinterpretation of the visual information being presented.
- Screenshots of EDS data are not acceptable. Data must be plotted in a graphing program.
- Halftones should have a minimum resolution of 300 dpi.

Combination art

- Definition: a combination of halftone and line art, e.g., halftones containing line drawing, extensive lettering, color diagrams, etc.
- Combination artwork should have a minimum resolution of 600 dpi.

Color art

- Color art is free of charge for online publication.
- If black and white will be shown in the print version, make sure that the main information will still be visible. Many colors are not distinguishable from one another when converted to black and white. A simple way to check this is to make a xerographic copy to see if the necessary distinctions between the different colors are still apparent.
- If the figures will be printed in black and white, do not refer to color in the captions.
- Color illustrations should be submitted as RGB (8 bits per channel).

Figure lettering

- To add lettering, it is best to use Helvetica, Calibri or Arial (sans serif fonts).
- Keep lettering consistently sized throughout your final-sized artwork, usually about 2–3 mm (8–12 pt).
- Variance of type size within an illustration should be minimal, e.g., do not use 8-pt type on an axis and 20-pt type for the axis label.
- Avoid effects such as shading, outline letters, etc.
- Do not include titles or captions within your illustrations.

Figure numbering

- All figures are to be numbered using Arabic numerals.
- Figures should always be cited in text in consecutive numerical order.
- Figure parts should be denoted by lowercase letters (a, b, c, etc.).
- If an appendix appears in your article and it contains one or more figures, continue the consecutive numbering of the main text. Do not number the appendix figures, "A1, A2, A3, etc." Figures in online appendices (Electronic Supplementary Material) should, however, be numbered separately.

Figure captions

- Each figure should have a concise caption describing accurately what the figure depicts. Include the captions in the text file of the manuscript, not in the figure file.
- Figure captions begin with the term Fig. in bold type, followed by the figure number, also in bold type.
- No punctuation is to be included after the number, nor is any punctuation to be placed at the end of the caption.
- Identify all elements found in the figure in the figure caption; and use boxes, circles, etc., as coordinate points in graphs.
- Identify previously published material by giving the original source in the form of a reference citation at the end of the figure caption.

Figure placement and size

- When preparing your figures, size figures to fit in the column width.
- For the *Journal of Materials Science*, the figures should be 84 mm wide for single-column figures or 174 mm wide for double-column figures, and not taller than 234 mm.

Cover art

- From June 2016, the Journal of Materials Science will feature large cover images.
- Suggestions for artwork can be uploaded at the time of submission.
- Artwork should be 8.5 in. × 8.5 in (21.6 cm × 21.6 cm) at a resolution of 300 dpi.
- The Journal of Materials Science does not charge authors a fee to feature their cover artwork.

Accessibility

- In order to give people of all abilities and disabilities access to the content of your figures, please make sure that:
  - all figures have descriptive captions (blind users could then use a text-to-speech software or a text-to-Braille hardware);
  - patterns are used instead of or in addition to colors for conveying information (color-blind users would then be able to distinguish the visual elements); and
  - any figure lettering has a contrast ratio of at least 4.5:1.

Permissions

If you include figures that have already been published elsewhere, you must obtain permission from the copyright owner(s) for both the print and online format. Please be aware that some publishers do not grant electronic rights for free and that Springer will not be able to refund any costs that may have occurred to receive these permissions. In such cases, material from other sources should be used.

Electronic supplementary material

Springer accepts electronic multimedia files (animations, movies, audio, etc.) and other supplementary files to be published online along with an article or a book chapter. This feature can add dimension to the author's article, as certain information cannot be printed or is more convenient in electronic form.

Submission

- Supply all supplementary material in standard file formats.
- Include in each file the following information: article title; journal name; author names; and affiliation and e-mail address of the corresponding author.
- To accommodate user downloads, keep in mind that larger files may require very long download times and that some users may experience other problems during downloading.

Audio, video, and animations

- Always use MPEG-1 (.mpg) format.

Text and presentations

- Submit your material in PDF format; .doc or .ppt files are not suitable for long-term viability.
- A collection of figures may also be combined in a PDF file.

Spreadsheets

- Spreadsheets should be converted to PDF if no interaction with the data is intended.
- If the readers should be encouraged to make their own calculations, spreadsheets should be submitted as .xls files (MS Excel).

Specialized formats

- Specialized format such as .pdb (chemical), .wrl (VRML), .nb (Mathematica notebook), and .tex can also be supplied.

Collecting multiple files

- It is possible to collect multiple files in a .zip or .gz file.

Numbering

- If supplying any supplementary material, the text must make specific mention of the material as a citation, similar to that of figures and tables.
- Refer to the supplementary files as “Online Resource”, e.g., "... as shown in the animation (Online Resource 3)", “... additional data are given in Online Resource 4”.
- Name the files consecutively, e.g. “ESM_3.mpg”, “ESM_4.pdf”.

Captions

- For each supplementary material, please supply a concise caption describing the content of the file.

Processing of supplementary files

- Electronic supplementary material will be published as received from the author without any conversion, editing, or reformatting.

Accessibility

- In order to give people of all abilities and disabilities access to the content of your supplementary files, please make sure that
- The manuscript contains a descriptive caption for each supplementary material
- Video files do not contain anything that flashes more than three times per second (so that users prone to seizures caused by such effects are not put at risk)

Publishing ethics

Springer is a member of the Committee on Publication Ethics (COPE) and subscribes to its principles. COPE's code of conduct, guidelines, and flowcharts are freely available from http://publicationethics.org/.

Text recycling (self-plagiarism)

The Journal of Materials Science bases its policy on text recycling, also known as self-plagiarism, on the COPE's guidelines available at http://publicationethics.org/text-recycling-guidelines.

Self-plagiarism occurs when sections of the same text appear (usually un-attributed) in more than one of an author's own publications. The term 'text recycling' has been chosen to differentiate from 'true' plagiarism (i.e., when another author's words or ideas have been used, usually without attribution).

The editors recognize that a certain degree of text recycling is unavoidable in scientific writing, especially in descriptions of techniques or experimental methods. In assessing cases of suspected self-plagiarism, the editors will consider how much of the text is repeated verbatim and in what context. Text recycling in the results section of an original research paper is always unacceptable if it duplicates published data. Text recycling in the discussion and conclusions sections is unlikely to be acceptable.

In the case of minor overlap, an editor may require the authors to re-write the sections of overlapping text and provide appropriate attribution. More significant overlap will result in the rejection of a submission. The assessment of the degree of overlap is at the discretion of the handling editor and editor-in-chief.

Article spinning

Article spinning is the use of software in attempt to bypass plagiarism-detection software. Submissions that include significant portions of text that have been processed in this way will be rejected.

Submissions that include experiments on samples of biological origin

Experiments involving in vivo testing on animal subjects

The Journal of Materials Science does not accept manuscripts where *in vivo* testing on animals is reported. Authors should consider submitting to Journal of Materials Science : Materials in Medicine.

Experiments involving human subjects and human tissue

The Journal of Materials Science does not accept manuscripts where testing on human subjects is reported.

For work which reports on the use of human tissue (including blood, saliva and urine), the authors must confirm at the point of submission that they obtained approval from an institutional review board or equivalent ethics committee and consent from the donor. A statement reflecting this approval must be given in the experimental section.

Experiments involving cell lines

At submission, authors must declare what cell lines were used and their origin.

Conflicts of interest

Conflicts of interest are situations in which personal, financial or other considerations from authors or reviewers has the potential to compromise or bias objectivity or professional judgment. Authors must explicitly declare conflicts of interest upon submission of an article for publication. Peer-reviewers must recuse themselves from refereeing manuscripts where they perceive a conflict of interest.

Conflicts of interest include consulting fees, honoraria, payments for expert testimony; support for travel to meetings for the study, manuscript preparation or other purposes; multiple affiliations; fees for participation in review activities; payment for writing or reviewing of a manuscript; provision of writing assistance; stock, stock options, equity ownership or other investment interest (including holdings of a spouse, children or other blood relative); intellectual property rights, patents and patent applications (including planned applications); and royalty payments. Beyond financial aspects, conflicts may arise from personal relationships or competing interests directly or indirectly tied to the research for publication, or professional interests or personal beliefs that may influence that research.

Research funding must be listed in the acknowledgements section and must include the funder and grant number.

Referees who suspect an undisclosed conflict of interest should contact the handling editor in the first instance.

The Journal of Materials Science does not allow publication of the content of peer reviews submitted to the journal because of the opportunities for abuse and inherent conflicts of interest. The editors may verify that a reviewer contributed to the Journal's peer-review process provided that no identifying information such as title, manuscript code or DOI are available to link the review to a specific publication.

Does Springer provide English language support?

All submissions must conform to accepted standards of written technical English. Either US or UK English is acceptable as long as the usage is consistent throughout.

The Journal's editors are not responsible for correcting errors in grammar or spelling. Articles that require extensive English revision may be rejected without review or referred to a professional copy editing service before acceptance.

Manuscripts that are accepted for publication will be checked by our copyeditors for spelling and formal style. This may not be sufficient if English is not your native language and substantial editing would be required. In that case, you may want to have your manuscript edited by a native speaker prior to submission. A clear and concise language will help editors and reviewers concentrate on the scientific content of your paper and thus smooth the peer review process.

Use of an editing service is neither a requirement nor a guarantee of acceptance for publication.

Please contact the editing service directly to make arrangements for editing and payment.

The following editing service provides language editing for scientific articles in all areas Springer publishes in:

For Authors from China

文章在投稿前进行专业的语言润色将对作者的投稿进程有所帮助。作者可自愿选择使用 Springer 推荐的编辑服务，使用与否并不作为判断文章是否被录用的依据。提高文章的语言质量将有助于审稿人理解文章的内容，通过对学术内容的判断来决定文章的取舍，而不会因为语言问题导致直接退稿。作者需自行联系 Springer 推荐的编辑服务公司，协商编辑事宜。

理文编辑

For Authors from Japan

ジャーナルに論文を投稿する前に、ネイティブ・スピーカーによる英文校閲を希望されている方には、Edanz 社をご紹介しています。サービス内容、料金および申込方法など、日本語による詳しい説明はエダンズグループジャパン株式会社の下記サイトをご覧ください。

エダンズ グループ ジャパン

For Authors from Korea

영어 논문 투고에 앞서 원어민에게 영문 교정을 받고자 하시는 분들께 Edanz 회사를 소개해 드립니다. 서비스 내용, 가격 및 신청 방법 등에 대한 자세한 사항은 저희 Edanz Editing Global 웹사이트를 참조해 주시면 감사하겠습니다.

Edanz Editing Global

After acceptance

Upon acceptance of your article you will receive a link to the special Author Query Application at Springer's web page where you can sign the Copyright Transfer Statement online and indicate whether you wish to order OpenChoice, offprints, or printing of figures in color.

Once the Author Query Application has been completed, your article will be processed and you will receive the proofs.

Open Choice

In addition to the normal publication process (whereby an article is submitted to the journal and access to that article is granted to customers who have purchased a subscription), Springer provides an alternative publishing option: Springer Open Choice. A Springer Open Choice article receives all the benefits of a regular subscription-based article, but in addition is made available publicly through Springer's online platform SpringerLink.

Springer Open Choice

Copyright transfer

Authors will be asked to transfer copyright of the article to the Publisher (or grant the Publisher exclusive publication and dissemination rights). This will ensure the widest possible protection and dissemination of information under copyright laws.

Open Choice articles do not require transfer of copyright as the copyright remains with the author. In opting for open access, the author(s) agree to publish the article under the Creative Commons Attribution License.

Offprints

Offprints can be ordered by the corresponding author.

Color illustrations

Online publication of color illustrations is free of charge. For color in the print version, authors will be expected to make a contribution towards the extra costs.

Proof reading

The purpose of the proof is to check for typesetting or conversion errors and the completeness and accuracy of the text, tables and figures. Substantial changes in content, e.g., new results, corrected values, title and authorship, are not allowed without the approval of the Editor.

After online publication, further changes can only be made in the form of an Erratum, which will be hyperlinked to the article.

Online First

The article will be published online after receipt of the corrected proofs. This is the official first publication citable with the DOI. After release of the printed version, the paper can also be cited by issue and page numbers.

Revised and approved by the editorial board on 11 January 2016.

http://www.springer.com/journal/10853

Journal of Materials Science
Editor-in-Chief: Carter, C.B.
ISSN: 0022-2461 (print version)
ISSN: 1573-4803 (electronic version)
Journal no. 10853

Journal 2 - *International Journal of Pharmaceutics*

INTERNATIONAL JOURNAL OF PHARMACEUTICS

ELSEVIER

AUTHOR INFORMATION PACK

TABLE OF CONTENTS

- Description p.1
- Audience p.1
- Impact Factor p.1
- Abstracting and Indexing p.2
- Editorial Board p.2
- Guide for Authors p.4

ISSN: 0378-5173

DESCRIPTION

The *International Journal of Pharmaceutics* is the journal for **pharmaceutical scientists** concerned with the physical, chemical and biological properties of devices and **delivery systems** for **drugs**, **vaccines** and **biologicals**, including their design, manufacture and evaluation. This includes evaluation of the properties of drugs, **excipients** such as surfactants and polymers and novel materials. The journal has special sections on **pharmaceutical nanotechnology** and personalized medicines, and publishes research papers, reviews, commentaries and letters to the editor as well as special issues.

Editorial Policy

The over-riding criteria for publication are originality, high scientific quality and interest to a multidisciplinary audience. Papers not sufficiently substantiated by experimental detail will not be published. Any technical queries will be referred back to the author, although the Editors reserve the right to make alterations in the text without altering the technical content. Manuscripts submitted under multiple authorship are reviewed on the assumption that all listed authors concur with the submission and that a copy of the final manuscript has been approved by all authors and tacitly or explicitly by the responsible authorities in the laboratories where the work was carried out. If accepted, the manuscript shall not be published elsewhere in the same form, in either the same or another language, without the consent of the Editors and Publisher.

Authors must state in a covering letter when submitting papers for publication the novelty embodied in their work or in the approach taken in their research. Routine bioequivalence studies are unlikely to find favour. No paper will be published which does not disclose fully the nature of the formulation used or details of materials which are key to the performance of a product, drug or excipient. Work which is predictable in outcome, for example the inclusion of another drug in a cyclodextrin to yield enhanced dissolution, will not be published unless it provides new insight into fundamental principles.

AUDIENCE

Pharmaceutical Scientists, Clinical Pharmacologists, Chemical Engineers, Biotechnologists.

IMPACT FACTOR

2014: 3.650 © Thomson Reuters Journal Citation Reports 2015

ABSTRACTING AND INDEXING

BIOSIS
Chemical Abstracts
MEDLINE®
International Pharmaceutical Abstracts
EMBASE
PASCAL M
Science Citation Index
CAB Abstracts
Current Contents (Life Sciences, Clinical Medicine)
Elsevier BIOBASE/Current Awareness in Biological Sciences
Scopus

EDITORIAL BOARD

GUIDE FOR AUTHORS

INTRODUCTION

The *International Journal of Pharmaceutics* publishes innovative papers, reviews, mini-reviews, rapid communications and notes dealing with physical, chemical, biological, microbiological and engineering studies related to the conception, design, production, characterisation and evaluation of drug delivery systems *in vitro* and *in vivo*. "Drug" is defined as any therapeutic or diagnostic entity, including oligonucleotides, gene constructs and radiopharmaceuticals.

Areas of particular interest include: pharmaceutical nanotechnology; physical pharmacy; polymer chemistry and physical chemistry as applied to pharmaceutics; excipient function and characterisation; biopharmaceutics; absorption mechanisms; membrane function and transport; novel routes and modes of delivery; responsive delivery systems, feedback and control mechanisms including biosensors; applications of cell and molecular biology to drug delivery; prodrug design; bioadhesion (carrier-ligand interactions); and biotechnology (protein and peptide formulation and delivery).

Note: For details on pharmaceutical nanotechnology, see Editorials in 279/1-2 281/1, and 288/1.

Types of paper

(1) **Full Length Manuscripts**

(2) **Rapid Communications**

(a) These articles should not exceed 1500 words or equivalent space.
(b) Figures should not be included otherwise delay in publication will be incurred.
(c) Do not subdivide the text into sections. An Abstract should be included as well as a full reference list.

(3) **Notes**

Should be prepared as described for full length manuscripts, except for the following:

(a) The maximum length should be 1500 words, including figures and tables.
(b) Do not subdivide the text into sections. An Abstract and reference list should be included.

(4) **Reviews and Mini-Reviews**

Suggestions for review articles will be considered by the Review-Editor. "Mini-reviews" of a topic are especially welcome.

BEFORE YOU BEGIN

Ethics in publishing

Please see our information pages on Ethics in publishing and Ethical guidelines for journal publication.

Human and animal rights

If the work involves the use of human subjects, the author should ensure that the work described has been carried out in accordance with The Code of Ethics of the World Medical Association (Declaration of Helsinki) for experiments involving humans; Uniform Requirements for manuscripts submitted to Biomedical journals. Authors should include a statement in the manuscript that informed consent was obtained for experimentation with human subjects. The privacy rights of human subjects must always be observed.

All animal experiments should comply with the ARRIVE guidelines and should be carried out in accordance with the U.K. Animals (Scientific Procedures) Act, 1986 and associated guidelines, EU Directive 2010/63/EU for animal experiments, or the National Institutes of Health guide for the care and use of Laboratory animals (NIH Publications No. 8023, revised 1978) and the authors should clearly indicate in the manuscript that such guidelines have been followed.

Declaration of interest

All authors are requested to disclose any actual or potential conflict of interest including any financial, personal or other relationships with other people or organizations within three years of beginning the submitted work that could inappropriately influence, or be perceived to influence, their work. More information.

Examples of potential conflicts of interest include employment, consultancies, stock ownership, honoraria, paid expert testimony, patent applications/registrations, and grants or other funding.

Submission declaration and verification

Submission of an article implies that the work described has not been published previously (except in the form of an abstract or as part of a published lecture or academic thesis or as an electronic preprint, see 'Multiple, redundant or concurrent publication' section of our ethics policy for more information), that it is not under consideration for publication elsewhere, that its publication is approved by all authors and tacitly or explicitly by the responsible authorities where the work was carried out, and that, if accepted, it will not be published elsewhere in the same form, in English or in any other language, including electronically without the written consent of the copyright-holder. To verify originality, your article may be checked by the originality detection service CrossCheck.

Contributors

Each author is required to declare his or her individual contribution to the article: all authors must have materially participated in the research and/or article preparation, so roles for all authors should be described. The statement that all authors have approved the final article should be true and included in the disclosure.

Authorship

All authors should have made substantial contributions to all of the following: (1) the conception and design of the study, or acquisition of data, or analysis and interpretation of data, (2) drafting the article or revising it critically for important intellectual content, (3) final approval of the version to be submitted.

Changes to authorship

Authors are expected to consider carefully the list and order of authors **before** submitting their manuscript and provide the definitive list of authors at the time of the original submission. Any addition, deletion or rearrangement of author names in the authorship list should be made only **before** the manuscript has been accepted and only if approved by the journal Editor. To request such a change, the Editor must receive the following from the **corresponding author**: (a) the reason for the change in author list and (b) written confirmation (e-mail, letter) from all authors that they agree with the addition, removal or rearrangement. In the case of addition or removal of authors, this includes confirmation from the author being added or removed.
Only in exceptional circumstances will the Editor consider the addition, deletion or rearrangement of authors **after** the manuscript has been accepted. While the Editor considers the request, publication of the manuscript will be suspended. If the manuscript has already been published in an online issue, any requests approved by the Editor will result in a corrigendum.

Article transfer service

This journal is part of our Article Transfer Service. This means that if the Editor feels your article is more suitable in one of our other participating journals, then you may be asked to consider transferring the article to one of those. If you agree, your article will be transferred automatically on your behalf with no need to reformat. Please note that your article will be reviewed again by the new journal. More information.

Copyright

Upon acceptance of an article, authors will be asked to complete a 'Journal Publishing Agreement' (see more information on this). An e-mail will be sent to the corresponding author confirming receipt of the manuscript together with a 'Journal Publishing Agreement' form or a link to the online version of this agreement.

Subscribers may reproduce tables of contents or prepare lists of articles including abstracts for internal circulation within their institutions. Permission of the Publisher is required for resale or distribution outside the institution and for all other derivative works, including compilations and translations. If

excerpts from other copyrighted works are included, the author(s) must obtain written permission from the copyright owners and credit the source(s) in the article. Elsevier has preprinted forms for use by authors in these cases.

For open access articles: Upon acceptance of an article, authors will be asked to complete an 'Exclusive License Agreement' (more information). Permitted third party reuse of open access articles is determined by the author's choice of user license.

Author rights
As an author you (or your employer or institution) have certain rights to reuse your work. More information.

Elsevier supports responsible sharing
Find out how you can share your research published in Elsevier journals.

Role of the funding source

You are requested to identify who provided financial support for the conduct of the research and/or preparation of the article and to briefly describe the role of the sponsor(s), if any, in study design; in the collection, analysis and interpretation of data; in the writing of the report; and in the decision to submit the article for publication. If the funding source(s) had no such involvement then this should be stated.

Funding body agreements and policies
Elsevier has established a number of agreements with funding bodies which allow authors to comply with their funder's open access policies. Some funding bodies will reimburse the author for the Open Access Publication Fee. Details of existing agreements are available online.

Open access

This journal offers authors a choice in publishing their research:

Open access
• Articles are freely available to both subscribers and the wider public with permitted reuse.
• An open access publication fee is payable by authors or on their behalf, e.g. by their research funder or institution.
Subscription
• Articles are made available to subscribers as well as developing countries and patient groups through our universal access programs.
• No open access publication fee payable by authors.

Regardless of how you choose to publish your article, the journal will apply the same peer review criteria and acceptance standards.

For open access articles, permitted third party (re)use is defined by the following Creative Commons user licenses:

Creative Commons Attribution (CC BY)
Lets others distribute and copy the article, create extracts, abstracts, and other revised versions, adaptations or derivative works of or from an article (such as a translation), include in a collective work (such as an anthology), text or data mine the article, even for commercial purposes, as long as they credit the author(s), do not represent the author as endorsing their adaptation of the article, and do not modify the article in such a way as to damage the author's honor or reputation.

Creative Commons Attribution-NonCommercial-NoDerivs (CC BY-NC-ND)
For non-commercial purposes, lets others distribute and copy the article, and to include in a collective work (such as an anthology), as long as they credit the author(s) and provided they do not alter or modify the article.

The open access publication fee for this journal is **USD 3500**, excluding taxes. Learn more about Elsevier's pricing policy: https://www.elsevier.com/openaccesspricing.

Green open access
Authors can share their research in a variety of different ways and Elsevier has a number of green open access options available. We recommend authors see our green open access page for further information. Authors can also self-archive their manuscripts immediately and enable public

access from their institution's repository after an embargo period. This is the version that has been accepted for publication and which typically includes author-incorporated changes suggested during submission, peer review and in editor-author communications. Embargo period: For subscription articles, an appropriate amount of time is needed for journals to deliver value to subscribing customers before an article becomes freely available to the public. This is the embargo period and it begins from the date the article is formally published online in its final and fully citable form.

This journal has an embargo period of 12 months.

Elsevier Publishing Campus
The Elsevier Publishing Campus (www.publishingcampus.com) is an online platform offering free lectures, interactive training and professional advice to support you in publishing your research. The College of Skills training offers modules on how to prepare, write and structure your article and explains how editors will look at your paper when it is submitted for publication. Use these resources, and more, to ensure that your submission will be the best that you can make it.

Language (usage and editing services)
Please write your text in good English (American or British usage is accepted, but not a mixture of these). Authors who feel their English language manuscript may require editing to eliminate possible grammatical or spelling errors and to conform to correct scientific English may wish to use the English Language Editing service available from Elsevier's WebShop.

Submission
Our online submission system guides you stepwise through the process of entering your article details and uploading your files. The system converts your article files to a single PDF file used in the peer-review process. Editable files (e.g., Word, LaTeX) are required to typeset your article for final publication. All correspondence, including notification of the Editor's decision and requests for revision, is sent by e-mail.

Authors must state in a covering letter when submitting papers for publication the novelty embodied in their work or in the approach taken in their research. Routine bioequivalence studies are unlikely to find favour. No paper will be published which does not disclose fully the nature of the formulation used or details of materials which are key to the performance of a product, drug or excipient. Work which is predictable in outcome, for example the inclusion of another drug in a cyclodextrin to yield enhanced dissolution, will not be published unless it provides new insight into fundamental principles.

Note:
The choice of general classifications such as "drug delivery" or "formulation" are rarely helpful when not used together with a more specific classification.

Referees
Please submit, with the manuscript, the names, addresses and e-mail addresses of at least four potential reviewers. Good suggestions lead to faster processing of your paper. Please note:
Reviewers who do not have an institutional e-mail address will only be considered if their affiliations are given and can be verified. Please ensure that the e-mail addresses are current. International reviewers who have recently published in the appropriate field should be nominated, and their areas of expertise must be stated clearly. Note that the editor retains the sole right to decide whether or not the suggested reviewers are contacted.
To aid the editorial process when suggested reviewers are not chosen or decline to review, ensure that the classifications chosen as the field of your paper are as detailed as possible. It is not sufficient to state "drug delivery" or "nanotechnology" etc.

PREPARATION
Use of word processing software
It is important that the file be saved in the native format of the word processor used. The text should be in single-column format. Keep the layout of the text as simple as possible. Most formatting codes will be removed and replaced on processing the article. In particular, do not use the word processor's options to justify text or to hyphenate words. However, do use bold face, italics, subscripts, superscripts etc. When preparing tables, if you are using a table grid, use only one grid for each individual table and not a grid for each row. If no grid is used, use tabs, not spaces, to align columns. The electronic text should be prepared in a way very similar to that of conventional manuscripts (see

also the Guide to Publishing with Elsevier). Note that source files of figures, tables and text graphics will be required whether or not you embed your figures in the text. See also the section on Electronic artwork.
To avoid unnecessary errors you are strongly advised to use the 'spell-check' and 'grammar-check' functions of your word processor.

Article structure

Subdivision - numbered sections
Divide your article into clearly defined and numbered sections. Subsections should be numbered 1.1 (then 1.1.1, 1.1.2, ...), 1.2, etc. (the abstract is not included in section numbering). Use this numbering also for internal cross-referencing: do not just refer to 'the text'. Any subsection may be given a brief heading. Each heading should appear on its own separate line.

Introduction
State the objectives of the work and provide an adequate background, avoiding a detailed literature survey or a summary of the results.

Material and methods
Provide sufficient detail to allow the work to be reproduced. Methods already published should be indicated by a reference: only relevant modifications should be described.

Results
Results should be clear and concise.

Discussion
This should explore the significance of the results of the work, not repeat them. A combined Results and Discussion section is often appropriate. Avoid extensive citations and discussion of published literature.

Conclusions
The main conclusions of the study may be presented in a short Conclusions section, which may stand alone or form a subsection of a Discussion or Results and Discussion section.

Appendices
If there is more than one appendix, they should be identified as A, B, etc. Formulae and equations in appendices should be given separate numbering: Eq. (A.1), Eq. (A.2), etc.; in a subsequent appendix, Eq. (B.1) and so on. Similarly for tables and figures: Table A.1; Fig. A.1, etc.

Essential title page information

• ***Title.*** Concise and informative. Titles are often used in information-retrieval systems. Avoid abbreviations and formulae where possible.
• ***Author names and affiliations.*** Please clearly indicate the given name(s) and family name(s) of each author and check that all names are accurately spelled. Present the authors' affiliation addresses (where the actual work was done) below the names. Indicate all affiliations with a lower-case superscript letter immediately after the author's name and in front of the appropriate address. Provide the full postal address of each affiliation, including the country name and, if available, the e-mail address of each author.
• ***Corresponding author.*** Clearly indicate who will handle correspondence at all stages of refereeing and publication, also post-publication. **Ensure that the e-mail address is given and that contact details are kept up to date by the corresponding author.**
• ***Present/permanent address.*** If an author has moved since the work described in the article was done, or was visiting at the time, a 'Present address' (or 'Permanent address') may be indicated as a footnote to that author's name. The address at which the author actually did the work must be retained as the main, affiliation address. Superscript Arabic numerals are used for such footnotes.

Abstract

A concise and factual abstract is required. The abstract should state briefly the purpose of the research, the principal results and major conclusions. An abstract is often presented separately from the article, so it must be able to stand alone. For this reason, References should be avoided, but if essential, then cite the author(s) and year(s). Also, non-standard or uncommon abbreviations should be avoided, but if essential they must be defined at their first mention in the abstract itself.

The abstract must not exceed 200 words.

Graphical abstract

A Graphical abstract is mandatory for this journal. It should summarize the contents of the article in a concise, pictorial form designed to capture the attention of a wide readership online. Authors must provide images that clearly represent the work described in the article. Graphical abstracts should be submitted as a separate file in the online submission system. Image size: please provide an image with a minimum of 531 × 1328 pixels (h × w) or proportionally more, but should be readable on screen at a size of 200 × 500 pixels (at 96 dpi this corresponds to 5 × 13 cm). Bear in mind readability after reduction, especially if using one of the figures from the article itself. Preferred file types: TIFF, EPS, PDF or MS Office files. See http://www.elsevier.com/graphicalabstracts for examples.

Keywords

Immediately after the abstract, provide a maximum of 6 keywords, using American spelling and avoiding general and plural terms and multiple concepts (avoid, for example, 'and', 'of'). Be sparing with abbreviations: only abbreviations firmly established in the field may be eligible. These keywords will be used for indexing purposes.

Chemical compounds

You can enrich your article by providing a list of chemical compounds studied in the article. The list of compounds will be used to extract relevant information from the NCBI PubChem Compound database and display it next to the online version of the article on ScienceDirect. You can include up to 10 names of chemical compounds in the article. For each compound, please provide the PubChem CID of the most relevant record as in the following example: Glutamic acid (PubChem CID:611). Please position the list of compounds immediately below the 'Keywords' section. It is strongly recommended to follow the exact text formatting as in the example below:

Chemical compounds studied in this article

Ethylene glycol (PubChem CID: 174); Plitidepsin (PubChem CID: 44152164); Benzalkonium chloride (PubChem CID: 15865)

More information.

Abbreviations

Define abbreviations that are not standard in this field in a footnote to be placed on the first page of the article. Such abbreviations that are unavoidable in the abstract must be defined at their first mention there, as well as in the footnote. Ensure consistency of abbreviations throughout the article.

Acknowledgements

Collate acknowledgements in a separate section at the end of the article before the references and do not, therefore, include them on the title page, as a footnote to the title or otherwise. List here those individuals who provided help during the research (e.g., providing language help, writing assistance or proof reading the article, etc.).

Formatting of funding sources

List funding sources in this standard way to facilitate compliance to funder's requirements:

Funding: This work was supported by the National Institutes of Health [grant numbers xxxx, yyyy]; the Bill & Melinda Gates Foundation, Seattle, WA [grant number zzzz]; and the United States Institutes of Peace [grant number aaaa].

It is not necessary to include detailed descriptions on the program or type of grants and awards. When funding is from a block grant or other resources available to a university, college, or other research institution, submit the name of the institute or organization that provided the funding.

If no funding has been provided for the research, please include the following sentence:

This research did not receive any specific grant from funding agencies in the public, commercial, or not-for-profit sectors.

Units

Follow internationally accepted rules and conventions: use the international system of units (SI). If other units are mentioned, please give their equivalent in SI.

Math formulae
Please submit math equations as editable text and not as images. Present simple formulae in line with normal text where possible and use the solidus (/) instead of a horizontal line for small fractional terms, e.g., X/Y. In principle, variables are to be presented in italics. Powers of e are often more conveniently denoted by exp. Number consecutively any equations that have to be displayed separately from the text (if referred to explicitly in the text).

Footnotes
Footnotes should be used sparingly. Number them consecutively throughout the article. Many word processors can build footnotes into the text, and this feature may be used. Otherwise, please indicate the position of footnotes in the text and list the footnotes themselves separately at the end of the article. Do not include footnotes in the Reference list.

Image manipulation
Whilst it is accepted that authors sometimes need to manipulate images for clarity, manipulation for purposes of deception or fraud will be seen as scientific ethical abuse and will be dealt with accordingly. For graphical images, this journal is applying the following policy: no specific feature within an image may be enhanced, obscured, moved, removed, or introduced. Adjustments of brightness, contrast, or color balance are acceptable if and as long as they do not obscure or eliminate any information present in the original. Nonlinear adjustments (e.g. changes to gamma settings) must be disclosed in the figure legend.

Electronic artwork
General points
• Make sure you use uniform lettering and sizing of your original artwork.
• Embed the used fonts if the application provides that option.
• Aim to use the following fonts in your illustrations: Arial, Courier, Times New Roman, Symbol, or use fonts that look similar.
• Number the illustrations according to their sequence in the text.
• Use a logical naming convention for your artwork files.
• Provide captions to illustrations separately.
• Size the illustrations close to the desired dimensions of the published version.
• Submit each illustration as a separate file.
A detailed guide on electronic artwork is available.
You are urged to visit this site; some excerpts from the detailed information are given here.
Formats
If your electronic artwork is created in a Microsoft Office application (Word, PowerPoint, Excel) then please supply 'as is' in the native document format.
Regardless of the application used other than Microsoft Office, when your electronic artwork is finalized, please 'Save as' or convert the images to one of the following formats (note the resolution requirements for line drawings, halftones, and line/halftone combinations given below):
EPS (or PDF): Vector drawings, embed all used fonts.
TIFF (or JPEG): Color or grayscale photographs (halftones), keep to a minimum of 300 dpi.
TIFF (or JPEG): Bitmapped (pure black & white pixels) line drawings, keep to a minimum of 1000 dpi.
TIFF (or JPEG): Combinations bitmapped line/half-tone (color or grayscale), keep to a minimum of 500 dpi.
Please do not:
• Supply files that are optimized for screen use (e.g., GIF, BMP, PICT, WPG); these typically have a low number of pixels and limited set of colors;
• Supply files that are too low in resolution;
• Submit graphics that are disproportionately large for the content.

Color artwork
Please make sure that artwork files are in an acceptable format (TIFF (or JPEG), EPS (or PDF), or MS Office files) and with the correct resolution. If, together with your accepted article, you submit usable color figures then Elsevier will ensure, at no additional charge, that these figures will appear in color online (e.g., ScienceDirect and other sites) regardless of whether or not these illustrations are reproduced in color in the printed version. **For color reproduction in print, you will receive information regarding the costs from Elsevier after receipt of your accepted article**. Please indicate your preference for color: in print or online only. Further information on the preparation of electronic artwork.

Figure captions
Ensure that each illustration has a caption. Supply captions separately, not attached to the figure. A caption should comprise a brief title (**not** on the figure itself) and a description of the illustration. Keep text in the illustrations themselves to a minimum but explain all symbols and abbreviations used.

Tables

Please submit tables as editable text and not as images. Tables can be placed either next to the relevant text in the article, or on separate page(s) at the end. Number tables consecutively in accordance with their appearance in the text and place any table notes below the table body. Be sparing in the use of tables and ensure that the data presented in them do not duplicate results described elsewhere in the article. Please avoid using vertical rules.

References

Citation in text
Please ensure that every reference cited in the text is also present in the reference list (and vice versa). Any references cited in the abstract must be given in full. Unpublished results and personal communications are not recommended in the reference list, but may be mentioned in the text. If these references are included in the reference list they should follow the standard reference style of the journal and should include a substitution of the publication date with either 'Unpublished results' or 'Personal communication'. Citation of a reference as 'in press' implies that the item has been accepted for publication and a copy of the title page of the relevant article must be submitted.

Reference links
Increased discoverability of research and high quality peer review are ensured by online links to the sources cited. In order to allow us to create links to abstracting and indexing services, such as Scopus, CrossRef and PubMed, please ensure that data provided in the references are correct. Please note that incorrect surnames, journal/book titles, publication year and pagination may prevent link creation. When copying references, please be careful as they may already contain errors. Use of the DOI is encouraged.

A DOI can be used to cite and link to electronic articles where an article is in-press and full citation details are not yet known, but the article is available online. A DOI is guaranteed never to change, so you can use it as a permanent link to any electronic article. An example of a citation using DOI for an article not yet in an issue is: VanDecar J.C., Russo R.M., James D.E., Ambeh W.B., Franke M. (2003). Aseismic continuation of the Lesser Antilles slab beneath northeastern Venezuela. Journal of Geophysical Research, http://dx.doi.org/10.1029/2001JB000884i. Please note the format of such citations should be in the same style as all other references in the paper.

Web references
As a minimum, the full URL should be given and the date when the reference was last accessed. Any further information, if known (DOI, author names, dates, reference to a source publication, etc.), should also be given. Web references can be listed separately (e.g., after the reference list) under a different heading if desired, or can be included in the reference list.

References in a special issue
Please ensure that the words 'this issue' are added to any references in the list (and any citations in the text) to other articles in the same Special Issue.

Reference management software
Most Elsevier journals have their reference template available in many of the most popular reference management software products. These include all products that support Citation Style Language styles, such as Mendeley and Zotero, as well as EndNote. Using the word processor plug-ins from these products, authors only need to select the appropriate journal template when preparing their article, after which citations and bibliographies will be automatically formatted in the journal's style. If no template is yet available for this journal, please follow the format of the sample references and citations as shown in this Guide.

Users of Mendeley Desktop can easily install the reference style for this journal by clicking the following link:
http://open.mendeley.com/use-citation-style/international-journal-of-pharmaceutics
When preparing your manuscript, you will then be able to select this style using the Mendeley plug-ins for Microsoft Word or LibreOffice.

Reference formatting
There are no strict requirements on reference formatting at submission. References can be in any style or format as long as the style is consistent. Where applicable, author(s) name(s), journal title/book title, chapter title/article title, year of publication, volume number/book chapter and the pagination must be present. Use of DOI is highly encouraged. The reference style used by the journal will be applied to the accepted article by Elsevier at the proof stage. Note that missing data will be highlighted at proof stage for the author to correct. If you do wish to format the references yourself they should be arranged according to the following examples:

Reference style
Text: All citations in the text should refer to:
1. *Single author:* the author's name (without initials, unless there is ambiguity) and the year of publication;
2. *Two authors:* both authors' names and the year of publication;
3. *Three or more authors:* first author's name followed by 'et al.' and the year of publication.
Citations may be made directly (or parenthetically). Groups of references should be listed first alphabetically, then chronologically.
Examples: 'as demonstrated (Allan, 2000a, 2000b, 1999; Allan and Jones, 1999). Kramer et al. (2010) have recently shown ....'
List: References should be arranged first alphabetically and then further sorted chronologically if necessary. More than one reference from the same author(s) in the same year must be identified by the letters 'a', 'b', 'c', etc., placed after the year of publication.
Examples:
Reference to a journal publication:
Van der Geer, J., Hanraads, J.A.J., Lupton, R.A., 2010. The art of writing a scientific article. J. Sci. Commun. 163, 51–59.
Reference to a book:
Strunk Jr., W., White, E.B., 2000. The Elements of Style, fourth ed. Longman, New York.
Reference to a chapter in an edited book:
Mettam, G.R., Adams, L.B., 2009. How to prepare an electronic version of your article, in: Jones, B.S., Smith , R.Z. (Eds.), Introduction to the Electronic Age. E-Publishing Inc., New York, pp. 281–304.
Reference to a website:
Cancer Research UK, 1975. Cancer statistics reports for the UK. http://www.cancerresearchuk.org/aboutcancer/statistics/cancerstatsreport/ (accessed 13.03.03).

Journal abbreviations source
Journal names should be abbreviated according to the List of Title Word Abbreviations.

Video data
Elsevier accepts video material and animation sequences to support and enhance your scientific research. Authors who have video or animation files that they wish to submit with their article are strongly encouraged to include links to these within the body of the article. This can be done in the same way as a figure or table by referring to the video or animation content and noting in the body text where it should be placed. All submitted files should be properly labeled so that they directly relate to the video file's content. In order to ensure that your video or animation material is directly usable, please provide the files in one of our recommended file formats with a preferred maximum size of 150 MB. Video and animation files supplied will be published online in the electronic version of your article in Elsevier Web products, including ScienceDirect. Please supply 'stills' with your files: you can choose any frame from the video or animation or make a separate image. These will be used instead of standard icons and will personalize the link to your video data. For more detailed instructions please visit our video instruction pages. Note: since video and animation cannot be embedded in the print version of the journal, please provide text for both the electronic and the print version for the portions of the article that refer to this content.

Supplementary material
Supplementary material can support and enhance your scientific research. Supplementary files offer the author additional possibilities to publish supporting applications, high-resolution images, background datasets, sound clips and more. Please note that such items are published online exactly as they are submitted; there is no typesetting involved (supplementary data supplied as an Excel file or as a PowerPoint slide will appear as such online). Please submit the material together with the article and supply a concise and descriptive caption for each file. If you wish to make any changes to supplementary data during any stage of the process, then please make sure to provide an updated

file, and do not annotate any corrections on a previous version. Please also make sure to switch off the 'Track Changes' option in any Microsoft Office files as these will appear in the published supplementary file(s). For more detailed instructions please visit our artwork instruction pages.

Data in Brief

Authors have the option of converting any or all parts of their supplementary or additional raw data into one or multiple Data in Brief articles, a new kind of article that houses and describes their data. Data in Brief articles ensure that your data, which is normally buried in supplementary material, is actively reviewed, curated, formatted, indexed, given a DOI and publicly available to all upon publication. Authors are encouraged to submit their Data in Brief article as an additional item directly alongside the revised version of their manuscript. If your research article is accepted, your Data in Brief article will automatically be transferred over to *Data in Brief* where it will be editorially reviewed and published in the new, open access journal, *Data in Brief*. Please note an open access fee is payable for publication in *Data in Brief*. Full details can be found on the Data in Brief website. Please use this template to write your Data in Brief.

Database linking

Elsevier encourages authors to connect articles with external databases, giving readers access to relevant databases that help to build a better understanding of the described research. Please refer to relevant database identifiers using the following format in your article: Database: xxxx (e.g., TAIR: AT1G01020; CCDC: 734053; PDB: 1XFN). More information and a full list of supported databases.

AudioSlides

The journal encourages authors to create an AudioSlides presentation with their published article. AudioSlides are brief, webinar-style presentations that are shown next to the online article on ScienceDirect. This gives authors the opportunity to summarize their research in their own words and to help readers understand what the paper is about. More information and examples are available. Authors of this journal will automatically receive an invitation e-mail to create an AudioSlides presentation after acceptance of their paper.

Interactive plots

This journal enables you to show an Interactive Plot with your article by simply submitting a data file. Full instructions.

Submission checklist

It is hoped that this list will be useful during the final checking of an article prior to sending it to the journal's Editor for review. Please consult this Guide for Authors for further details of any item.

Ensure that the following items are present:

One Author designated as corresponding Author:

- E-mail address
- Full postal address
- Telephone and fax numbers

All necessary files have been uploaded

- Keywords
- All figure captions
- All tables (including title, description, footnotes)

Further considerations:

- Use continuous line numbering (every 5 lines) to facilitate reviewing of the manuscript.
- Manuscript has been "spellchecked" and "grammar-checked"
- References are in the correct format for this journal
- All references mentioned in the Reference list are cited in the text, and vice versa
- Permission has been obtained for use of copyrighted material from other sources (including the Web)
- Color figures are clearly marked as being intended for color reproduction on the Web (free of charge) and in print or to be reproduced in color on the Web (free of charge) and in black-and-white in print
- If only color on the Web is required, black and white versions of the figures are also supplied for printing purposes

For any further information please visit our customer support site at service.elsevier.com.

AFTER ACCEPTANCE

Online proof correction

Corresponding authors will receive an e-mail with a link to our online proofing system, allowing annotation and correction of proofs online. The environment is similar to MS Word: in addition to editing text, you can also comment on figures/tables and answer questions from the Copy Editor. Web-based proofing provides a faster and less error-prone process by allowing you to directly type your corrections, eliminating the potential introduction of errors.

If preferred, you can still choose to annotate and upload your edits on the PDF version. All instructions for proofing will be given in the e-mail we send to authors, including alternative methods to the online version and PDF.

We will do everything possible to get your article published quickly and accurately. Please use this proof only for checking the typesetting, editing, completeness and correctness of the text, tables and figures. Significant changes to the article as accepted for publication will only be considered at this stage with permission from the Editor. It is important to ensure that all corrections are sent back to us in one communication. Please check carefully before replying, as inclusion of any subsequent corrections cannot be guaranteed. Proofreading is solely your responsibility.

Offprints

The corresponding author will, at no cost, receive a customized Share Link providing 50 days free access to the final published version of the article on ScienceDirect. The Share Link can be used for sharing the article via any communication channel, including email and social media. For an extra charge, paper offprints can be ordered via the offprint order form which is sent once the article is accepted for publication. Both corresponding and co-authors may order offprints at any time via Elsevier's Webshop. Corresponding authors who have published their article open access do not receive a Share Link as their final published version of the article is available open access on ScienceDirect and can be shared through the article DOI link.

AUTHOR INQUIRIES

Track your submitted article
Track your accepted article
You are also welcome to contact the Elsevier Contact Center.

ANNEXURE C - Poster Presentations

Poster 1 – 17th World Congress of Basic and Clinical Pharmacology (WCP 2014)

WCP 2014 was an international conference held at the Cape Town International Convention Centre (CTICC) in South Africa from the 13th to the 18th July 2014. The scientific abstracts from this conference are published in Basic & Clinical Pharmacology & Toxicology by John Wiley & Sons. http://www.wcp2014.org/

The following poster presented at this congress was published under the "Pharmacology and Technology" theme and was published as follows:

Chelopo M., Hayeshi R., Grobler A; Physicochemical and *In Vivo* Characteristics of a Combined Drug Delivery System for Selected Anti-Tuberculosis Drugs, *Basic & Clinical Pharmacology & Toxicology*, 115 (Suppl. 1), 1–374, Pharmacology and Technology (p.323) (Abstract number:1042) © 2014 Nordic Pharmacological Society

(URL: http://onlinelibrary.wiley.com/doi/10.1111/bcpt.12259_11/pdf)

#1042

our future through science

Physicochemical and *In Vivo* Characteristics of a Combined Drug Delivery System for Selected Anti-Tuberculosis Drugs

Madichaba P Chelopo[1,2*], Lonji Kalombo[1], Matthew Glyn[2], Brendon Naicker[1], Hulda Swai[1], Anne Grobler[2], Rose Hayeshi[1]

[1]CSIR Materials Science and Manufacturing, PO Box 395, Pretoria, 0001
[2]DST/NWU Preclinical Drug development Platform, NWU, PUK Campus, Potchefstroom, 2520
* Mchelopo@ csir.co.za

BACKGROUND

South Africa has one of the highest tuberculosis (TB) burdens in the world [1]. Current TB therapy requires daily and lengthy administration periods resulting in poor patient compliance and poor therapeutic outcomes. Drug delivery systems have been investigated to improve these therapeutics so as to reduce dosing frequency and shorten the treatment period [2]. Examples include lipid-based delivery systems and polymeric nanoparticles (NP). Hybrid delivery systems, which combine the advantages of polymeric NP and lipid-based systems, have emerged to be a robust and promising delivery platform [3].

OBJECTIVES

To develop a novel hybrid system where poly lactic-co-glycolic acid (PLGA) NP are entrapped within lipid-based Pheroid® vesicles resulting in a potentially robust drug delivery technology, with excellent stability, sustained drug release and enhanced drug delivery. The PLGA NP confer extended systemic circulation and sustained release and the Pheroid® enhance absorption of drugs.

The specific objective is to entrap anti-TB drug (rifampicin and isoniazid)-loaded PLGA NPs within Pheroid® vesicles (Figure 1) and evaluate the capability of this hybrid system to enhance the pharmacokinetics (PK) of these two anti-TB drugs.

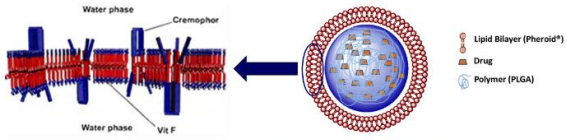

Figure 1: Hypothetical illustration of NP-Pheroid® system. Drug loaded PLGA core and the surrounding lipid bilayer (Pheroid®) - enlarged on the left to highlight its components

EXPERIMENTAL METHODS

NP were incorporated into Pheroid® vesicles during manufacture of Pheroid® (pre-mix) or post manufacture of Pheroid® (post-mix), see Figure 2. The particle size and zeta potential were measured using dynamic light scattering and laser diffraction techniques.

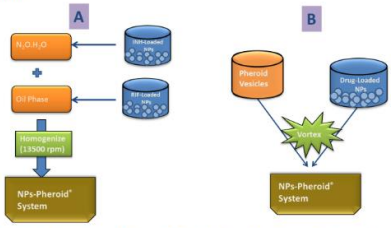

Figure 2: Methods of combining NP with Pheroid ®. Pre-mix (A) and post-mix (B) methods

The effect of the hybrid system on bioavailability of rifampicin (RIF) and isoniazid (INH) was determined in mice (Figure 3). Test formulations were administered via oral gavage at doses of 10 and 5 mg/kg for RIF and INH respectively.

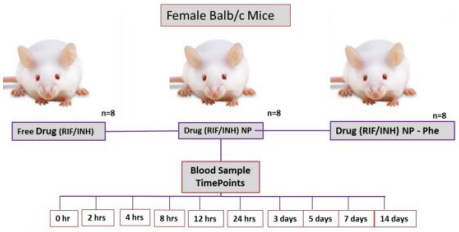

Figure 3: Mouse study design (NWU ethics approval # NWU-00128-11-A5)

RESULTS

NP size ranged from 250 nm to 400 nm and zeta potential (ZP) from 14.5 to 35.5 mV. The average particle size of free Pheroid® increased from 1990 nm to 2450 nm when combined with 1% (w/w) of NP using both pre-mix and post-mix methods. The ZP of the Pheroid® and hybrid system ranged from -18 to -30 mV.

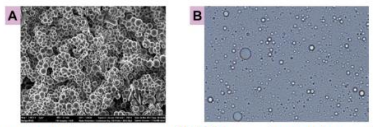

Figure 4: (A) Scanning electron microscopy (SEM) image showing the morphology of PLGA NP and (B) Pheroid® vesicles observed under light microscope

Visual analysis using confocal laser scanning microscopy showed that the NP (labelled with Coumarin 6) were entrapped within the Pheroid® vesicles (stained with Nile Red). The optimal mixing ratio was 2.5% (w/w) of NP to Pheroid®, beyond which a morphological disruption of the Pheroid® vesicles was observed.

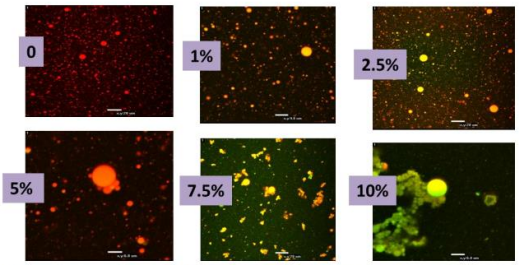

Figure 5: Confocal images of Pheroid ® vesicles with varying ratios of NP

The bioavailability of INH and RIF are indicated by the plasma concentration profiles in Figure 6. An in-depth statistical analysis will confirm any significant differences in the hybrid system profile versus the controls.

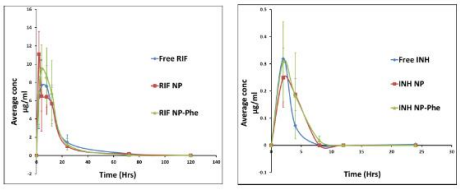

Figure 6: Plasma concentration level curves for INH ((left) and RIF (right)

CONCLUSION

The fabrication of a novel PLGA NP-Pheroid® delivery system has been successful, the NP core is entrapped within the Pheroid® vesicle shell. In-depth statistical analysis is required to prove whether the NP-Pheroid® hybrid system enhanced the bioavailability of either RIF or INH. Further characterisation of the system is required to understand the interaction of the two delivery systems.

ACKNOWLEDGEMENTS

Department of Science and Technology (DST) and National Research Foundation (NRF) for funding. A special thank you to Antoinette Fick and Hylton Bunnting for their exceptional help during the animal study.

REFERENCES

1. WHO, 2012, Global Tuberculosis Report. World Health Organization.
2. YVES, L. Y. et.al., 2007. Antituberculosis drugs: Ten years of research. Bioorg Med Chem,15, 35
3. Zhang, L., et al., 2008. Self-Assembled Lipid−Polymer Hybrid Nanoparticles: A Robust Drug Delivery Platform. ACS Nano, 2, 696

science & technology
Department: Science and Technology
REPUBLIC OF SOUTH AFRICA

PCDDP
DST/NWU Preclinical Drug Development Platform

NORTH-WEST UNIVERSITY
YUNIBESITI YA BOKONE-BOPHIRIMA
NOORDWES-UNIVERSITEIT

Poster 2 – From Rising Stars to a Nobel Star

After participation at the 67th Lindau Noble Laureate Meeting, Madichaba P Chelopo, who is a Next Generation Scientist (NGS) fellow, was invited to present the Lindau meeting feedback and current PhD work in a poster (on the following page) at Novartis AG, Basel, Switzerland, on the 4th July 2017.

Novartis meeting invitation: “Meet Kurt Wüthrich, a Nobel Chemistry laureate and get inspired by two former Next Generation Scientist fellows and a NIBR post-doctoral fellow, all of whom were participants at the Lindau conference, an annual conference where Nobel laureates meet to coach and mentor young rising star scientists.”

The Fabrication of PLGA Nanoparticle – Pheroid® Hybrid Drug Delivery System with the Potential to Improve the Therapy of High-Burden Diseases in South Africa

Madichaba P Chelopo[1,2*], Lonji Kalombo[1], James Wesley-Smith[1], Brendon Naicker[1], Anne Grobler[2], Rose Hayeshi[1]

[1]Materials Science and Manufacturing, CSIR, , Pretoria, 0001
[2]DST/NWU Preclinical Drug development Platform, NWU, PUK Ca PO mpus, Potchefstroom, 2520
* Madichaba.PC@gmail.com

BACKGROUND

Drug delivery systems (DDSs) formulations assist in the effective transport of therapeutic drugs to optimise their activity. A Hybrid DDS combines the unique attributes of polymeric nanoparticles (NPs) and lipid-based systems to obtain a more robust drug delivery platform [1]. However, the capacity of these hybrid DDS are yet to be explored in the therapy improvement for nfectious diseases such as tuberculosis (TB), which burden most South Africans [2].

OBJECTIVES

1. To fabricate a novel hybrid DDS where poly lactic-co-glycolic acid (PLGA) NPs are entrapped within lipid-based Pheroid® vesicles.

2. To conduct a case study for tuberculosis (TB) therapy: The pharmacokinetic (PK) properties of anti-TB drug, rifampicin (RIF) or isoniazid (INH) will be evaluated to determine the effect of the hybrid DDS..

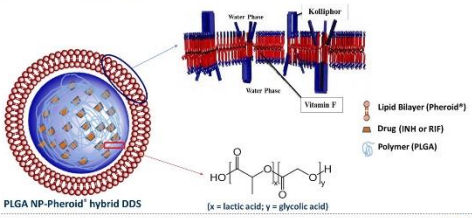

METHODS

NPs were incorporated into Pheroid® vesicles either through the pre-mix (A) or the post-mix (B) approach and physicochemical characterization was done.

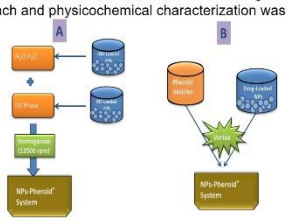

In the *in vivo* case study drug formulations were administered to mice via oral gavage at 10 and 5 mg/kg dosages for RIF and INH respectively. (Ethics approval # NWU-00128-11-A5)

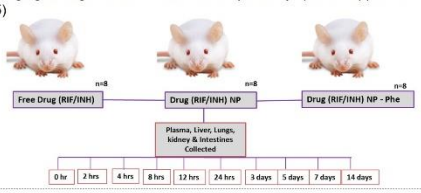

RESULTS

The average particle size of free Pheroid® increased from 1990 nm to 2450 nm when combined with 1% (w/v) of NPs while the zeta potential (ZP) ranged between -18 and -30 mV. The pre-mix method resulted in relatively higher ZP of the NP-Pheroid® hybrid DDS. The maximum optimal NP to Pheroid® mixing ratio was 2.5% (w/v).

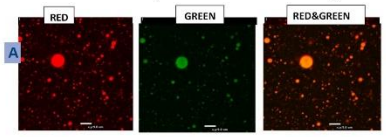

Fig. 1: Confocal laser scanning microscopy (CLSM) images (A) showed that the NPs (labelled with coumarin 6) were co-localised with the Pheroid® vesicles (stained with nile red).

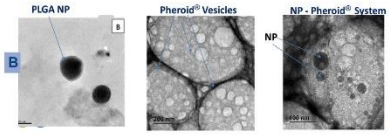

Fig. 2: Transmission electron microscopy (TEM) images (B) suggesting the co-localisation of NPs with the Pheroid® vesicles (negatively stained with uranyl acetate).

INH	AUC_{0-t} (µg/ml h)	C_{max} (µg/ml)	T_{max} (h)	$t_{1/2}$ (h)
	Mean ± SD	Mean ± SD	Mean ± SD	Mean ± SD
Free INH	0.946 ± 0.397	0.327 ± 0.128	2.00 ± 0.61	2.549 ± 2.532
INH NP	1.657 ± 1.294	0.282 ± 0.053	2.50 ± 0.62	2.119 ± 0.790
INH NP-Phe	1.449 ± 1.216	0.330 ± 0.163	2.25 ± 1.10	1.521 ± 0.790
RIF	AUC_{0-t} (µg/ml h)	C_{max} (µg/ml)	T_{max} (h)	$t_{1/2}$ (h)
	Mean ± SD	Mean ± SD	Mean ± SD	Mean ± SD
Free RIF	145.30 ± 35.52	9.65 ± 1.57	6.50 ± 3.51	12.65 ± 1.77
RIF NP	157.49 ± 23.53	11.43 ± 1.92	4.29 ± 2.93	11.03 ± 1.82
RIF NP-Phe	172.10 ± 44.01	11.01 ± 2.14	7.50 ± 3.34	11.91 ± 3.29

Phe = Pheroid®

Tab. 1: The mice plasma PK data of INH (top) and RIF (bottom) over a period of time. There was no significant difference (P>0.05) in all the PK parameters among the three formulations for both drugs

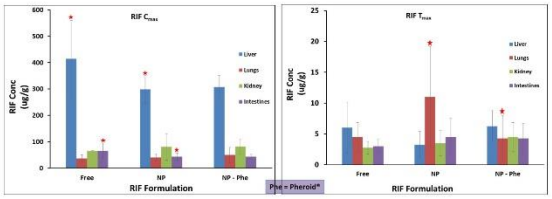

Fig. 3: The PK parameters of RIF in various mouse organs. The NP-Pheroid® (Phe) hybrid DDS did not significantly alter the RIF C_{max} in any organ. The effect of this hybrid system was observed to be the significant reduction of RIF T_{max} in the lungs (P = 0.02), in comparison with the RIF NPs. This system also led to the longest retention of RIF in the lungs (5 days), comparison to all other organs (3 days).

CONCLUSION

In the development of a novel hybrid DDS, the PLGA NP core was confirmed to be co-localised with the Pheroid® vesicle shell, suggesting a successful fabrication.

The PLGA NP-Pheroid® hybrid DDS did not alter the PK parameters of both INH and RIF drugs in the plasma. The effect of this hybrid DDS was observed in the distribution RIF to the lungs, where it significantly reduced T_{max} and that it also resulted in the longest detection of RIF in the lungs.

More studies to conclude the potential of this novel hybrid DDS to improve the therapy of pulmonary TB are required.

ACKNOWLEDGEMENTS

Department of Science and Technology (DST) and National Research Foundation (NRF) for funding; Matthew Glyn for his technical assistance with the CLSM; Antoinette Fick and Hylton Buntting for their exceptional help during the animal study.

REFERENCES

1. Zhang, L., et al., 2008. Self-Assembled Lipid−Polymer Hybrid Nanoparticles: A Robust Drug Delivery Platform. ACS Nano, 2, 696
2. WHO, 2015, Global Tuberculosis Report. World Health Organization

ANNEXURE D - Oral Presentations

The following are the details and cover pages of all the oral presentations given at various conferences for the work presented in this thesis.

Oral Presentation 1 – APSSA/ SAAPI Conference

The Academy of Pharmaceutical Sciences of the Pharmaceutical Society of South Africa (APSSA) / South African Association of Pharmacists in Industry (SAAPI) Conference was held on the 17th - 19th September 2015 at CedarWoods Conference Centre in Sandton, South Africa. The talks given at this conference by postgraduate students were presented to both local and international delegates.

http://confpro.co.za/SPWTS2.htm

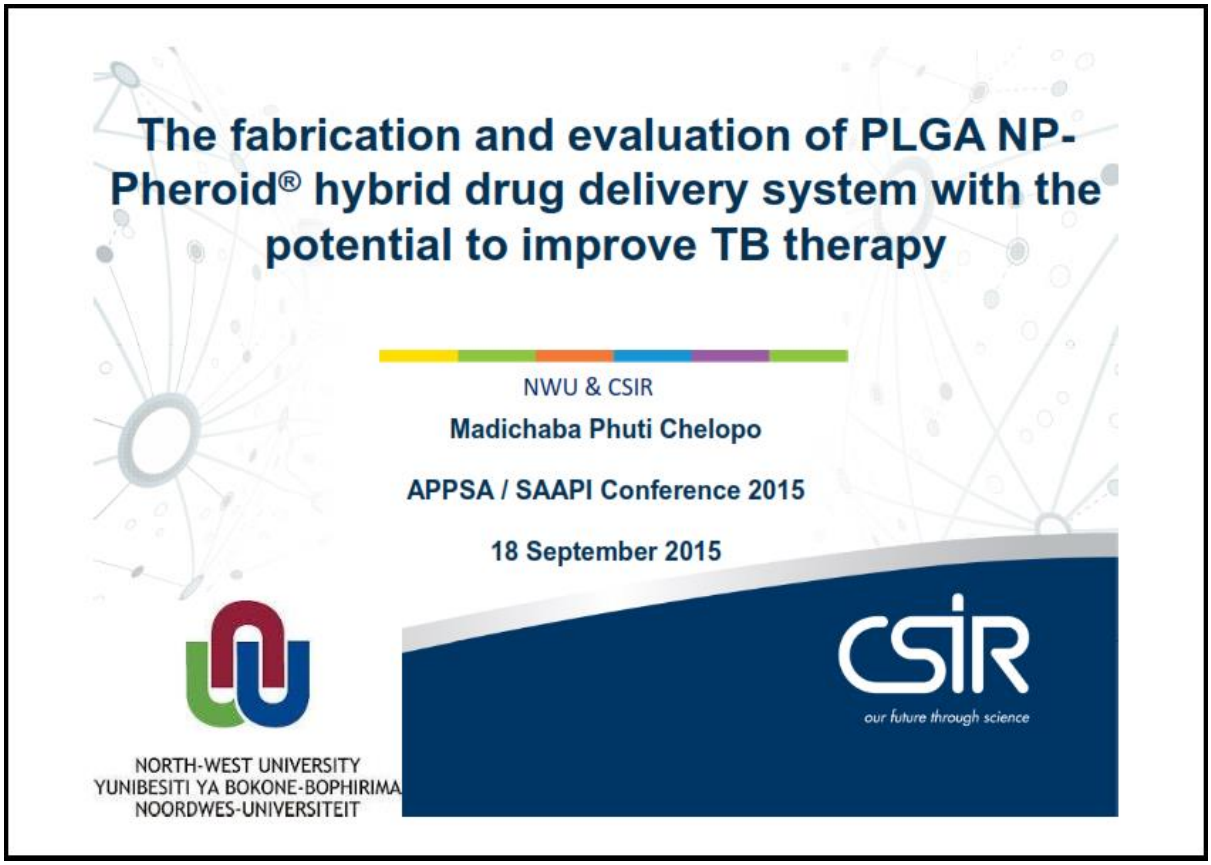

Oral Presentation 2 - 6th International Conference on Nanoscience & Nanotechnology in Africa (Nano Africa 2016)

The NanoAfrica 2016 conference was held on the 3rd - 6th April 2016 at the University of South Africa (UNISA), Florida campus, South Africa.

http://www.npep.co.za/newsletters/16-nanoannounce/128-the-6th-international-conference-on-nanoscience-and-nanotechnology-2

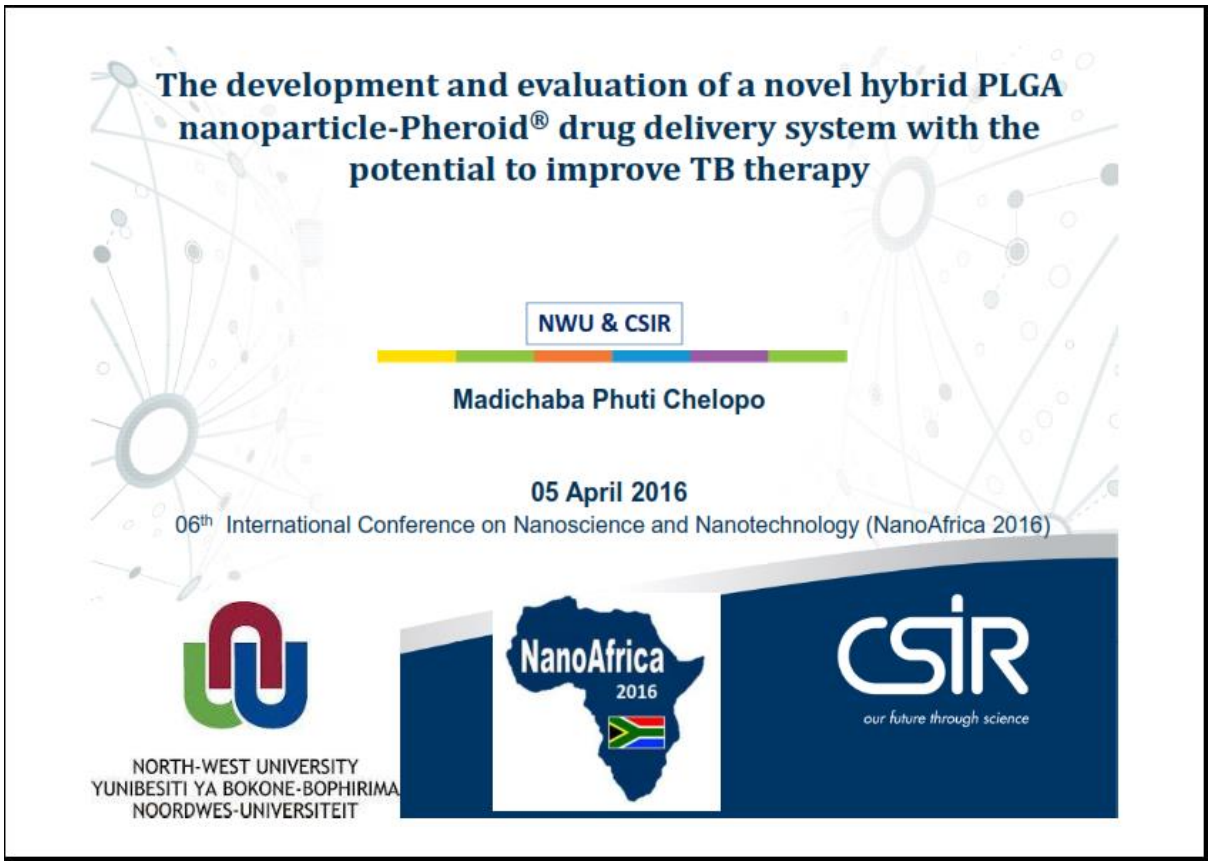

Oral Presentation 3 – 2nd Edition of Nanotech France International Conference and Exhibition (Nanotech France 2016)

The Nanotech France 2016 was an international conference held on the 1st – 3rd June 2016 at the Pôle Universitaire Léonard de Vinci, in La Défense – Paris, France. The following talk given at this meeting was presented under the theme of "Nanotech in Life Sciences and Medicine".

http://www.setcor.org/conferences/Nanotech-France-2016

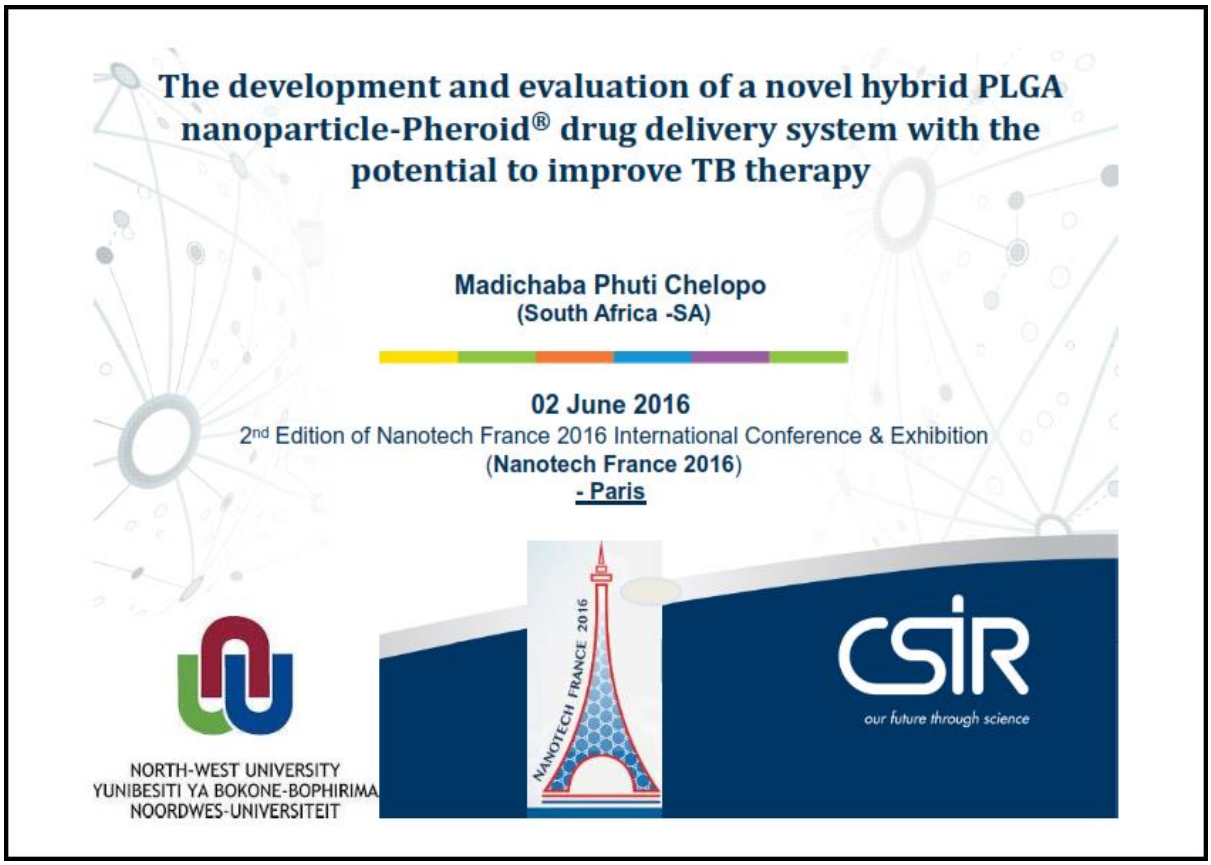

Oral Presentation 4 – 2nd Symposium on Nanomedicine and HIV/AIDS

The SA Nano HIV/AIDS 2016 was held on the 2nd December 2016 at The South African Agency for Science and Technology Advancement (SAASTA), Pretoria, South Africa.

http://www.npep.co.za/october-2016/213-2nd-symposium-on-nanomedicine-and-hiv-aids-in-south-africa-2

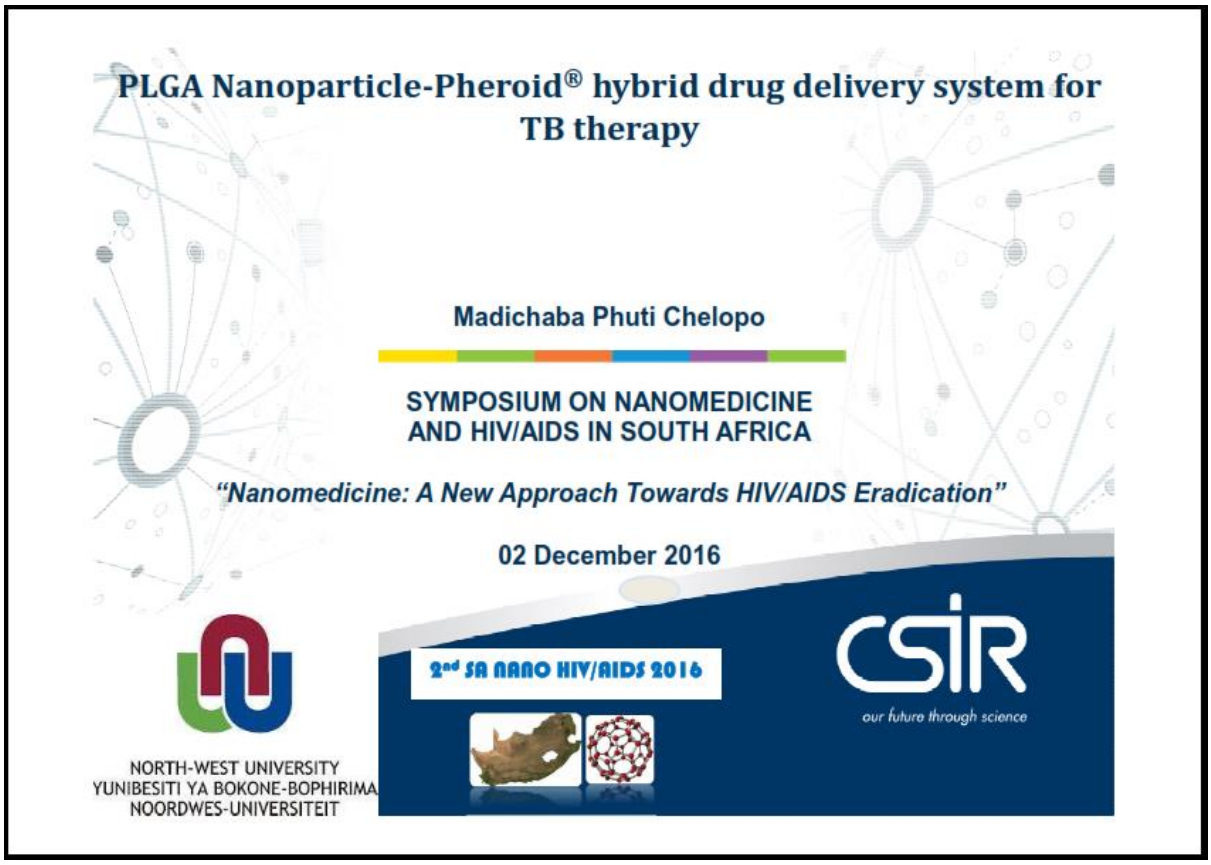

ANNEXURE E – Language Editing

This section contains proof of the English language editing.

M: +27 (0) 73 3414395
+27 (0) 78 129 0653
E: mmathabomakhanya@gmail.com
A: 209 Crown Gardens | 1236 Bottrill Street | Queenswood

konibo communications

EDITOR'S NOTE

The thesis submitted by Ms M P Chelopo-Mgobozi for the degree of Doctor of Philosophy in Pharmaceutical Chemistry at the North West University, titled 'The development and evaluation of a novel hybrid PLGA nanoparticle-Pheroid with the potential to improve tuberculosis therapy', has been edited by Ms Kefilwe Makhanya (Editor: Konibo Communications).

Kefilwe is a former Communication Lecturer (UFH) with extensive writing and editing experience in various disciplines, including science, technology, trade and business.

17 November 2017

SIGNATURE **DATE**